Universitat Autònoma de Barcelona

# Catechol Poly(disulfide)s: a new platform for adhesives in the medical industry

**Miguel Ángel Moreno Villaécija**

**Department of Chemistry**

**Faculty of Science**

# Catechol Poly(disulfide)s: a new platform for adhesives in the medical industry

Miguel Ángel Moreno Villaécija

PhD in Materials Science

2021

**Director**
Dr. Daniel Ruiz Molina

**Tutor**
Dr. Félix Busqué Sánchez

*Memoria presentada para aspirar al Grado de Doctor por Miguel Ángel Moreno Villaécija*

Dr. Daniel Ruiz Molina

Bellaterra, 9 de diciembre de 2021

‘Con estos bueyes hemos de arar’
by *Dni*

‘B******t!’
by *J.*

# Acknowledgements

Me gustaría comenzar dando las gracias a mi director de tesis Daniel, por darme la oportunidad de realizar este trabajo del que tanto he podido disfrutar y aprender en el grupo Nanosfun. Gracias por la confianza que me has dado a lo largo de los años en el grupo, donde me he sentido apoyado e importante en todo momento. Tu visión científica y tu gestión de las personas hace que seas un excelente director para cualquier estudiante. Quiero agradecer también a Josep toda su implicación en la primera parte de la tesis. Pese a no ser finalmente director de la tesis, en los primeros compases me supervisó como tal, enseñándome a ser riguroso y autocrítico en cada paso que dábamos. Ambos habéis sido cruciales para poder llevar a cabo este trabajo del que estoy orgulloso.

Quiero agradecer a toda la gente que forma y ha formado parte de la familia *Nanosfun* por los grandes momentos que he pasado y lo mucho que he aprendido de ellos. A Fabi, a quien considero mi "madre científica" siendo mi supervisora en mis primeros pasos en el ámbito de la investigación, y que me enseño a ser meticuloso y a cuestionarme todos los resultados. A Juan, principal culpable del proyecto de esta tesis y que me enseño los primeros trucos de síntesis orgánica. Agradecer a Salvi, compañero antes y durante la tesis, siempre predispuesto a ayudar en todo, y por las risas con él en los ratos de marujeo del bueno. También a A. Julià, compañero y amigo, con el que he tenido la suerte de compartir momentos increíbles a lo largo de los años durante la carrera y durante el doctorado. Muy buen compañero dando soporte moral como "Event Manager" del grupo. Junda, thank you for the great times during these years sharing moments in and outside the lab, always available for ordering chinese food for me. Ivana, aka Ragazza, grazie mille por ser siempre una buenísima compañera, aunque desertaras a la *Mafia* del CM3... También a Noe, que ha tenido que aguantar más que nadie mis bromas y quien finalmente ha perdido en la carrera de ver quién presentaba más tarde la tesis. Gracias Claudio y Fer, lo seniors al pie del cañon,

Jaume, Hector, Aleix (CM3 *Mafia*), María y su *real coffee*, José, su infinidad de viales y su dieta que le hace romper batas, Pau mi pequeño saltamontes, Eva mi última compi de oficina... todos vosotros habéis hecho que esta tesis y últimos meses en el grupo *Nanosfun* hayan sido especiales. No puedo dejar de mencionar a todos los que en un momento u otro habéis compartido momentos conmigo durante mi periodo en el grupo, haciendo de esta familia que es *Nanosfun* un grupo espectacular en el que la gente se siente como en casa. Bea, Xiao, Ayala, Christian, Nahia, Mire, Pablo, Nuria, Ferran, Karolina, Payam, Faezeh, Anton, Belén, Olga, Alexis, Roger, Carolina,... todos y cada uno de vosotros habéis formado parte de mi camino para poder llegar a presentar este trabajo, haciendo que todo sea más sencillo.

Me gustaría agradecer también a la gente del Departamento de Orgánica. En especial a Carolina y a Sergio que han estado ligados de una forma u otra a este proyecto y que me han ayudado aportándome ideas y consejos de química orgánica cuando los he necesitado. También dar las gracias a Félix y Ramon que han estado implicados en el proyecto y que me han ayudado en algunos aspectos de química orgánica de la tesis.

Quiero agradecer también a Haritz Sardon de POLYMAT por acogerme en su grupo en Donosti durante unos meses y por ayudarme y enseñarme en todo lo relacionado con la química de polímeros que ha sido vital para poder llevar a cabo gran parte de la tesis. Muchísimas gracias a todos los compañeros de POLYMAT y la UPV/EHU con los que he tenido el placer de compartir buenos momentos en el lab, de pintxopote o de sidreria. Fermin, Iñaki, Naroa, Andere, Antonio, Jeremy, Marine, Amaury, Nicolas, Elena. Pero sobre todo mil gracias a Sara y Álvaro por recibirme siempre con los brazos abiertos cuando se lo he pedido. Con vosotros he podido disfrutar de las mejores experiencias allí, con buenas anécdotas como el día día de la mudanza en que estrené piso con vosotros o el día de la nevada en la playa de La Concha. Sabéis que siempre vais a tener un buen amigo por Barcelona que vais a tener la puerta de mi casa siempre abierta. Eskerrik asko!

También dar las gracias a Nora, Itziar, Lidia y Ainhoa del Grupo de Procesados de POLYMAT y UPV/EHU por darme la oportunidad de ir a usar sus equipos, aunque fuera pagando la tasa correspondiente de una caja de bombones.

Me gustaría también dar las gracias a la Dra. Julia Lorenzo y al Dr. David Montpeyó por su ayuda y colaboración para realizar los ensayos *in vitro* que se presentan en la tesis.

저는 이 해신 교수님 에게 감사합니다. 저는 한국에 멋진 경험 했어요. 그리고

저는 많이 배웠어요. 나는 친구들에게도 감사 인사를 전하고 싶습니다. 지희 'mi amiga' 나에게 특별합니다. 우리는 함께 즐거운 시간을 보냈습니다. 나는 우리의 대화가 그리워요. 윤한 '요가 맨' 나를 많이 도왔어요. 나는 축구에 대한 우리의 토론을 즐긴다. 정한 Jingxian 내 중국 친구. 당신은 항상 행복해요. 감사합니다. 은숙 'the shy girl' 항상 똑똑했어요. 나는 BTS을 들어서 너를 기억해요. 윤선 '박사님'. 우리는 바르셀로나에서 만났어요. 너는 항상 나를 도와줘요. 나는 너에게 많이 맥주를 빚졌어요. 여러분 모두는 제 마음에 영원히 이겠어요. 그리고 나는 실험실 동료에게도 감사 인사를 전하고 싶습니다. 수현과 대헌과 해성과 재관과 흥기와 감사합니다. 내 한국어 미안. 나는 배우고 있어요. I tried my best ㅋㅋㅋ

Quiero agradecer también a mi amigo y doctorando en bioinformática José, Apa para los amigos, quien me ha ayudado en el análisis conformacional de los compuestos cíclicos de este trabajo y con el que tengo discusiones distendidas sobre ciencia y fútbol. No nos cansamos nunca de repetir una y otra vez los mismos temas...

Por último quiero agradecer a mi familia todo el soporte que me han dado a lo largo de estos años. A mis padres, Chari y Rafa por apoyarme en cada uno de mis pasos y aguantarme en casa. A mi hermana, que siempre me ha ayudado en lo que le he pedido y quien es la gran artista de los dibujos y portada de la tesis que han quedado espectacular. Y también a Laura. Mi compañera, mi confidente, la persona que me alegra por las mañanas. Muchísimas gracias por todo tu cariño y respaldo incondicional. Nunca te lo voy a poder agradecer lo suficiente.

Muchísimas gracias a todas las personas que habéis puesto vuestro granito de arena para que esta tesis haya salido adelante.

**Funding Sources**

This work was supported by the Spanish Government through project SEV-2013-0295-16-1 encompassed within the Severo Ochoa (SO) Program. I thank the *Ministerio de Educación, Cultura y Deporte* for the predoctoral grant BES-2016-076924 associated to the project of SO Program.

**Abstract**

Catechols are widely present in nature taking part on crucial mechanisms in some organisms. The fascinating properties of catechols in terms of adhesion, redox activity and chelating properties have raised the recent interest in catechol containing polymers for the development of new functional materials.

An area of active research is the design of new bioinspired catechol containing adhesives. The presence of catechol functionality has allowed to achieve materials with adhesion on multiple substrates and, furthermore, has enhanced the adhesion on wet conditions. This adhesion on wet conditions has opened the possibility of using these materials in the biomedical field as adhesives in medical devices and tissue adhesives/sealants. Despite the great advances in the field during last decades, new approaches to achieve adhesives based on catechols with full biodegradability potential and bonding/debonding on demand properties are still required. Poly(disulfide)s, which are characterized by the presence of disulfide bonds (-S-S-), are polymers with special interesting dynamic behavior due to their reversibility through thiol-disulfide exchange and homolytic cleavage with light and temperature.

Within this context, in the present thesis a new family of catechol poly(disulfide)s is introduced to combine the most interesting features of catechols and disulfides functionalities. During this work the synthesis of a novel catechol containing compound bearing two thiols readily for polymerization is performed. Then, oxidative polymerization of free thiols with iodine is optimized looking for a proper modular approach with fine-tuning of the molecular weight of catechol poly(disulfide)s obtained. Seeking for potential applications, the adhesion on diverse substrates and the use of these materials as tissue adhesive and sealant is evaluated. Furthermore, to study the full potential of these materials on the biomedical field, in vitro and in vivo studies following ISO 10993 are carried out, as well as the assessment of the feasible degradation on different media. Besides, the finding and characterization of catechol disulfides macrocycles from polymerization reactions has led to the development of an alternative adhesive formulation from ring opening polymerization (ROP) disulfide macrocycles.

## Abbreviations

**ACN**: Acetonitrile

**AFM**: Atomic Force Microscopy

**AIBN**: Azobisisobutyronitrile

**ASTM**: American Society for Testing and Materials

**COSY**: Correlated Spectroscopy

***D***: Diffusion coefficient

**Đ**: Polydispersity index

**DCM**: Dichloromethane

**DMA**: Dopamine methacrylate

**DMEM**: Dulbecco's Modified Eagle Medium

**DODT**: 3,6-dioxa-1,8-octanedithiol

**DoE**: Design of Experiments

**DOSY**: Diffusion-ordered spectroscopy

**DSC**: Differential Scanning Calorimetry

**DTT**: Dithiothreitol

**EDX**: Energy-dispersive X-ray spectroscopy

**EMA**: European Medicines Agency

**FDA**: Food and Drug Administration

**GPC**: Gel Permeation Chromatography

**HDPE**: High-density polyethylene

**ISO**: International Organization of Standardization

**L-DOPA**: L-3,4-dihydroxyphenylalanine

**MALD-TOF**: Matrix Assisted Laser Desorption Ionization Time of Flight

**mfp**: mussel foot protein

**NMR**: Nuclear Magnetic Resonance

**NOE**: Nuclear Overhauser Effect

**$PBu_3$**: Tributylphosphine

**PDA**: Polydopamine

**PEG**: Polyethylene glycol

**PGA**: Poly(glycolic acid)

**PLA**: Poly(lactic acid)

**PTFE**: Polytetrafluoroethylene

**PVA**: Polyvinyl alcohol

**rms**: Root mean square

**rt**: Room Temperature

**TEA**: Triethylamine

**TFA**: Trifluoroacetic acid

**TGA**: Thermogravimetric Analysis

**THF**: Tetrahydrofuran

**TLC**: Thin Layer Chromatography

**ROP**: Ring-opening polymerization

**$S_a$**: Arithmetical mean height

**SFA**: Surface Force Apparatus

**STM**: Scanning Tunneling Microscopy

**USP**: United States Pharmacopeia

**UTM**: Universal Testing Machine

**VC**: Vinyl catechol

**XTT**: 2,3-Bis-(2-Methoxy-4-Nitro-5-Sulfophenyl)-2H-Tetrazolium-5-Carboxanilide

# Formula Index

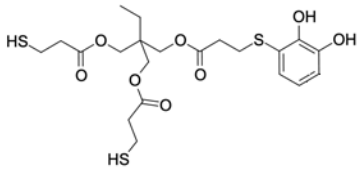


1

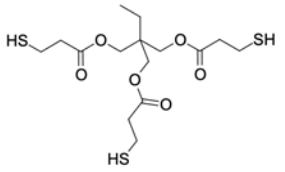


2


3


4

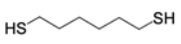


5

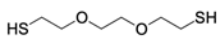


6

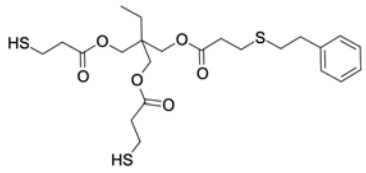


7

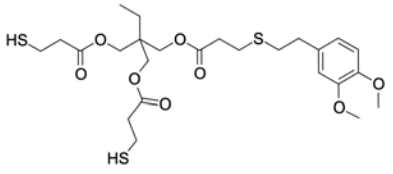


8

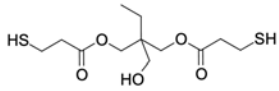

**9**

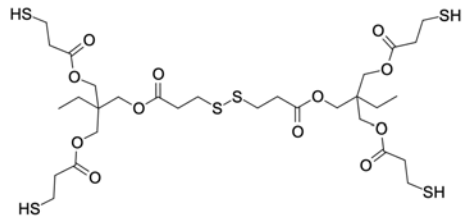

**10**

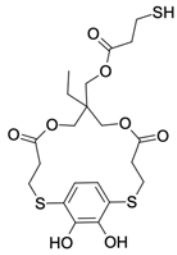

**11**

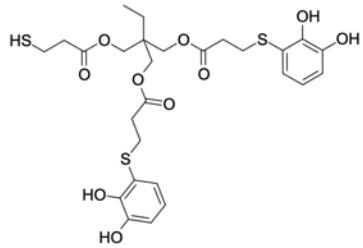

**12**

**13**

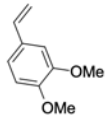

**14**

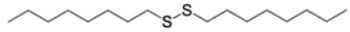

**15**

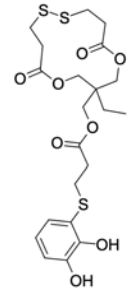

**c1**

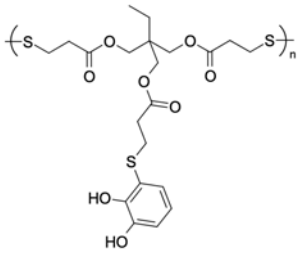

**p1**

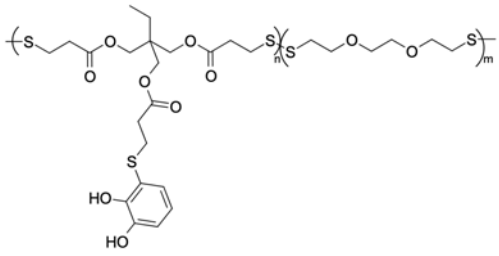

**p(1–6)**

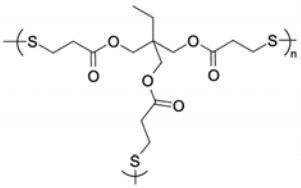

**p2**

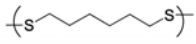

**p5**

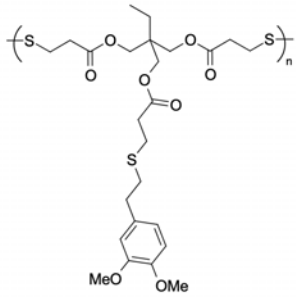

**p8**

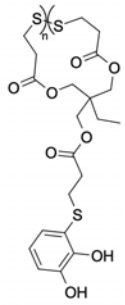

**p1-cyc**

# Contents

# CHAPTER 1

# Catechols, poly(disulfide)s, and the design of bioinspired polymers

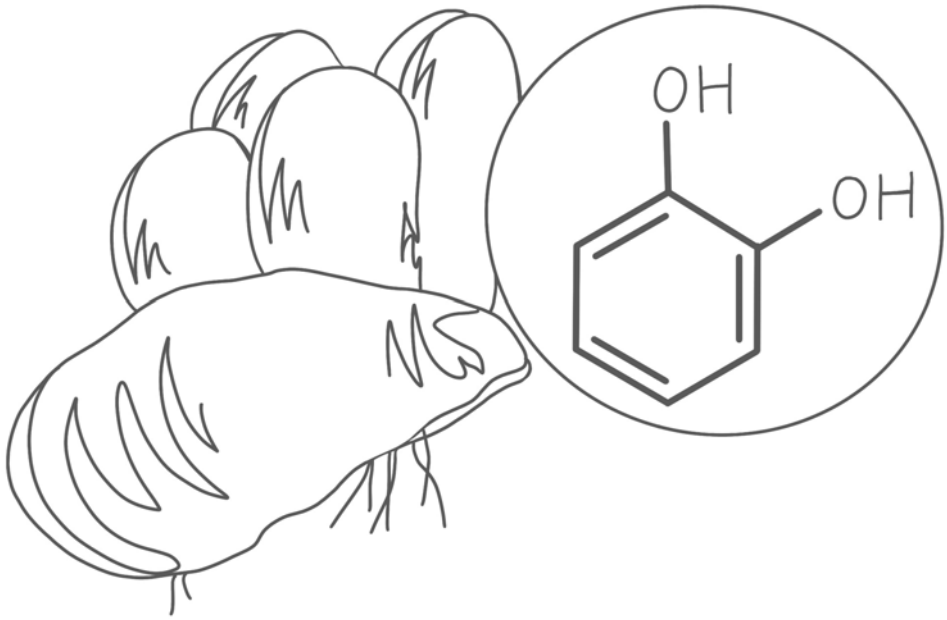

## 1.1 Catechols in nature – A source of inspiration

Nature has been always a great source of inspiration. Recently, the concept of biomimicry, defined as innovation inspired by nature, has reemerged. Nowadays, research in so distinct fields as economy, architecture or materials science is paying further attention in how nature works. In order to achieve an efficient and sustainable world, knowing how the organisms have reached current complexity is the key. In the field of chemistry and material sciences, the knowledge acquired from natural systems has given insights for the new design and development of new human-made materials.

Among all chemical structures, catechols have awaken strongly the interest during last decades for the improvement of bioinspired materials, especially due to their redox activity, adhesive and chelating properties. Naturally, catechols are widely present in many organisms either in isolated compounds or in polymeric structures (Figure 1.1). Catechol derivatives are found in fruits and vegetables being involved in the browning process produced by the enzymatic oxidation of compounds such as chlorogenic acid, catechin or epicatechin present in apples, avocados and green tea, for example.[1] In mammals, pigmentation of skin, eyes and hair is due to melanin, a catechol containing biopolymer.[2] Melanin is also present in the ink of marine organisms and is crucial in the tanning process of insects for the exoskeleton stiffening.[3]

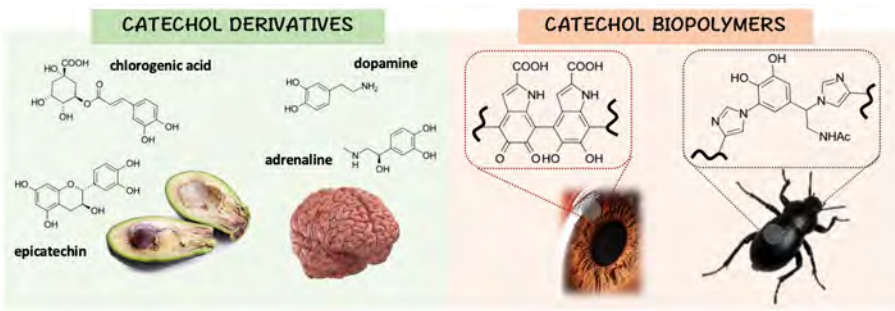


**Figure 1.1.** Examples of catechol derivatives and catechol containing biopolymers present in natural systems.

However, if there is a case where the presence of catechol moiety deserves special attention for the present work, this is mussels. The secretion of adhesive material through their byssal thread allows blue mussels to remain anchored robustly to a plethora of surfaces underwater and even under turbulent conditions, which is unthinkable for conventional synthetic adhesives. The first studies of these systems by Waite et al. reported the existence of different mussel foot

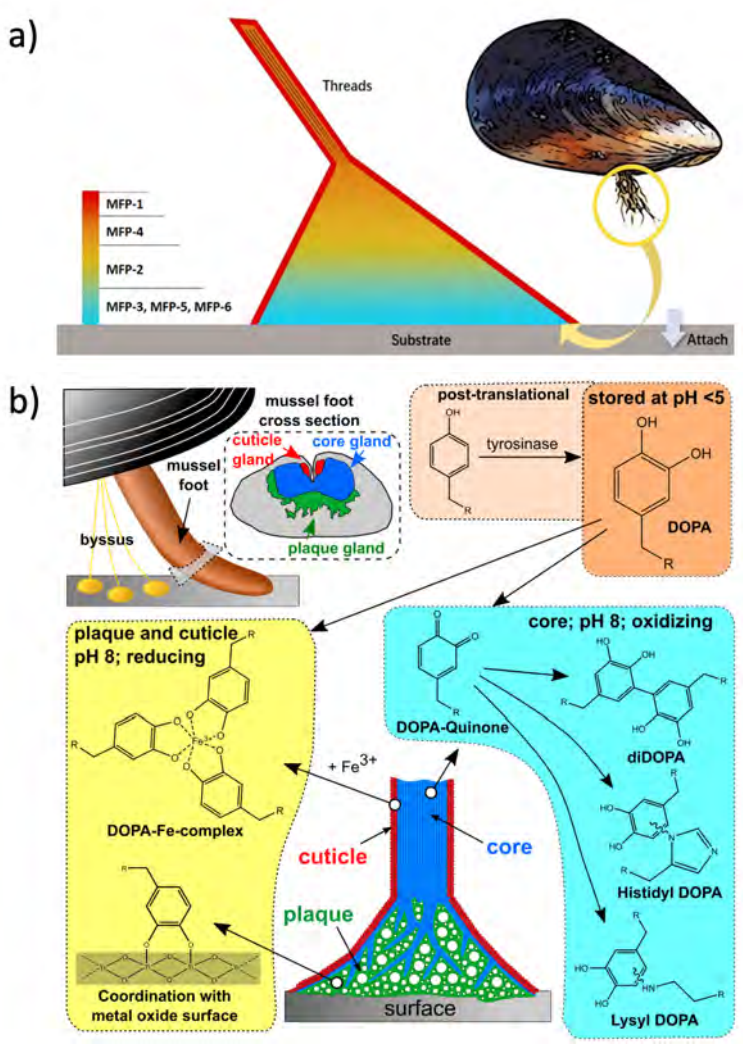


**Figure 1.2.** a) Schematic distribution representation of the different mfps along the mussel byssus;[4] b) representation of the different mechanisms involving catechols occurring on the different compartments of the mussel byssus.[5]

proteins (mfps) taking part in the adhesion of these organisms (Figure 1.2).[6] Studies focused on the polypeptide chains of mfp-1, mfp-2 and mfp-3, showed the presence of the catecholic amino acid 3,4-dihydroxyphenyl-L-alanine (DOPA) in

amounts between 2 to 30 mol%, revealing the importance of this functionality in the adhesive properties of mussels. More recent studies have elucidated the chemical structure of other mfps which allow to enlighten the role of lysine and cysteine enriched proteins participating in the process, both in the adhesion and the cohesion of this natural glue.[7,8]

Despite the efforts for determining the structure of catechol containing biopolymers, there are still unraveled questions about their structures and mechanisms of action due to the high complexity of natural systems such as melanins and mfps. The most relevant are analyzed in next sections.

## 1.2 Properties of catecholic compounds

### 1.2.1 Reactivity of catechols and *o*-quinones

#### 1.2.1.1 Redox activity

Catechol can be present in three different oxidation states: the reduced form of catechol ($QH_2$), the semi-oxidized form semiquinone ($QH^{\bullet}$) and the fully oxidized *o*-quinone (Q). Upon exposure with atmospheric oxygen, catechols are spontaneously oxidized to *o*-quinones via two electron electron abstraction and two hydrogen loss, through the less stable $QH^{\bullet}$ state.[9]

An important feature of $QH_2/QH^{\bullet}/Q$ system is their interconversion. When two $QH^{\bullet}$ are formed, fast disproportionation occur to form the corresponding $QH_2$ and Q or both $QH^{\bullet}$ can be combined forming a new covalent bond between catechols. Oppositely, in a slower process, comproportionation can occur between $QH_2$ and Q in solution.[10]

This reversible redox activity of $QH_2/Q$ has led to the design of catechol containing materials for their use on energy storage devices. An exhaustive review about the use of catechol-derived polymers for energy storage and environment has been published recently by Detrembleur et al.[11]

Another important issue regarding $QH_2/Q$ system is their radical scavenging activity, present in most natural polyphenols. In an experimental and computational study of different phenols it was concluded that radical scavenging is mainly contributed by the presence of $-OH$ in *ortho* position.[12]

Radical scavenging properties of natural compounds such as chlorogenic acid and caffeic acid have been seen to contribute to the inhibition of oxidative stress and ROS production.[13] However, while the radical scavenging property of catechols could reduce ROS, the oxidation of catechols by oxygen can generate ROS species as byproducts and, consequently, can increase the oxidative stress in cells as well.[14] This close relation between catechols and inhibition/generation of ROS

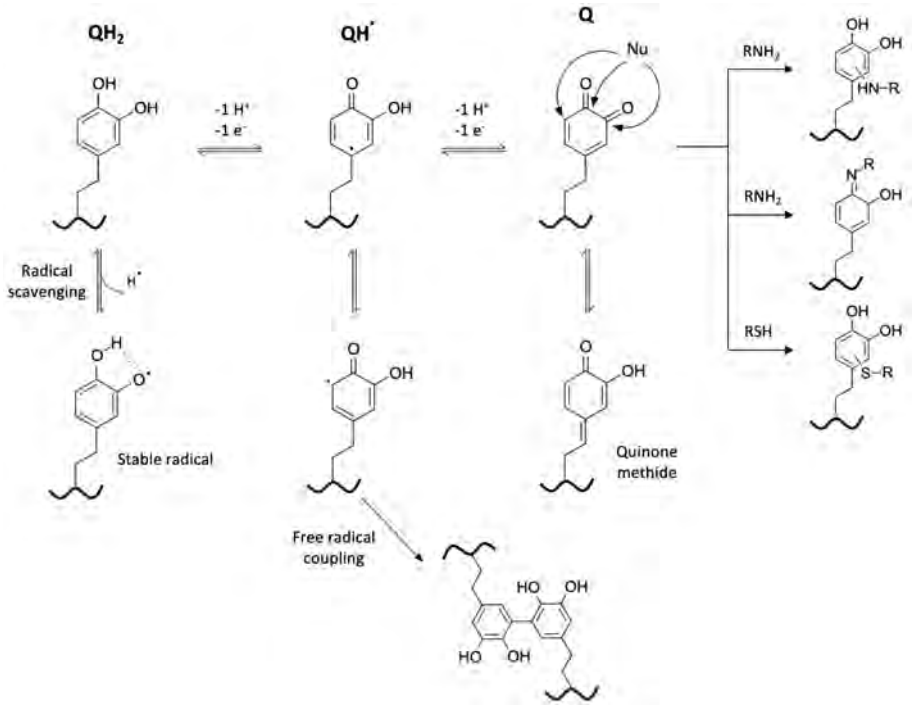


**Figure 1.3.** General scheme of the redox behavior and reactivity of catechols and *o*-quinones.

species is an issue of especial interest for those materials containing catechols aimed for biological applications.

#### 1.2.1.2 Catechol-amine reactivity

The oxidized form of catechol, *o*-quinone (Q), is a highly reactive electrophilic group that can undergo different reaction with nucleophiles such as amines and thiols.

For years, the reaction between catechols and amines has been subject of study due to its relation with the formation of natural melanins.[2,15] However, nowadays a full understanding of these complex systems has not been achieved yet.

About the different reactions between amines and catechols, reactions via Michael-type or via Schiff base reaction have been described.[9] This reactivity has been broadly employed for the design of melanin-like materials through oxidative polymerization of catechols in combination with amines (see Section 1.3.1). For

more information about Michael-type and Schiff base reaction between amines and catechols, the extensive review by Kamperman et al. provides further details.[9]

#### 1.2.1.3 Catechol-thiol reactivity

Initial studies of catechol-thiol reactivity were focused on pheomelanins, which are sulfur-containing pigments obtained from the oxidative polymerization of 5-S-cysteinyldopa and 2-S-cysteinyldopa within the group of melanins.[16] Besides taking part in melanogenesis process, pheomelanins have been related to red hair color and its presence in high contents has been associated to UV-induced melanoma due to the their more prominent pro-oxidant properties front eumelanins.[17–19] The intriguing properties of this type of sulfur-containing melanins led to the research in the synthesis of cysteinyldopa derivatives in the late '70s by S. Ito and G. Prota.[20] Their study using tyrosinase revealed the formation of the well-known 5-S-cysteinyldopa and 2-S-cysteinyldopa as well as 2,5-S,S-dicysteinyldopa and 6-S-cysteinyldopa as side products, the later in lower amounts. This study exposed the preference of the 1,6-addition of cysteine to dopaquinone and the feasibility of a double thiol addition in the case of 2,5-S,S-dicysteinyldopa.

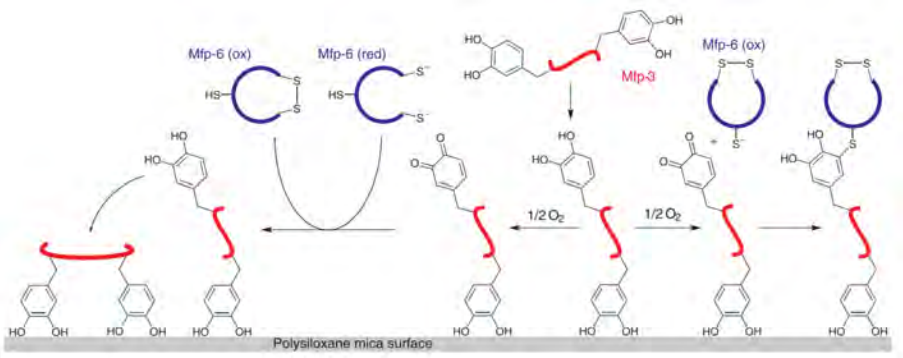


**Figure 1.4.** Redox control process of catechol/quinone system in mfp3 with thiol-rich mfp-6.[8]

Thiol addition has been found to be also important in mussels, playing a crucial role in the action of mfp-6. The presence of this thiol-rich protein (containing presumably two disulfides and nine free thiols) would confer an antioxidant action mechanism by mfp-6 by reducing the dopaquinone formed in mfp-3, restoring the adhesion of mfp-3 (Figure 1.4).[8] In fact, nearly 1 % of 5-S-cysteinyldopa was detected in mfp, which would confirm thiol-Dopa coupling on these systems.[21] Recently, a structural study of the core/shell architecture of mussel byssal threads

have shown how thiol-rich proteins are highly present in the interlayer between the cuticle and the core, preventing catechol oxidation and making possible catechol restoration through this cysteinyldopa formation.[22]

This reactivity between catechol/quinone pair and thiols has been also used frequently in the design of polymers and hydrogels, for enhancing cross-linking of the system. Lee et al. used this reactivity for promoting the cross-linking in hyaluronic acid/pluronic composite hydrogels with interesting thermo-sensitive properties for biological application.[23] In a more recent work, Krüger and Börner took advantage of this reactivity to synthesize catechol containing polymers up to 15.9 kDa.[24] This reaction showed fast kinetics, with the consumption of bisquinones in less than 2 minutes and leading to the formation of cyclic products.

In view of the reactivity between *o*-benzoquinones and thiols, recently Dr. Mancebo-Aracil developed a synthetic approach achieving conjugate addition of the thiol. Through this strategy, a wide range of new bioinspired functional catechol derivatives were obtained, showing high potential for uses such as surface modification and metal-coordination.[25]

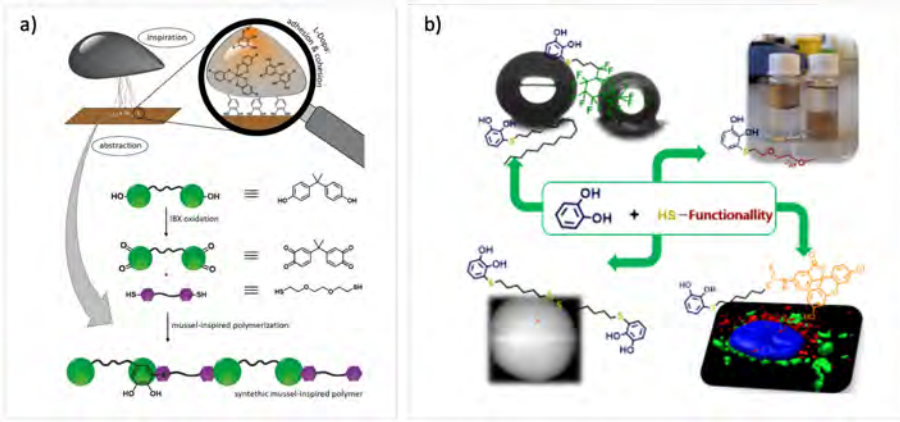


**Figure 1.5.** a) Bioinspired polymerization approach reported by Krüger and Börner combining bisquinones and dithiols,[24] b) synthetic approach for the development of novel catechol derivatives reported by Mancebo-Aracil et al.[25]

In summary, a few examples combining catechol and thiol chemistries have been reported in natural and synthetic systems, but their versatility open a new venue for the design of new materials with interesting properties, such as the self-repairing and adhesion restoring found in natural systems.

### 1.2.2 Adhesive properties

One of the most interesting characteristics of catechols is their role in the adhesion mechanism in some marine organism. Focusing on the adhesion of catechol based materials, several works have tried to unravel the mechanism behind the adhesion of natural catechol containing systems. For adhesive materials, proper performance is achieved when there is efficient balance between the adhesion and cohesion contributions. Adhesive contribution is related to the catechol-surface interactions while cohesive contribution is connected with the cross-linking mechanisms of catechol containing materials. In next sections the most relevant key players in the adhesion and cohesion of catechol containing materials are detailed.

#### 1.2.2.1 Adhesion: catechol/surface interaction

Chemical structure of catechol, a benzene ring bearing two neighboring hydroxyl groups, is the essence of its versatility for the adhesion. Catechols have the ability of interact with multiple surfaces via covalent and non-covalent interactions.[26]

Concerning non-covalent interactions hydrogen bonding allows the adhesion of catechol groups on hydrophilic surfaces. The studies of mfps adhesion on mica surfaces by Waite and Israelachvili using atomic force microscopy (AFM) and surface force apparatus (SFA) revealed the role of hydrogen bonding on the reversible adhesion of mfps on these substrates.[27,28] This interaction is highly dependent on the pH and the presence of oxidants. At elevated pHs and/or in presence of oxidants, where quinone form prevails over catechol, the adhesion can be reduced up to 60 %, confirming the importance of hydroxyls groups for the interaction via hydrogen bonding.[29]

Interactions via $\pi$-$\pi$ are also important in catechol containing systems. Scanning tunneling microscopy (STM) studies of the interaction of alkylcatechols on graphite showed well-defined oriented patterns confirming the adsorption of catechols on materials containing $\pi$ systems.[30] The $\pi$-$\pi$ stacking capability of catechols have been used to improve the coating on substrates such as carbon nanotubes (CNTs).[31]

Concerning metal containing surfaces, studies on alumina ($Al_2O_3$) and titania ($TiO_2$)[32] have shown the predominancy of bidentate coordination between catechols and these surfaces. The possibility to achieve coordination is, however, determined by the oxidation state of catechols. Recent electrochemical studies of Lee et al. have revealed the reduction of catechol-titanium interaction upon catechol oxidation to quinone.[33]

Finally, catechols, in its oxidized formed *o*-quinone, can react covalently via Michael addition with organic surfaces with pendant amines of thiols, as described in previous section. This strategy is broadly used in the design of catechol based adhesives aimed for biomedical use in order to promote their adhesion on wet

tissues.[34,35]

#### 1.2.2.2 Cohesion: cross-linking mechanisms of catechols

In order to enhance the cohesion of the systems, catechol containing polymers can be cross-linked through reversible and irreversible pathways.

In natural mfps, reversible cross-linking via $\pi$-cation interactions is present. These interactions has been seen to play and important role in the cohesion of marine organisms, as demonstrated in the work of Israelachvili et al. about lysine-rich peptides with SFA.[7] The $\pi$-cation interactions have been found to be also important in melanin-like materials containing free amines, such as polydopamine (PDA). In fact, the nature of the cations has been reported to be determinant allowing assembling and disassembling by changing between $K^+$ and $Na^+$.[36]

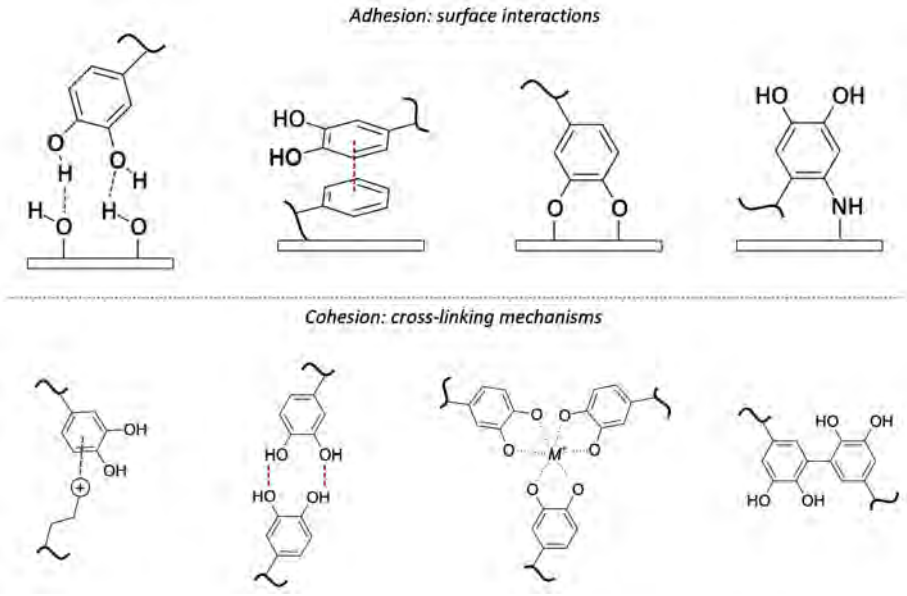


**Figure 1.6.** On the top, possible covalent and non-covalent interactions of catechols with surfaces depending the exposed functional groups. On the bottom, possible cross-linking mechanisms of catechol containing polymers through catechol oxidation and metal coordination.

Another way to get reversible cross-linking is by using coordination of catechols with metal ions, as occurs in mfps.[37] Metal-catecholate complexes with Fe(III), Cu(II), Co(II), Zn(II), Ni(II) and Ti(IV) have been studied in solution by Wilker et al. showing the mono-, bis- and tris- complexes depending the pH and type of ion.[38] The formation of this complexes and their pH dependency has

been extensively used for the design of pH responsive hydrogels with self-healing properties.[34,39–43] In the case of catechol-iron complexes, it is well stablished the formation of monocatecholate complex below pH 4, biscatecholate complex between pH 5-7 and triscatecholate complex above pH 9.[34] However, parameters such as the type of salt, temperature and concentration of catechol and ferric ions have also an impact in the final structure of the complexes formed.[44]

Irreversible covalent cross-linking can be achieved by the coupling of two highly reactive semiquinones $QH^{\bullet}$. This reaction is reached through $QH_2$/Q comproportionation mentioned previously and can be triggered by oxidizing catechol containing polymers with $NaIO_4$ or enzimes, such horse radish peroxidase or tyrosinase, and $H_2O_2$.[9]

## 1.3 Bioinspired catechol-based polymers

The unprecedented properties of natural catechol containing systems has open up new avenues for the development of novel bioinspired materials. The use of polymeric structures containing catechol functionalities has thrived due cooperative and synergic effects. Certainly, the inclusion of catechol moiety within myriad of different polymeric structures has allowed to take advantage of the adhesive, chelating and redox activity of catechols, broadening their range of application and use on a great variety of substrates.[45–50] Many other distinctions could be employed for the classification of catechol containing polymers, though, for the purpose of the present work, the main approaches for the incorporation of catechol functionality are divided in three groups by differentiating the role in the polymerization and position of catechol moiety in the polymeric backbone. More precisely, catechol-based polymers will be divided in those polymerized via catechol oxidation, the ones obtained after post-functionalization of preformed polymers and the catechol-based polymers obtained from modular polymerization of catechol derivatives (see Figure 1.7).

### 1.3.1 Polymerization via catechol oxidation

Oxidative polymerization of catechol derivatives is, probably, the most popular approach for the synthesis of bioinspired catechol containing polymers. Pioneering in this concept, Messersmith et al. found in 2007 a strategy for obtaining catecholamine polymeric coatings from dopamine with adhesion on multiple substrates. The material known as polydopamine (PDA) was obtained through simple dip coating in diluted aqueous solution of dopamine buffered with Tris at pH 8.5.[51] The robust biocompatible coatings reported stablished a precedent in the development of this polymerization approach.

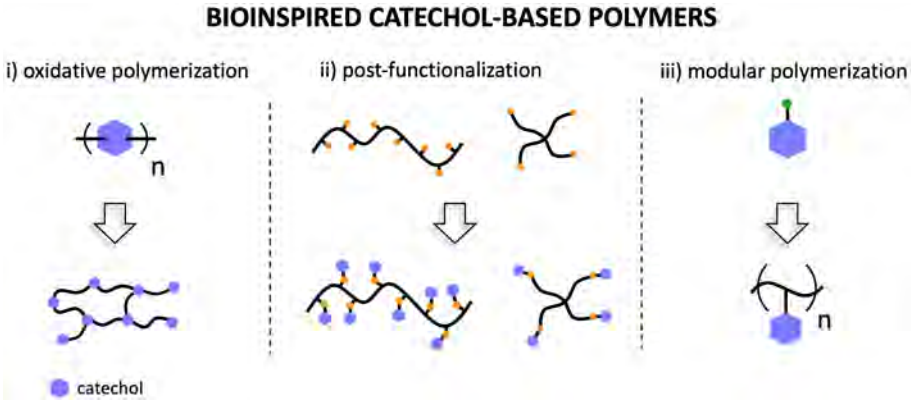


**Figure 1.7.** Schematic classification of the principal approaches reported for the synthesis of catechol containing polymers

Thanks to the straightforward synthesis and the adhesion to virtually all surfaces, the use of PDA increased rapidly as a potential candidate for universal surface modification. Following similar strategies, other catecholamines like norepinephrine[52–54] and L-3,4-dihydroxyphenylalanine (L-DOPA)[55,56] were polymerized as well. While presenting similarities with dopamine, these polymers provided new functionalities to the final coatings formed by presenting free carboxylic groups exposed. Several studies have tried to determine the self-polymerization mechanism of catecholamines, but the poor solubility of these polymers has limited their structural examination. Although still unclear, the most accepted models for PDA structure consist on different oligomeric building blocks containing uncyclized catecholamine/quinones and cyclized 5,6-dihydroxyindole units with covalent and/or supramolecular organization through H-bonding and $\pi$-stacking (Figure 1.8).[15] Detailed analysis of PDA and eumelanin structure elucidation have been presented by D' Ischia et al. and Liebscher et al. in their respective reviews.[2,15,57] Another issue surrounding the study of the chemical structure of PDA and melanin-like materials lays on the diversity of polymerization conditions reported. Aiming for controlling thickness, robustness, surface charge and functionality, a great variety of oxidants, buffers and additives have been suggested.[58] This aspect enlarges chemical complexity of the systems, giving versatility but limiting a proper control in the chemical structure of the polymers.

First polymeric systems obtained through catechol oxidation were focused on catecholamines due to the fragile polymers obtained from catecholic compounds lacking amine groups. Although some natural phenolic and polyphenolic compounds containing catechol moieties can be oxidized to obtain nanocoatings,[59] the presence of amines within polymeric backbone has been found to be rele-

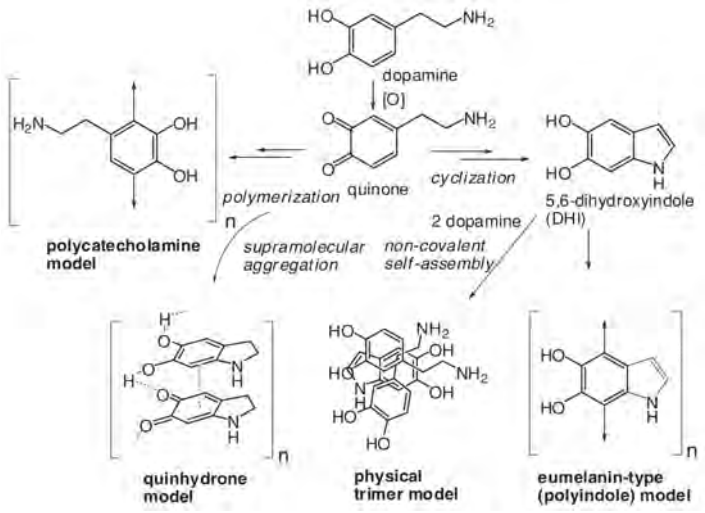


**Figure 1.8.** Some of the models of the unraveled structured of polydopamine. Reproduced from literature.[15]

vant in the final robustness of the coating.[54] Presence of amines provides further cross-linking via Schiff base and Michael addition reaction and allows $\pi$-stacking interaction through protonated pendant groups. In this way, the combination of catechols lacking amine groups with diamines or polyamines has favored the synthesis of more robust coatings.[60–64] This approach boosted the flexibility of the systems by removing the limitation of catecholamines precursors and reducing the cost of production.

A huge collection of polymers obtained via catechol oxidation and their combination with amines have been broadly studied and exploited in applications such as biosensing, membrane filtration, drug delivery or optoelectronics, among others, thanks to their great versatility.[58,65,66] Nonetheless, the mayor limitation of these systems remain in the processability due to their poor solubility and the lack of control in the final polymeric structures. This strategy has been broadly studied by our research group during last decade, achieving interesting properties of a great variety of polydopamine-like materials without clear control of their chemical structure.[31,63,67,68]

Despite the versatility of these polymeric materials, their application has been mostly limited for coating and surface modification purposes. For these reason, other alternatives have been developed to exploit further the potential of catechol containing systems, specially for adhesive purposes.

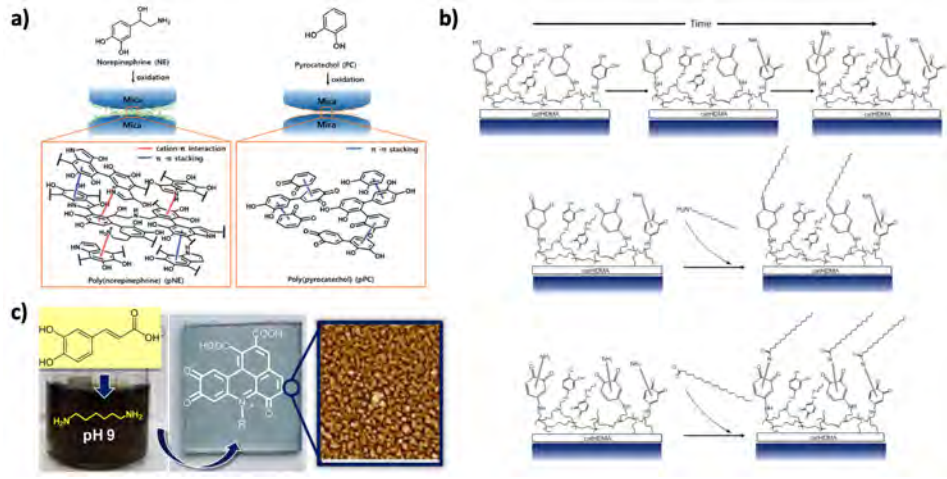


**Figure 1.9.** Reported examples of coatings obtained via catechol oxidation. a) Mechanistics studies with SFA of poly(catecholamine) coatings;[54] b) tentative chemical structure of coatings after reaction of catechol with diamines and their posterior functionalization;[63] and c) synthesis of multifunctional films from caffeic acid cross-linked with diamines.[62]

### 1.3.2 Post-functionalized polymers catechol containing polymers

In order to overcome some limitations found in polymeric materials from the previous section, several biopolymers such as chitosan,[69–71] hyaluronic acid,[72,73] cellulose,[74–76] gelatin,[77] dextran,[78] xanthan gum,[79] elastin,[80] chondroitin[81] or silk[82] have been modify introducing catechol functionality. The presence of reactive functional groups such as $-NH_2$, $-COOH$, $-CHO$ and OH, among others, allows the functionalization of these biopolymers. For example, amidation through EDC/NHS coupling is widely used to add catechol moiety in the biopolymers using dopamine or caffeic acid.[69–81] The use of biopolymers modified with catechol has been mainly focused in the design of tissue adhesives, where biocompatibility is a priority. In the same direction, polymers approved by FDA such as PLA, PGA or PVA have been functionalized with catechol derivatives for improving adhesive properties of the polymers.[64,83,84]

Other polymeric structures such as star-shape poly(ethylene glycol)s (PEGs) have been also employed for synthesizing catechol containing gels with potential medical application thanks to PEG biocompatibility (see Figure 1.11). One of the first examples of this approach was introduced in 2002 by Messersmith et al. describing the synthesis of linear and branched PEGs functionalized with catechols and their gelation via oxidative cross-linking.[85] This idea has been

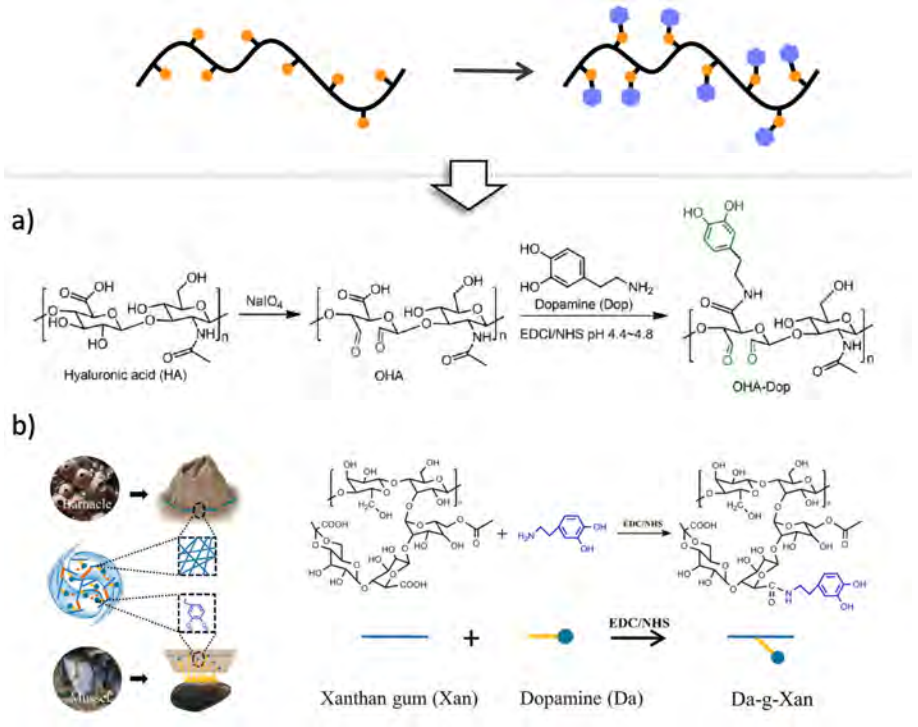


**Figure 1.10.** Reported examples of catechol containing polymers obtained via post-functionalization of biopolymers. In a) synthesis of reported catechol containing polymer obtained from hyaluronic acid and dopamine;[73] in b) the synthetic approach of reported catechol containing polymer obtained from xanthan gum and dopamine.[79]

improved during last decades modifying PEGs and cross-linkers with a clear focus on biomedical application.[39,86,87] In a most recent study, these star-shape PEGs functionalized with catechols have been used for the development of dynamic inks with potential use in 3D bioprinting, a field with clear growth of interest.[42]

The most determining point of post-functionalization is the amount of catechol incorporated in the polymeric chain. Mismatches on the amount on catechol incorporation could cause considerable differences on the final adhesive performance.[88] Another disadvantage of this approach is the lack of control on the functionalization, commonly presented as random.

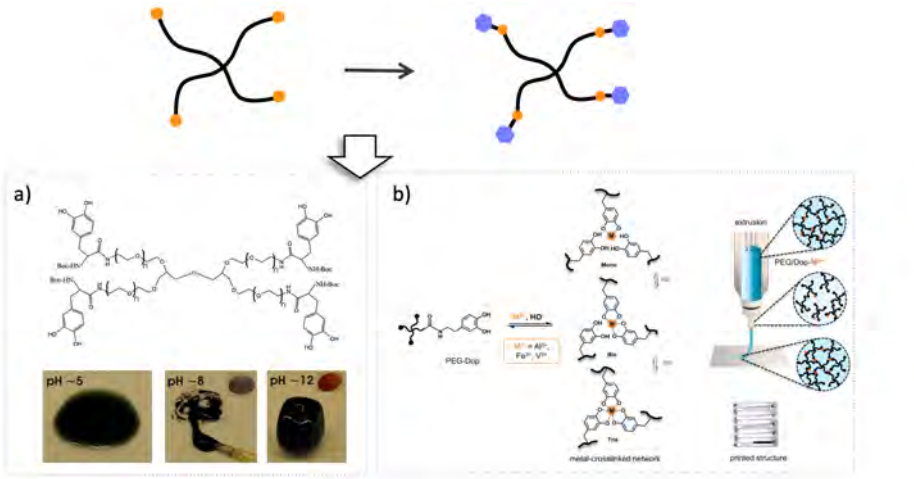


**Figure 1.11.** Reported examples of catechol containing polymers obtained via post-functionalization of star-shape PEGs. In a) synthesis of reported catechol functionalized 4-arm PEG and the gelation with iron(III) at different pHs;[39] in b) the synthetic approach for the development of dynamic inks based on catechol modified PEGs.[42]

### 1.3.3 Modular polymerization of catechol derivatives

The last approach for the synthesis of catechol containing polymers is the modular polymerization of catechol derivatives bearing polymerizable groups. Controlled peptidic synthesis containing DOPA, which is one of the most common strategy, has been of high importance for the understanding of mussel-inspired systems.[7,8,27,89–91] For example, the study of short peptidic sequences combining DOPA, tyrosine and lysine residues and modifying their position within the chain, allowed to determine the synergistic effect of lysine residues close to catechol groups to enhance underwater adhesion in mfps.[7] However, despite the high importance of catechol containing peptides for the study of natural systems, this approach is limited in terms of scalability, requiring alternative systems for synthesizing catechol containing polymers to reach applicability.

Beyond peptidic sequences, other catechol derivates can be found in the literature as monomers and comonomers. Generally, these derivatives can be separated in two clear groups: i) the non-protected and ii) the protected derivatives (see Figure 1.12).

One of the most used non-protected catechol monomers is dopamine methacrylate (DMA). In recent reported studies, the copolymerization of DMA with ethylene glycol monomers to obtain coatings on polytetrafluoroethylene (PTFE), a material well-known for its antiadherent properties.[92] Also, the copolymeriza-

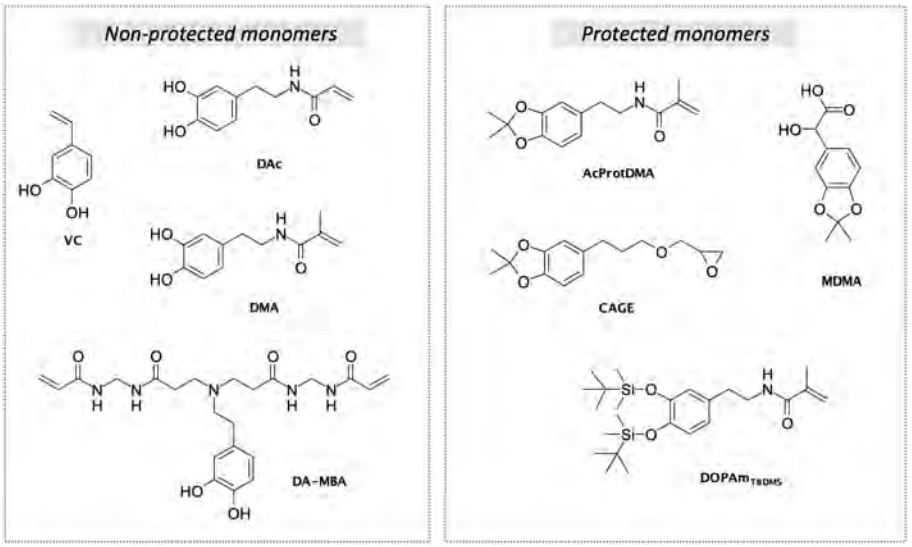


**Figure 1.12.** Examples of protected and non-protected catechol derivatives used as monomers and comonomers to obtain catechol containing polymers following modular polymerization.

tion of DMA with phosphate functionalized monomers has been used to study the synergy between catechols and positive charges already seen on peptides,[7] observing an increase of the adhesion from 1.0 to 2.5 MPa on steel for the catechol containing polymers bearing phosphate groups.[93] Some examples with other non-protected catechol monomers such as vinyl catechol (VC) or more complex difunctional acrylates like DA-MBA (see Figure 1.12) can be also found in literature for the design of functional coatings and tissue adhesives.[94,95]

However, the polymerization of non-protected derivatives via radical polymerization is limited by the radical scavenging ability of catechols, which can lead to undesired cross-linking and branching of the polymer. In fact, homopolymerization of DMA cannot be controlled and its use has been limited as a comonomer.[11,96] In other reported examples, the radical polymerization of catechol-bearing vinyl monomers has ended in the formation of hyperbranched or cross-linked polymers with the use of a derivative from DMA.[97]

This problematic has driven this approach to the use of protected monomers, specially in those cases of vinyl, acrylate and methacrylate derivatives polymerized via radical polymerization. The copolymerization of styrene and 3,4-dimethoxystyrene and its use as underwater adhesive has been studied in deep by Wilker et al. after deprotection with $BBr_3$ and an acidic workup to get the final catechol functionality.[88,98] The adhesion of these polymers showed dependence

with the molecular weight, going from 2 to 5.5 MPa when the molecular weight increased from 20 to 40 kDa.[88] Moreover, the addition of $NaIO_4$ to promote further cross-linking improved the adhesion up to 7 MPa.[98] In another example of the same author, 3,4-(methylenedioxy)mandelic acid (MDMA) was copolymerized with PLA to achieve a bio-based and degradable adhesive containing catechol after removal of protecting group using $Sn(oct)_2$ and *p*-toluenesulfonic acid as catalysts.[50]

This last strategy allows the proper control over the polymerization and the final chemical structure, but requires a posterior deprotection step to obtain the final catechol functionality. The design of new monomers and polymerization strategies with high control over the final chemical structure without the need of protection/deprotection steps is one of the current challenges in the development of catechol containing polymers. Further development and the arrival of new strategies for modular polymerization would give the opportunity to ease and scale up the synthesis of controlled polymeric structures incorporating catechol functionality.

## 1.4 Poly(disulfide)s

Poly(sulfide)s and poly(disulfide)s are a special family of polymeric structures with one shared feature, the presence of -S-S- bond. The dynamic nature of this group, provides to these materials particularly interesting properties such as self-healing, stress resistance and adaptability.[99] In natural systems, this dynamic behavior of disulfides have an essential role in the folding of proteins through cysteine residues. Another relevant example is the vulcanization process of rubber, where the addition of sulfur leads to the formation of oligosulfides improving its mechanical properties.

The reversibility of disulfide bonds and its thiol-disulfide exchange, has focused the interest of these materials on the development of biodegradable and stimuli responsive structures, cleaving the disulfide bond on demand under certain conditions like a reducing environment.[100]

Concerning the synthesis of poly(disulfide)s, two main pathways are found: i) the oxidative polymerization of dithiols, and ii) the chain extension through disulfide cleavage (see Figure 1.14).

### 1.4.1 Oxidative polymerization of dithiols

There is a large variety of reactions affording the oxidation of thiols to disulfides, though few of them have been employed for the synthesis of poly(disulfide)s from dithiol monomers, since harsh oxidation conditions could produce over oxidation of thiols to sulfonic acid (e.g. thiol oxidation to sulfonic with concentrated

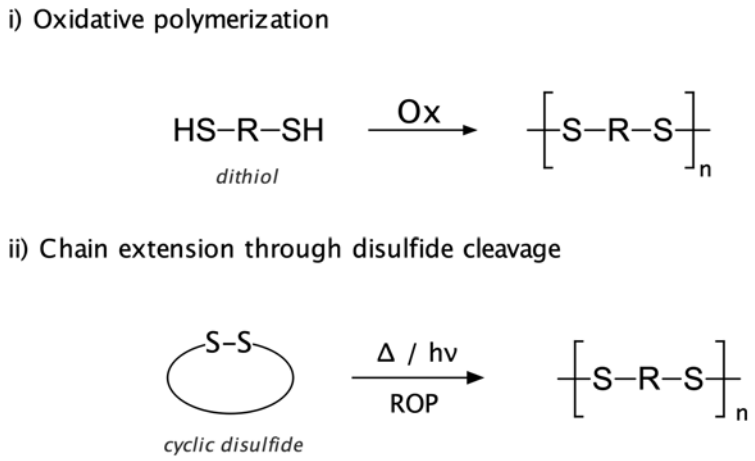


**Figure 1.13.** General scheme of main approaches for the synthesis of poly(disulfide)s.

$HNO_3$). Among the most studied ones for the oxidation of thiols to disulfides, the oxidation via $O_2$, DMSO, $H_2O_2$ and $I_2$ deserve a special mention.

The oxidation of dithiols with $O_2$, or air, is probably the most pioneering and well-known strategy for synthesizing poly(disulfide)s. To achieve poly(disulfide)s of high molecular weight, this approach requires the addition of catalysts. First studies by Marvel and Olson described the use lauric acid plus potassium hydroxide and compressed air to promote the polymerization of dithiols after prolonged times.[101] More recently, similar strategy was used by Choi et al.[102] to polymerize dithiols obtained from mono- and bifunctional five-membered cyclic dithiocarbonates, achieving $M_n$ values of 20 kDa and Đ of 1.45 in presence of TEA after 100 h. By using CuCl and *N,N,N',N'*-tetramethylethylenediamine (TMEDA), different works reported the synthesis of cyclic(arylene disulde) oligomers within few hours.[103,104]

Poly(disulfide)s can be also obtained in the oxidation of thiols mediated by sulfoxides, concretely with DMSO. This polymerization reaction described by Goethals et al. allowed the polymerization of $\alpha,\omega$-alkyldithiols after 8 hours at 160 °C achieving polymers below 10.5 kDa.[105] However, scarce examples in the literature can be found where this procedure is used for the polymerization of dithiols.[105–107]

The use of harsh oxidizing agents such as hydrogen peroxide can be used as well for the polymerization of dithiol, but problems with over oxidation of thiols and formation of sulfonic acid species have been found. Optimized conditions reached by Rosenthal et al.[100,108,109] allowed the formation of high molecular poly(disulfide)s above 200 kDa from 3,6-dioxa-1,8-octanedithiol (DODT) avoid-

ing over oxidation. Combining $H_2O_2$ and TEA, polymers from 14 to 230 kDa with narrow Đ below 1.2 in less than 3 hours were reported.[108]

Considered as a mild oxidant for the oxidation of thiols, $I_2$ has been used long time ago for the titration of thiol containing samples.[110] In the '60s, a series of works reported by Danehy et al. provided deeper understanding of the reaction, elucidating diverse equilibria and key factors involved in the reaction.[111–113] Despite this knowledge, few reported examples using $I_2$ for polymerizing dithiols can be found. In the aforementioned work of Choi et al.,[102] dithiols obtained from mono- and bifunctional five-membered cyclic dithiocarbonates were oxidized by 0.6 equivalents of $I_2$ and excess of TEA, achieving polymeric species below 15 kDa which depolymerized in prolonged reaction times. In other works, the oxidation by $I_2$ has been used for the synthesis of cyclic oligomeric disulfides, commonly by using high diluted conditions (see Figure 1.14).[114–117]

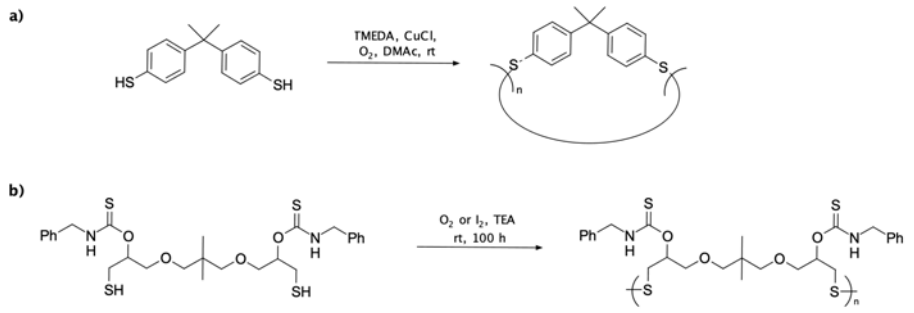


**Figure 1.14.** Reported synthesis of poly(disulfide)s via oxidative polymerization of a) cyclic(arylene disulde) oligomers and b) dithiols from bifunctional five-membered cyclic dithiocarbonates. Reproduced from the works of Hay et al.[103] and Choi et al.[102]

### 1.4.2 Chain extension through disulfide cleavage

The synthesis of poly(disulfide)s through chain extension via disulfide cleavage is a broadly used approach. Disulfide bond can suffer an homolytic cleavage, generating two free thiyl radicals which can induce the expansion of the chain through the attack of another disulfide bond, like in the case of ring-opening polymerization (ROP).

The ROP of six-membered ring disulfides 1,2-dithiane and 1,4-dihydro-2,3-benzodithiine have been reported and studied extensively by Endo et al., showing yields over 80 % after 8 hours in the polymerization in bulk above the melting temperature of these cyclic compounds.[107,117,118] Thermal analysis of the resulting polymeric materials has led the authors to hypothesized about potential physical entanglement through ring closing in the form of polycatenane structure.

Another cyclic disulfide polymerized through ROP is the five-membered ring disulfide $\alpha$-lipoic acid (LA).[107,119–122] Only by heating the system above LA melting temperature (60-62 °C), poly-LA up to 13.7 kDa and Đ of 1.5 can be obtained. Since the nature of the final poly-LA could lead to depolymerization, the combination of LA with acrylic acid (AA)[119] or 1,3-diisopropenylbenzene (DIB)[121] can enhance the stability of the systems through thiol-ene reaction of free thiyl radicals formed to get high stretchable and self-healing materials. Thanks to the dynamic behavior of disulfide bond, these materials present high reprocessability and fully reciclability upon heating. First studies about the polymerization of LA described the formation of polycatenane structure in the ROP of LA.[122] However, more recent studies using AFM to elucidate the architecture of the system suggested the formation of branched structures instead of an interlocked one.[120]

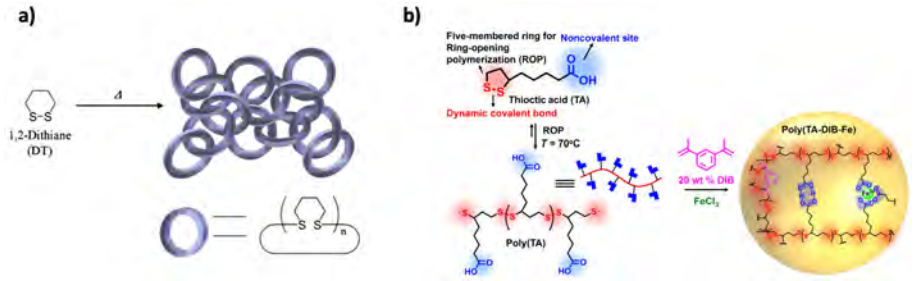


**Figure 1.15.** a) ROP of 1,2-dithiane and the interlocked structure suggested and b) ROP of LA in combination of DIB and $FeCl_3$ to achieve cross-linked system with high adaptability and self-healing properties. Reproduced from the works of Endo et al.[118] and Zhang et al.[121]

Cyclic aromatic disulfide oligomers have been also used as initiators for the ROP of poly(disulfide)s.[103,104,123,124] These aromatic disulfides present higher melting temperature that can be tune combining cocyclic(arylene disulfide)s. These cyclic oligomers undergo ROP at high temperatures, presenting good adhesive properties with shear strength up to 4.6 MPa achieved by their heat-induced ROP at 200 °C during 5 min.[104]

Other strategies for synthesize poly(disulfide)s through disulfide cleavage is the use 2,2′-dithiodipyridine in combination with dithiols. The high reactivity of pyridine disulfide toward thiols allows the chain extension to obtain poly(disulfide)s with $M_n$ values up to 12 kDa.[125]

## 1.5 Scope of the thesis

Within this context, the recent development of a novel straightforward synthetic approach through the reaction between *o*-quinones and thiols opened up a new

venue for the synthesis of different catechol derivatives with further polymerization possibilities.[25] In a work carried out by Dr. Juan Mancebo-Aracil, a wide variety of catechol containing compounds were presented, being the dithiolated catechol monomer **1** an interesting derivative for the design of catechol based polymers (see Figure 1.16).[126]

Following this synthetic strategy, a full process from synthesis to application has been followed in the present thesis, with an in depth evaluation of the synthesis and polymerization reactions, as well as the final potential use as adhesives of the new family of catechol poly(disulfide)s materials presented. The main challenge of the present work has been to achieve proper control over the synthesis of catechol poly(disulfide)s and determine the potential use as adhesives, specially for biomedical applications. Focusing on the final use of the materials, the main results of the thesis are divided in two extensive chapters, Chapter 3 and Chapter 4.

In Chapter 3, the development of catechol poly(disulfide)s **p1** is centered on the use of the polymer as reversible medical grade adhesives. First, the synthesis of dithiolated catechol containing monomer **1** is faced using the tristhiol compound trimethylolpropane tris(3-mercaptopropionate) **2** and pyrocatechol **3** (through the *o*-quinone **4**). Then, its posterior polymerization is studied and optimized in order to achieve catechol poly(disulfide)s **p1** in a controlled manner, looking for a modular approach to obtain high and low molecular weight polymers. The polymerization is evaluated in parallel with the polymerization of 1,6-hexanedithiol **5** as a model reaction. Besides, two 'blank' monomers containing pendant benzyl **7** or 3,4-dimethoxy benzyl **8** groups are synthesized for comparative means. Then, the adhesion and reversible adhesion performance on different substrates is studied, and biocompatibility (*in vitro* and *in vivo*) of catechol poly(disulfide)s is assessed aiming for its potential use as medical grade adhesives.

In Chapter 4, the synthesis of catechol poly(disulfide)s **p1** and copolymerization with 3,6-dioxa-1,8-octanedithiol **6** is focused for their use as tissue adhesives and sealants which is one of the most interesting fields of application of catechol containing polymers with a clear added value. The performance on porcine skin and porcine intestine is evaluated, as well as their biocompatibility (*in vitro* and *in vivo*), following standardized protocols. Moreover, the stability and potential degradability of these novel materials is assessed on different media with and without enzymes to simulate physiological conditions.

Figure 1.16 summarizes the strategic pathway followed along the project to face the challenges previously mentioned with these materials.

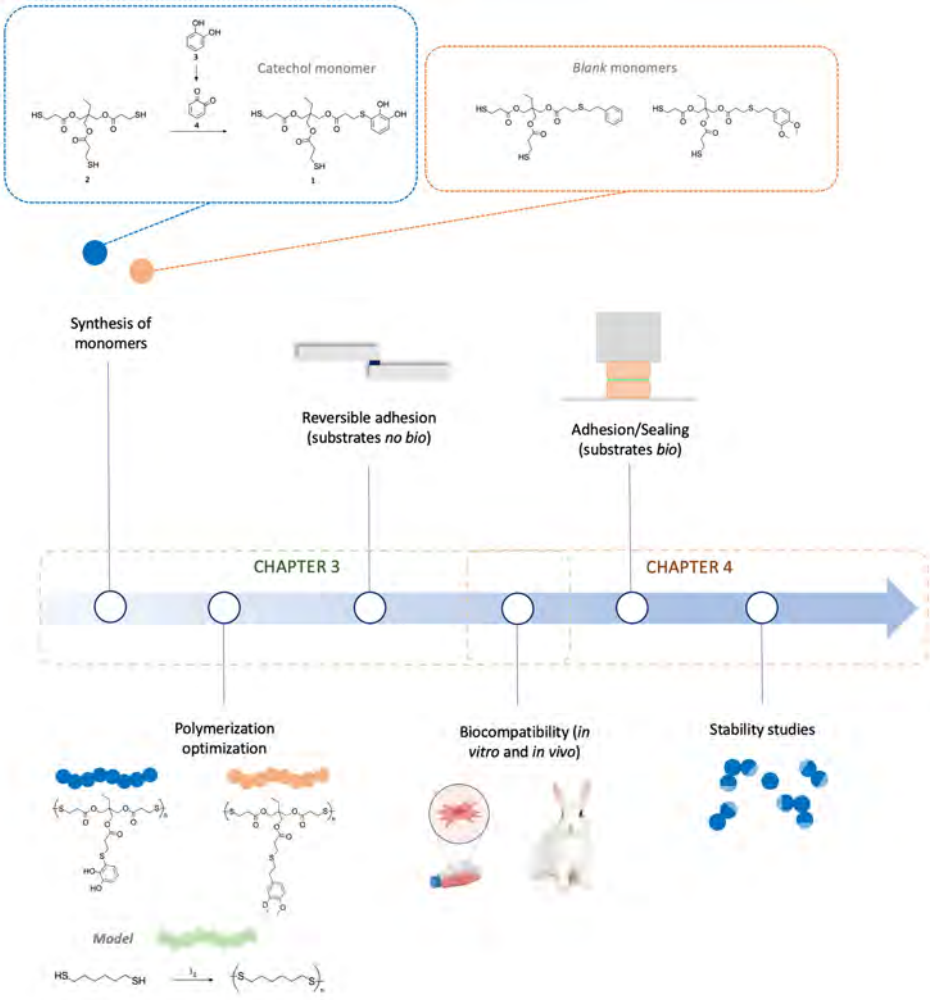


**Figure 1.16.** Schematic representation of the main steps followed throughout the whole thesis.

# CHAPTER 2

# Objectives

In accordance to all precedents in catechol containing polymers presented in the introduction and considering the scope of this thesis, the general objectives set for the present PhD project are the following ones:

1. To optimize the synthesis of catechol poly(disulfide)s **p1** from the catechol containing monomer **1** through oxidative polymerization by iodine.

2. To study the adhesive role of catechol poly(disulfide)s on different substrates and its reversibility.

3. To evaluate potential biological application of catechol poly(disulfide)s as medical grade adhesives and tissue adhesives/sealants.

To achieve these main objectives, the following specific objectives were set:

- To synthesize, purify and characterize the dithiolated catechol derivative, monomer **1**.

- To study the oxidative polymerization of dithiols using the model 1,6-hexanedithiol **5**.

- To synthesize and polymerize dithiolated 'blank' monomers **7** and **8** as a references for studying adhesive properties of catechol poly(disulfide)s.

- To study adhesion through of 'blank' polymers obtained from to polymerization of **p7** and **p8**.

- To evaluate the cytotoxicity *in vitro* and *in vivo* and the adhesion on wet tissues of catechol poly(disulfide)s.

- To study copolymerization of monomer **1** with commercial dithiols such as 3,6-dioxa-1,8-octanedithiol **6** through oxidative polymerization.

- To study the stability of **p1** on different simulated physiological media.

# CHAPTER 3

# Synthesis of catechol poly(disulfide)s and their use as reprocessable medical grade adhesives

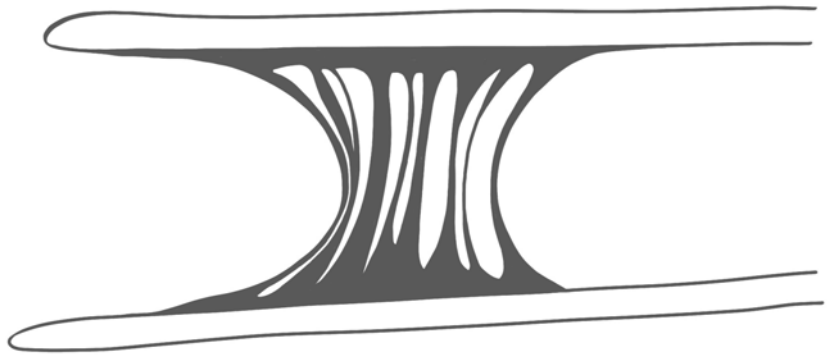

## 3.1 Medical grade and reprocessable adhesives based on catechols and disulfides

As defined by the European Medicines Agency (EMA), medical devices 'are products or equipment intended generally for a medical use',[127] which comprises a great variety of materials and products. From devices used outside the body such as a wheelchair or a thermometer, to devices such as a pacemaker or an orthopedic implant which have a direct interaction within the body, all of them must fulfill a strict regulation. Depending the country, the regulation and classification of medical devices can vary substantially in the final requirements of the regulatory agency due to differences in their classification (see Figure 3.1). Moreover, these regulations are in constant change and are becoming more limiting as occurred with the last update applied from 26 May 2021 by the EMA. The aim of these new regulations is to provide a safer environment looking for the protection of the patients, by demanding higher requirements of the materials in terms of biocompatibility.

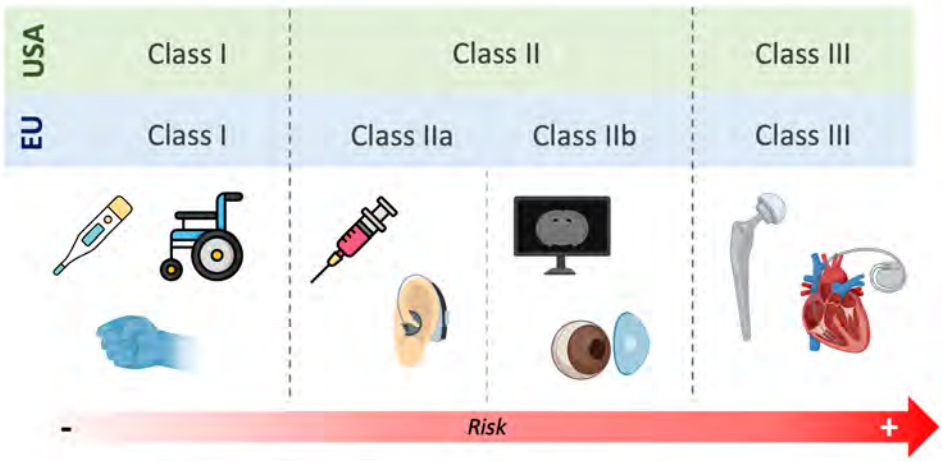


**Figure 3.1.** Schematic representation of the classification of medical devices devices in Europe, USA and Australia, showing the difference between subgroups defined by USA respect Europe and Australia agencies.

Within this context, the use of adhesives has gained importance recently. To achieve permanent joining and sealing in medical devices such as needles, blood bags or endoscopic guides, among others, medical grade adhesives are required. This medical grade adhesives must be certified with the ISO 10993 'Biological evaluation of medical devices' by passing *in vitro* and *in vivo* evaluations.

Some commercial brands such as Henkel have already in their portfolio some adhesives fulfilling these requirements.[128] Other adhesives based on UV-curing acrylic, epoxy, cyanoacrylate or silicone formulations have also emerged as alternatives.[129]

Although most medical devices cannot be reused and are hardly recycled by safety reasons, more concerns have raised recently about the reuse and recyclability of medical products as a consequence of the stunning amount of waste generated by the biomedical sector. Regarding medical devices, recovering high-valued components to be used in other instruments or devices could be a compelling alternative to reduce waste. Within this framework finding medical grade adhesives that allow reusability has become and interesting niche in the adhesive industry.

An interesting approach to reach reusability of adhered components is by controlling the attachment of the adhesives when required, what is called bonding/debonding on demand. This strategy requires the application of an external stimuli to control the adhesion of the material. Traditional hot melt adhesives could be considered as adhesives with bonding/debonding on demand behavior upon heating. By increasing the temperature above the melting point of the thermoplastic, hot melt adhesives loss their adhesion and can recover their adhesive behavior after a second thermal cycle. Another stimuli to achieve bonding/debonding on demand is light.[130] Light-induced bonding/debonding can be achieved by photoisomerization,[131] supramolecular chemistry (through H-bonding,[132] coordination chemistry[133] or host-guest interactions[134]) and dynamic covalent bonds (Figure 3.2a).[135]

Of special interest are the adhesives based on poly(disulfide)s chains (Figure 3.2b). Thanks to the dynamic behavior of disulfide bonds, dual responsive systems can be achieved with poly(disulfide)s, since they can respond both to light ($\lambda = 320 - 390$ nm) and temperature (above 150 °C).[135,136]

Despite the compelling properties of catechols and disulfides separately, scarcely any example has been reported. Recently, catechol based polymers containing disulfide bonds have been described for the synthesis of hydrogels with fast degradation in presence of dithiothreitol (DTT) (Figure 3.2c).[43] However, their use was focused on the design of degradable hydrogels and neither their adhesion nor biocompatibility have been studied.

Combining the high adhesion of catechol containing polymers and the dynamic nature of disulfide bonds, in the present work the polymerization of the catechol containing monomer **1** has been optimized to obtain a new family of catechol (polydisulfide)s adhesives. Adhesion and rebonding properties of these adhesives formulations have been studied on different substrates to assess the reprocessability and the role of the different functional groups of the system. Aiming for the development of a potential medical grade adhesive, *in vitro* and *in vivo* studies following ISO 10993 have been carried out as well.

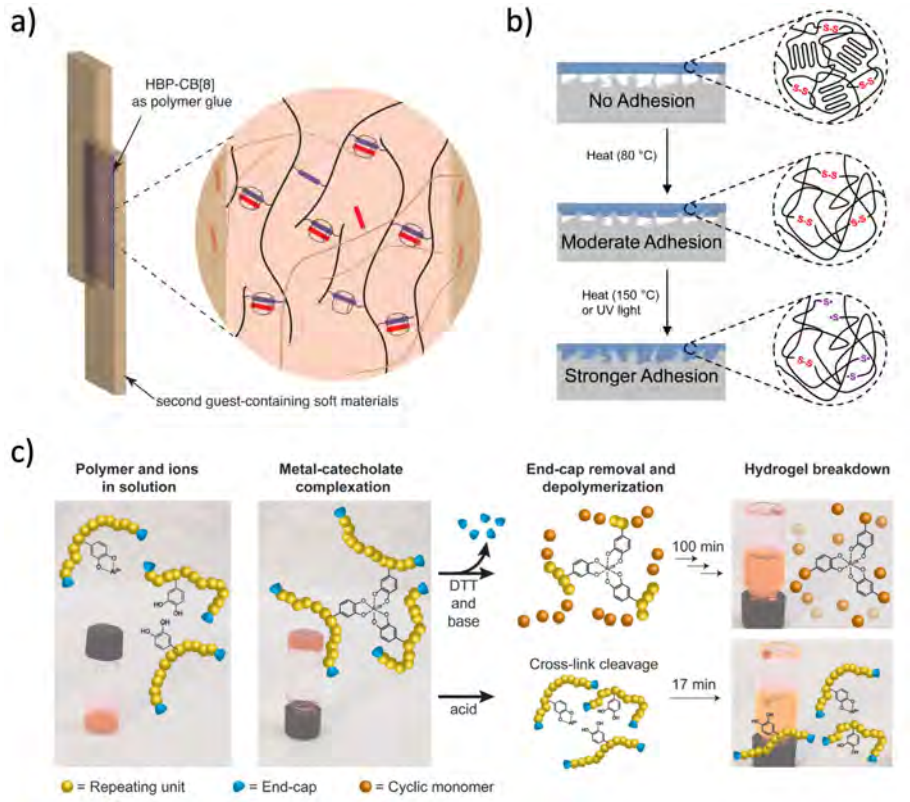


**Figure 3.2.** a) Reported example of adhesive using cucurbit[n]uryl host-guest interactions;[134] b) adhesive based on the dual response of poly(disulfide)s;[135] and c) catechol poly(disulfide) hydrogel formation through metal coordination with degradation behavior under reductive environments.[43]

## 3.2 Synthesis and characterization of dithiolated monomers

### 3.2.1 Synthesis of catechol dithiolated monomer 1

The synthetic approach for obtaining monomer **1** was based on the previous work developed by Dr. Juan Mancebo Aracil[25] (see Figure 3.3a).[a]

[a]Note that similar monomeric structures containing two free thiols and a pendant catechol could be obtained through other synthetic approaches. For example, commercial catechols such as dopamine methacrylate, dopamine acrylate or vinyl catechol could be reacted with tristhiol

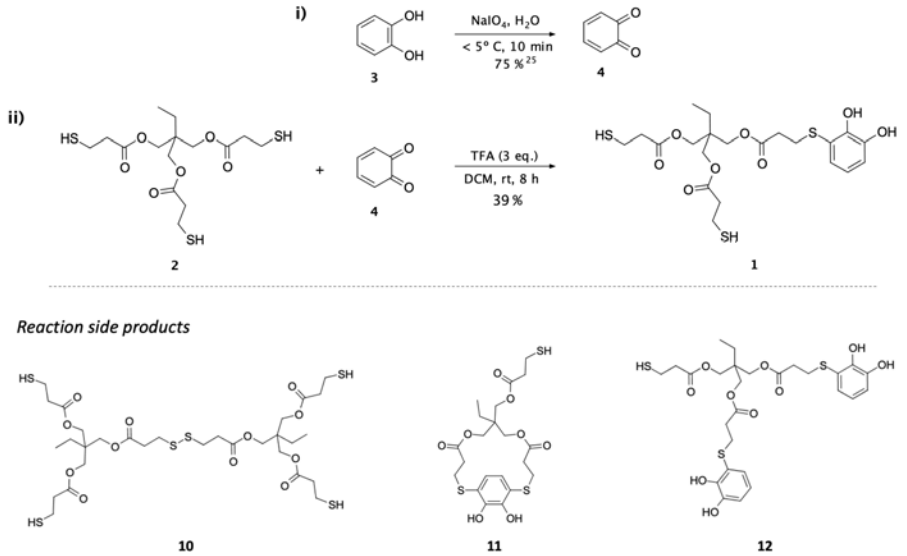


**Figure 3.3.** On the top, the reaction scheme of the synthesis of catechol monomer **1**. On the bottom, some of the side products formed in the reaction.

Before starting the synthesis of monomer **1**, the starting commercial trimethylolpropane tris(3-mercaptopropionate) **2** (tristhiol, from now on) was purified, as it presents a purity around 95 %. Around 5 % of the dithiolated alcohol compound **9** is present in the commercial tristhiol **2**, which could be originated in the production of commercial tristhiol **2** due to uncompleted esterification. The removal of this impurity was initially attempted by adsorption on active carbon, silica and Celite® in EtOAc and $CHCl_3$, all of them without showing selective adsorption of the impurity **9**. At the end, flash column chromatography was required for its complete removal (eluent conditions of hexanes:EtOAc 7:3). The presence of **9** can be followed clearly either by the presence of a blue spot in TLC after vanillin staining or the presence of a singlet at 3.44 ppm in $^1$H NMR (see Figure 3.4).[b]

For the synthesis of monomer **1**, pyrocatechol **3** was oxidized to *o*-quinone

**2** via thiol-ene chemistry to achieve resembling monomers, with the main difference of the conjugation position. In fact, an approach to develop similar catechol-containing compounds was presented by Hwang et al. using pentaerythritol tetra (3-mercaptopropionate) and a silyl-protected catechol through thiol-ene coupling.[137]

[b]Removing impurity **9** is important to avoid side products on the posterior reaction which has been observed to be coeluted during purification process of monomer **1** due to their similar polarities.

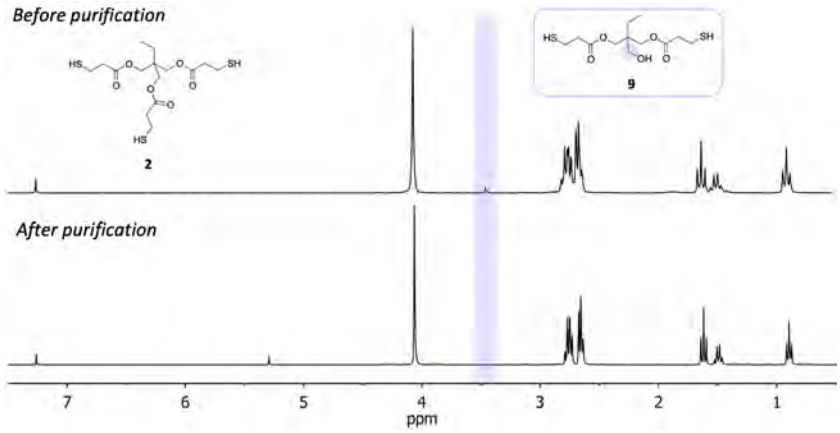


**Figure 3.4.** $^1$H NMR spectra of compound **2** before and after purification by flash column chromatography showing the disappearance of the singlet at 3.44 ppm from the removal of impurity **9**.

**4** with $NaIO_4$ in aqueous solution in an ice bath. The temperature and time of this oxidation process resulted critical, as high temperature and excess of time lead to the formation of insoluble side products from catechol self-polymerization. Specifically, the *o*-quinone **4** is formed rapidly within less than a minute and the extension of the reaction time over 10 minutes has resulted in the formation of side products that have a detrimental effect in the posterior reaction steps, as monitored by TLC. Overall, a time of 5 minutes was the most appropriate to get high conversion and avoid self-polymerization of the *o*-quinone.

Afterwards, *o*-quinone **4** was extracted with DCM and reacted with **2** in presence of 3 equivalents of TFA during 8 h. After complete removal of TFA, the crude of reaction was purified by flash column chromatography isolating **1** in the third fraction with a yield of 34-39 %, but not pure enough due to the presence of disulfide **10**. The reaction progress and products determination were properly followed by TLC during the whole synthesis and purification process, being $FeCl_3$ and vanillin stains the most useful, as well as UV due to the absorbance of catechols. While only catechol containing compound were stained by $FeCl_3$, vanillin allowed us to identify thiol containing impurities. The details of product and impurities determination by both stains are presented in Table 3.1.

Disulfide **10** can be formed as a side product from redox pairs involved in the synthesis, as seen in other similar cases.[25] Accordingly, compound **10** was removed upon reduction to **10** upon treatment with $PBu_3$. This step resulted crucial because the similar polarities of monomer **1** and disulfide **10** precluded the complete isolation of **1** in the previous chromatography column. Dragging a

small amount of disulfide **10** would result in a dramatic effect in the next polymerization step of monomer **1** and would have a huge impact in the reproducibility of the materials developed along this work. Monomer **1** was ultimately isolated by purifying the final crude of reaction through flash column chromatography, with 24-30 % overall yield after the two purification steps.

Just after the fraction of **1** in the first column, it was possible to recover the side products from double addition, the cyclic compound **11** and the double functionalized compound **12**. Although these compounds were isolated and fully characterized, they were not used for further studies. Cyclic compound **11** resulted in the least side product (<4 % overall yield) and was clearly identified by $^{1}$H NMR by the appearance of a singlet of proton H-14 at 6.95 ppm (2H) and the appearance of protons H-8 and H-8' as two doublets at 3.88 and 3.67 ppm with strong coupling corresponding to the diastereotopic protons from the conformational restriction of this structure (see assignments on Figure 6.3 in Annex). The formation of this cyclic impurity would be expected to be related with the concentration of the reaction, since more diluted systems would favor the intramolecular reaction. In this case, furthermore, a previous oxidation of catechol moiety from **1** should occur to proceed the second nucleophilic attack (see Figure 3.7). As this compound was not of high importance for the present work, no further studies were performed. The structure of side product **12** was determined in $^{1}$H NMR by the decrease of the signal ratio between signals of H-6, and H-7 at 2.80-2.60 ppm and the triplets from H-7' and H-6' at 2.95 and 2.54 ppm after catechol conjugation.

$^{1}$H NMR and $^{13}$C NMR of pure monomer **1** are presented in Figure 3.5. The triplet and quadruplet at 2.75 and 2.65 ppm corresponds to the protons H-7 and H-6 from the chains with a free thiol as seen in the starting material (Figure 6.1 in Annex), while the appearance of triplets at 2.95 and 2.54 ppm from H-7' and H-6' respectively confirms the addition of catechol. The ratio between the integrals of this signals are crucial to ensure purity of the compound and discard the presence of **10**. In Figure 3.6, it is presented this $^{1}$H NMR region before and after $PBu_3$ treatment and posterior purification, which confirms the presence of disulfide **10** after the first purification step due to the excess of integration corresponding to H-6 and H-7 corresponding to the chains without catechol functionality.

Overall, the variety of side products with similar polarities and almost identical signals by $^{1}$H NMR hinders the process of isolation of monomer **1**. The whole complexity of the reaction lays on the several side reactions that can be formed and the redox pairs catechol/quinone and thiol/disulfide as can be seen in the general scheme of Figure 3.7. Additional electrochemical studies out of the scope of this thesis would be required to determine the different roles of all the species involved in the reaction.

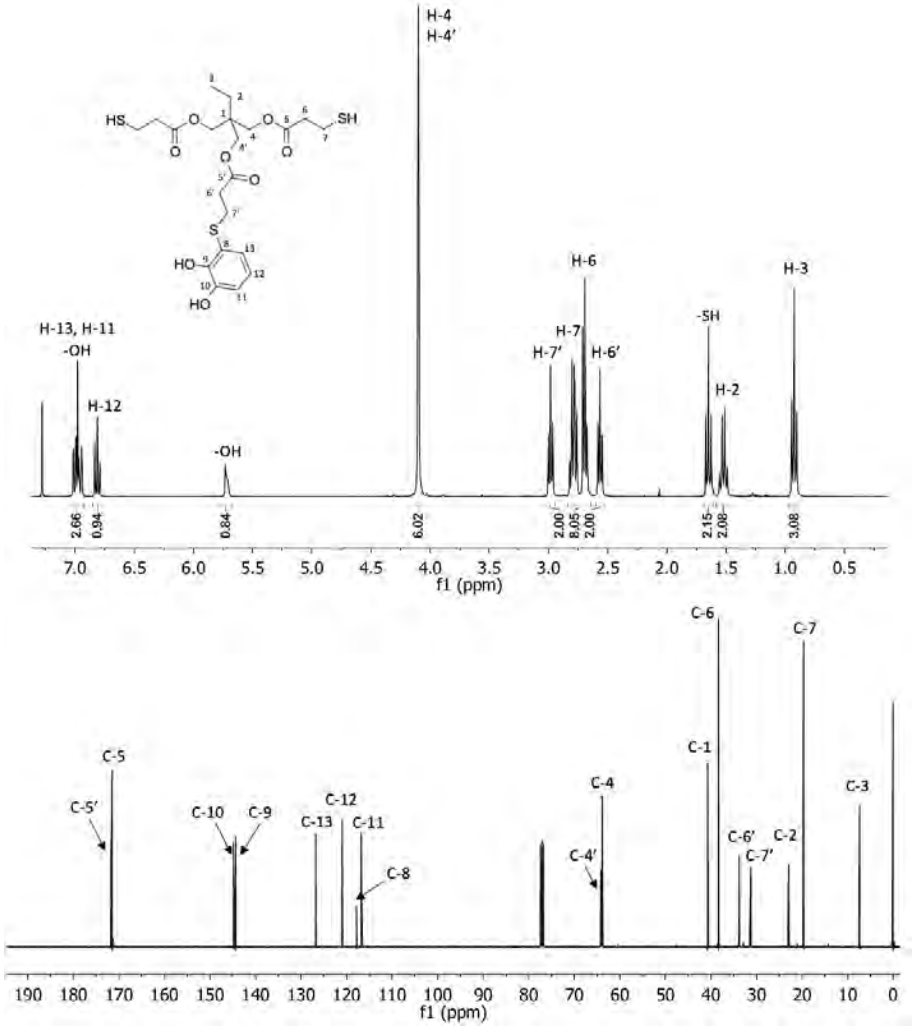


**Figure 3.5.** $^{1}$H NMR and $^{13}$C NMR spectra and assignments of monomer **1**.

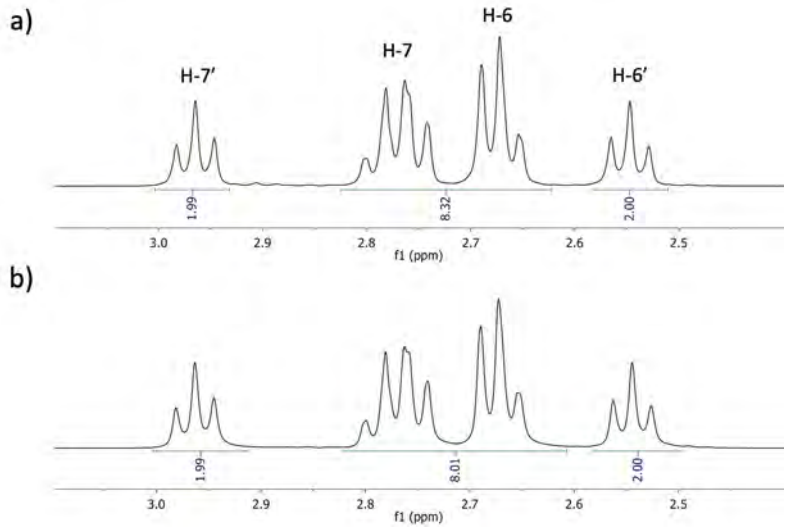


**Figure 3.6.** $^{1}$H NMR of the region 3.00 - 2.50 ppm of monomer **1** a) before $PBu_3$ treatment and b) after $PBu_3$ treatment demonstrating the presence of impurities due to the higher integral of the region of analysis.

**Table 3.1.** Compound determination by TLC stains. Elution conditions: Hex/EtOAc - 4.5/5.5. ND: not determined.

| **Compound** | **Rf** | **$FeCl_3$ stain** | **Vanilin stain** |
|---|---|---|---|
| monomer **1** | 0.28 | dark blue | orange |
| tristhiol **2** | 0.49 | turquoise | orange |
| pyrocatechol **3** | 0.38 | dark blue | pink |
| *o*-quinone **4** | 0.35 | black | pink |
| alcohol **9** | 0.26 | ND | blue |
| disulfide **10** | 0.24 | ND | orange |
| adduct **11** | 0.20 | black | orange |
| adduct **12** | 0.14 | black | orange |

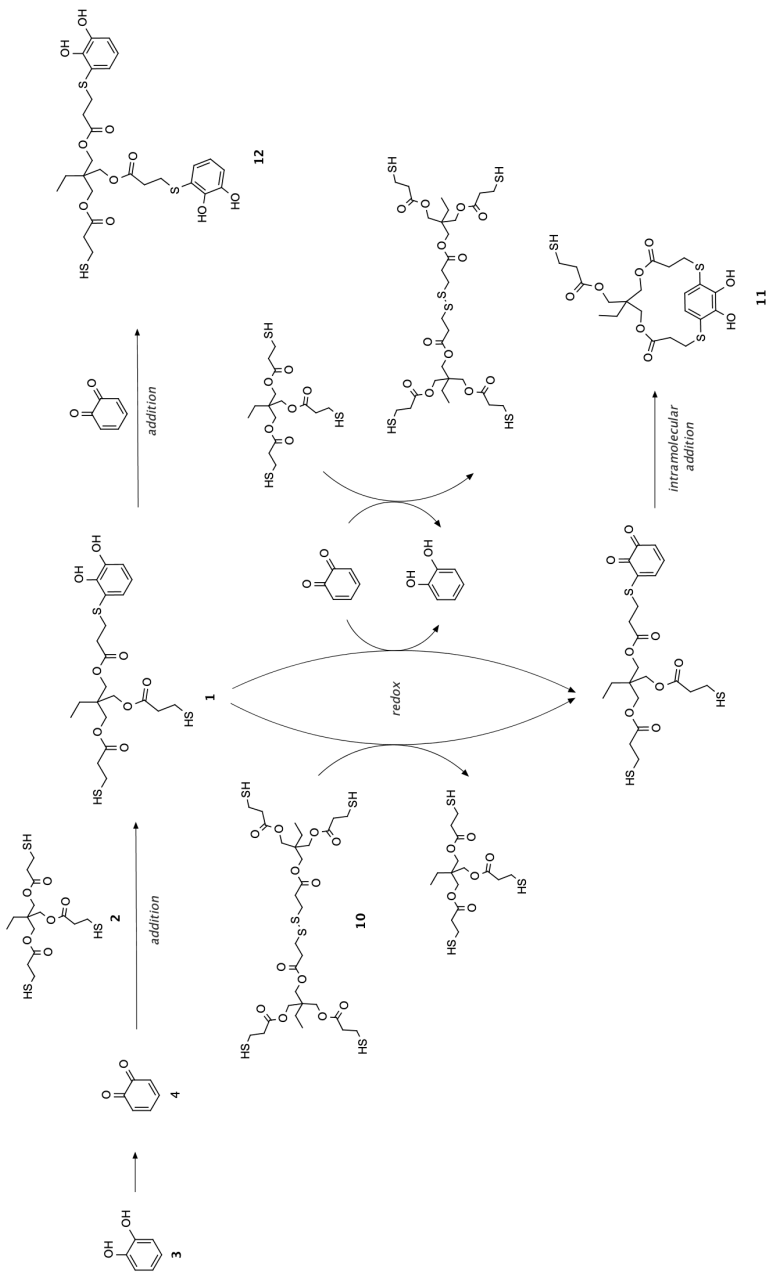


**Figure 3.7.** Scheme of suggested redox equilibria and potential side reactions in the synthesis of monomer **1**.

### 3.2.2 Synthesis of 'blank' monomers

To evaluate the role of catechols in the adhesion of this new family of poly(disulfide)s, dithiolated monomers with pendant aromatic ring or protected catechol were synthesized. The 'blank' monomers were obtained from styrene **13** and 3,4-dimethoxystyrene **14** through thiol-ene click chemistry,[c] which has been broadly used for the design of novel materials.[139]

#### 3.2.2.1 Synthesis of monomer 7

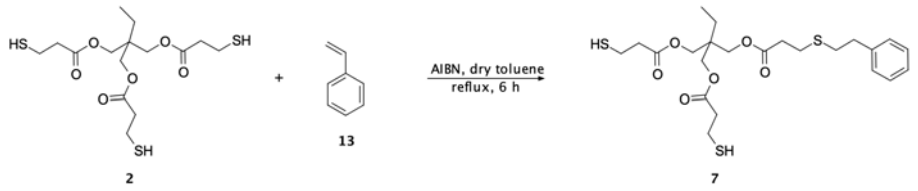


**Figure 3.8.** Synthesis scheme of styrenic monomer **7**.

Synthesis of compound **7** was attempted by a radical-catalyzed thiol-ene reaction, using purified tristhiol **2** and commercial styrene **13** in a molar ratio 1:1 (see Figure 3.8). The reaction was performed in toluene under reflux conditions and adding azobisisobutyronitrile (AIBN, 0.2 eq.) as free radical initiator. The reaction was monitored by $^1$H NMR, showing complete disappearance of olefinic protons and, hence, achieving full conversion after 6 h (see Figure 6.6a in Annex). $^1$H NMR signals of the crude of reaction did not match with a pure compound despite visualizing a unique spot in TLC with different elution mixtures (hexanes:EtOAc; 9:1, 7:3 and 6:4). A flash column chromatography was carried out, separating nine fractions with almost identical polarities. The analysis by MALDI-TOF of the first three fractions isolated allowed us to demonstrate the presence of some side products present in the crude of reaction (see Figure 3.9 a, b and c). First fraction had a single peak at 733.236 Da, corresponding to the $Na^+$ adduct of the product from triple addition of styrene. Analysis of the second fraction revealed the presence of $Na^+$ adducts of the non-reacted tristhiol **2** (421.069 Da), the compound **7** (525.115 Da), the product from double addition (629.163 Da) and the product from triple addition (733.236 Da). In third fraction, non-reacted tristhiol **2**, compound **7**, product from double addition were also found.[d] From all the fractions recovered, only the product from the triple

[c] Another alternative would be the protection of the catechols of compound **1** via the formation of cyclic acetals and ketals or cyclic esters,[138] though this approach was not attempted.

[d] The peak observed at 696.191 Da could correspond to the water adduct from a trimer of dithranol used as a matrix for the analysis.

addition could be isolated, but it did not have interest for the present work. So, compound **7** was discarded for further polymerization due to the impossibility of its proper isolation with the conditions studied.

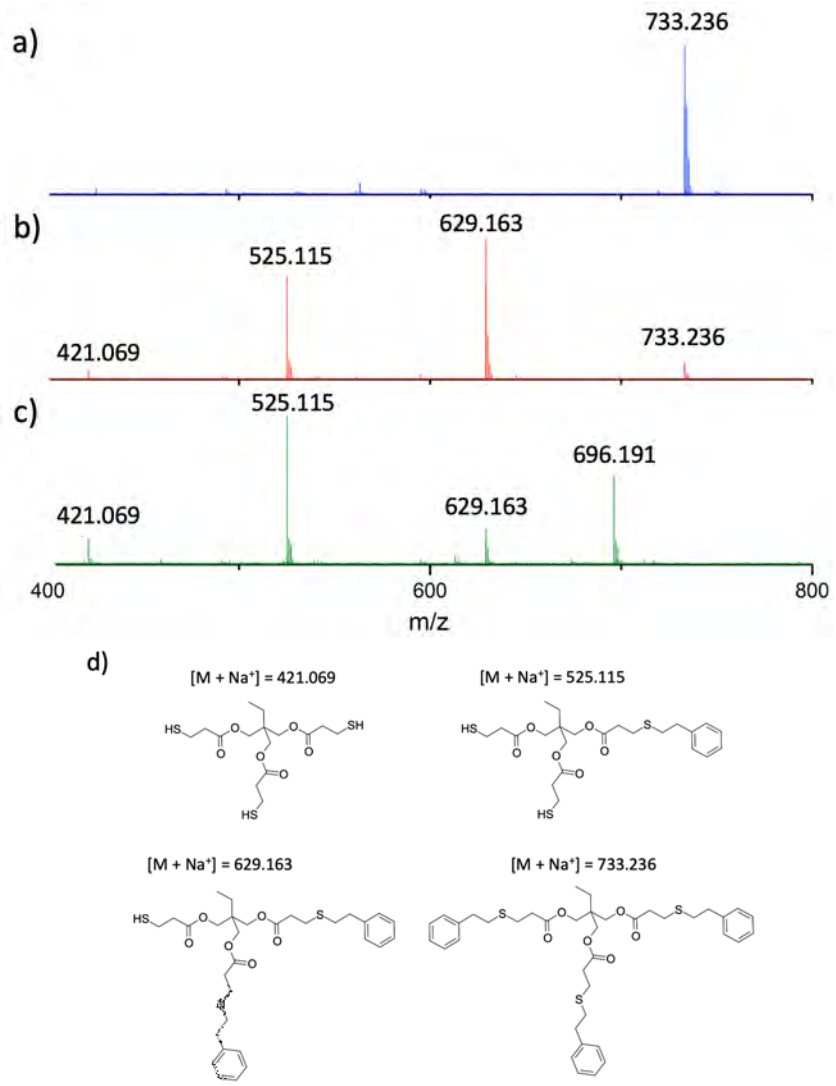


**Figure 3.9.** Characterization of products from the synthesis of **7**. In a) MALDI-TOF of first fraction, b) MALDI-TOF of second fraction, c) MALDI-TOF of third fraction recovered, and in d) chemical structure of the different peaks found by MALDI-TOF.

#### 3.2.2.2 Synthesis of monomer 8

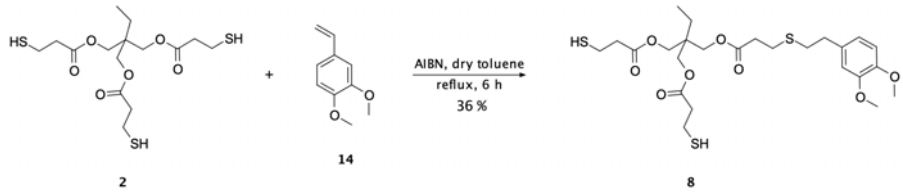


**Figure 3.10.** Synthesis scheme of monomer **8**

Looking for an alternative 'blank' monomer, the radical-catalyzed thiol-ene reaction was performed using purified tristhiol **2** and commercial 3,4-dimethoxystyrene **14** in a molar ratio 1:1 (Figure 3.10). Like in the previous case, the reaction was carried out in toluene under reflux conditions and adding AIBN (0.2 eq.), showing complete disappearance of olefinic protons in the $^{1}$H NMR after 6 hours. Oppositely to the synthesis of **7**, TLC analysis of the reaction crude showed clear different polarities of products formed. To achieve proper isolation of monomer **8**, the crude of reaction was treated with $PBu_3$, to avoid any presence of **10** which was confirmed by the appearance of tristhiol **2** after $PBu_3$ treatment. This disulfide from the starting thiol can be formed as a side product during the radical-catalyzed thiol-ene reaction from the termination mechanism by two thiyls.[139] After $PBu_3$ treatment and solvent removal, the crude was purified by flash column chromatography, achieving pure monomer **8** in 36 % yield. $^{1}$H NMR and $^{13}$C NMR of monomer **8** are presented in Figure 3.11. Aromatic protons H-11, H-12 and H-15 appeared as the sum of two doublets and a singlet, as expected, and the integral of this region matched completely with the ethyl signals of H-2 and H-3. Protons H-4 and H-4' have a close chemical shift with certain overlap between both singlets. The presence of H-16 and H-17 ensures that no deprotection occurred during the reaction. Besides, −SH signal integrated 1.8 which can be considered in agreement with the two pendant thiols of monomer **8**.

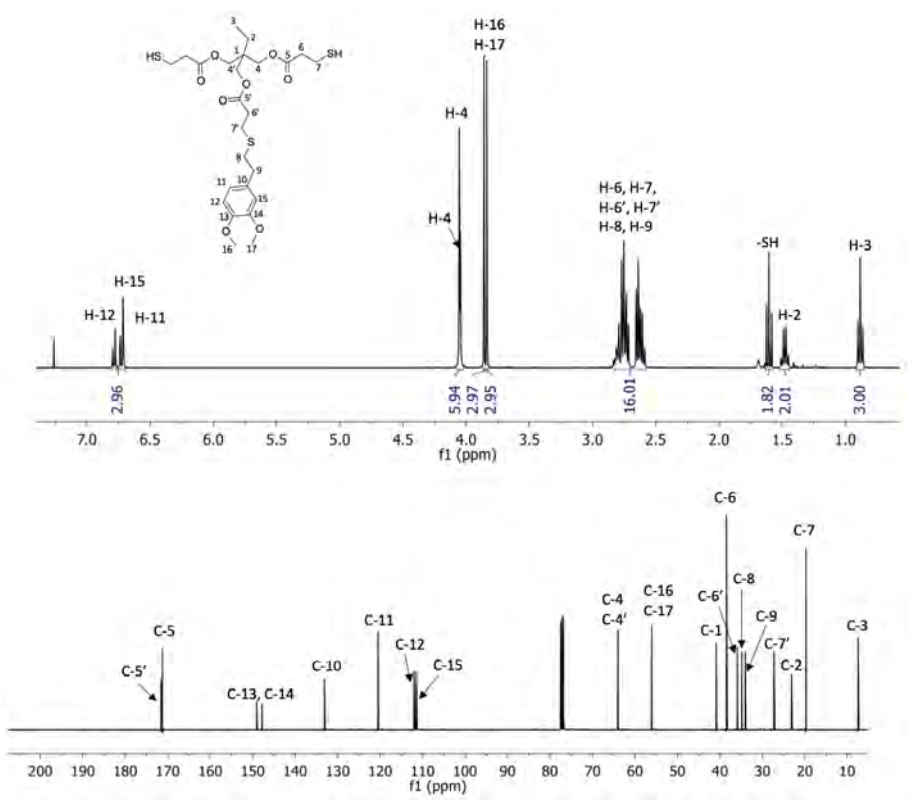


**Figure 3.11.** $^{1}$H NMR and $^{13}$C NMR spectra and assignments of monomer **8**.

## 3.3 Polymerization optimization of poly(disulfide)s via thiol oxidation by iodine

The polymerization of monomer **1** was carried out through the oxidation with iodine to obtain the final catechol poly(disulde) **p1**.[e] In parallel, a model polymerization reaction with dithiol **5** was evaluated to gain insights in the reaction without using monomer **1** (see Figure 3.12).

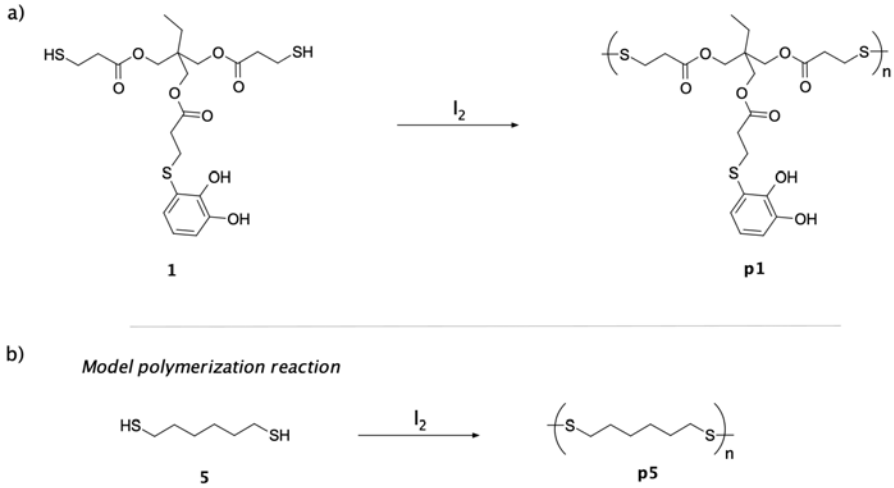


**Figure 3.12.** Reaction scheme of a) polymerization of monomer **1** and, b) polymerization model reaction of dithiol **5**.

### 3.3.1 Solvent effect on poly(disulfide)s synthesis

The polymerization of monomer **1** was described previously by Dr. Juan Mancebo Aracil, without further optimization.[126] That polymerization was performed in EtOH and ended in the precipitation of **p1** from the media. Looking for other possible solvents, dithiol **5** was polymerized by using iodine in EtOH, ACN and THF.

The reaction of **5** was performed in EtOH and 1.1 equivalents of iodine, showing fast consumption of the iodine and precipitation of **p5-16k** in the media,

[e]From now on, the description of the polymers synthesized will follow the general nomenclature **px-nk** where $x$ is an integer number corresponding to the monomer naming and $n$ is the $M_n$ in kDa obtained by GPC analysis. For those case where $M_n$ is not specified, the general nomenclature **px** will be used.

like in the case of **p1**. Polymerization of **5** through disulfide formation is clearly observed in $^1$H NMR. By comparing with the $^1$H NMR spectrum of the monomer, it can be observed that the triplet at 1.35 ppm from the free thiol disappears and the quadruplet at 2.54 ppm from the adjacent methylene to free thiol becomes a triplet at 2.70 ppm corresponding to the one next to disulfide bond (see Figure 3.13a).

The use of ACN and THF as solvent led to side reactions in both cases affecting the synthesis of **p5**.

In the case of ACN, despite the formation of disulfide bond, $^1$H NMR spectrum showed the appearance of new signals: (t) 1.25, (s) 2.32, (s) 2.80, (t) 3.45, (m) 3.75, (bs) 10.43 and (bs) 11.50 ppm (see Figure 3.13b), which do not correspond to free ACN (singlet at 2.10 ppm in $CDCl_3$). Some of these signals could be related to the formation ethanimidothioate group from the reaction of thiol with ACN which has been described elsewhere.[140] The reaction mixture becomes more complex when the reaction is left for longer times as seen in the Figure 6.7 in the Annex. Disulfide formation in ACN with $I_2$ has been described in the literature, achieving high conversion rates, but no comments about possible side products are mentioned.[141]

In the case of the reaction in THF, five additional signals on top of those expected for **p5** appeared (Figure 3.13 c): (m) 1.92, (s) 2.16, (m) 2.50, (t) 3.22 and (t) 3.70 ppm. The signals at 1.92 and 3.76 ppm could be directly related with THF. However, these signals still remained after long periods under reduced pressure, which would discard the presence of free solvent in the system. The appearance of the other signals observed at 2.55 and 3.27 ppm and their relation by comparing integrals suggested a side reaction involving the solvent, more precisely, the polymerization of THF. In acidic media or in presence of proper initiators, THF can polymerize through cationic ring opening polymerization.[142] In fact, it has been reported that iodine can catalyze this ring opening polymerization of THF.[143] Disulfide formation in the oxidation of thiols by iodine leads to HI release which could favor this side reaction related to THF polymerization.[112,143]

Considering the outcomes obtained in ACN and THF, the use of EtOH was stablished as the most convenient one for the polymerization of dithiols with iodine in our case. Besides the satisfactory results and the good solubility of iodine in EtOH, it is considered a green solvent by being one of the solvents with less environmental impact.[144]

### 3.3.2 Experimental design of monomer 1 polymerization

In a first design of experiments (DoE) of the polymerization of monomer **1** in EtOH, the parameters monomer concentration, stoichiometry ($I_2$/monomer **1**) and reaction time were evaluated at two different levels ([monomer]: 0.04 and 0.4

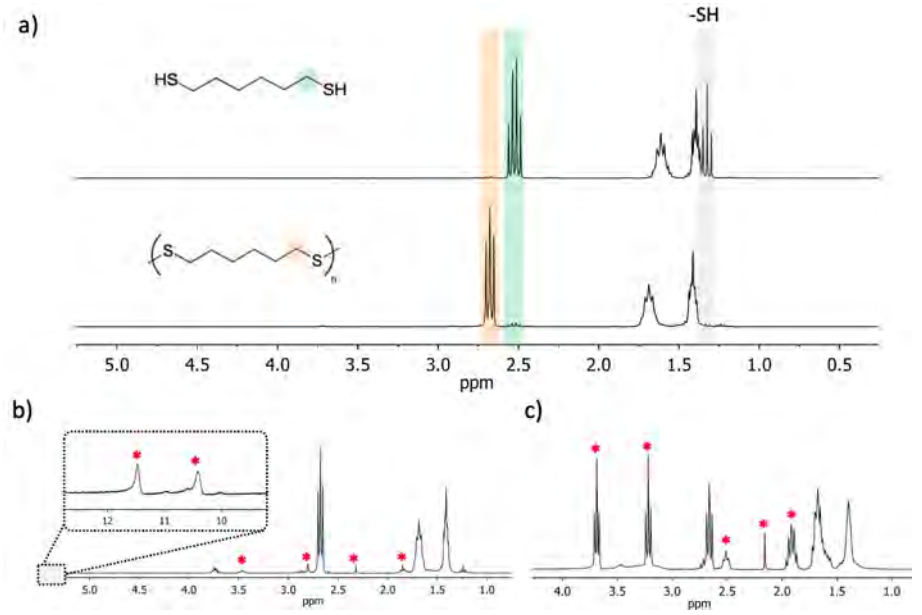


**Figure 3.13.** $^{1}$H NMR spectra of a) **5** and **p5-16k** from reaction in EtOH, b) reaction product of the polymerization in ACN and c) reaction product of polymerization in THF. The asterisk mark indicates the new peaks observed corresponding to side products in the polymerization reaction

M; stoichiometry: 0.8 and 1.05 equivalents of $I_2$; and reaction time: 10 minutes and 4 hours) in a total of eight synthesis (see Table 3.2).[f]

The yield of precipitated fraction is related to the initial monomer concentration. Concentrated conditions yielded higher amount of polymer than diluted ones. Higher concentrations lead to faster precipitation of shorter polymeric chains coprecipitating low molecular species due to supersaturation of the system. On the contrary, diluted conditions would keep the system below saturation and the polymeric chains would be expanded further, until reaching the solubility limit, when the polymer precipitates.

The adhesion was considered the main outcome for the go/no go of the resulting polymers. Only diluted conditions (0.04 M) and 1.05 equivalents of iodine ended with an adhesive polymer, regardless the reaction time. In all the other reaction conditions, the polymer **p1** obtained had no adhesion at all, slipping

[f]These parameters were selected for being expected to be some of the most relevant parameters affecting the reaction. Other parameters such as temperature (room temperature used) and addition rate of iodine (300 $\mu$L/min) were kept constant in all reactions. For more details check the corresponding Experimental Section at the end of the chapter

**Table 3.2.** Detailed reaction conditions and yield of the design of experiments of the polymerization of monomer **1**. Adhesion results obtained from lap shear measurements on glass. Values above 100 kPa could not be tested due to fragility of the glass specimens used above this value.

| | **[Monomer 1] (M)** | **Equivalents of $I_2$** | **Post addition time** | **Yield** | **Shear strength (kPa)** |
|---|---|---|---|---|---|
| Reaction 1 | 0.04 | 0.8 | 10 min | 36 | $< 5$ |
| Reaction 2 | 0.4 | 0.8 | 10 min | 73 | $< 5$ |
| Reaction 3 | 0.04 | 1.05 | 10 min | 29 | $> 100$ |
| Reaction 4 | 0.4 | 1.05 | 10 min | 65 | $< 5$ |
| Reaction 5 | 0.04 | 0.8 | 4 h | 30 | $< 5$ |
| Reaction 6 | 0.4 | 0.8 | 4 h | 71 | $< 5$ |
| Reaction 7 | 0.04 | 1.05 | 4 h | 31 | $> 100$ |
| Reaction 8 | 0.4 | 1.05 | 4 h | 64 | $< 5$ |

upon traction with a negligible force ($< 5$ kPa).

### 3.3.3 Impurity assessment of monomer 1 polymerization

The obtained polymers from previous experimental design were analyzed by MALDI-TOF with positive reflectron mode. The mass spectrum of the different reactions showed different series of peaks that corresponds to polymers containing the monomeric unit of **1**. A detailed analysis of all reaction products from Table 3.2 allowed a proper assessment of impurities present.

In all cases, the set of signals separated by 504 Da of higher intensities would correspond to the $Na^+$ adducts from homopolymerization ($n = 1, 2, 3, 4$, etc.) of monomer **1**. Besides this main series of peaks, other sets of signals separated by 504 Da, i.e. containing subunit from monomer **1**, can be found in the different reactions. In Figure 3.14 the MADI-TOF spectrum of 'reaction 5' is presented as example showing multiple series. MALDI-TOF spectra from the other reactions can be found on page 181 in the Annex.

The series at $n - 196$ Da would be related to sodium adducts of oligomers containing **9** within the chain. The growth of the chain would not be altered in this case, but the amount of catechol functionalities would be affected.

The series of peaks at $n - 88$ Da would correspond to the sodium adduct of an oligomer with one free thiol due to the hydrolysis of one branch of monomer **1**. Contrary from the previous case, the incorporation of this subunit would involve the end of the polymeric growth on that side.

Series of $n + 106$ Da would coincide with oligomeric chains ended with a disulfide from propionic acid, which would trigger the end of the chain as well.

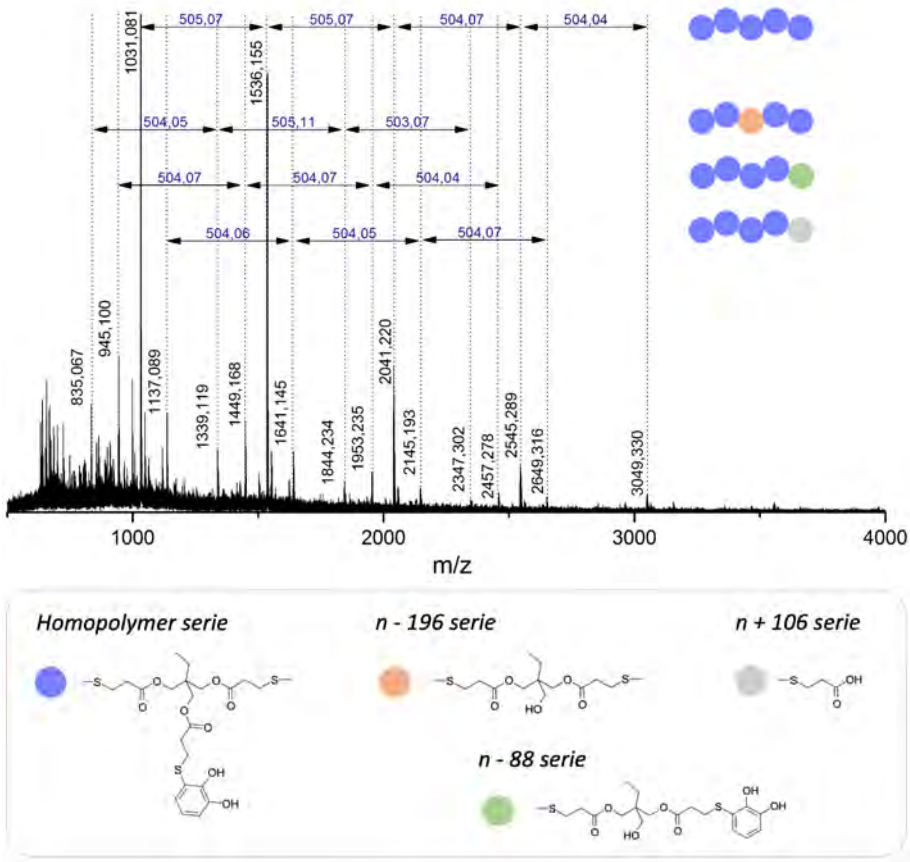


**Figure 3.14.** MALDI-TOF and the corresponding peak assignments of **p1-nk** from the polymerization reaction at 0.4 M, 0.8 equivalents of iodine and 4 h of reaction time.

Although the series of $n - 196$ Da could come from the presence of impurity **9** in the starting material for the polymerization, series of $n - 88$ and $n + 106$ Da would be formed as side product during the polymerization process. Of special interest is the set of signals of $n + 106$, which can be correlated to the addition of mercaptopropionic acid and appears in all the products obtained at 0.4 M. A possible explanation for these signals in concentrated reactions could be the ester hydrolysis of monomer **1**. As a result of the polymerization reaction, HI is formed and could induce the ester hydrolysis of the core of the monomer, due to the exothermic nature of the reaction. This effect would be more evident in the case of high concentration since the final pH of the hydroalcoholic media would

be much lower.

Apart from previous set of peaks, other series at $n + 88$ and $n + 286$ Da have been observed in other reactions (see Figure 6.12 and 6.16 in the Annex). More precisely, $n + 88$ would coincide with the proton adducts of oligomeric chains ended with the bis-adduct impurity **12** and the one at $n + 286$ Da could be related to a water adduct of oligomers containing disulfide **10**. These two sets of signals, though, would not be formed during the polymerization process, but should come from impurities in the starting material. These results highlight the importance of the purity of the starting material, since any presence of impurities could have a relevant effect in the final chemical structure of the polymer.

### 3.3.4 Stoichiometry effect on dithiol polymerization by iodine

The effect of the stoichiometry was evaluated in the model reaction with dithiol **5**. Generally, the reaction of disulfide formation by using iodine is dependent on the amount of iodine as described elsewhere.[112] Given the step-growth nature of poly(disulfide)s formation from the oxidation of dithiols, higher degree of polymerization is expected to be obtained at higher conversion rates.[g]

The kinetics of the reaction of polymerization of **p5-nk** was evaluated at 0.25, 0.5, 1, 2 and 4 equivalents of iodine following the conversion by $^1$H NMR. Conversion was calculated by relating the integral from signals at 2.5 and 2.7 ppm corresponding to the adjacent methylene to the thiol or the disulfide respectively. It was observed that conversion reaches a maximum between 15 and 30 minutes of reaction and then suffered a decrease. As seen in Figure 3.15c conversion increases with the amount of $I_2$ equivalents.

As described by Danehy et al., the whole oxidation reaction by iodine involves two steps and a series of equilibria (see Figure 3.15a).[111–113] By increasing and exceeding the amount of iodine it is possible to push the equilibria towards the formation of disulfide. Although high conversion is achieved with 2 equivalents of iodine, full conversion is only achieved with 4 equivalents. $^1$H NMR spectra show a signal displacement and distortion which could be in agreement with the fact that higher molecular weight species are formed (Figure 3.15b). The decrease of the conversion with time could be related with the acid formation and the precipitation of the polymer. Initially, polymer formed precipitates, protecting the polymer from the effect of the acidic media. With time, the acid formed could induce the disulfide cleavage, going back in the reaction.

Analysis of the precipitated **p5** by GPC shown in Table 3.3 are in agreement with the conversion of the reaction. While oligomeric species of 535 Da of $M_n$

[g] As described by Carothers equation for step-growth polymerizations, where the degree of polymerization is defined as $\bar{X}_n = 1/(1-p)$ with $p$ corresponding to the conversion to polymer.

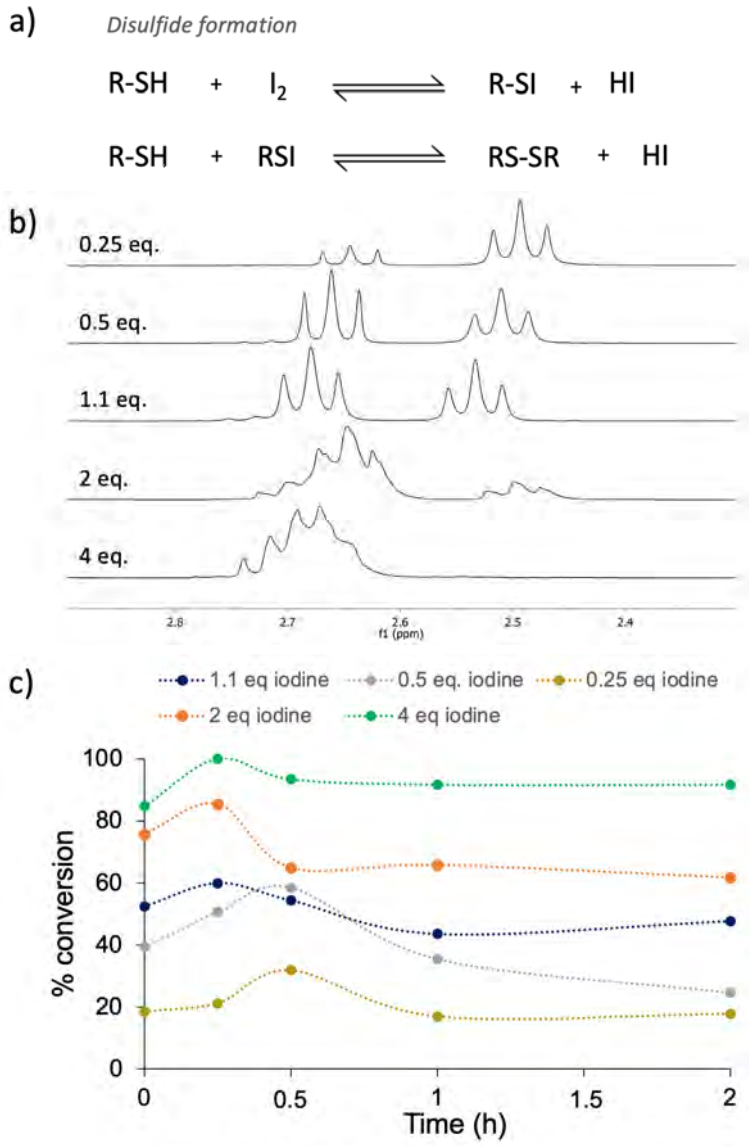


**Figure 3.15.** a) Reaction equilibria of the disulfide formation through the oxidation by iodine, b) $^{1}$H NMR spectra of reaction product after 15 minutes and c) kinetic studies results of polymerization of **5** in EtOH at different $I_2$ equivalents.

**Table 3.3.** GPC results of **5** polymerizations at different equivalents of $I_2$ and yields of purified **p5** after obtained after purification by precipitation

| Equivalents $I_2$ | Mn (kDa) | Polydispersity (Đ) | Yield |
|---|---|---|---|
| 0.25 | 0.5 | 3.7 | 20 |
| 0.5 | 2.2 | 1.7 | 23 |
| 1.1 | 16.5 | 1.7 | 41 |
| 2 | 50 | 1.7 | 55 |
| 4 | 49 | 1.8 | 56 |

and high polydispersity (Đ) of 3.7 are obtained at 0.25 equivalents of iodine, polymers of 50 kDa of $M_n$ and Đ of 1.7 are achieved with 2 and 4 equivalents, which are common values for polymers with step-growth polymerization nature. The amount of polymer precipitated increased with the equivalents of iodine used, enhancing the final yield.

The results obtained with the model could be correlated with the results obtained in the first DoE, because only reactions performed with 1.05 equivalents of iodine had good adhesion and higher molecular weights would be expected.

### 3.3.5 The effect of the addition of base in dithiol polymerization by iodine

As seen in the equilibria shown in Figure 3.15a, the formation of HI has an impact in disulfide formation, pushing the reaction towards disulfide cleavage. This aspect was faced with the model of dithiol **5** by adding different bases. To confront this issue, in reported polymerizations of dithiols with iodine by Choi et al., $Et_3N$ was used to neutralize the acidic media.[102] In the case of **p5** formation, the addition of $Et_3N$ with the $I_2$ solution, the addition of $Et_3N$ before and after starting the polymerization reaction were studied, in all cases without showing conversion increase in the formation of disulfides (see Figure 3.16). This outcome could have similarities with the observations of Choi et al., who described that although achieving polymerization in the system, it was observed that prolonged reaction times had an adverse effect.[102] However, no explanation about it was given. This detrimental effect in the addition of $Et_3N$ could be related to the fact that $Et_3N$ would be affecting only the amount of protons in the media, while the equilibrium of iodide remains invariable due to the solubility of the triethylammonium salt in EtOH. Furthermore, a precise control over the amount of $Et_3N$ should be needed to avoid a high increase of the

pH and, hence, disulfide/thiol exchange which is favored upon thiolate presence.

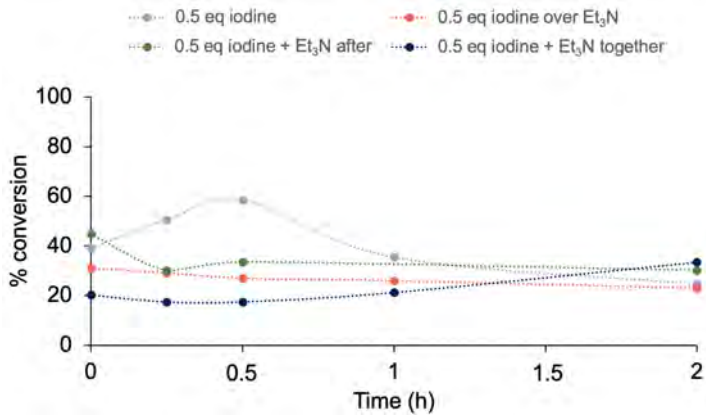


**Figure 3.16.** Kinetics of **p5** formation in presence of $Et_3N$ at different combinations.

In order to affect also the iodide equilibrium, polymerization of **5** was carried out in presence of $NaHCO_3$ since NaI is insoluble in EtOH. This reaction was done in heterogeneous conditions due to the poor solubility of $NaHCO_3$ in EtOH, adding 2 equivalents of iodine.

As shown in the graph of Figure 3.17, full conversion is achieved when $NaHCO_3$ was added within the reaction process. GPC analysis supported the results obtained by $^1$H NMR, achieving a $M_n$ of 244 kDa and Đ of 1.7, almost five fold greater than the reached without $NaHCO_3$.

Despite the low solubility of $NaHCO_3$, once polymerization initiates and first protons are released, the slight amount of $NaHCO_3$ solubilized neutralizes the media, being released $CO_2$ and precipitating NaI as products of this neutralization process. In this way, both the protons and iodide can be withdrawn from the reaction media and the equilibria can be push further towards the formation of disulfide.

Another base tried due to its solubility in EtOH was sodium salicylate. Polymerization of **5** in presence of sodium salicylate and 2 equivalents of iodine resulted in the formation of **p5-140k** with $M_n$ of 140 kDa and Đ of 1.4. Although the resulting polymer has a lower molecular weight than the one obtained with $NaHCO_3$ (244 kDa), the use of salicylate ended in a 3-fold increased of the growth of the chain with respect to the polymerization with 2 equivalents of iodine and without base. This difference between sodium salicylate and $NaHCO_3$ could lay in the different neutralization process involved in each case. Although $pK_b$ of sodium salicylate ($\approx$ 11.0) is higher than the one from $NaHCO_3$ ($\approx$ 7.7), the neutralization by $NaHCO_3$ generates $CO_2$ which is released, pushing the neutral-

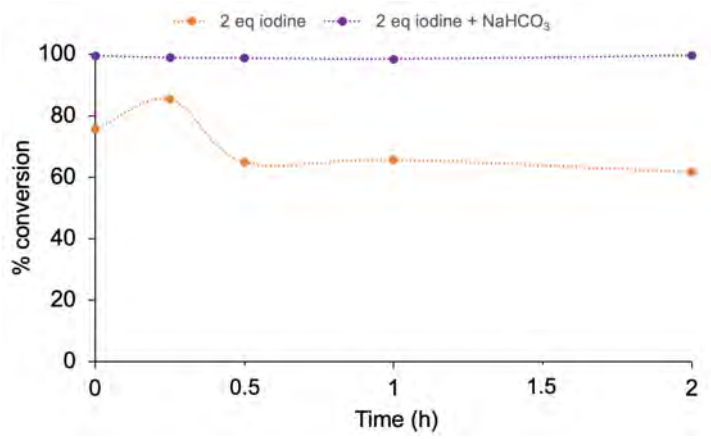


**Figure 3.17.** Kinetic results of polymerization of dithiol **5** with 2 equivalents of $I_2$ in presence and absence of $NaHCO_3$.

ization equilibrium further.

Having in mind all considerations extracted from the results obtained in the model polymerization of dithiol **5**, polymerization reactions of monomer **1** were tuned to maximize molecular weight, i.e. reaction conditions of 1 M monomer in EtOH, 2 equivalents of $I_2$ and presence of $NaHCO_3$.

Unfortunately, these conditions ended in the formation of a gel-type material, insoluble in acetone, ACN, THF, DCM, chloroform, DMF and DMSO. Having catechol as an extra functionality in **p1** system and considering its broad reactivity, it was decided to study any effect of catechol in the polymerization of dithiols by iodine in view of this results.

### 3.3.6 Effect of catechol in the polymerization of dithiol 5 by iodine

Kinetics of the polymerization of dithiol **5** were studied in presence of catechol with different equivalents of iodine (Figure 3.18a). For these studies, a ratio 1:1 of dithiol **5** and pyrocatechol **3** was used to resemble closer the conditions of polymerization of monomer **1**. In parallel, possible oxidation of pyrocatechol **3** in EtOH with iodine was studied, without observing any detectable formation of *o*-quinone **4** by $^1$H NMR (see Figure 3.18b).

$^1$H NMR analysis of the crude and the purified **p5** did not show formation of *o*-quinone **4**, and the signals of pyrocatechol remain without the presence of

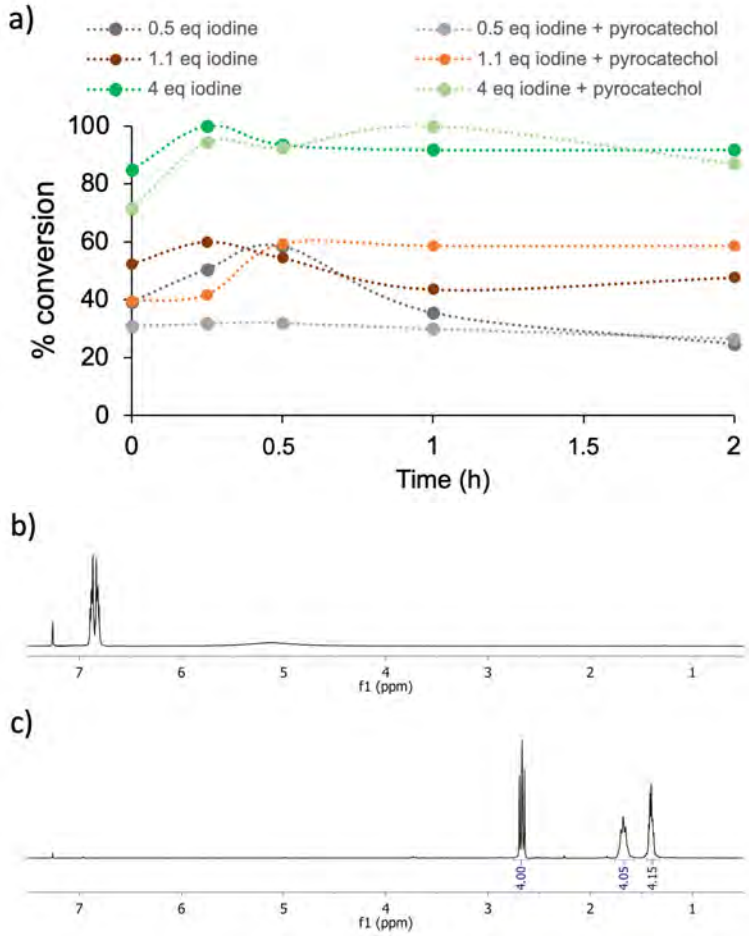


**Figure 3.18.** a) Kinetic studies results of polymerization of **5** in EtOH in presence of catechol and different $I_2$ equivalents; b) $^1$H NMR of final product from pyrocatechol **3** in presence of iodine; and c) $^1$H NMR of **p5** obtained from the reaction at 1.1 equivalents of iodine and addition of pyrocatechol **3**.

any new peak, which seems to indicate no relevant effect of catechol in the final chemical structure (Figure 3.18c). However, the $M_n$ of the precipitated polymer in the reaction with 1.1 equivalents of iodine in the presence of catechol was 32.5 kDa by GPC, twice the molecular weight under the same conditions without catechol. Given the differences observed in the kinetics and $M_n$, it could be thought that catechol has some influence in the reaction, although its role could not be

determined. Further and more specific studies would be required to understand the whole complexity of the system.

### 3.3.7 Final optimization of polymerization of monomer 1 by iodine

Initial DoE presented in previous section of the chapter showed that diluted conditions and high stoichiometry worked better to obtain an adhesive material, with no relevant influence of the reaction over periods of 4 hours. To study the effect of the higher equivalents of iodine and the presence of $NaHCO_3$ as a base, these parameters were combined in a new set of experiments (see Table 3.4).[h] The use of bicarbonate this time to neutralize the acid and displace the equilibrium of reaction towards disulfide formation would affect the hydrolysis of the monomer core as well, which is expected to provide a better control in the final chemical structure. The precipitated polymer for each reaction condition was isolated, washed with EtOH three times and dried.

**Table 3.4.** Detailed reaction conditions and yield of the second design of experiments of the polymerization of monomer **1**.

| [Monomer 1] (M) | Equivalents of $I_2$ | Presence of $NaHCO_3$ | Yield |
|---|---|---|---|
| 0.04 | 1.05 | No | 32 |
| 0.04 | 2 | No | 27 |
| 0.04 | 1.05 | Yes | 31 |
| 0.04 | 2 | Yes | 27 |

GPC elugrams of the reactions at 0.04 M looked similar (Figure 3.19a) regardless the presence/absence of $NaHCO_3$ and the use of 1.05 or 2 equivalents of iodine, showing practically the same molecular distribution of the precipitated polymers. The small differences between them could be related perfectly to minor experimental deviations. In all the cases, a bimodal distribution of polymeric species is observed. This result could mean that low molecular weight species coprecipitated with high molecular polymeric species. Surprisingly, the ratio between them seems to be quite consistent in all the reactions, but no clear understanding of this behavior has been determined yet. The fraction of shorter elution

[h] Considering previous optimization, room temperature was used, the addition rate of iodine was set at 300 $\mu$L/min and a post addition time of 20 min was set. These parameters were kept constant in all reactions.

times, corresponding to higher molecular species, presented a $M_n$ between 70 - 96 kDa ($n$ = 140 - 180) and a Đ of 1.8 - 1.9.

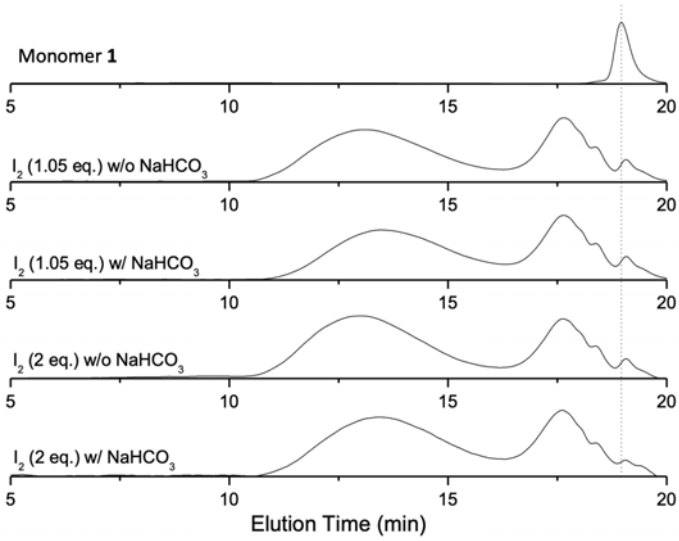


**Figure 3.19.** GPC elugrams of DoE of the synthesis of **p1-nk** at 0.04 M at different ratios of iodine and presence/absence of base.

After this optimization process, the parameters chosen as the optimal for the polymerization of monomer **1** were: concentration of 0.04 M, 1.5 equivalents of iodine, and without presence of base.[i] Working under this conditions, polymerization of monomer **1** ended in the formation of **p1-50k** with good reproducibility.

Figure 3.20 shows the $^1$H NMR of polymer **p1-50k**. As it can be seen, -SH signal completely disappears as expected from poly(disulfide) formation. Furthermore, signal of H-7 shifts towards higher ppm as a consequence of disulfide formation.

As mentioned along the present section, we have been focused of the precipitated part formed in the polymerization of monomer **1**. GPC elugrams in all precipitated samples show a bimodal distribution, presenting low molecular species coprecipitated along with **p1-50k**. In order to remove low molecular weight species, the final product can be precipitated in EtOH, since they remain soluble. By dissolving in DCM and precipitating **p1-50k** in cold EtOH three times it was possible to eliminate most of short oligomeric species (Figure 3.21a),

[i]The use of 1.5 equivalents was selected to avoid any experimental error when working close to 1 equivalent. Besides, the ineffectiveness of the presence of $NaHCO_3$ at 0.04 M permits avoiding its addition which would cause further work-up steps.

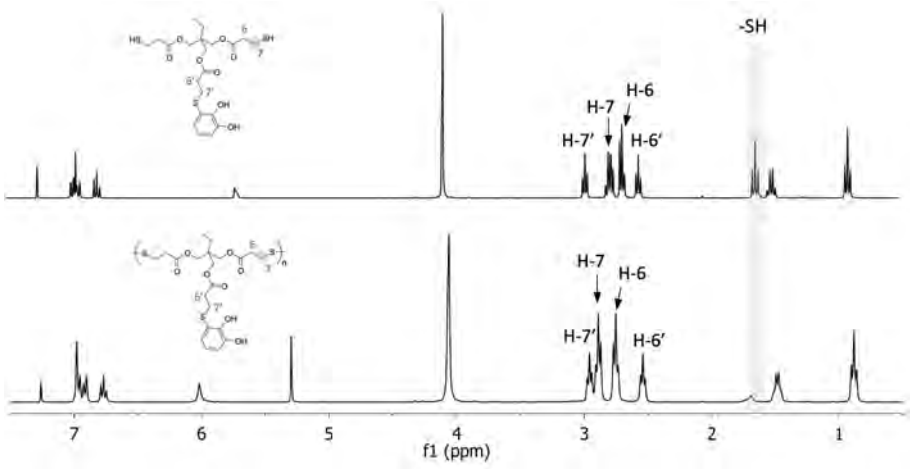


**Figure 3.20.** $^{1}$H NMR of **1** (top) and **p1-50k** (bottom) showing main differences between them.

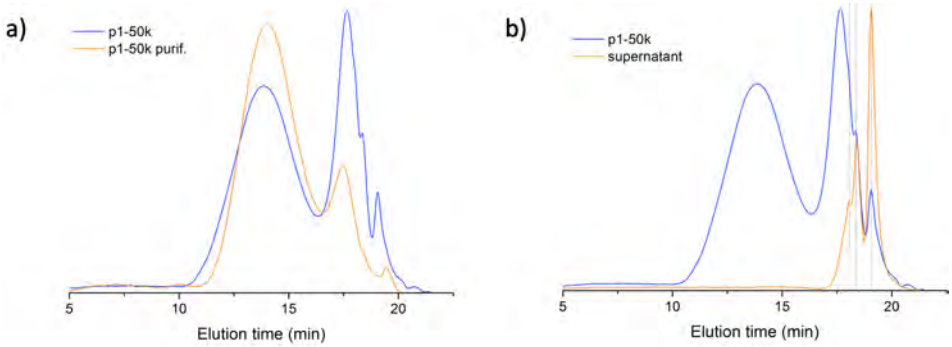


**Figure 3.21.** a) GPC elugram of **p1-50k** before and after purification by precipitation, and b) GPC elugram of precipitated and soluble part in EtOH for **p1-50k** synthesis.

but the final yield was reduced considerably. Despite the presence of oligomeric part, in the adhesives test described in Section 3.4 it was decided to work with the polymer without purification by precipitation.[j]

Soluble part which represents between 65 - 75 % of the reaction yield, is composed by oligomeric mixtures with $M_n$ below 1.5 kDa, as found by GPC

[j]Due to the limitation of pure monomer **1** and its reduced yield in polymerization in diluted conditions ($25 - 35$ %), it was decided to focus the efforts on the study of the properties and potential applications of this new family of poly(disulfide)s.

analysis (Figure 3.21b). Further characterization of these species are detailed in Section 3.6.

### 3.3.8 Development of reference 'blank' polymer p8

As mentioned previously, the synthesis of a 'blank' polymer has been done in this project in order to evaluate more in detail the adhesive role of catechols in this family of poly(disulfide)s.

Oxidative polymerization of monomer **8** by $I_2$, considering previous results from the polymerization of **p1** and **p5**. In this way, the reaction conditions were adapted in order to have the closest values of $M_n$ between **p8** and **p1-50k**.

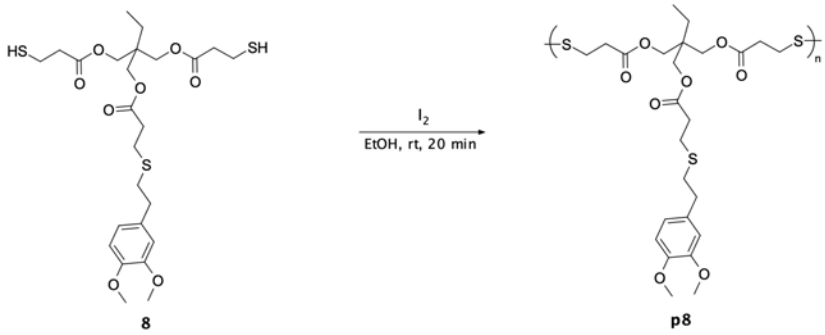


**Figure 3.22.** Reaction scheme of the synthesis of **p8-nk**.

Polymerization above $I_2$ stoichiometry (1.5 equivalents) led to the formation of poly(disulfide)s with $M_n$ of 25 kDa ($n \approx 44$) and Đ of 1.6 (**p8-25k**), presenting also bimodal molecular weight distribution like in the case of **p1-50k**. The lower solubility of monomer **8** in EtOH with respect to monomer **1** results in a faster precipitation of the former one. Increasing the reaction temperature to 45 °C to improve monomer solubility led to a minimal change in the final polymer, obtaining a polymer with $M_n$ of 29 kDa and Đ of 1.7 (**p8-29k**). In order to increase the molecular weight further, polymerization was done with 1.5 equivalents of iodine and addition of sodium salicylate, which resulted in a molecular weight increase in the reaction model of **p5**. Under this conditions $M_n$ reached a value of 37 kDa ($n \approx 66$).

$^1$H NMR analysis of **p8-37k** shows the disappearance of −SH indicating disulfide formation (Figure 3.23a) and a clear displacement of the signals from adjacent methylene to disulfide towards higher ppm, like in the case $^1$H NMR of **p1-50k** from Figure 3.20. MALDI-TOF of the resulting polymer also confirmed the proper formation of the polymer **p8** from the presence of the series of

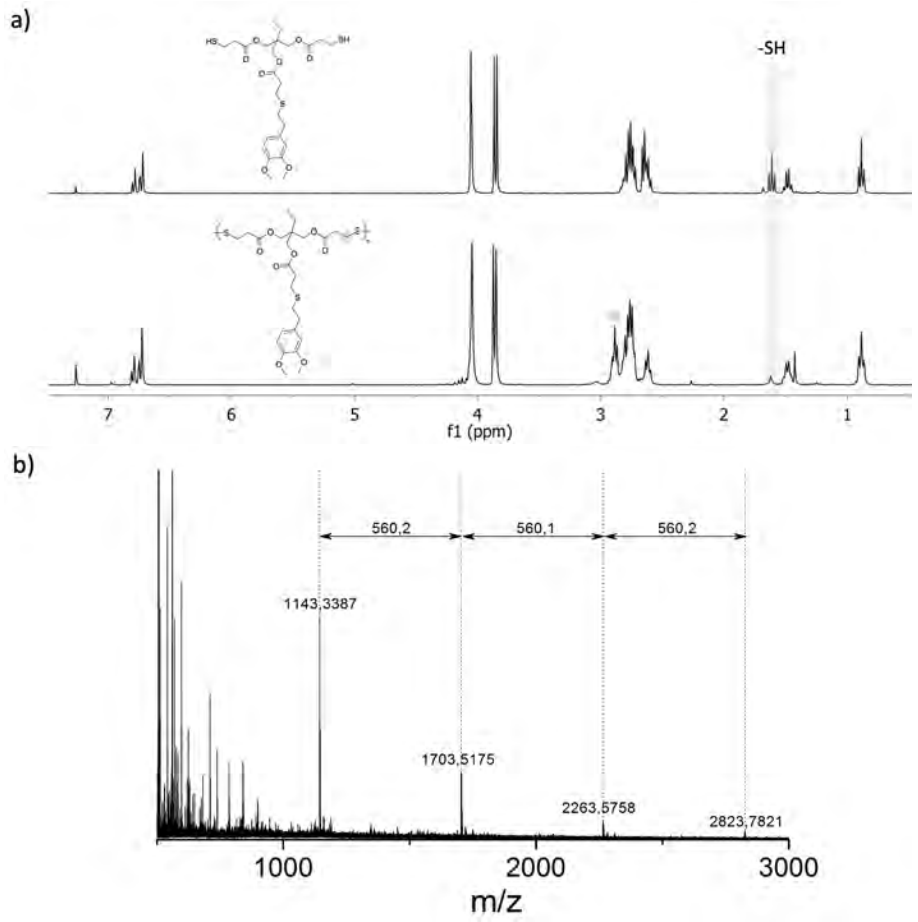


**Figure 3.23.** a) On the top, $^{1}$H NMR of **8** and $^{1}$H NMR of **p8-37k** on the bottom showing the displacement of methylene from free thiol to disulfide formation; and b) MALDI-TOF of analysis of **p8-37**.

peaks separated by 560.2 Da corresponding to the $Na^{+}$ adducts of homopolymers (Figure 3.23b).

## 3.4 Adhesive properties of catechol poly(disulfide)s

The adhesion of catechol poly(disulfide)s, **p1-50k**, was evaluated on glass, copper, aluminum, stainless steel and titanium following ASTM D 1002-99. To do so, ≈ 10 mg of the polymer dissolved in $CHCl_3$ were added on one side of the corresponding substrate covering and area of 12.7 x 25.4 mm. Once the solvent was dried, two substrates were tightly joined and left curing at 120 °C during 30 minutes. For further details check the full procedure described in the corresponding Experimental section 3.8.

In all cases, an adhesive strength in the order of MPa for the different substrates was obtained (see Figure 3.24). As a blank for evaluating the role of catechol in the adhesion on the substrates, the poly(disulfide) containing dimethoxylated functional group (**p8-37k**) was studied as well. The adhesion was tested after four different bonding/debonding cycles, applying a heating process of 120 °C during 30 minutes between the cycles of bonding/debonding for both polymers. Both polymers are stable at this temperature as determined by the TGA analysis of **p1-50k** and **p8-37k** (see Figures 6.8 and 6.9 in the Annex).

In all substrates **p8-37k** presented poor adhesion in comparison to **p1-50k** which would indicate that in this family of poly(disulfide)s the adhesion would come from the presence of the catechol moiety and its interaction with the substrate. Furthermore, generally cohesive failure was observed since polymeric material remained attached on both sides of the substrates after lap shear test, except on glass where substrate failure occurred in some cases from the fracture of the sample before adhesive detachment (see Figure 6.19 in Annex).

On glass substrates, the adhesion reaches values between 2 - 2.5 MPa after being rejoined. It is worth to mention that the maximum values obtained in this case was limited to the load cell used in the UTM, which was the only one provided with rubber clamps to avoid substrate fissure. In some cases, the maximum force of the loading cell was achieved, so the real maximum adhesion could not be registered. Besides, two samples suffered substrate failure, meaning that the substrate was broken before being separated apart. The high adhesion of **p1-50k** would be in accordance to the good interaction of catechol to silicates trough H-bonding.[26] It must be noted that this high adhesion would not be possible if catechol were oxidized to quinone, since this last one is unable to form H-bonding on glass substrate.[145]

The adhesion on copper has a special behavior as it went down with the number of rejoining cycles. Interestingly, the initial adhesion is 3.7 ± 1.2 MPa, which is by far the highest adhesion of all substrates tested. However, this adhesion was reduced up to 1.4 ± 0.2 MPa in the last cycle. The effects observed

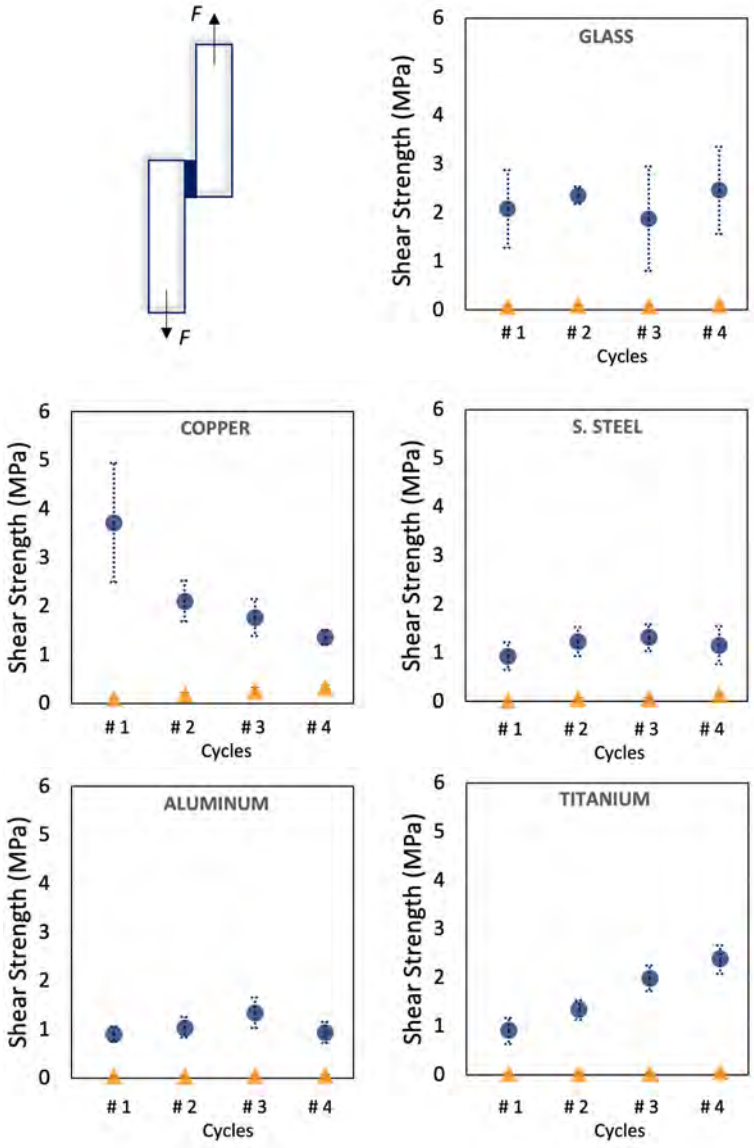


**Figure 3.24.** Shear strength results of **p1-50k** and **p8-37k** on different substrates and rejoining cycles. Deviation standard (n = 5) of the measurements are represented as well.

in this case could indicate that, on copper, catechols are not the only players in the interaction polymer/substrate. While catechols could interact with copper through coordination bonding, thiols and disulfides can interact as well with the copper substrate. In fact, it has been reported the use of thiols and disulfides for the preparation of self-assembly monolayers (SAMs) on copper.[146,147] The high decrease in the adhesive strength with the cycles could be caused by the reduction of disulfide bonds catalyzed by the copper with the time and heat,[148] which would break the backbone of the polymeric chains decreasing the physical cohesion of the system. Taken into account the presence of thiols and the high number of disulfides in our system, this idea of the role of thiols and disulfides would support the higher initial adhesion of **p1-50k** observed on copper with respect to the other substrates and the progressive loss of adhesion with the rejoining cycles.

In the case of stainless steel, the adhesive strength reaches an initial value of 0.9 ± 0.3 MPa and reaches a maximum of 1.3 ± 0.3 MPa in the third cycle, meaning that there is not significant difference between the adhesion along with the cycles. A similar behavior is observed in aluminum, where the adhesion is 0.9 ± 0.2 MPa at the beginning and increases up to 1.3 ± 0.3 MPa. In both cases, catechol can interact with the substrate through coordination bond with the metal, which has been extensively described in the literature with various systems.[39,42,47,48,149] The constant adhesion over time through the bonding/debonding cycles could indicate that catechol moiety remain in the reduced form since the oxidized quinone could have a negative impact on the interaction between catechols and the metallic substrates.

On titanium, the adhesion tends to increase with time, and it would seem that it did not reach the maximum adhesion after the fourth cycle (2.4 ± 0.3 MPa). Although the adhesion of catechols is expected to be important in the substrate of titanium,[33,150] until now there is not clear explanation why in the case of **p1-50k** the adhesion increases and does not remain constant like in the case of glass, stainless steel and aluminum. This promising result extols the potential of this material in applications were titanium is broadly used, such as implants in the biomedical field.

Several processes could affect the system when temperature is applied. On one side, disulfide can suffer metathesis with temperature, affecting the final molecular distribution of the system.[151,152] Also, thia-Michael addition between *o*-quinones (from catechol oxidation in curing process) and free thiols from polymer end-chain could proceed. This reaction could induce cross-linking of the system. However, this effect should be less relevant due to the limited amount of free thiols, since only the ones from the end chain would be the available. Catechol-catechol cross-linking could also occur from the reaction between *o*-quinones and catechol. Due to the nature of catecholic compounds it seems reasonable to con-

sider that a minimal amount of catechol could be readily oxidized to *o*-quinone just from the contact with atmospheric oxygen present during all the process of bonding/debonding.

A less familiar mechanism could be hypothesized in this system containing catechols and disulfides. Thiyl radical formation through homolytic disulfide cleavage, in presence of catechol, could be followed by hydrogen abstraction of catechol moiety. If this process takes place, quinone/semiquinone and free thiol system will be formed, allowing the Michael type addition (see Figure 3.25a). However, studies with a model reaction between an alkyl disulfide **15** and pyrocatechol **3** did not show any reaction by $^1$H NMR after heating at 120 °C overnight (see Figure 3.25c). Also, this potential reaction was tested with the poly(disulfide) **p5-16k** ($n \approx 100$) and pyrocatechol **3** heating up to 120 °C for 1 hour, without showing reaction by $^1$H NMR or change in the molecular weight by GPC (see Figure 6.20 and 6.21 from Annex). These results suggest that this potential reaction between thiyl radicals and catechols would not be the most relevant mechanism if happened, since no evidence of the reaction could be found yet.

### 3.4.1 Surface characterization

In order to gain more insights in the possible interaction polymer/surface, lap shear test specimens where characterized by optical microscopy, profilometry and UV-Vis.

Among all parameters affecting adhesion, the roughness of the surface is relevant, since those substrates with higher roughness tend to enhance adhesion due to their larger surface of contact. Surface of the pristine substrates was examined by optical microscopy and roughness of the systems was analyzed with an optical 3D profiler to give precise information about the substrates used in this work (see Figure 3.26).

The surface analysis of the different materials showed a considerable roughness difference between them (Table 3.5). The parameter of mean roughness, $S_a$ (nm), increases in the following order: glass << copper << titanium < stainless steel << aluminum. Copper and stainless steel display a linear pattern (on y and x respectively) on the substrate which is consequence of the laminating process during their fabrication.

Concerning adhesion results presented previously, they do not seem to follow any correlation with the roughness of the systems, as the roughest substrates are not the ones presenting highest adhesive performance and the flattest ones do not present the lowest adhesion. So, adhesion should be ultimately related to the interaction of catechols with the material.

The interaction of the polymer with the metallic substrates was studied by an-

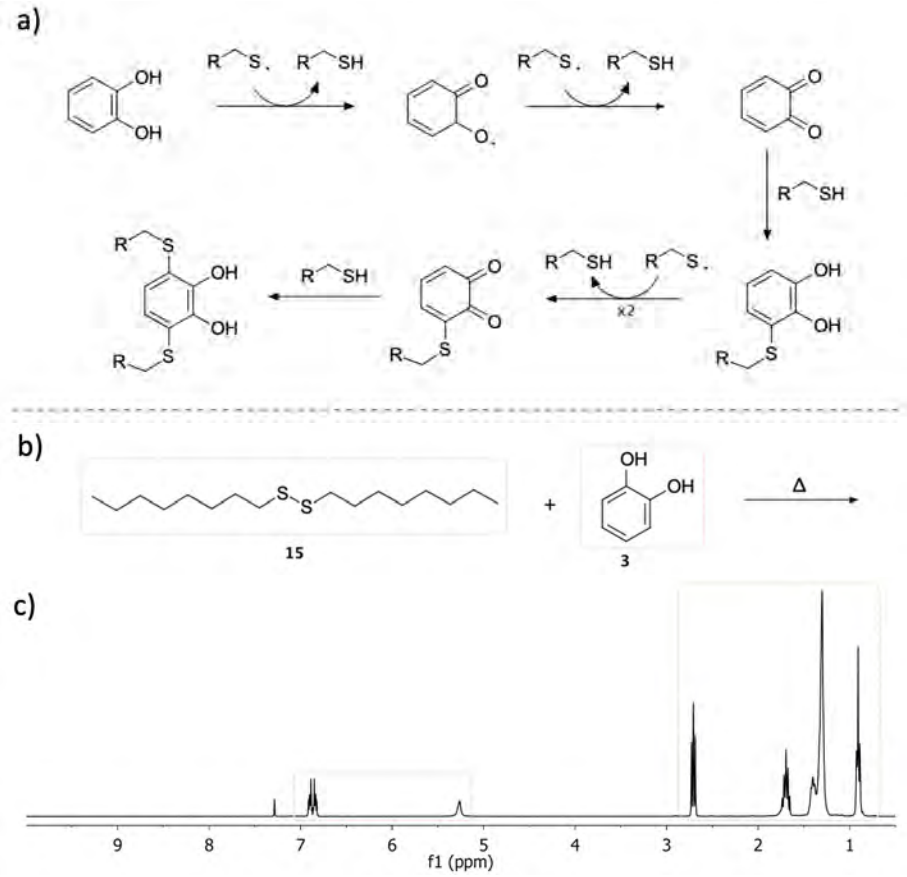


**Figure 3.25.** a) Suggested possible reaction between catechol and thyil radicals; b) reaction scheme of the model reaction for the heat-induced disulfide cleavage in presence of catechol and c) $^{1}$H NMR of the reaction mixture of the model reaction for the heat-induced disulfide cleavage in presence of catechol overnight showing no changes in composition from starting materials.

alyzing the UV-Vis absorption bands. Absorption spectra were obtained from the diffuse reflectance on the substrate after lap shear test. Only metallic substrates were feasible to be studied, since glass did not give reliable reflectance signal to be processed. Although the reported visible absorption studies of metal-catecholate complexes in literature are described in liquid state,[38] the absorption ranges of metal-catecholate complexes could be used as a guide to determine possible coordination of the catechol containing polymer with the substrate.

The analysis on copper revealed a broad band for **p1-50k** between 300 and

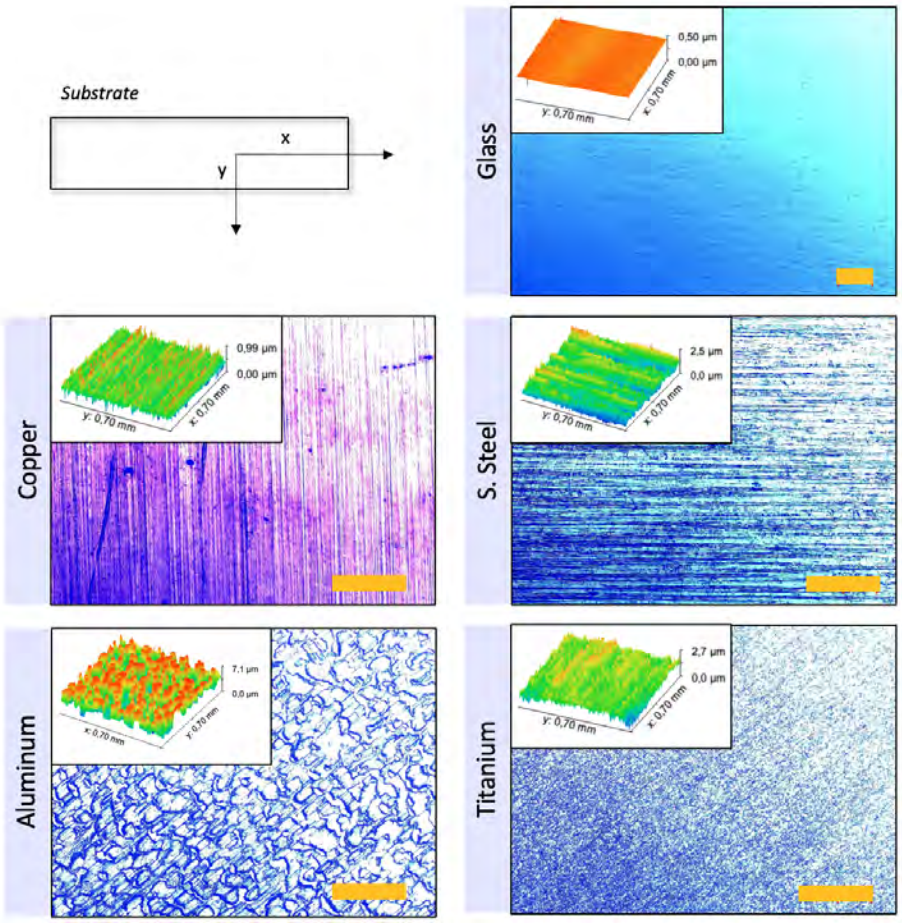


**Figure 3.26.** Optical microscopy images of the pristine substrates tested and surface profiles (insets). Scale bars: 200 $\mu$m.

500 nm which was not observed in **p8-37k**. This band could be related with the bis complex $[Cu(cat)_2]^{2-}$ which presents an absorption with a $\lambda_{max}$ around 401 nm.

On stainless steel substrate, a broad band with low intensity in the visible range between 400 and 700 nm was observed for **p1-50k**. This band can be correlated with the well-known bis complex between $Fe(cat)_2$ with a $\lambda_{max}$ around 576 nm. Moreover, dark blue spots could be observed on the adhesive region as can be seen on Figure 6.22 of the Annex. Substrates containing **p8-37k** presented

**Table 3.5.** Roughness parameters of pristine substrates obtained from the surface analysis by optical profilometer.

| Substrate | $S_a$ (nm) |
|---|---|
| Glass | 6.8 |
| Copper | 79.8 |
| S. Steel | 256.5 |
| Aluminum | 1433 |
| Titanium | 219.4 |

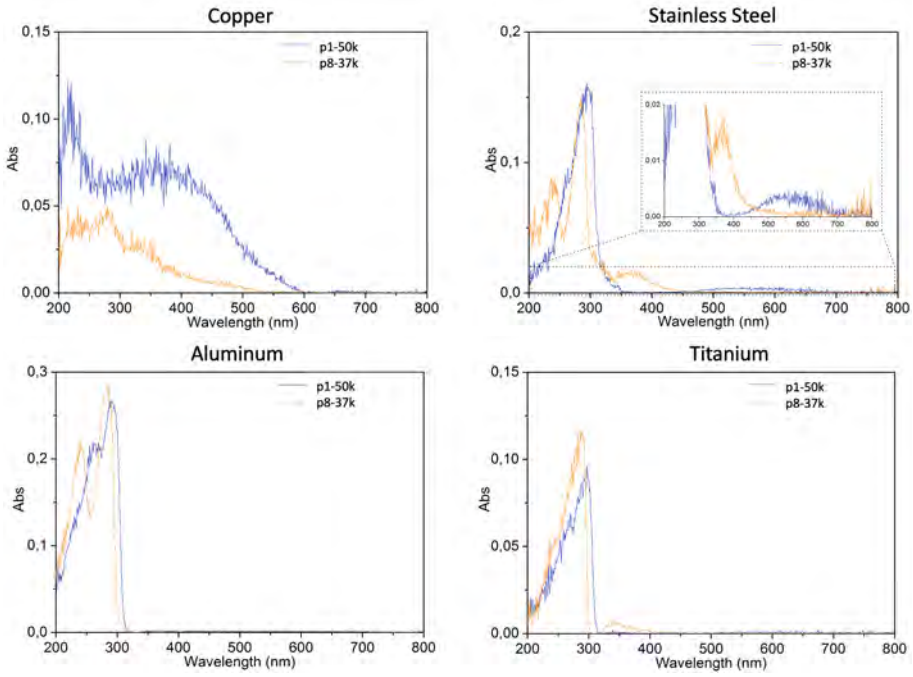


**Figure 3.27.** UV-Vis absorption of lap shear specimens' surface after last debonding process in copper, stainless steel, aluminum and titanium substrates.

an absorption band centered around 380 nm that could not be associated to any possible described interaction of **p8-37k**.

In the case of aluminum and titanium, no absorption band was observed in the visible region, only UV absorption between 200 and 300 nm. This bands are directly related to the absorption of aromatic rings in both polymers. Although

it would be expected coordination between catechol moieties and Ti(IV) and Al(III) present on their respective oxidized surfaces,[38,40,41,43] these interactions were not observed with this technique in these cases.

## 3.5 Biocompatibility studies

One of the main concerns about the design of new materials is their biosafety. To evaluate the potential toxicity of the new family of catechol poly(disulfide)s adhesives as potential medical grade products, **p1-50k** was studied following the procedures of ISO 10993 'Biological evaluation of medical devices'. Consisting on 24 different sections, ISO 10993 series is considered one of the most strict standards that all materials must pass if they are ultimately used in healthcare, especially those classified as Class III medical devices with higher risks for human body.

Although catechol containing polymers have been introduced as potential materials in biomedical applications, concerns about their potential toxicity have arose recently. Catechol derivatives have been seen to affect the production and metabolism of reactive oxygen species (ROS), which are closely related with inflammatory responses as mentioned in the Section 1.2.1.1. For these reason, a precise evaluation of potential toxicity is required.

To performed this biocompatibility assessment, ISO 10993-5 'Test for in vitro toxicity', ISO 10993-10 'Test for irritation and skin sensitization' and ISO 10993-12 'Sample preparation and reference materials' have been followed to assess the fulfillment of the requirements in the case of polymer **p1-50k**.

### 3.5.1 *In vitro* cell viability of p1-50k

Following ISO 10993-5, cell viability of **p1-50k** extracts on NIH3T3 fibroblasts with XTT assay was studied in collaboration with Dr. Julia Lorenzo and Dr. David Montpeyó at IBB (Institut de Biotecnologia i de Biomedicina). The blank corresponded to the extraction media which was the cell culture media, Dulbecco's Modified Eagle Medium (DMEM). As negative control, the extracts of USP Reference Standard of high-density polyethylene (HDPE) was considered as defined by ISO 10993-12. The extracts of **p1-50k** were obtained after keeping the material on DMEM at 37 °C for 24 and 72 h.

The results of the extracts of **p1-50k** presented good biocompatibility, showing cell viabilities of 92.4 ± 3.2 % and 103.5 ± 7.1 % for the extracts obtained at 24 and 72 h respectively as presented in Figure 3.28. These results demonstrate that the extracts does not contain any potential toxicity which could come from remaining solvents or monomers retained within the material from the synthesis process.

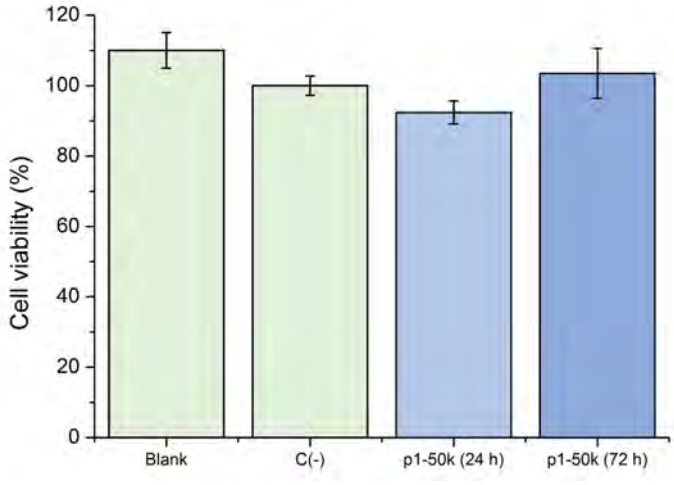


**Figure 3.28.** Cell viability results of XTT assay from the extracts in DMEM of **p1-50k** at 24 and 72 h extraction times

The high cell viabilities of **p1-50k** would indicate its safety regarding the extraction products, boosting the use of this polymer in biological application.

### 3.5.2 *In vivo* intradermal reactivity of p1-50k

To evaluate further the potential of **p1-50k**, *in vivo* toxicity of the extracts after intradermal subcutaneous administration on New Zealand White rabbits was studied following the procedures described in ISO 10993-10 for the corresponding test.

Extract solutions of **p1-50k** products from polar (physiological saline solution) and apolar media (cottonseed oil) were prepared and injected intradermally on different sites from the back of New Zealand White rabbits (n = 2). Erythema and edema formation were monitored during 72 h (see Figure 3.29). The overall mean score of erythema and edema formation was calculated considering the different spots and times in each case (results presented in Figure 3.30).

Interestingly, none of the extracts produced reactivity throughout the assay, since all erythema and edema scoring were below 1.[k] Current results show that **p1-50k** do not present immunologic response after extraction in saline media or cottonseed oil and so they are promising candidates for the development of novel medical grade adhesives to be used in medical devices.

[k]ISO 10993-10 establishes that the assay requirements are accomplished if the final scoring of the sample tested is equal or below 1.

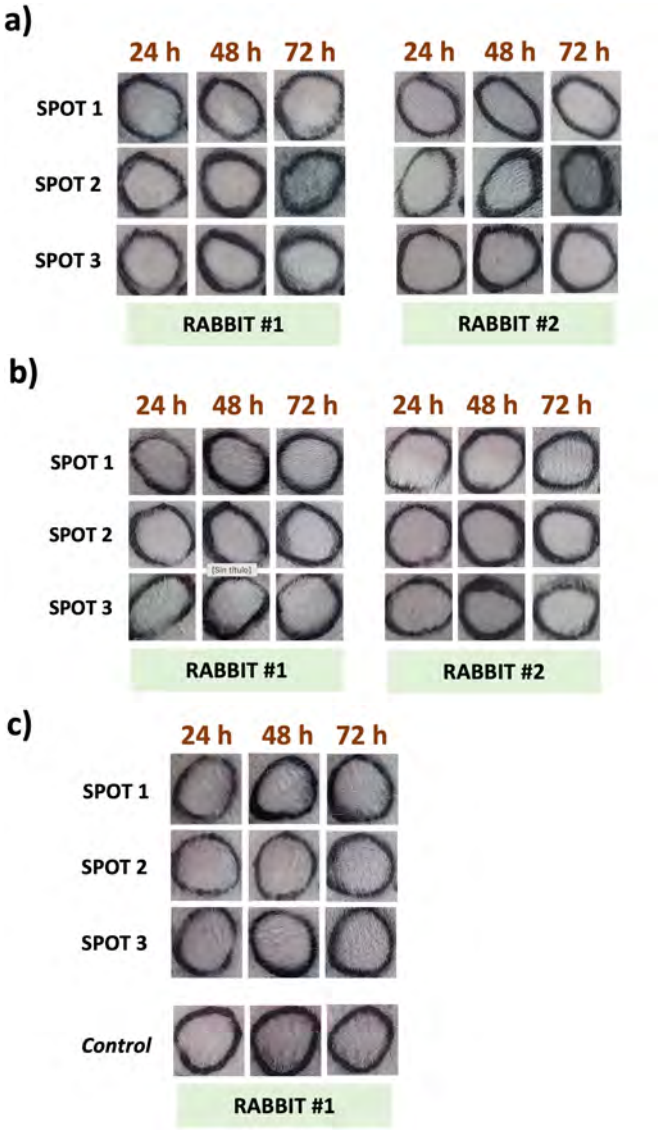


**Figure 3.29.** Images of the progress of the different injection sites of a) control of physiological saline media, b) extract of **p1-50k** in physiological saline media, and c) extracts of **p1-50k** in cottonseed oil and the control, showing no detrimental evolution during the 72 h monitoring.

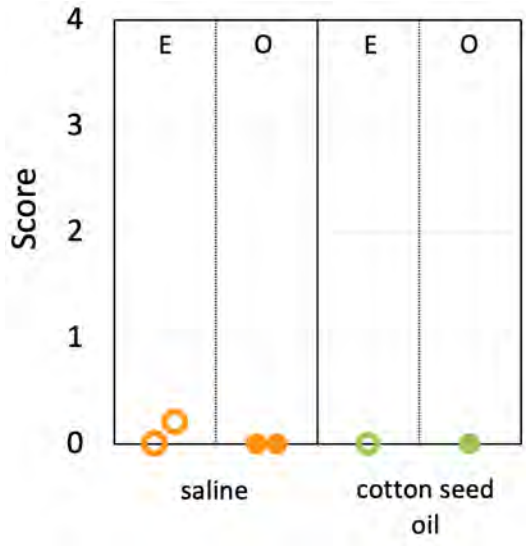


**Figure 3.30.** Results of the scoring of erythema (E) and edema (O) of **p1-50k** extracts in physiological saline media and cotton seed oil.

## 3.6 Cyclic catechol disulfides

### 3.6.1 Synthesis and characterization of cyclic catechol disulfides

As presented in previous sections, the polymerization of monomer **1** under optimized conditions afforded the precipitation of high molecular weight species ($25 - 35\,\%$), while short oligomeric species remained soluble in EtOH media as observed in the GPC elugrams presented previously on Figure 3.21b of page 77.

Similar process occurred in the model polymerization of dithiol **5**. The precipitated part represented between $30 - 75\,\%$ of the final product depending on the reaction conditions as seen previously on Table 3.2.

To check and follow the supernatant over time, polymerization of **5** was done in EtOD-d6 and supernatant was placed into a NMR tube. Reaction conditions were 2 equivalents of iodine with and without $NaHCO_3$, and data was collected from 5 min to 45 min. In none of them, there was observed any variation in the signals with time (see Figure 3.31b and c). Compared to the previous $^1H$ NMR spectrum of **p5-16k** shown (check Figure 3.13 on page 66), supernatant of the reactions presented a new signal at 1.90 ppm. This broad signal corresponds

to the eight-membered ring compound **c5** which is formed as a side product of polymerization reaction from the cyclization reaction of the monomer as described elsewhere for dithiol oxidation[114] (check COSY experiment in Figure 6.23 of Annex). Reported results of oxidation of dithiol **5** are in agreement with this observation.[153] The $^1$H NMR analysis indicates that supernatant is formed by a mixture of **c5** and oligomeric species of **p5**. These oligomeric species of **p5** could be formed by a combination of cyclic and linear species. The presence of a small peak from −SH from its chain end points out the presence of linear species, but cyclic species are expected to be formed as well.[114]

Concerning supernatants of **p1-50k** polymerization, the soluble fraction was isolated after treatment with thiosulfate to reduce the excess of iodine, followed by an extraction in DCM/$H_2O$ to recover the oligomeric product in the organic fraction. $^1$H NMR and MALDI-TOF analysis of these oligomers (Figure 3.32) determined that the product is formed by a mixture of cyclic oligomers (**p1-cyc**). The absence of thiol signals in $^1$H NMR and the unique monoisotopic peak found in MALDI-TOF confirms the formation of cyclic species.[1]

$^1$H NMR showed some clear differences in the spectrum of **p1-cyc** with respect the one of monomer **1** and **p1-50k**. Signals corresponding to H-4 found around 4.1 ppm in $^1$H NMR of monomer **1** and **p1-50k** (check Figures 3.5 and 3.20 on pages 57 and 77, respectively) became a more complex set of signals. There was also the new appearance of a broad signal at 3.05 which must be related to H-6 and H-7 methylenes for the corresponding integration.

Of special interest is the region from 5.5 to 6.0 ppm corresponding to one of the −OH of the catechol moiety. While this signal is a broad singlet in monomer **1** and **p1-50k**, in **p1-cyc** it appears as a set of singlets ending in a broad band.

DOSY analysis of the −OH region of **p1-cyc** showed a clear linear correlation of the signals with the $logD$. With this NMR experiment, signals of different molecular weight species can be separated thanks to their difference diffusion coefficients ($D$). In the case of **p1-cyc** it can be seen how each singlet of −OH region can be related to one different $D$ value (Table 3.6), showing a clear linear correlation of the signals which can be related to oligomers of **p1** up to the hexamer (Figure 3.33).

To analyze more in detail the different species of this system of cyclic disulfides, **p1-cyc** was purified through flash column chromatography as they could be separated clearly by TLC in hexanes:AcOEt (1:3) (Figure 6.24 of Annex). The elution conditions for the column were a gradient of hexanes:AcOEt from 8:2 to 4:6. Six fractions with close retentions were extracted.

$^1$H NMR and $^{13}$C NMR of the third fraction determined the isolation of the

[1]From now on, the mixture cyclic oligomers will be named as **px-cyc** where $x$ is the molecule number.

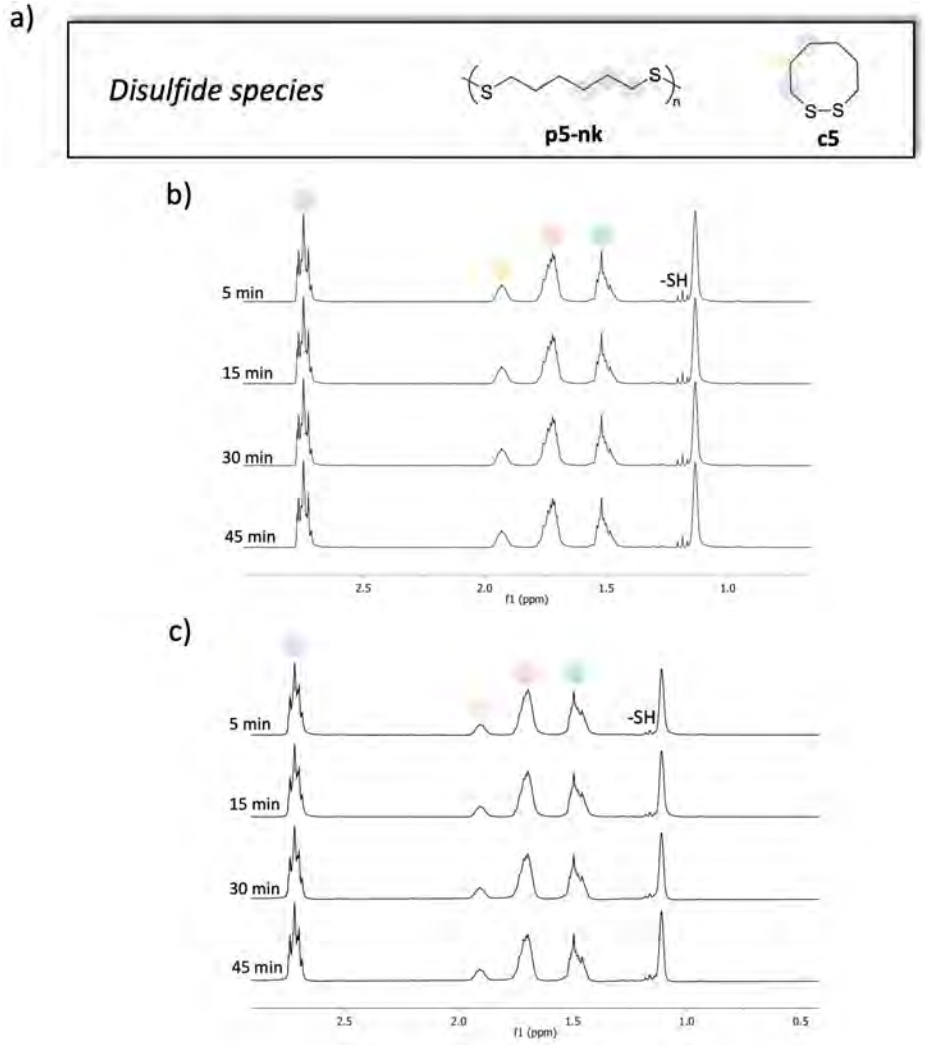


**Figure 3.31.** a) Disulfide species formed during the polymerization of **5**; b) $^{1}$H NMR of supernatant in polymerization of **5** with 2 equivalents of iodine without $NaHCO_3$; and c)$^{1}$H NMR of supernatant in polymerization of **5** with 2 equivalents of iodine with $NaHCO_3$. EtOD-d6 with 4 % $D_2O$ was used as solvent for $^{1}$H NMR.

cyclic disulfide **c1**. The corresponding $^{1}$H NMR and $^{13}$C NMR assignments of this catechol pendant macrocycle are presented in Figure 3.34. All these assignments

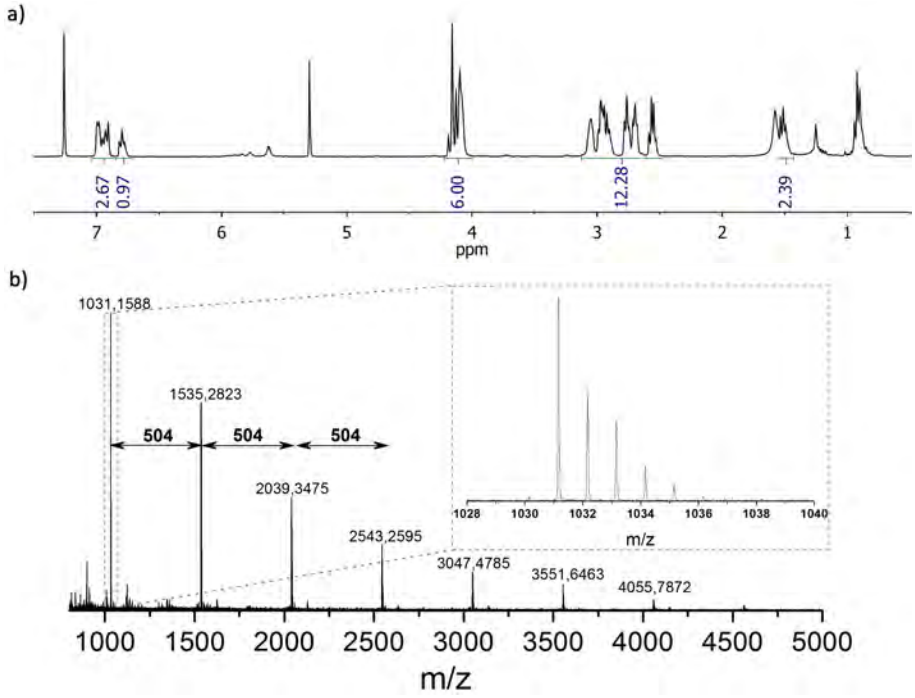


**Figure 3.32.** a) $^1$H NMR of oligomeric mixture of **p1**, and b) MALDI-TOF analysis of oligomeric mixture and zoom in of the dimer peak showing its corresponding isotopic distribution.

**Table 3.6.** Experimental diffusion coefficient of cyclic catechol poly(disulfide)s obtained from DOSY experiments in $CDCl_3$.

| **n** | $D \cdot 10^{10}$ **(m$^2$/s)** |
|---|---|
| 1 | 9.10 |
| 2 | 6.90 |
| 3 | 5.93 |
| 4 | 5.30 |
| 5 | 4.94 |
| 6 | 4.86 |

were supported by COSY, DEPT135, HSQC and HMBC experiments. As it can be seen in the $^1$H NMR spectrum, just one singlet at 5.65 from −OH appears, which coincides with the first peak of the −OH region of the DOSY of Figure

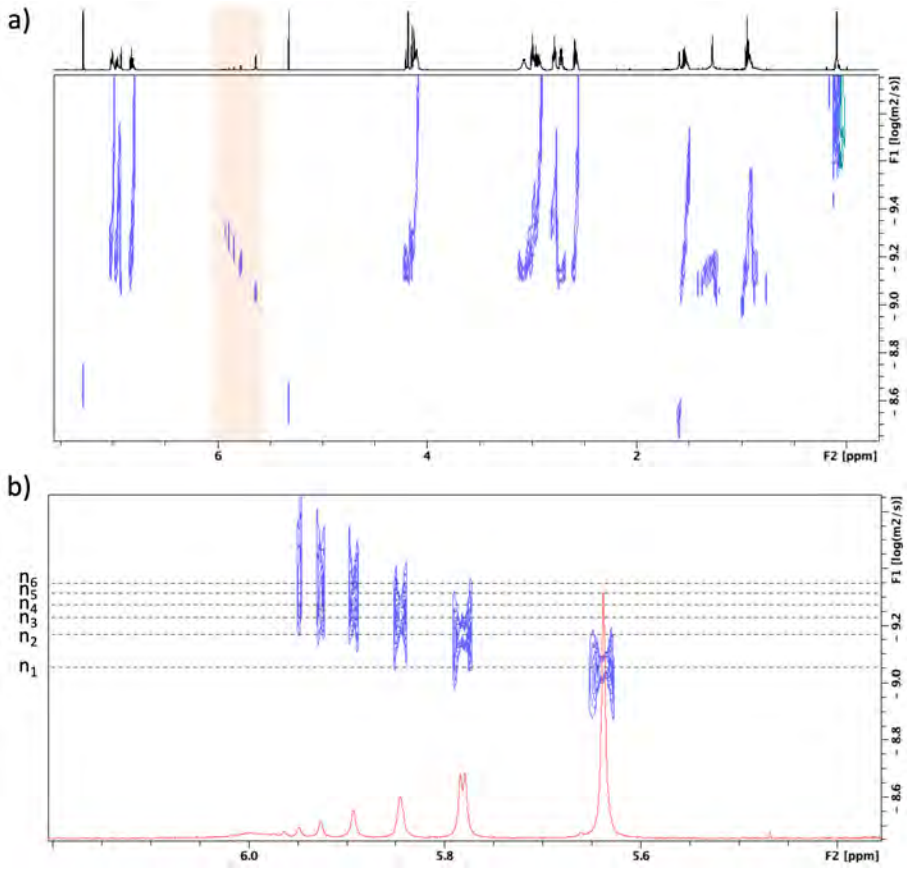


**Figure 3.33.** a) DOSY of **p1-cyc** in $CDCl_3$ with −OH region pointed out, and b) overlapped DOSY and $^1$H NMR of the −OH region of interest, with the assignment of the different cyclic $n$-mers.

3.33. Signals corresponding to protons H-4 and H-4' are shown as the sum of a singlet and two doublets with high coupling ($J_{HH} = 11.3$ Hz). While all these six protons (H-4 and H-4') are homotopic in monomer **1** from the free rotation, four of them become diastereotopic in cyclic compound **c1** due to the conformational restriction of the cycle. Protons H-4' from the branch containing pendant catechol remain homotopic and, hence, still a singlet. Protons H-4 turn into two doublets (one of them overlapped with H-4') from the coupling with each partner. The four protons H-4 appear as two doublet suggesting certain symmetry in the molecule. Concerning $^{13}$C NMR of **c1**, C-7 is displaced towards higher ppm in **c1** with

respect monomer **1** which is directly related with disulfide formation. The signals of other carbons remain similar to those in monomer **1** with minimum changes in chemical shift.

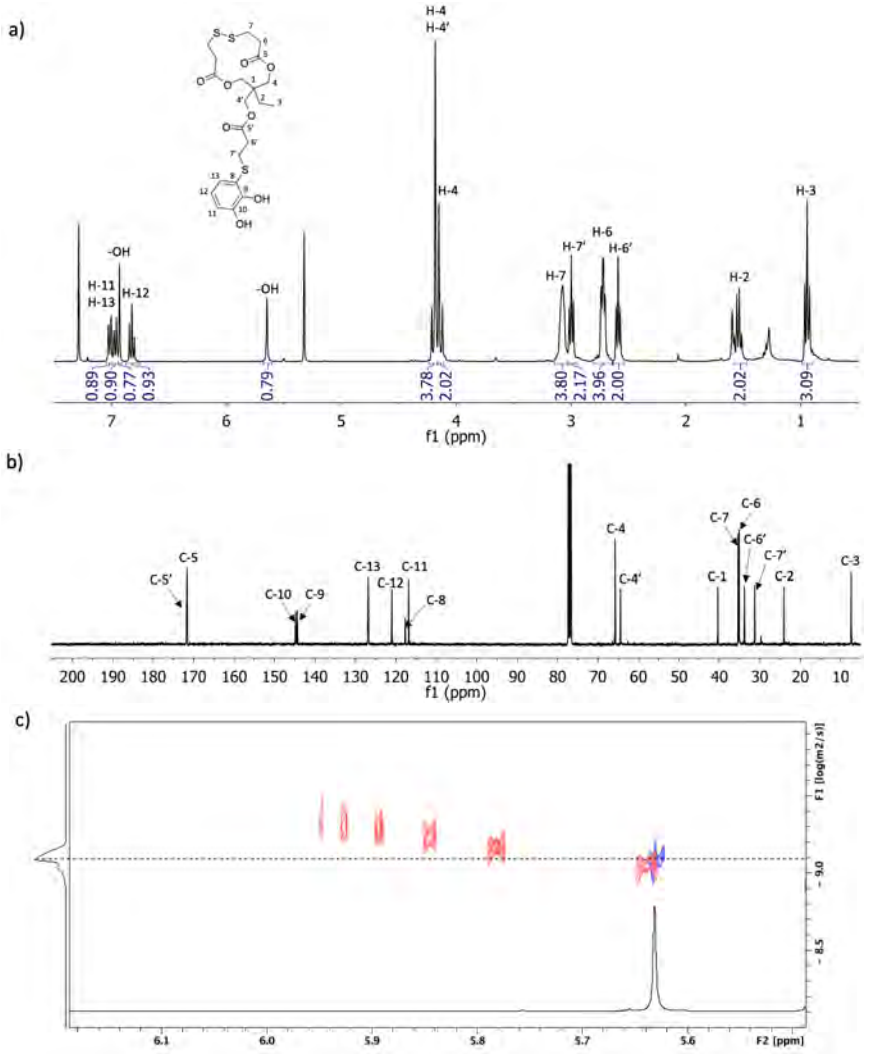


**Figure 3.34.** a) $^{1}$H NMR, and b) $^{13}$C NMR assignments of cyclic catechol disulfide **c1**; c) DOSY of **c1** (blue) overlapped with $^{1}$H NMR of **c1** (black) and DOSY of **p1-cyc** (red) in the −OH region.

For the case of **c1** the most stable conformer of the 13-membered ring macrocycle is presented in Figure 3.35a.[m] This conformer of lower energy, obtained using the improved ETKDG conformer generator,[154] would present one pair of H-4 oriented within the cycle and the other H-4 pair facing the outer part of the cycle. NMR studies were done at 300 K and no further analysis varying temperature were done with this compound to get further conformational information of this compound. To fully assign properly protons H-4, it would be required more specific studies with NMR that are out of the scope of this work.

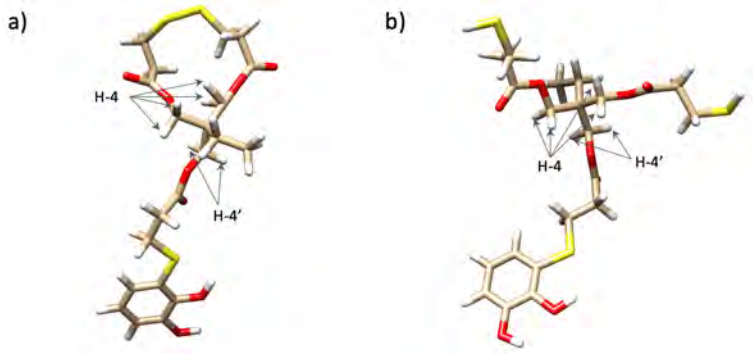


**Figure 3.35.** 3D structure of most stable conformers of a) compound **c1** and b) monomer **1** showing H-4 and H-4' protons and the conformational restriction due to cyclization through disulfide formation.

$^1$H NMR and DOSY of other fractions obtained from the flash column chromatography of **p1-cyc**, showed that they were composed by mixture of cycles. Fourth fraction analysis in Figure 3.36a (next after **c1** isolation), presented two peaks in the −OH region at 5.68 and 5.80 ppm, which clearly corresponds to $n_1$ (**c1**) and $n_2$. Analysis of fifth fraction (Figure 3.36b) showed peaks at 5.80, 5.87 and 5.92 ppm, without any signal of the singlet at 5.68 from **c1**. These results confirmed that each singlet of the −OH region between 5.6 and 6.0 ppm can be related to a given cyclic *n*-mer as suggested by DOSY of **p1-cyc** and, hence, these −OH signals can be used to determine the mixture of cycles present in a sample of **p1-cyc**.

The formation of cyclic oligomers is known to be driven by the concentration of the system since higher dilutions favors the intramolecular reaction. To know this effect of the polymerization of monomer **1**, the undergraduate student Pau Delgado Melgares, as a part of his final bachelor's project, carried out a series of

[m]To check the conformers of other oligomeric macrocyclic catechol disulfides see Figures in the Annex

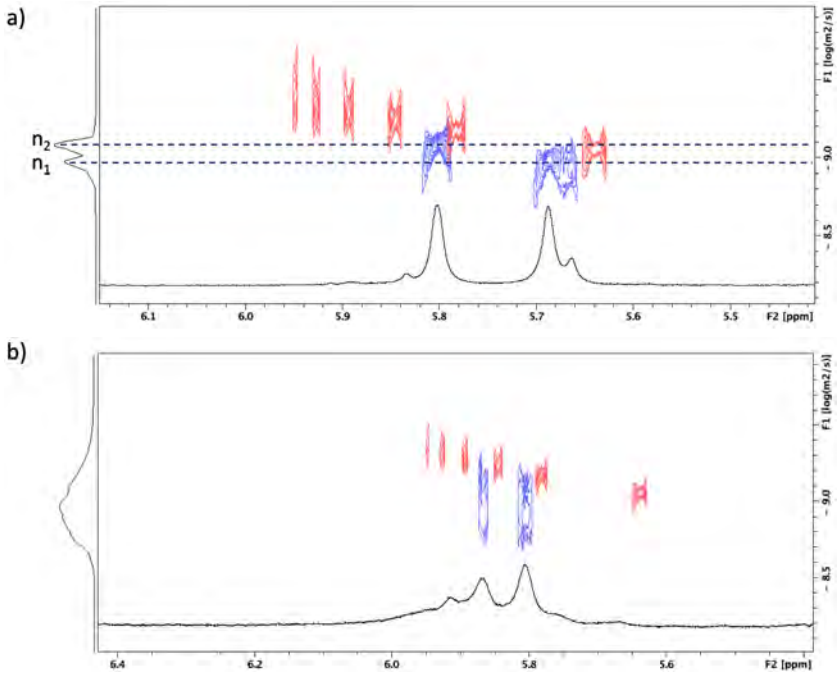


**Figure 3.36.** a) DOSY of fourth fraction (blue) overlapped with its $^{1}$H NMR (black) and DOSY of **p1-cyc** (red) in the −OH region, and b) DOSY of fifth fraction (blue) overlapped with its $^{1}$H NMR (black) and DOSY of **p1-cyc** (red) in the -−OH region.

experiments oxidizing monomer **1** with 1.5 equivalents of iodine at 1, 5, 10 and 20 mM, and isolating and analyzing the supernatant. That study revealed the clear tendency towards the formation of **c1** at higher diluted reactions, and could be followed properly through the pattern of the −OH region between 5.6 and 6.0 ppm (Figure 3.37). These results proves the possibility of tuning the distribution of the cycles, increasing the amount of **c1** with respect to bigger disulfide macrocycles. However, high diluted systems below 1 mM would be required to obtained pure **c1** without presence of other extended cyclic disulfides.

Furthermore, in the same study, reactions with 0.75 equivalents of iodine were also performed, to consider the mixtures of cyclic and linear species. Interestingly, the region between 5.6 and 6.0 ppm (see Figure 6.26 in Annex) did not present any distinguished pattern of signals like in the case of **p1-cyc**, but instead the −OH region has a highly noisy undefined signal patterning. These clear difference could indicate that the cyclic configurations can affect to this −OH signal patterning due to intramolecular interactions of the cyclic structures. To confirm

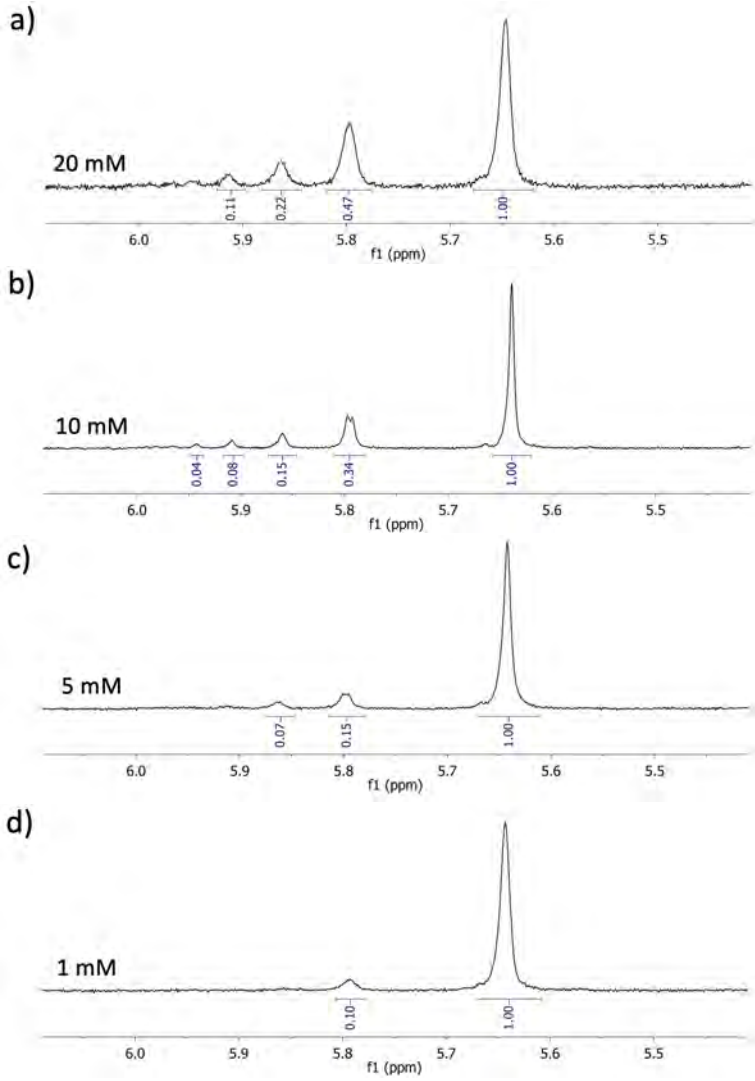


**Figure 3.37.** $^{1}$H NMR of −OH region from the synthesis of cyclic oligomeric catechol disulfides at different concentrations, a) 20 mM, b) 10 mM, c) 5 mM and d) 1 mM. Data courtesy of Pau Delgado Melgares.

this hypothesis, specific simulation and molecular dynamics studies that are out of the scope of the present work should be performed.

### 3.6.2 Heat-induced ROP of cyclic catechol disulfides

Although polymerization via ROP can be achieved above $T_m$ of disulfide cycles as explained in Section 1.4 Poly(disulfide)s, generally disulfide bonds are cleaved above 150 °C to produce fast reactions.[104,135,151,152]

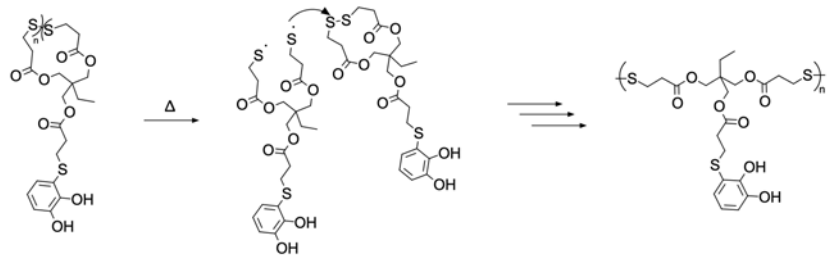

**Figure 3.38.** Reaction scheme of ROP of cyclic oligomeric mixture of catechol poly(disulfide)s **p1-cyc**

Cyclic catechol disulfides **p1-cyc** were polymerized by heating up the mixture at 175 °C without solvent (see scheme of Figure 3.38). The mixture started completely liquid upon heating and became rubbery after 10 minutes of reaction. $^1$H NMR analysis of the product at different times confirmed the polymerization by ROP. On one side, the singlet at 4.1 ppm corresponding to the protons H-4 and H-4' increases with time, while the set of signals corresponding to cyclic monomer **c1** are reduced (see Figure 3.39a). Moreover, signals corresponding to H-6 and H-7 also change, which is partially in accordance with the chain extension through ROP as well. DOSY analysis of the −OH region of the final product soluble in $CDCl_3$ also indicated the extension of the chain from the decrease of the peaks coming from low $n$ oligomers and the appearance of a broader band with lower diffusion coefficient (see Figure 3.39b).[n]

The presence insoluble product in $CHCl_3$ led to the hypothesis of a cross-linking in the system, since **p1-50k** is completely soluble in $CHCl_3$. Catechol functionality of the polymer is one of the potential inducers to the cross-linking of the system. If oxidized to *o*-quinone, it could be produced covalent bonding between catechols. Furthermore, the radical scavenging nature of catechols could also interfere by removing thiyl radicals formed in the ROP and resulting in side reactions. Aromatic region in $^1$H NMR of the soluble fraction seems to suffer some variation, but no apparent differences can be determined to extract clear conclusions.

[n] It is worth to mention that above 10 minutes of reaction when the final product became rubbery, there was always a fraction completely insoluble in $CDCl_3$ which could not be characterized by $^1$H NMR.

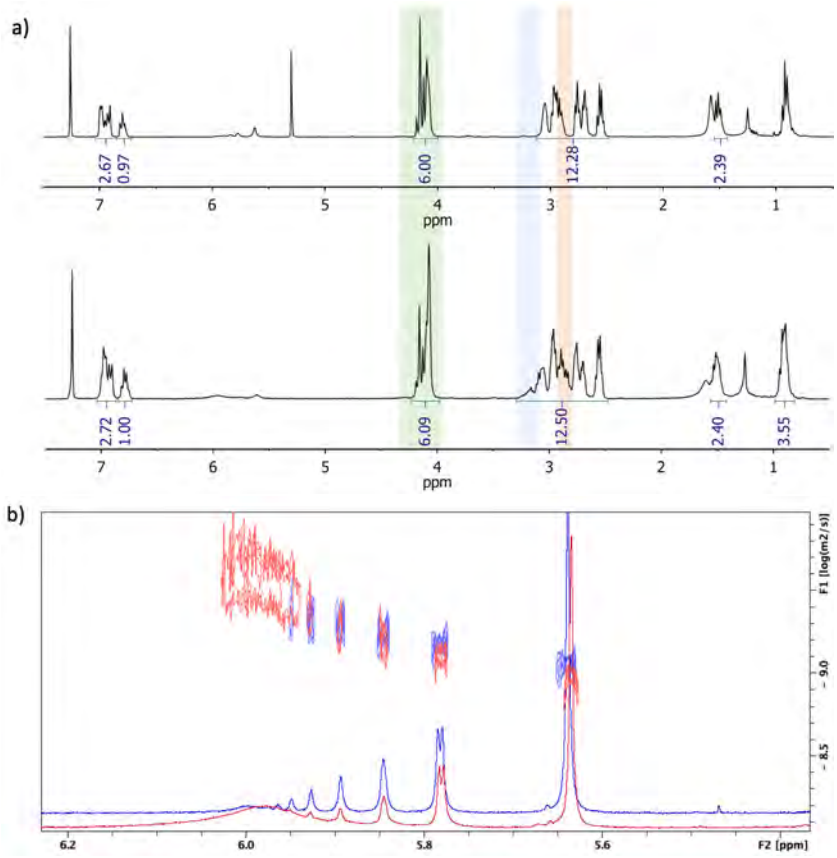


**Figure 3.39.** a) On top, $^{1}$H NMR of **p1-cyc**, on the bottom $^{1}$H NMR of **p1-cyc** after heat-induced ROP; and b) overlapped $^{1}$H NMR and DOSY analysis of −OH region of **p1-cyc** before and after heat-induced ROP (blue and red respectively).

With respect to the signals close to disulfide, $^{1}$H NMR of ROP product from **p1-cyc** shows changes and the appearance of new peaks in the region of H-6 and H-7 which do not fit with the signals of **p1-50k**. Among the possible effects causing these changes in the signals of H-6 and H-7 it could be considered: i) a reaction with catechol/quinone after the homolytic cleavage of disulfide, ii) the over oxidation of disulfide to higher oxidation states from the presence of atmospheric oxygen or iii) changes in chemical shifts due to local environment in an interlocked polycatenane-like structure.

The reaction of a thyil radical with catechol could be a possibility and has been

previously discussed in Section 3.4. With the data from $^{1}$H NMR analysis this hypothesis cannot be neither confirmed nor completely discarded. To evaluate further this hypothesis, the model reaction between an alkyl disulfide **15** and pyrocatechol **3** was studied heating up to 175 °C overnight, without observing reaction by $^{1}$H NMR.

The possibility of over oxidation of disulfides to thiouslfinates or thiosulfonates, among others, could also explain the appearance of these signals with higher chemical shift.[155] Although the over oxidation of disulfides after ROP at high temperatures has not been described after heat-induced disulfide cleavage in similar reported systems,[104,135,151,152] the oxidation to thiosulfinates has been already described in acetylated catechol derivatives.**??** MALDI-TOF analysis of ROP product from **p1-cyc** showed the presence of oxygenated species which would confirm the presence of thiosulfinates and thiosulfonates. In Figure 3.40 it is presented the MALDI-TOF spectrum of the region corresponding to the macrocycle of the dimer. As is can be seen, there can be found different sequential peaks separated by 32 Da, indicating the possible oxidation of the two disulfide bonds presented in the dimeric macrocycle. Despite the fact that over oxidation can be demonstrated by MALDI-TOF, this oxidation should not affect the cross-linking of the system, so this effect would not be the only one occurring during the heat-induced ROP of cyclic catechol disulfides, but could explain the appearance of new $^{1}$H NMR signals in the region of H-6 and H-7.

Another possibility for the cross-linking of the system could be the physical interlocking between macrocycles. Some reported examples involving the polymerization of cyclic disulfides has suggested the formation of interlocked system after ROP in polycatenane-like architecture,[107,117,118] although other studies have discarded this idea.[120] To study more in detail our system and with the aim of elucidating final structure, selective NOE experiments were performed looking for further information about the local environments in the system.

The use of NOE experiments could help in the elucidation of the final structure since the appearance of new NOE peaks of the oligomeric mixture of catechol poly(disulfide)s **p1-cyc** before and after ROP could be related to local interlocking.

Selective NOE of different isolated species (monomer **1** and cyclic monomer **c1**) were tackled before the study of **p1-cyc** to obtain a full picture of the system (see NOE assignments in Figures 6.27 and 6.28 in the Annex).

Region of protons H-6 and H-7 was considered the most interesting to be studied. On one side, the NOE experiments showed that protons H-6 and H-7 had less couplings in both monomer **1** and cyclic monomer **c1**. On the other side, this region was the one presenting differences in the $^{1}$H NMR of ROP product from **p1-cyc**. Selective NOE of the new signals from H-6 and H-7 region (Figure 3.41) showed the coupling between them and no other protons, which did not

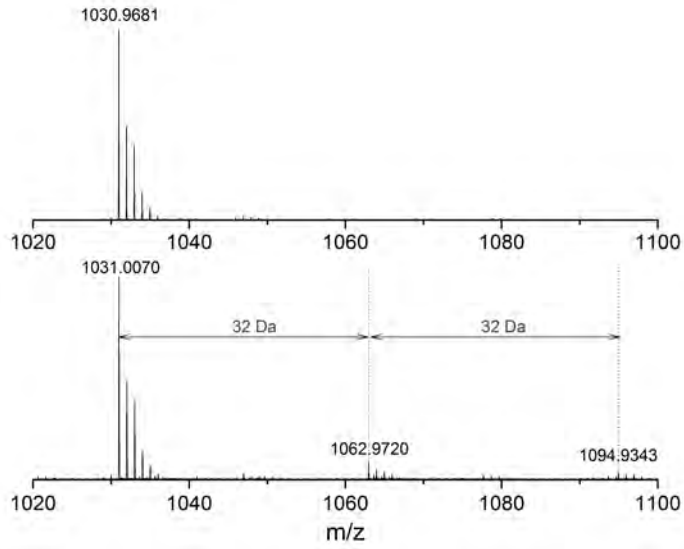


**Figure 3.40.** On top, MALDI-TOF peaks observed in the region corresponding to the dimer showing a single set of peaks. On the bottom, MALDI-TOF peaks observed in the region corresponding to the dimer showing different set of peaks separated by 32 Da demonstrating the possible oxidation of the cyclic macrocycles.

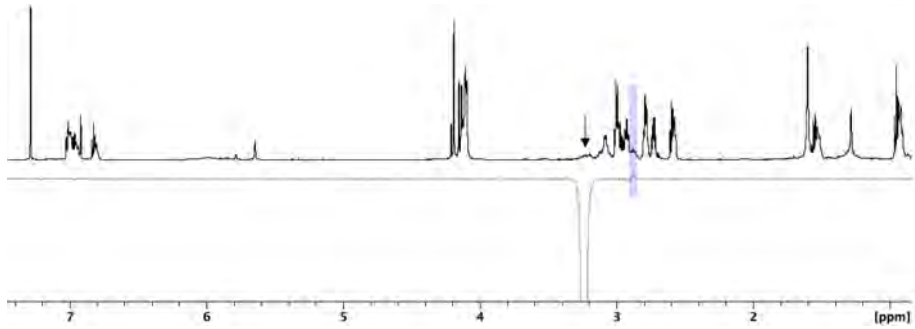


**Figure 3.41.** Overlapped $^{1}$H NMR spectra and selective NOE experiment of the signal at 3.22 ppm

contribute in gaining more structural information.

Despite the efforts in elucidating the structure of the final polymer from the ROP of **p1-cyc** and confirming the oxidation of disulfides by MALDI-TOF, the suggested hypotheses about cross-linking through catechol or via chain interlock-

ing in polycatenane-like structure could not be confirmed or discarded. Further studies would be required to reach full understanding of this complex system involving cyclic disulfides and catechols.

### 3.6.3 The use of cyclic catechol disulfides for the design of adhesives via ROP

ROP of **p1-cyc** was used to develop a new strategy for obtaining adhesive formulations based on this catechol poly(disulfide)s. For testing the adhesion of these materials, **p1-cyc** was applied on different substrates and the joints were cured during 30 minutes at 175 °C. Same process was used for the 'blank' reference **p1-cyc**, which was obtained form the soluble fraction of the synthesis of **p8-29k**. TGA of the products of ROP are presented in Figures 6.10 and 6.11 in the Annex.

The results of adhesion after lap-shear testing on glass, copper, aluminum, stainless steel and titanium with different bonding and rebonding cycles are presented in Figure 3.42. In all substrates, **p1-cyc** products showed good adhesion compared to **p8-cyc**.

Glass substrates experienced fissure and substrate failure after the first tests. Maximum adhesion recorded for **p1-cyc** products reached a value of 2.7 ± 0.4 MPa. Substrates from **p8-cyc** had an increase of the adhesion from 0.3 ± 0.1 MPa to 0.7 ± 0.2 MPa in the third rebonding cycle. This increase could come as a consequence of further polymerization from the cumulative curing process between cycles of bonding/rebonding. The forth and last cycle could not be tested in **p8-cyc** samples due to substrate failure of three specimens of five. Both **p1-cyc** and **p8-cyc** presented cohesive failure.

In copper substrates the adhesion of **p1-cyc** products reached a maximum of 2.1 ± 0.4 MPa after the third bonding/rebonding cycle. The adhesion remained similar along the bonding/rebonding cycles. However, **p8-cyc** presented a shear strength of 0.3 ± 0.1 MPa without a clear increase in time. Both **p1-cyc** and **p8-cyc** presented cohesive failure.

The adhesion of **p1-cyc** products in aluminum increased from 1.7 ± 0.1 MPa in the first bonding/rebonding cycle to 2.3 ± 0.2 MPa in the third one. In case of **p8-cyc** the adhesion also increased from 0.07 ± 0.03 MPa in the first bonding/rebonding cycle to 0.5 ± 0.1 MPa in the fourth. Both **p1-cyc** and **p8-cyc** presented cohesive failure.

Stainless steel presented the lower results of all of them. For **p1-cyc** and adhesion of 0.7 ± 0.2 MPa was achieved in the first bonding/rebonding cycle and increased up to 1.6 ± 0.1 MPa in the third cycle. Specimens from **p8-cyc** presented poor adhesion, with a maximum value of 0.010 ± 0.003 kPa in the fourth cycle. Both **p1-cyc** and **p8-cyc** presented cohesive failure.

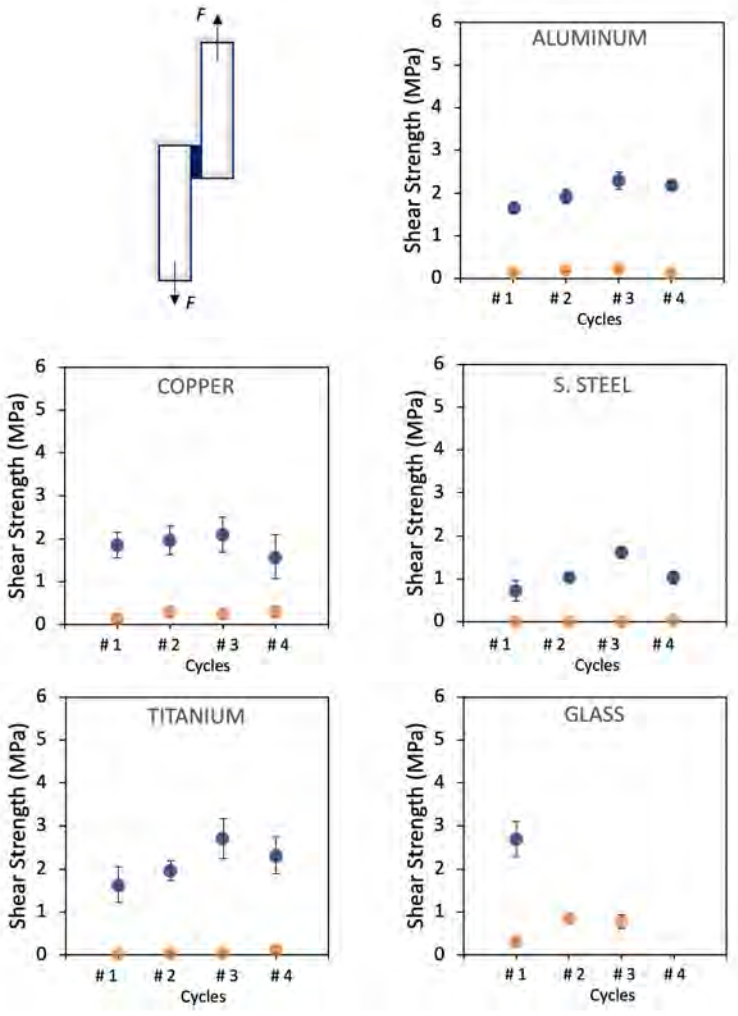


**Figure 3.42.** Shear strength results of **p1-cyc** (blue dots) and **p8-cyc** (orange dots) after ROP on aluminum, copper, stainless steel, titanium and glass.

The adhesion of **p1-cyc** on titanium was similar to the aluminum case. The adhesion values increased from 1.6 ± 0.4 MPa in the first bonding/rebonding cycle to 2.7 ± 0.5 MPa in the third one. Regarding **p8-cyc**, the adhesion also increased from 0.007 ± 0.001 kPa in the first bonding/rebonding cycle to 0.13 ± 0.08 kPa in the fourth. Both **p1-cyc** and **p8-cyc** presented cohesive failure.

## 3.7 Adhesive benchmarking and summary

The adhesion of a commercial EVA based hot melt adhesive and a cyanoacrylate (Loctite®, Henkel) were studied as for comparative means with the catechol poly(disulfide)s **p1-50k** and **p1-cyc** following the same procedure (see Figure 3.43). In the case of the EVA based hot melt, bonding/debonding cycles with temperature were performed taking advantage of its high reprocessability at 100 °C. Both adhesive formulations presented high shear strength results between 3 – 4 MPa in all substrates. Glass substrates suffered substrate failure and fracture due to the high adhesion. Both for EVA based hot melt and cyanoacrylate, adhesive failure was observed. Furthermore, through the bonding/debonding cycles of the commercial EVA based hot melt adhesive the material did not present significant increase or decrease of the performance.

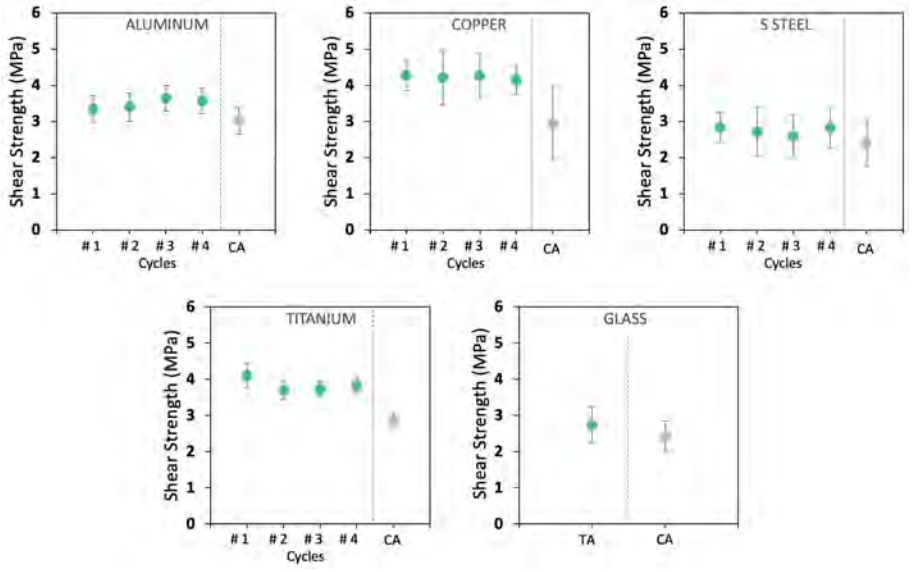


**Figure 3.43.** Shear strength results of a commercial EVA based hot melt adhesive (green dots) during bonding/debonding cycles and a commercial cyanoacrylate (gray dots, CA) on aluminum, copper, stainless steel, titanium and glass.

Previous results with **p1-50k** and **p1-cyc** set a precedent for these new approaches based on catechol containing polymers. In most of the substrates, the adhesion strength was above 1 MPa and could reach maximums close to 4 MPa, which is within the range of commercial adhesive formulations. While commercial hot melts and cyanoacrylates tend to fail in the adhesive component, catechol

poly(disulfide)s have failure from cohesion. To improve the cohesion of the system several points such as the optimization of curing process (temperature, timing, etc.) or the addition of fillers could enhance the final performance to achieve adhesion values closer or greater than commercial adhesives tested.

## 3.8 Experimental section

### 3.8.1 Materials

All commercially available reagents were purchased from Sigma Aldrich and used as received unless specified otherwise. Synthesis-grade solvents were purchased in Scharlab S.L and used without further purification. When needed, reactions were performed avoiding moisture by standard procedures and under $N_2$ or Ar atmosphere. Mili-Q water (18.2 m$\Omega$·cm) was used in all cases.

### 3.8.2 Characterization

**NMR**

$^1$H NMR and $^{13}$C NMR spectra were recorded with Bruker DPX360 and 400 MHz Bruker Avance III spectrometers. DOSY and NOE experiments were performed in a 600 MHz Bruker Avance II. Mestre Nova and TopSpin softwares were use for the analysis and treatment of the data. NMR signals were assigned by correlating the data acquisition of $^1$H NMR and $^{13}$C NMR, COSY, DEPT 135, HSQC and HMBC experiments.

The abbreviations used to describe multiplicities are: s (singlet), bs (broad singlet), d (doublet), t (triplet), q (quartet), dd (double doublet), m (multiplet).

In DOSY experiments, 15 mg/mL samples were prepared in $CDCl_3$. Acquisition parameters set in all cases were a gradient range of 2-95 %, a diffusion delay of 100 ms, 16 gradient steps, temperature of 300 K and sample spinning to avoid convection issues. Pulse sequence used was ledbpgp2s. Selective NOE experiments were performed with sample concentration of 15 mg/mL.

**GPC**

Molecular weights were found by gel permeation chromatography (GPC) using an Agilent Technologies 1260 Infinity chromatograph and THF solvent. The instrument is equipped with three gel columns: PLgel 5 $\mu$m Guard/50x7.5 mm, PLgel 5 $\mu$m 1000 Å MW 4K-400K, and PL Mixed gel C 5 $\mu$m MW 200-3M. Calibration was made by using PMMA standards. In each experiment, the polymer sample of interest was dissolved in THF (2 mg/mL) and analyzed by GPC (1 mL/min flow; 40 °C column temperature). Before GPC analysis the presence of peroxides in the THF was checked with an iodide salt to confirm its absence. Presence of peroxides in the THF must be avoided due to their impact in the analysis of catechol poly(disulfide)s due to side reactions.

**MALDI-TOF**

Mass analysis was performed on a Bruker Daltonics Ultraflextreme MALDI-TOF

using positive reflectron mode. Samples for MALDI-TOF were prepared by mixing 50 $\mu$L of the analyte solution in $CHCl_3$ (1 mg/mL) and 50 $\mu$L of dithranol solution in $CHCl_3$ (1.7 mg/mL) as a matrix. A volume of 1.5 $\mu$L of the sample solution was deposited on the target plate (MP 384 Polished Steel, Bruker Daltonics). Calibration was done by using Peptide Calibration Standard of Bruker following recommended sample preparation protocol with HCCA matrix. The software mMass was used for the visualization and analysis of the data.

**IR**
Fourier transform infrared spectroscopy (FTIR) was carried out with a Bruker Tensor 27 FTIR spectrometer. Each spectrum was acquired from 400 to 4000 $cm^{-1}$ at a spectral resolution of 2 $cm^{-1}$. OPUS software was used for the analysis and treatment of the data.

**UV-Vis**
The absorption spectra of solid samples were measured through diffuse reflectance mode, using an external integrating sphere connected with a fiber optic from a Cary 60 spectrophotometer. As a reference, the pristine materials without adhesives were used. The absorption spectra were estimated from the measured diffuse reflectance spectra through the Kubelka-Munk equation ($F(R) = (1–R)2/2R$).[156]

**DSC**
Measurements were carried out in a Perkin Elmer DSC8500 LAB SYS differential scanning calorimeter equipped with a CRYOFILL liquid $N_2$ controller. Scanned temperature range went from - 20 to 200 °C and the scanning rate was 10 K/min for the heating and the cooling process with $N_2$ atmosphere.

**TGA**
Thermal decomposition was studied with a NETZSCH-STA 449 F1 Jupiter with $N_2$ atmosphere. All samples were heated at a heating rate of 10 K/min.

**Optical Microscopy (OM)**
Optical microscopy images were obtained with a Zeiss Axio Observer Z-1 inverted optical microscope, equipped with five magnification lenses (5x, 10x, 20x, 50x and 100x). Images of non-transparent substrates were obtained in reflectance mode.

**Profilometry**
Characterization of surface roughness was obtained from a Profilm3D Optical 3D Profiler (Filmetrics, San Diego, CA, USA). Acquisition was started when interference pattern was formed on the surface of study. Data collected was analyzed with Gwyddion v2.49 software.

## 3.8.3 Synthetic procedures

### 3.8.3.1 Synthesis of monomer 1

For the preparation of **1**, purified trimethylolpropane tris(3-mercaptopropionate) (4.6 g, 11.5 mmol) was dissolved in DCM (10 mL) and TFA (2.3 mL, 30.0 mmol) was added over the previous solution. Separately, a solution of $NaIO_4$ (2.3 g, 10.7 mmol) in miliQ $H_2O$ (350 mL) was prepared and cooled down in an ice bath. Pyrocatechol (1.1 g, 10.0 mmol) dissolved in $Et_2O$ (5 mL) was added to the aqueous solution when temperature was below 5 °C, keeping vigorous stirring for 10 min. The orange-reddish *o*-benzoquinone formed was then extracted with DCM (5 x 200 mL) and the organic phase was dried with anhydrous $Na_2SO_4$, filtered and added immediately to the thiol containing solution. The reaction mixture was stirred at room temperature for 8 h. After this time, the solvent and the TFA were evaporated in a rotary evaporator under reduced pressure. The crude was purified by flash column chromatography through silica gel (using a gradient of hexanes:EtOAc, 9:1, 7:3, 6:4) affording **1**. Purification yielded 2.0 g (40 %). As a general procedure, product obtained required further purification because of the presence of disulfide **10** from the starting trimethylolpropane tris(3-mercaptopropionate). To remove the disulfide impurity, the obtained product (2.0 g, 4.0 mmol) was dissolved in 10 % aqueous MeOH (300 mL). Then, tributylphosphine (200 $\mu$L, 0.8 mmol) dissolved in acetone (3 mL) was added over the previous solution, leaving the reaction progress during 1 hour at room temperature and aerobic conditions. After this time, the solvent was evaporated under vacuum and the crude of reaction purified by flash column chromatography trough silica gel using (hexanes:EtOAc, 6:4). Monomer **1** was obtained as a colorless oil (1.9 g, 3.9 mmol, 39 %).

**$^1$H NMR** (600 MHz, $CDCl_3$): $\delta$(ppm) 6.99 (dd, $J$ = 7.8, 1.7 Hz, 2H), 6.94 (bs, 1H), 6.93 (dd, $J$ = 8.0, 1.7 Hz, 1H), 6.79 (dd, $J$ = 8.0, 7.8 Hz, 1H), 5.65 (bs, 1H), 4.19 (s, 6H), 2.97 (t, $J$ = 6.4 Hz, 2H), 2.77 (q, $J$ = 7.0 Hz, 4H), 2.68 (t, $J$ = 6.3 Hz, 4H), 2.54 (t, $J$ = 6.4 Hz, 2H), 1,64 (t, $J$ = 8.1 Hz, 1H), 1.51 (q, $J$ = 7.7 Hz, 2H), 0.92 (t, $J$ = 7.7 Hz, 3H).

**$^{13}$C NMR** (100.6 MHz, $CDCl_3$): $\delta$(ppm) 171.8, 171.5, 144.9, 144.5, 126.8, 121.0, 117.9, 116.9, 64.2, 63.9, 40.8, 38.5, 33.9, 31.3, 23.0, 19.8, 7.4.

**IR** (neat): ($cm^{-1}$) 3405, 2967, 2942, 2565, 1727, 1587, 1458, 1388, 1354, 1245, 1223,1189, 1137, 1056, 1010, 935, 898, 777, 727, 674, 638, 567, 534, 482.

**Elemental Anal.** Calcd for $C_{21}H_{30}O_8S_3$: C, 49.79; H, 5.97; S, 18.98. Found: C, 49.67; H, 6.00; S, 19.34.

#### 3.8.3.2 Synthesis of monomer 7

For the preparation of monomer **7**, purified trimethylolpropane tris(3-mercaptopropionate) (0.7 g, 1.7 mmol) and styrene (0.2 mL, 1.7 mmol) were dissolved in dry toluene (10 mL) in a Schlenk round-bottom flask. Azobisisobutyronitrile (AIBN, 49 mg, 0.3 mmol) was added and the reaction was heated up to reflux with vigorous stirring under inert atmosphere for 7 h. After this time, the solvent was evaporated in a rotary evaporator under reduced pressure obtaining a pale-yellowish oil. The obtained crude was purified by flash column chromatography trough silica gel using a gradient of hexanes:EtOAc (hexanes:EtOAc, 1:0, 9:1, 8:2, 7:3). Pure compound **7** could not be obtained as mentioned in the corresponding section.

#### 3.8.3.3 Synthesis of monomer 8

For the preparation of monomer **8**, purified trimethylolpropane tris(3-mercaptopropionate) (4.0 g, 10.0 mmol) and 3,4-dimethoxystyrene (1.5 mL, 10.1 mmol) were dissolved in dry toluene (100 mL) in a Schlenk round-bottom flask. Azobisisobutyronitrile (AIBN, 164 mg, 1 mmol) was added and the reaction was heated up to reflux with vigorous stirring under inert atmosphere for 7 h. After this time, the solvent was evaporated in a rotary evaporator under reduced pressure obtaining a pale-yellowish oil. The obtained crude was dissolved in 300 mL of 10 % aqueous MeOH and then tributylphosphine (200 $\mu$L, 0.8 mmol) dissolved in 3 mL of acetone was added, leaving the reaction progress during 1 hour at room temperature and aerobic conditions. Finally, the solvent was evaporated under vacuum and the crude of reaction purified by flash column chromatography trough silica gel using (hexanes:EtOAc, 7:3). Monomer **8** was obtained as a colorless oil (2.0 g, 3.6 mmol, 36 %).

**$^1$H NMR** (400 MHz, $CDCl_3$): $\delta$(ppm) 6.78 (d, $J$ = 8.0 Hz, 1H), 6.73 (d, $J$ = 8.0 Hz, 1H), 6.71 (s, 1H), 4.06 (s, 2H), 4.05 (s, 4H), 3.86 (s, 3H), 3.84 (s, 3H), 2.75-2.61 (m, 16H), 1.48 (q, $J$ = 7.6 Hz, 2H), 0.88 (t, $J$ = 7.6, 3H).

**$^{13}$C NMR** (100.6 MHz, $CDCl_3$): $\delta$(ppm) 171.6, 171.3, 149.1, 147.8, 133.1, 120.5, 112,0, 111.5, 64.0, 63.9, 56.0, 55.9, 40.9, 38.5, 35.9, 34.9, 34.1, 27.3, 23.1, 19.8, 7.5.

**IR** (neat): ($cm^{-1}$) 2963, 2939, 2835, 2573, 2563, 1730, 1607, 1590, 1514, 1464, 1417, 1387, 1353, 1257, 1236, 1189, 1142, 1026, 935, 855, 807, 763, 711, 675, 618, 596, 556.

**Elemental Anal.** Calcd for $C_{25}H_{38}O_8S_3$: C, 53.36; H, 6.81; S, 17.09. Found: C, 52.99; H, 6.83; S, 17.72.

#### 3.8.3.4 Synthesis of p1

In a general reaction, monomer **1** (100.0 mg, 0.20 mmol) was dissolved in EtOH 96 % (5 mL) in a round bottom flask. For those reactions where pH was neutralized, $NaHCO_3$ (36.4 mg, 0.43 mmol, 1.1 equivalents) was added and mixed homogeneously with monomer **1** with magnetic stirring. Then, a solution of iodine (75.5 mg, 0.30 mmol for 1.5 equivalent reaction) dissolved in EtOH 96 % (1.5 mL) was added over the previous one at 300 $\mu$L/min with a syringe pump.[o] Once added, the reaction was left under magnetic stirring at 500 rpm for 20 min at room temperature. The white precipitated polymer obtained was washed 5 times with EtOH 96 % until excess of iodine was fully removed. The final product was dried under reduced pressure for 24 h obtaining between 32 mg. The amount of $NaHCO_3$ and iodine were modified depending the equivalents of study.

**$^1$H NMR** (360 MHz, $CDCl_3$): $\delta$(ppm) 6.99 (bs, 1H), 6.96 (dd, $J$ = 7.9, 1.7 Hz, 1H), 6.91 (dd, $J$ = 8.0, 1.8 Hz, 1H), 6.77 (dd, $J$ = 8.0, 7.9 Hz, 1H), 6.04 (bs, 1H), 4.06 (s, 6H), 2.96 (t, $J$ = 6.7 Hz, 2H), 2.89 (t, $J$ = 6.9 Hz, 4H), 2.75 (t, $J$ = 6.9 Hz, 4H), 2.54 (t, $J$ = 6.7 Hz, 2H), 1.48 (q, $J$ = 7.4 Hz, 2H), 0.88 (t, $J$ = 7.4 Hz, 3H).

**IR** (neat): ($cm^{-1}$) 3407, 2968, 2938, 1726, 1635, 1587, 1559, 1541, 1458, 1411, 1387, 1350, 1277, 1223, 1159, 1131, 1056, 1015, 991, 928, 898, 852, 824, 777, 728, 701, 667, 638, 567.

#### 3.8.3.5 Synthesis of p5

In a general reaction for the optimization studies of the polymerization of 1,6-hexanedithiol **5**, the corresponding amount of iodine 672, 336, 185, 84 or 42 mg for the reactions of 4, 2, 1.1, 0.5 and 0.25 equivalents, respectively) was dissolved in 1.25 mL of EtOH 96 %. In the studies of pH neutralization, 1.05 equivalents of $Et_3N$, $NaHCO_3$ or sodium salicylate was added, considering the release of two protons for each disulfide formed. Then, 1,6-hexanedithiol **5** (100 mg, 0.66 mmol) was added keeping the reaction under magnetic stirring for 15 minutes. The precipitated white polymer was washed with EtOH 96 % three times and precipitated in cold $Et_2O$ twice. The final white powder was dried under reduced pressure.

#### 3.8.3.6 Synthesis of p8

In the optimal conditions, monomer **8** (111.2 mg, 0.20 mmol) and sodium salicylate (76.8 mg, 0.48 mmol) were dissolved in EtOH 96 % (5 mL) in a round

[o]For all the procedures where iodine has to be added, it is strongly recommended to use plastic spatula. Different chrome on metallic spatula has been seen to affect the final polymer obtained due to impurity traces.

bottom flask. Then, a solution of iodine (75.5 mg, 0.30 mmol) dissolved in EtOH 96 % (1.5 mL) was added over the previous one at 300 $\mu$L/min with a syringe pump. Once added, the reaction was left under magnetic stirring at 500 rpm for 20 min at room temperature. The white precipitated polymer obtained was washed between 5-8 times with EtOH 96 % until excess of iodine was fully removed. The final product was then dissolved in the minimum amount of DCM and precipitated in cold $Et_2O$ for removing remaining salicylate/salicylic acid and dried under reduced pressure for 24 h affording 52 mg of **p8-37k** as a white polymer.

**$^1$H NMR** (360 MHz, $CDCl_3$): $\delta$(ppm) 6.79 (d, $J$ = 7.8 Hz, 1H), 6.74 (d, $J$ = 7.8 Hz, 1H), 6.73 (s, 1H), 4.05 (s, 6H), 3.87 (s, 3H), 3.85 (s, 3H), 2.93 – 2.87 (m, 3H), 2.85 – 2.69 (m, 10H), 2.66 – 2.57 (m, 3H), 1.49 (q, $J$ = 7.7 Hz), 0.88 (t, $J$ = 7.7 Hz).

**IR** (neat): ($cm^{-1}$) 2962, 2932, 2835, 1730, 1607, 1590, 1514, 1464, 1417, 1387, 1349, 1258, 1234, 1179, 1133, 1026, 993, 929, 852, 808, 763, 711, 667, 618, 597, 556.

#### 3.8.3.7 Synthesis of c1

To obtain **c1**, polymer **p1-50k** was synthesized following the procedure described previously. The supernatant from the corresponding polymerization was isolated and treated with a 20 mM aqueous solution of $Na_2S_2O_3$ which was added until the excess of iodine was completely reduced, changing from dark amber to colorless solution. Then, and extraction with DCM was performed three times isolating the organic phase composed by the mixture of cyclic compounds **p1-cyc**. A flash column chromatography of **p1-cyc** was performed with a gradient of hexanes:AcOEt starting at 9:1 during column preparation and changing gradually up to 1:1 which was kept, obtaining pure **c1** in the third fraction.

**$^1$H NMR** (400 MHz, $CDCl_3$): $\delta$(ppm) 6.98 (d, $J$ = 7.9 Hz, 1H), 6.93 (d, $J$ = 7.8, 1H), 6.89 (bs, 1H), 6.79 (dd, $J$ = 7.9, 7.8 Hz, 1H), 5.72 (s, 1H), 4.17 (d, $J$ = 11.3 Hz, 2H), 4.15 (bs, 2H), 4.11 (d, $J$ = 11.3 Hz, 2H), 3.09-3.02 (m, 4H), 2.97 (t, $J$ = 6.7 Hz, 2H), 2.74-2.65 (m, 4H), 2.56 (t, $J$ = 6.7 Hz, 2H), 1.52 (q, $J$ = 7.6 Hz, 2H), 0.92 (t, $J$ = 7.6 Hz, 2H).

**$^{13}$C NMR** (100.6 MHz, $CDCl_3$): $\delta$(ppm) 171.8, 171.6, 144.8, 144.4, 126.8, 121.0, 117.7, 116.9, 65.8, 64.5, 40.4, 35.4, 34.1, 33.8, 31.3, 24.0, 7.4.

**IR** (neat): ($cm^{-1}$) 3404, 2965, 2927, 2854, 1726, 1634, 1587, 1458, 1418, 1388, 1349, 1331, 1277, 1223, 1185, 1129, 1056, 1017, 999, 901, 854, 823, 777, 727, 647, 567.

**Elemental Anal.** Calcd for $C_{21}H_{28}O_8S_3$: C, 49.98; H, 5.59; S, 19.06. Found: C, 49.58; H, 5.79; S, 18.26.

### 3.8.4 Conformational optimization

The most stable conformers of catechol disulfides macrocycles have been obtained with the improved ETKDG conformer generator for macrocycles implemented in the RDKit Python library.[154] These analyses were carried out by José Emilio Sánchez Aparicio from the Chemistry Department of the UAB.

### 3.8.5 Lap shear adhesion test

**Substrates**
Lap shear substrates of float glass, copper (SF-Cu F25), stainless steel (1.4301), aluminum (6016) and titanium (grade 1) were purchased in Rocholl GmbH (Eschelbronn, Germany). Substrates were cleaned with water, ethanol and acetone three times during 30 min. No further surface treatment was applied.

**Sample preparation**
For **p1-50k** and **p8-37k**, polymer solutions in DCM (0.33 g/mL, 30 $\mu$L) were added to each substrate and left dried. Once solvent was evaporated, the substrates were overlapped at 12.7 x 25.4 mm following configuration described at ASTM D 1002 – 99 and kept tightly joined with two clamps for paper sheets and left 1 hour at 120 °C and 23 h at room temperature before testing. For the study of bonding/debonding adhesion cycles, each sample was rejoined after the measurement and left 1 h at 120 °C followed by 23 h at room temperature between cycles.

For **p1-cyc** and **p8-cyc**, 27 ± 3 mg were added to each substrate and overlapped at 12.7 x 25.4 mm. While tightly joined with a clamp, the substrates were left 1 hour at 175 °C and 23 h at room temperature before testing. For the study of bonding/debonding adhesion cycles, each sample was rejoined after the measurement and left 1 h at 175 °C followed by 23 h at room temperature between cycles.

**Adhesion measurement**
Lap shear adhesion measurements were conducted on an Instron 5569 equipped with 1 kN load cell with rubber grips in the case of glass and 5 kN load cell for the rest of substrates. Adherends were pulled apart at a rate of 1 mm/min. Final adhesive strength in MPa was obtained by dividing the maximum load at failure by the overlapping area. As a general rule, a total amount of five replicates was analyzed for each sample. Any variation of these conditions is described in each corresponding section.

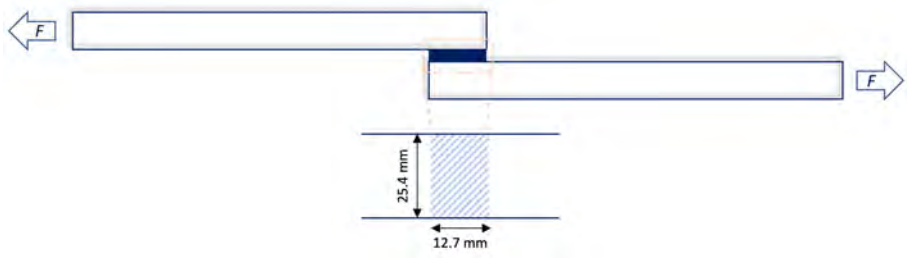


**Figure 3.44.** Scheme with the corresponding dimensions of the lap shear test performed along this work.

### 3.8.6 *In vitro* cell viability test

**Extract preparation**. Polymer **p1-50k** was adsorbed on PP textile (DH Material Medico, Barcelona, Spain) which was cut in substrates of 5 x 1 cm in size with a laser cutter. The adsorption was achieved by immersing the PP textile substrate into 50 mg/mL solution of **p1-50k** in DCM and drying it under reduced pressure to get a fully coated substrate. PP textile substrates were properly coated with 2.1± 0.3 mg/cm$^2$ of **p1-50k** on average (n=5). An extraction ratio of 6 cm$^2$/mL was applied following the considerations described in ISO10993-12. Negative control was prepared with USP Reference Standard of high-density polyethylene of 2.0 x 1.5 cm in size by immersing the substrate in 2 mL (extraction ratio 3 cm$^2$/mL. The extractions were performed in Dulbecco's Modified Eagle Medium (DMEM, Invitrogen) during 24 or 72 h at 37 °C. Before testing, the extract solutions were sterilized by filtration through a 0.2 $\mu$m pore nylon syringe filter.
**XTT Assay**. Mouse embryonic NIH3T3 fibroblasts were obtained from European Collection of Authenticated Cell Cultures (ECACC 93061524). The cells were routinely cultured in Dulbecco's Modified Eagle Medium (DMEM, Invitrogen) containing 10 % heat-inactivated fetal bovine serum and 1 % antibiotic-antimycotic solution (GIBCO) at 37 °C in a humidified 10 % $CO_2$ atmosphere. The cell viability was evaluated using XTT Assay (Canvax Biotech). Untreated cells were used as blank and the extract of high-density polyethylene was used as negative control. Cells were plated in 96-well plates at a density of $5 \cdot 10^3$ cells/well in 100 $\mu$L of culture medium and were allowed to grown overnight. After this time, cells were treated with 100 $\mu$L of the extracts of polymeric samples obtained in DMEM in the initial concentration and dilutions 1:2. After 24 h of incubation, 50 $\mu$L of XTT/PMS solution per well was added and incubated for 3 hours. After incubation, absorption at 450 nm (reference 630 nm) was measured using a Victor3 multiwell microplate reader (Perkin Elmer). The relative

cell viability (%) for each sample related to the negative control was calculated. Each sample was tested in triplicate. Cell manipulation and viability quantification was carried out by Dr. David Montpeyó from Institut de Biotecnologia i Biomedicina (IBB).

### 3.8.7 *In vivo* intradermal reactivity assay

**Animals**

All animal experimental procedures were performed with the approval of the Animal Care Committee of the Korea Advanced Institute of Science and Technology (KA2017-44) and carried out in the facilities of Knotus Co. Ltd (Incheon, Republic of Korea). Three male New Zealand White (NZW) rabbits were acquired from a commercial breeder (Hallim Experiment Animal, Republic of Korea). These rabbits were acclimated two weeks prior the study in an animal room maintained at 23 ± 3 °C and 55 ± 15 % humidity, on a 12-hour light-dark cycle (beginning at 08:00) between 150-300 lx with 10 to 20 air changes per hour. Food (Dream Bio, Republic of Korea) and tap water sterilized by UV and microfiltration were provided ad libitum. At the time of the study the rabbits were 18 weeks old. Fur was clipped 12 h before the test.

**Extract preparation**

Polymer **p1-50k** was adsorbed on PP textile (DH Material Medico, Barcelona, Spain) which was cut in substrates of 5 x 1 cm in size with a laser cutter. The adsorption was achieved by immersing the PP textile substrate into 50 mg/mL solution of **p1-50k** in DCM and drying it under reduced pressure to get a fully coated substrate. PP textile substrates were properly coated with 2.1± 0.3 mg/cm$^2$ of **p1-50k** on average (n=5). An extraction ratio of 6 cm$^2$/mL was applied following the considerations described in ISO10993-12. The extractions were performed in sterile saline media CLEANCLE® (JW Pharmaceutical, Republic of Korea) or cottonseed oil (Sigma Aldrich, South Korea) during 72 h at 37 °C. Before being injected, extract solutions were sterilized by filtration through a 0.2 $\mu$m pore nylon syringe filter.

**Procedure**

Animals were anesthetized by administering subcutaneously a mixture of Zoletil 50 (VIRBAC, France, 5 mg/kg) and xylazine (Rompun, Bayer AG, Germany, 2.5 mg/kg) prior the injections of the extracts. The intradermal reactivity of **p1-50k** was determined by injecting 200 $\mu$L of the extract solutions on three different spots on the back of the animals (n = 2). The injection sites were observed every 24 h throughout three days. Evaluation was carried out considering the scoring grading system for intracutaneous reactions described in ISO 10993-10

and adapted to the current sampling. Animal manipulation and injection procedure was carried out by Dr. Kim Geum Yeon. Erythema and edema scoring was supervised by Dr. Kim Geum Yeon.

# CHAPTER 4

# Catechol poly(disulfide)s for the development of tissue adhesives and sealants

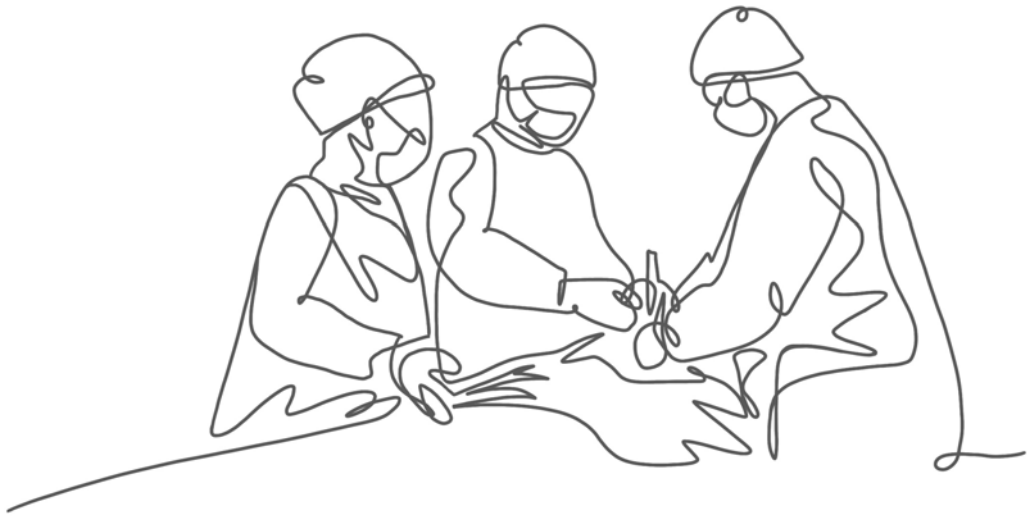

# 4.1 Introduction. The use of catechol adhesives in healthcare

## 4.1.1 Tissue adhesives and sealants

Since last century, the development of adhesives with potential use in biomedical applications attracted the focus as promising alternatives for the replacement and reinforcement of traditional methods employed in wound healing such as sutures, staples and clips. Regardless of the improvement of sutures and staples through the use of bioabsorbable materials, these traditional methods are insufficient in those cases where fast and precise action is required and, besides, produce extra damage to the target tissue to be healed.

Despite the clear benefits that tissue adhesives could provide, traditional methods are still the most common practices and the 'standard of care' for many surgical procedures. However, for those operations where there is high risk of post-surgical infection and/or when perfect sealing is required, the use of sutures is not enough and tissue adhesives are becoming more frequent. For example, infections from leakage after colorectal anastomosis is one of the main risks found where tissue adhesives and sealants could improve the current 'standard of care'. Air leakage after pulmonary surgery is another example were the use of traditional methods are still insufficient.

Depending the mechanism of action, tissue adhesives are classified in glues (or adhesives) when used for joining to tissues without extra requirements, hemostats when producing blood clots, and sealants when the material is used to create a barrier to prevent leakage (see Figure 4.1).[157]


**Figure 4.1.** Schematic representation of some applications of tissue adhesives depending their mechanism of action as tissue glue on epidermis, hemostat on blood vessels and sealant on lung surgery.

Apart from good adhesion on wet biological substrates, biocompatibility of

the tissue adhesives and their degradation products is a must.[158] Other physical properties such as stiffness, viscoelasticity, strength, toughness, porosity, roughness or deformation are parameters of interest for the design of proper tissue adhesives which are becoming more important. Common approaches for the design of tissue adhesives are centered in the development of adhesives useful for all kind of tissues.[159] However this 'one-size-fits-all' approach is inadequate to achieve the optimal performance of tissue adhesives.[160] The complexity and difference between mechanical and physical properties of the diverse biological tissues must be taken into account for the correct design of the adhesive materials.[159] In terms of elasticity, for example, tissue adhesives must be able to support dynamic behaviors when applied on heart and lungs since they suffer high deformations repeatedly. This variety implies, not only a proper match between tissue and adhesive properties, but also the study and conditioning of the products as function of the local environments within the biological tissues, considering parameters such as temperature, humidity, UV exposure, local pH, oxygen and ezymatic action which can differ drastically between tissues. Future trends on the design of tissue adhesives will be clearly focused on this direction, looking for especific tissue/adhesive physico-chemical properties matching, but further studies towards this direction are still required with already commercial products to asses the importance of this point.

Another aspect important in the development of tissue adhesives is achieving biodegradation of the adhesive material after complete recovery of the target tissue. It is generally assumed that tissue adhesives must keep functional for periods longer than three weeks without losing properties.[161] However, this periods will be closely related to the final application and, hence, considerations about the healing process of the specific tissue must be contemplated as mention previously.

#### 4.1.1.1 Commercial products: considerations, use and impact

First applications of tissue adhesives are dated on the middle of last century with the use of fribrinogen in the '40s and cyanoacrylate in the '50s. Although it is known that cyanoacrylate sprays were used in the battlefield during the Vietnam War to control bleeding rapidly,[162] the use of cyanoacrylates for topical application was approved by FDA on 1998.

Commercial tissue adhesives can be divided clearly in two big groups: those based on natural and the ones based on synthetic polymers.

From natural polymeric formulations, fibrin-based tissue adhesives are the most broadly employed. Encompassed by the formulations containing fibrin, fibrinogen and thrombin, this materials take advantage of the cascade reaction of blood clotting mechanism, being applied mostly in cases where bleeding management is required. TISEEL®, TachoSil® and Artiss (Baxter); Evicel®, Evarrest®

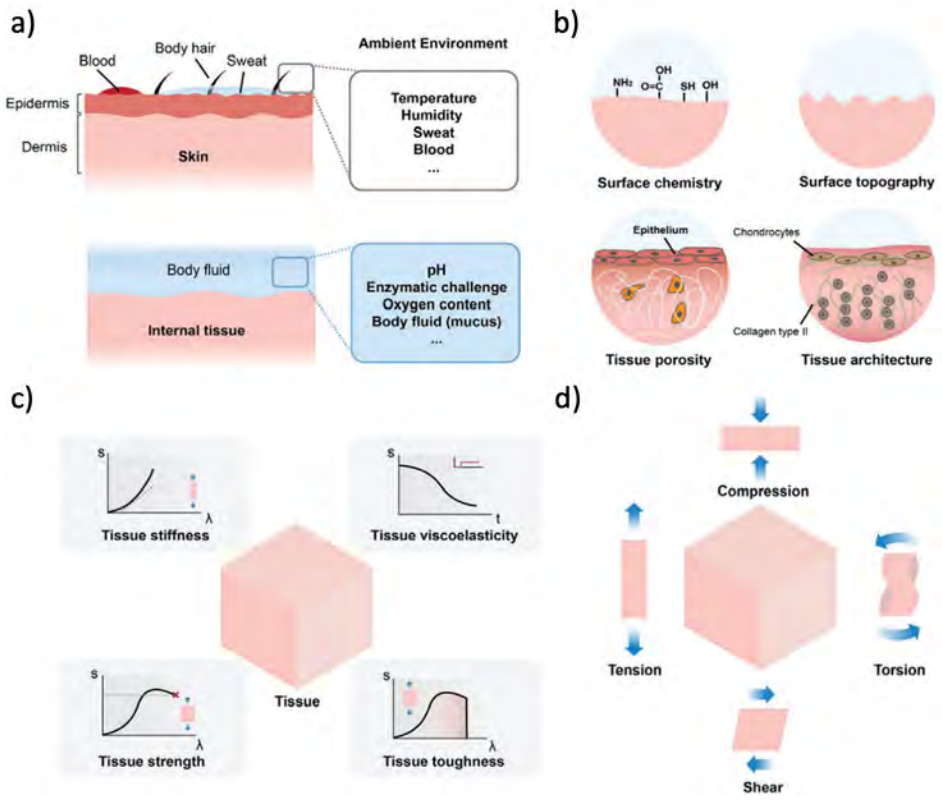


**Figure 4.2.** Representation of some important parameters to consider to the design of tissue adhesives. In a) the different local environment depending the target tissue; in b) surface and structural consideration; in c) the different mechanical properties of tissues; and d) the variety of forces a tissue can suffer (compression, tension, torsion and shear).[159]

and Evithrom (Ethicon); or CoStasis® are some of the commercial fibrin glues. The most important advantage of fibrin glue is the high biocompatibility. In fact, patient-specific application can be obtained from the plasma of the same patient.[163] However, the poor adhesive performance has limited their use to hemostatic applications. Other commercial adhesive formulations with natural biopolymers are obtained with gelatin (LifeSeal™ from LifeBond; or GRF from Microval), collagen (FloSeal® from Baxter; or SurgiFlo® from Ethicon) and albumin (PREVELEAK™ from Baxter; BioGlue® from Cryolife; or Progel™ from Davol). These alternatives have been developed and presented to the market, improving the adhesive performance and broadening the range of application from hemostasis to air leak sealing after thoracotomy in Progel™.[164]

Regarding synthetic polymer approaches, we can find cyanoacrylates, polyethylene glycol (PEG) and polyurethane-based tissue adhesives, among others. As mentioned previously, cyanoacrylate-based formulations were one of the first adhesives tested on tissues. Although cyanoacrylates got the approval by the FDA for topical use on 1998 for Dermabond® from Ethicon, its approval for internal uses was not achieved until 2010 with the product OMNEX™ from Ethicon for limited cardiovascular surgeries. Despite the great adhesive performances, the main limitation of cyanoacrylates is their cytotoxicity. Although the composition has been modified to reduce toxicity, there are still limitations of their use and are contraindicated for patients with hypersensitivity to cyanoacrylates or formaldehyde released.(poner doc OMNEX) Alternatively, PEG-based formulations such as FocalSeal® (Focal Inc.), CoSeal™ (Baxter), DuraSeal® (Integra LifeSciences Corp.) entered in the market providing adhesion performances close to cyanoacrylates but with greater biocompatibility. The main complication found in PEG-based approaches lays on the high swelling ratio of these materials, which can produce high stresses to the surrounding tissues and can end in detachment of the adhesive. Also, a polyurethane-based tissue adhesive named TissuGlu® (Cohera Medical Inc.) got CE mark on 2011 and FDA approval on 2015 for its application in abdominoplasty, but its used has not been employed broadly.[a]

Despite the huge variety of commercial tissue adhesives, all of them fail at some point, either on poor adhesive performances on the wet tissues or in low biocompatibility. In terms of adhesion, fibrin-based formulations present performances below 20 kPa, cyanoacrylates have adhesion over 200 kPa and the other approaches such as PEG-based formulations reach values from 50-150 kPa. Concerning biocompatibility, the trend is completely the opposite, being fibrin glues the most compatible and cyanoacrylates the most toxic, limiting their use to topical application in general. For these reasons, new approaches are required to fill the needs of the medical sector combining high performances and biocompatibility.

As regulatory is concerned, tissue adhesives are considered Class III medical devices since their internal application requires of a stricter control. Furthermore, due to the novelty of most tissue adhesive formulations, they must go through a premarket approval (PMA) process which implies several preclinical and clinical studies. In general, for the more recent formulations, periods around 8-12 years have lasted from the description of the adhesive until its corresponding approval (see Figure 4.3). Some new approaches on tissue adhesive developments are reported to incorporate drugs or bioactive species such as growth factors to

[a]This technology had no successful implantation leading to the closure of Cohera Medical Inc. and the selling of the IP assets on private auction.[165] Nowadays, patent rights of IP assets of Cohera Medical Inc. are terminated due to non-payment of the annual fees.

promote wound healing.[159] However, from the regulatory perspective, these new formulations would not be classified as medical devices due to the incorporation of biologically active components and, consequently, their regulatory would be substantially modified requiring more stringent processes. An extensive review about the full translational path of tissue adhesives was reported recently providing a whole view of adhesive design and regulatory issues.[160]

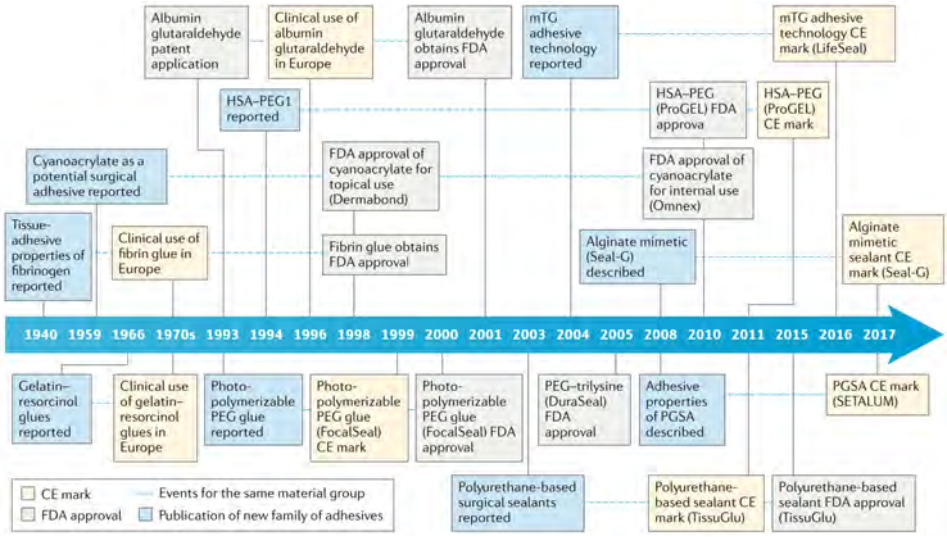


**Figure 4.3.** Chronogram of the research on tissue adhesives and the corresponding market development.[160]

For further information of current reported commercial and non-commercial tissue adhesives the reading of recent published reviews extensively detailed is recommended.[157,159–161]

### 4.1.2 Current trends on catechols based formulations

The unfulfilled requirements of commercial tissue adhesives has encourage the development of new approaches. In this context, catechol containing polymers (also referred in literature as 'mussel-inspired' formulations) have appeared as potential candidates to overcome main issues concerning the low adhesive performance on the wet surfaces of tissues.

Several approaches using catechol functionality as adhesive motif have been described, showing performances above commercial formulations. The performance of some relevant reported catechol based tissue adhesives are presented in

Table 4.1 and 4.2. Both the functionalization of polymers with catechol and the copolymerization of catechol derivatives are convenient strategies for the design of tissue adhesives, as already exposed on Chapter 1. For example, biopolymers such as chitosan modified with catechol functionality can present adhesion from 7.5 to 50 kPa on pig skin.[69–71,166–168] Other biopolymers such as catechol functionalized gelatin, have adhesions ranging from 16 kPa to values up to 77 kPa.[169] In the case of PEG-based catechol containing formulations values from 12 kPa up to 107 kPa have been reported.[170–174] Higher adhesions from 120 to 223 kPa have been achieved with formulations combining catechols and citrate and after cross-linking with $FeCl_3$ or $NaIO_4$.[175–177] In general, however, most reported adhesive results of catechol containing polymers are below 100 kPa (see Figure 4.4). Compilation about the performance and application of other relevant catechol containing formulations can be found in other noteworthy reviews published elsewhere.[178–180]

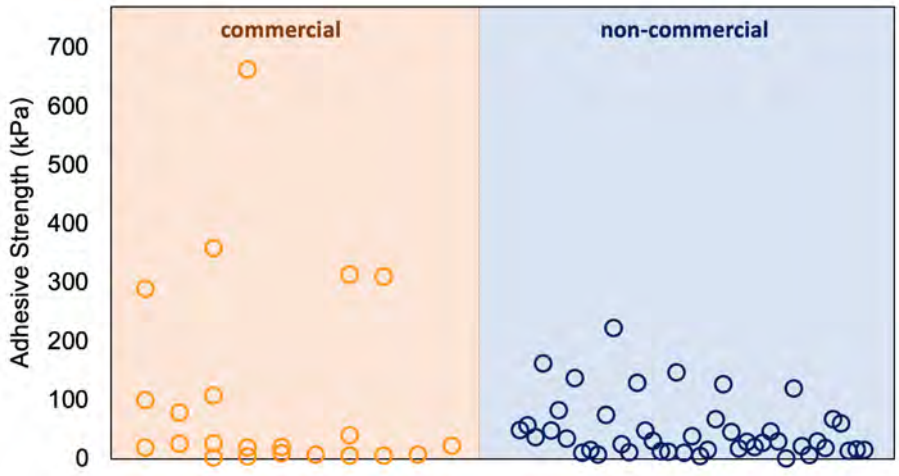


**Figure 4.4.** Compilation graph of reported adhesion values of commercial products and non-commercial catechol based formulations reported on the literature.

Concerning the industrial interest of catechol containing polymers as tissue adhesive, a total of 1593 patents have been filled about catechol containing adhesives aimed for medical application.[b] From these patents, 1341 ($\approx$ 84 %) have

[b]This search has been carried out in Espacenet patent database. The Boolean operator OR was applied for the terms 'catechol', 'dopa', 'dihydroxybenzene' and 'mussel' and for the terms 'adhesive', 'glue', 'polymer' and 'gel*' applying a restriction for their presence within the title, abstract or claims. A classification filter for IPC A61K corresponding to 'Preparations for medical, dental, or toilet purposes' was added. (Last update: October 6$^{th}$ 2021.)

been published after the year 2000, which shows the huge and recent interest of these materials in the field during last decade. A tendency of these published patents are present in Figure 4.5. Despite this interest and potential product development, few companies of catechol formulations focused on medical applications have been stablished. One of the pioneering companies in this area was Nerites Corp., founded on 2004 by Prof. Phil Messersmith and acquired by Kensey Nash Corp. on 2011 for $20 million.[181] Although no clear trail of their technology could be found to see if the materials reached the market, the truth is that the main IP related to their technology are still active as the fees are paid annually.[182–184] Another relevant example is the development of catechol containing products by Innotherapy Inc., founded on 2010 by Prof. Haeshin Lee. Having a broad portfolio of materials for bleeding management, leakage prevention and wound dressing,[185] the product InnoSEAL (an externally applied hemostatic agent) is one of the first bioinspired approaches containing a catechol-based technology that has already reached the market.[c]

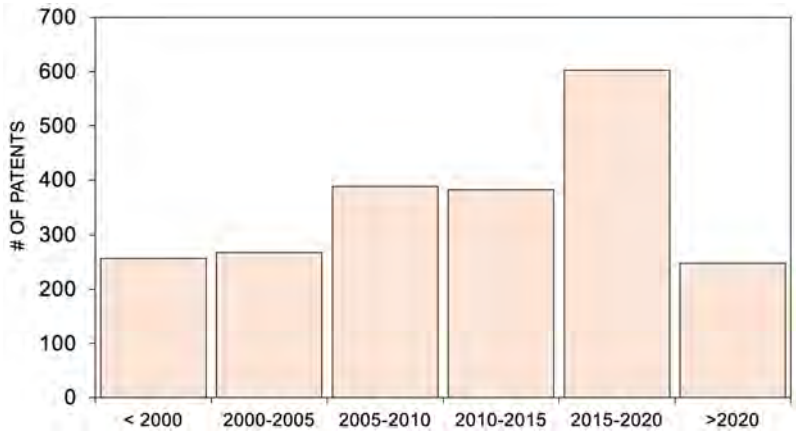


**Figure 4.5.** Number of patents published during last decades using Espacenet database for catechol containing adhesives aimed in biomedical applications

Despite all the efforts in designing novel strategies based on catechol chemistry to take advantage of the adhesion on wet tissues, few commercial examples can be found as presented previously. Introducing new functionalities to the system such as disulfide bond and having a proper fine-tuning of the final polymer obtained are some interesting developments that could boost the use of this materials. In the present chapter the aim is to synthesize adhesive formulations based on

[c]InnoSEAL is on market in Korea and is already approved by the corresponding agencies on USA, Japan, Hong Kong, Pakistan, Israel, Argentina, Malaysia and UE.[185]

catechol poly(disulfide)s which will be lately tested as potential tissue adhesives and sealants.

Looking for a material with easy application, polymerization is optimized to achieve adhesive formulations with sufficient fluidity. In some cases, oligomeric mixtures are interesting for their use as prepolymer mixtures in the case of adhesive and coatings. Moreover, copolymerization of monomer **1** with dithiol **6** containing a short ethylene glycol chain is performed, expecting to obtain polymers with higher solubility in aqueous media and enhanced biocompatibility.

**Table 4.1.** Reported examples of catechol containing tissue adhesives obtained from natural biopolymers or bioinspired polypeptides.

| **Composition** | **Adhesive strength (kPa)** | **Cross-linker** | **Curing time (min)** | **Application** |
|---|---|---|---|---|
| Alginate-catechol | $21.8 \pm 3.1$[186] | - | 120 | - |
| | 6.5[187] | - | - | - |
| Cellulose-catechol | 15-20[74] | acrylamide | - | wound healing |
| | 21.2[75] | $FeCl_3$ | - | epidermal sensor |
| | $88 \pm 15$[76] | $FeCl_3$ | 15 | - |
| Chitosan-catechol | $15.0 \pm 3.5$[166] | - | 5 | hemostat |
| | $45.8 \pm 16.0$[167] | $FeCl_3$ | 30 | - |
| | 18.1[168] | $FeCl_3$ + light | 60 | - |
| | 7.5[69] | - | - | - |
| | 45[70] | $NaIO_4$ | - | wound healing |
| | $16.9 \pm 0.9$[71] | - | 6 | wound healing |
| Chondritin-catechol | 30[188] | - | - | cartilage repair |
| BSA-catechol | $162.5 \pm 34.7$[177] | $FeCl_3$ | 120 | seroma prevention |
| Collagen-catechol | 15[189] | - | 720 | - |
| Dextran-catechol | 10[78] | - | - | wound healing |
| Elastin-catechol | 37[80] | $NaIO_4$ | - | - |
| Gelatin-catechol | $24.7 \pm 3.3$[190] | $FeCl_3$ | 120 | - |
| | $77.0 \pm 1.5$[169] | $FeCl_3$ | - | - |
| | 16[191] | $FeCl_3$ | 15 | - |
| Hyaluronic-catechol | $7.2 \pm 0.9$[23] | - | 5 | - |

| | | | | |
|---|---|---|---|---|
| | $90.0 \pm 6.7$[72] | $NaIO_4$ | 5 | - |
| Xanthan gum-catechol | 28[79] | - | - | anastomosis |
| Mussel peptide | $200 \pm 60$[192] | $FeCl_3/NaIO_4$ | 120 | - |
| | $48.2 \pm 10.1$[193] | light | 120 | wound healing |
| Polypeptide | 120[194] | - | 720 | - |

**Table 4.2.** Reported examples of catechol containing tissue adhesives obtained from synthetic polymers.

| **Composition** | **Adhesive strength (kPa)** | **Cross-linker** | **Curing time (min)** | **Application** |
|---|---|---|---|---|
| Poly(dopamine-co acrylate) | $37.0 \pm 5.6$[195] | fibrinogen | 15 | topical |
| | $76.0 \pm 13.4$[195] | $HRP/H_2O_2$ | 1440 | topical |
| | 18.3[196] | - | 30 | intestinal sealing |
| Citrate-catechol | $123 \pm 13.2$[197] | $NaIO_4$ | 120 | topical |
| | $223.1 \pm 15.9$[175] | $NaIO_4$/CuAAc | 120 | antifungal |
| | $127.0 \pm 14.0$[198] | MgO | 140 | - |
| Dopamine glutamic | 30[199] | $HRP/H_2O_2$ | 10 | - |
| Poly-lysine catechol | 147[200] | $HRP/H_2O_2$ | 30 | wound healing |
| | 15[201] | $FeCl_3$ | 30 | - |
| | 15[83] | $FeCl_3$ | 30 | wound healing |
| PEG-catechol | $35.0 \pm 12.5$[198] | $NaIO_4$ | 1440 | - |
| | $107.0 \pm 24.7$[171] | $NaIO_4$ | 120 | hernia repair |
| | $11.8 \pm 4.0$[173] | - | 10 | - |
| Pluronic-catechol | $83.2 \pm 8.7$[202] | $HRP/H_2O_2$ | 180 | topical |
| PGA-catechol | 140[64] | $HRP/H_2O_2$ | 10 | bladder sealing |
| PLGA-catechol | $38.7 \pm 10.9$[203] | - | 10 | bucal |
| Polyester-catechol | $13.1 \pm 1.7$[193] | $Fe(Ac)_3$ | 5.5 | - |
| | $10.6 \pm 2.1$[204] | $NaIO_4$ | 240 | - |
| | 20[205] | light | 5 | - |
| PVA-catechol | 10.5[84] | - | 0.5 | bucal |

## 4.2 Optimization of p1 for biomedical application

Considering all parameters of the polymerization reaction previously studied on Chapter 3, the synthesis of **p1** was carried out with an amount of iodine below the stoichiometry, high concentration (0.4 M) and presence of sodium bicarbonate. These conditions would allow to obtain low molecular weight species of high fluidity, due to fast precipitation (limiting chain extension) and, besides, protecting end groups by neutralizing the acid media formed.

The synthesis of **p1**, was studied at different stoichiometries of $I_2$ (0.75, 0.8 and 0.9 equivalents). All the polymer formed was isolated by extraction in $DCM/H_2O$, removing all the excess of salts. GPC elugrams (Figure 4.6) showed how the molecular weight distribution changes toward higher molecular weights, i.e. lower elution times, when increasing the amount of iodine as seen in Table 4.3. Besides, the peak at higher elution times in comparison with the monomer indicates the presence of molecules with lower apparent molecular weight.

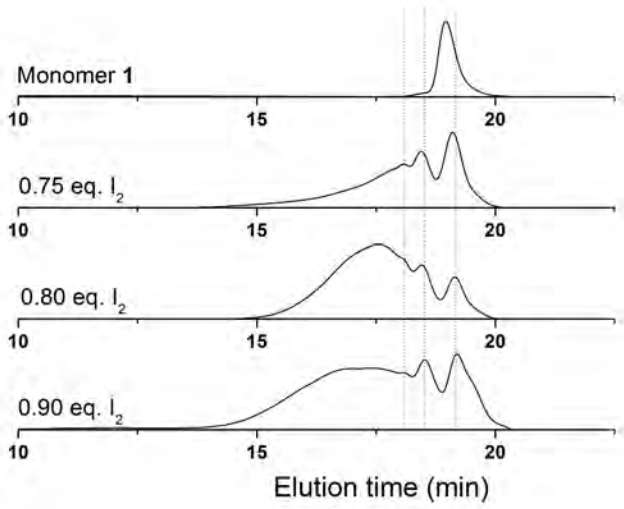


**Figure 4.6.** GPC elugrams of **p1** from the reaction at 0.75, 0.8 and 0.9 equivalents of $I_2$.

These low molecular weight species were analyzed by MALDI-TOF in positive reflectron mode. Interestingly, the peaks obtained did not show the common isotopic distribution. The signals observed suggested the presence of two different species, with their respective monoisotopic peaks separated by 2 Da. Such differ-

**Table 4.3.** GPC results of the **p1** synthesis in substoichiometric amounts of iodine.

| **Stoichiometry** | $\mathbf{M_n}$ **(g/mol)** | $\mathbf{M_w}$ **(g/mol)** | **Đ** |
|---|---|---|---|
| 0.75 | 870 | 3270 | 3.8 |
| 0.8 | 1500 | 4400 | 2.9 |
| 0.9 | 1200 | 6230 | 5.5 |

ence could be associated to different species: i) the $Na^+$ adduct with one catechol oxidized to quinone or ii) the $Na^+$ adduct of a cyclic compound coming from the oxidation of the ending thiol groups to disulfides. In the MALDI-TOF of Figure 4.7 it can be seen this phenomenon in the peak around 1031 Da corresponding to the $Na^+$ adduct of the dimeric compound. If considered that the monoisotopic peaks separated by 2 Da come from the presence of the quinone form, it would be mean that in MALDI-TOF we are observing the dimer with two catechols and the dimer with one catechol and one quinone, but none with two quinones. Although this hypothesis is valid since the species can have a completely different way of desorption in the matrix for MALDI analysis, the idea of quinone presence could be considered less feasible than the cyclic formation through end thiols. Moreover, taking into account $^1$H NMR spectra (see Figures 6.29, 6.30 and 6.31 in the Annex), no signals of *o*-quinone is observed, which would reinforce the idea of the cycle formation. Hence, most probably when synthesizing **p1** using substoichiometric amounts of $I_2$, a mixture of linear and cyclic species is obtained. Clear differences in the isotopic distributions in MALDI-TOF can be found up to $n = 4$. Above tetramer peak, the isotopic distribution becomes more complex and cyclic/linear species cannot be identified easily. Furthermore, the presence of cyclic species would be in agreement with the observation by GPC, since cyclic species have a lower hydrodynamic radius than linear counterpart and, hence, it results in an increase of its elution time.

In terms of fluidity, only **p1-0.9k**, obtained from 0.75 equivalents reaction, had low viscosity allowing easy handling and spreading of the material. For this reason, **p1-0.9k** was chosen for the adhesion studies in biological tissues described in following sections.

## 4.3 Synthesis of copolymer p(1-6)

An approach to tune the final properties of catechol containing poly(disulfide)s could be the copolymerization of monomer **1**, using other dithiols as chain extender groups. For the present study, the copolymerization of monomer **1** with dithiol

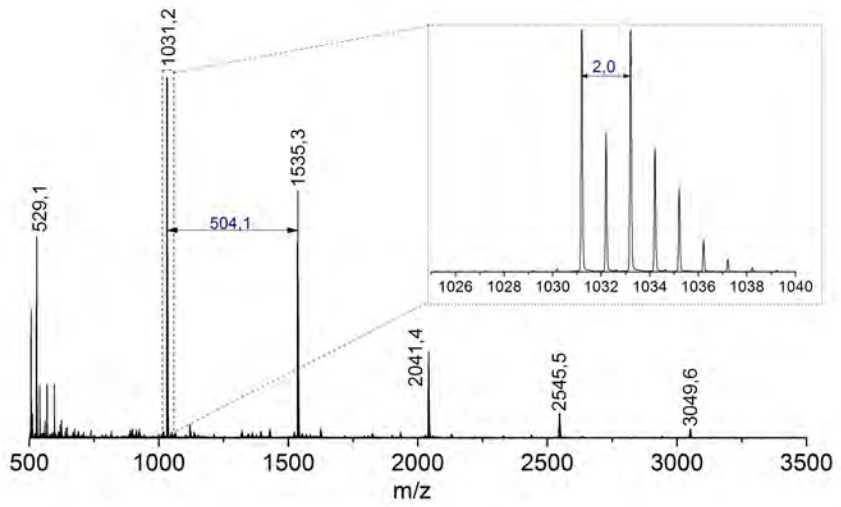


**Figure 4.7.** MALDI-TOF spectrum of **p1-0.9k** obtained with the reaction of 0.75 equivalents of $I_2$. In the inset, a zoom in of the region corresponding to the signal of the dimer.

**6** for the formation of new catechol poly(disulfide)s has been faced.[d] Dithiol **6** was chosen to get ethylene glycol domains in the polymeric chain, which were expected to enhance solubility in water and biocompatibility.

The copolymerization of monomer **1** with dithiol **6** was done at different monomer molar ratios (monomer **1**:dithiol **6**; 0.75:0.25, 0.50:0.50 and 0.25:0.75). Reactions were performed at 0.04 M of monomer, 1.5 equivalents of iodine and without presence of base looking for high molecular weight polymers. Like in the case of **p1-50k**, the precipitated polymer was isolated and characterized by $^1$H NMR, GPC and MALDI-TOF.

From $^1$H NMR spectra of final polymers (see Figure 6.32 in the Annex), the ratio between both monomeric subunits was obtained by integrating all the signals in the range 3.2 - 2.4 ppm with respect to the singlet at 4.0 ppm. In Table 4.4 the theoretical and the experimental ratios obtained by $^1$H NMR are presented.

Even though the experimental values differ slightly from theoretical values,

[d]Other copolymers could be synthesized by using thiol-ene approach. However, this chemistry has not been explored in this work.

**Table 4.4.** Ratios of monomer subunits obtained in the synthesis of **p(1-6)**. Theoretical ones correspond to the ratios tested and experimental to the ratios obtained by $^1$H NMR analysis.

| **Theoretical** | | **Experimental** | |
|---|---|---|---|
| % monomer **1** | % dithiol **6** | % monomer **1** | % dithiol **6** |
| 25 | 75 | 25.4 | 74.6 |
| 50 | 50 | 42 | 58 |
| 75 | 25 | 65 | 35 |

both starting monomers are found in the final polymer. GPC analysis showed a similar bimodal molecular weight distribution as seen for homopolymer **p1-nk** (see Figure 4.8). The $M_n$ of the high molecular weight species were 61 kDa, 45 kDa and 39 kDa for the ratios **1**:**6** of 75:25, 50:50 and 25:75, respectively. These results would indicate that the degree of polymerization is similar in all the cases if considered the molecular weight of the monomers (506,64 g/mol for monomer **1** and 182,30 g/mol for dithiol **6**).

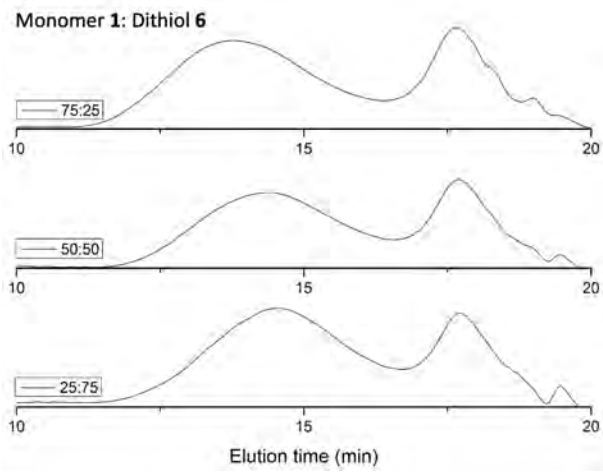


**Figure 4.8.** GPC elugrams of **p1-6** from the reaction at different **1**:**6** ratios showing an increase of the molecular weight at higher ratios of **1**.

Although $^1$H NMR and GPC results are in agreement with the copolymerization, MALDI-TOF analysis was done to confirm properly the copolymerization. In the MALDI spectra of the copolymers **(p1-6)-61k**, **(p1-6)-45k** and **(p1-6)-39k**, different set of signals can be clearly identified, corresponding to the molecular weights of the series with the subunits of **1** and **6** monomers. Gather-

ing all the peaks and sequences obtained in the spectra of the different polymers, it was possible to build a mapping of the species found in the different copolymers **p(1-6)** (see Figure 4.9 a, b and c). While the product from the ratio **1**:**6** of 75:25 has presence of species with more subunits of **1**, the one from the ratio **1**:**6** of 25:75 has more presence of species with higher amount of **6**. These results are in consonance with the expected product taking into account the initial ratio between **1** and **6** monomers which would indicate that copolymerization was successful without prevailing the homopolymerization of one monomer above the other.

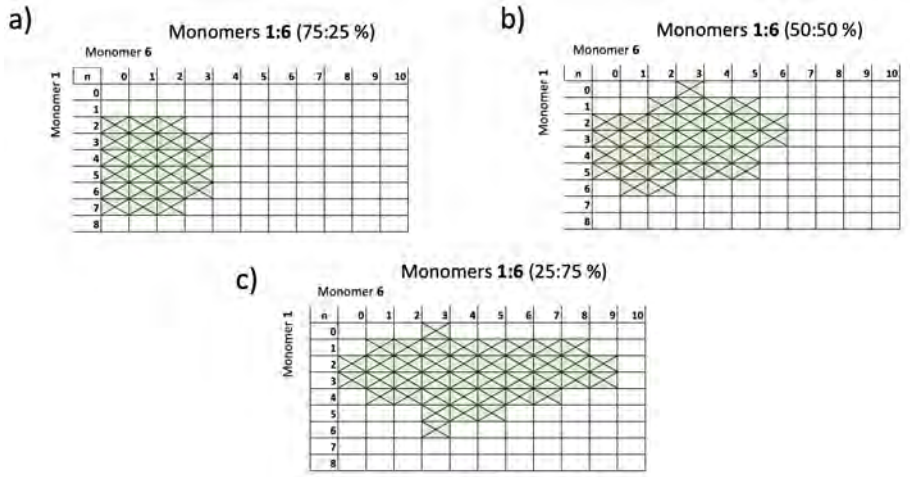


**Figure 4.9.** a) Mapping of peaks found in MALDI-TOF analysis of **p(1-6)-61k** 25:75 **1**:**6**, b) mapping of peaks found in MALDI-TOF analysis of **p(1-6)-45k** 50:50 **1**:**6**, and c) mapping of peaks found in MALDI-TOF analysis of **p(1-6)-39k** 75:25 **1**:**6**. Marked sections means that the corresponding copolymer combination is found by MALDI-TOF.

Despite obtaining different chemical structures in **(p1-6)-61k**, **(p1-6)-45k** and **(p1-6)-39k** by modifying the ratio of **1** and **6**, none of the final polymers presented a minimum solubility in aqueous media. The poor handling of these formulations, besides, hindered their direct application as tissue adhesive and/or sealant. For these reason, lower molecular weight formulation were synthesized to improve solubility and obtain a material with proper handling.

Copolymerization of monomer **1** with dithiol **6** was carried out with a ratio of monomers 1:1 and 0.83 equivalents of iodine.[e]

[e]The stoichiometry of iodine was stablished considering the theoretical final weight of the polymer **p1-0.9k** (0.75 eq. of iodine, $n \approx 4$, $M_{n(th)} = 2018$ g/mol). To get **p(1-6)** with similar

GPC analysis determined a $M_n$ of 1035 g/mol, $M_w$ of 4600 g/mol and Đ of 4.4. $^1$H NMR of the polymer, from now on **p(1-6)-1k**, confirmed that the ratio of monomeric subunits **1**:**6** was 1:1 by comparing the signals between 3.60-3.85 ppm from **6** segment and the signals between 4.00-4.25 ppm from **1** segment (see Figure 4.10a). MALDI-TOF analysis of **p(1-6)-1k** (Figure 4.10b) showed different set of signals corresponding to the molecular weights of the series with the monomeric subunits of **1** and **6**.

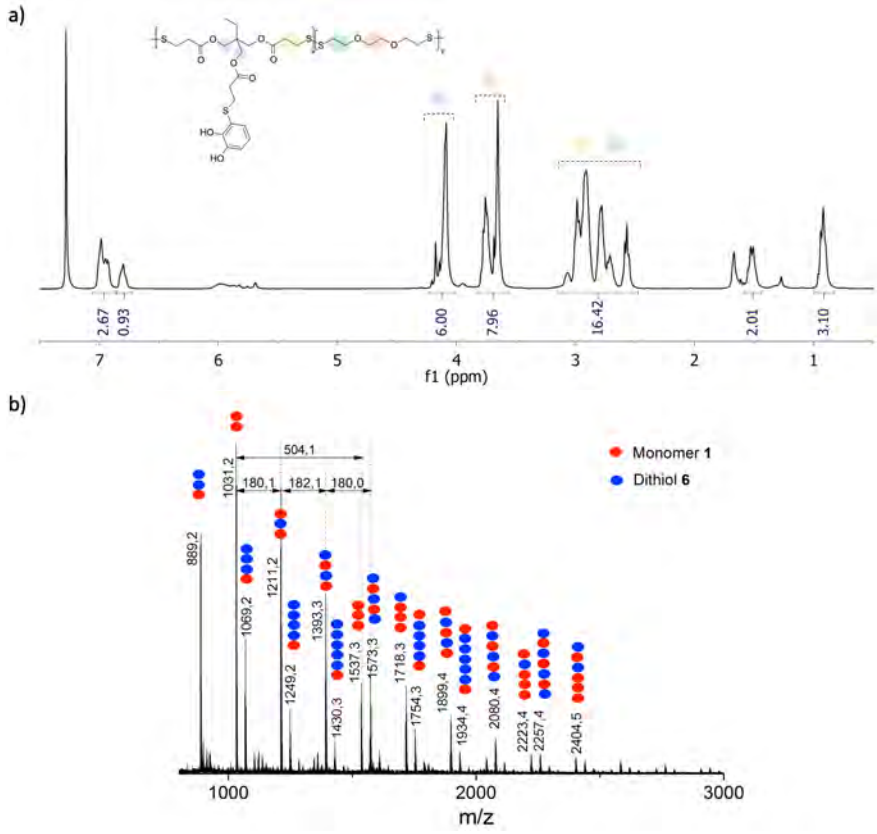


**Figure 4.10.** a) $^1$H NMR of **p(1-6)-1k** with the corresponding integrals, and b) MALDI-TOF and peak assignment of **p(1-6)-1k** (a tentative representation of the possible subunits arrangement is shown with blue and red dots).

expected molecular weight, a copolymer between monomer **1** and dithiol **6** at 1:1 ratio should have $n \approx 6$. Full conversion to polymer an Carothers equation $\bar{X}_n = 1/(1-p)$ have been considered for these estimations.

## 4.4 Adhesive and sealant properties on biological substrates

### 4.4.1 Adhesion on porcine skin

Adhesion of homopolymer **p1-0.9k** was evaluated on porcine skin with pull-off geometry (Figure 4.11a). Porcine skin is generally used and defined as the standard in ASTM due to the high similarity to human skin in terms of composition, thickness and mechanical properties. The adhesion was tested after 5 min and 6 h of the application.[f] Despite the viscous nature of **p1-0.9k**, the adhesive formulation was spread on the porcine skin successfully.

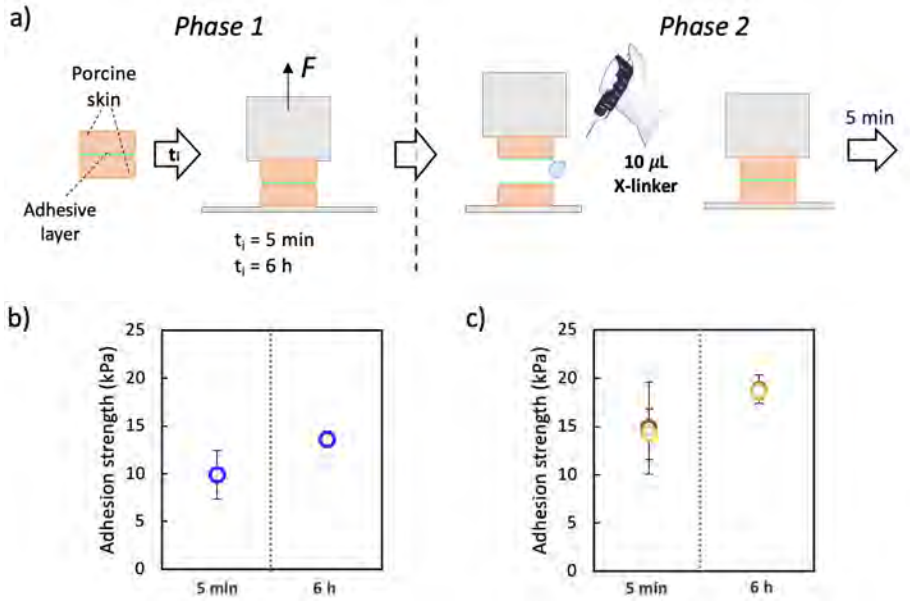


**Figure 4.11.** a) Scheme of adhesion measurement in pull-off geometry, phase 1 corresponding to the measurements before cross-linking and phase 2 corresponding to the measurements after cross-linking, b) results of **p1-0.9k** adhesion on porcine skin after 5 min and 6 h, and c) **p1-0.9k** adhesion on porcine skin after 5 min and 6 h with cross-linking via $NaIO_4$ (red) or $FeCl_3$ (yellow).

The adhesion of **p1-0.9k** after 5 min was 9.9 ± 2.5 kPa (n=11) and it increases

[f]These times were selected from the results of a first screening with **p(1-6)-1k** which revealed a performance improvement of the system as a consequence of the curing process with time from 2 to 6 h when a plateau was observed. Results are present in Annex

up to 13.6 ± 0.9 kPa (n=12) after 6 hours being cured (see Figure 4.11b).

Moreover, the adhesion was evaluated after 5 min of curing by applying $FeCl_3$ or $NaIO_4$ which are broadly used to cross-link catechol containing polymers. Adhesion of **p1-0.9k** after 5 min was 14.8 ± 4.8 kPa (n=6) with $NaIO_4$ and 14.2 ± 2.6 kPa (n=5) with $FeCl_3$. In the case of adding the cross-linker after 6 h curing, the adhesive strength was 18.9 ± 1.5 kPa (n=6) with $NaIO_4$ and 18.6 ± 0.8 kPa (n=6) with $FeCl_3$. Despite the low molecular weight of **p1-0.9k**, it showed high elasticity after first detachment as can be seen in Figure 4.12b, keeping adhesion between adhesive and tissue interface. This behavior could come from the cohesion of **p1-0.9k** from intermolecular interactions, especially H-bonding between catechols.

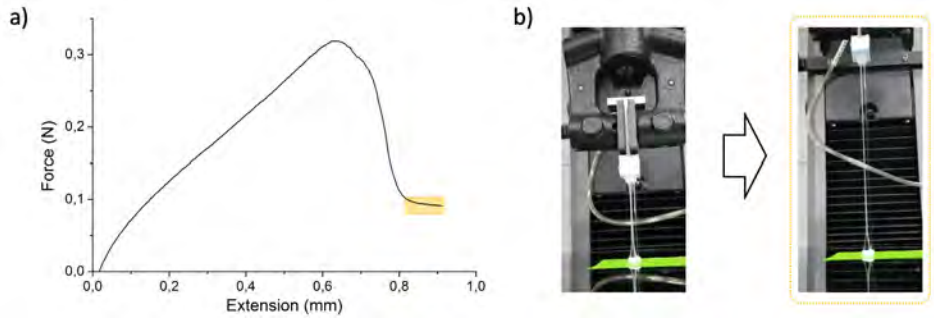


**Figure 4.12.** a) Pull-off test graph of the adhesion of **p1-0.9k** on porcine skin, and b) pictures of the specimens during the adhesion test, showing the high elasticity of the material.

For comparative means two other formulations were analyzed under the same conditions. On one side the copolymer **p(1-6)-1k** was evaluated to analyze the role of the amount of catechol functionality within the final chemical structure of the adhesive polymer. Also, a new formulation obtained from the oxidative polymerization of tristhiol **2** using 0.75 equivalents of iodine was synthesized (from now on named as **p2-2k**) for being used as reference material of a poly(disulfide) formulation of low molecular weight without containing catechol functionality.

Adhesion of **p(1-6)-1k** on porcine skin was 5.1 ± 0.7 kPa (n=12) after 5 min and 10.8 ± 1.1 kPa (n=12) after 6 h, showing a similar tendency like **p1-0.9k** but with poorer performance (Figure 4.13a). Either catechol or thiols could play an important role in this curing process through catechol-catechol reaction, catechol-thiol addition or disulfide formation as mentioned before. In the case of **p2-2k**, however, the adhesion did not change with time, being 2.1 ± 0.8 kPa (n=12) after 5 min and 2.2 ± 0.8 kPa (n=12) after 6 h (Figure 4.13b). These results could indicate that disulfide formation through free thiol oxidation could

not be the most relevant for increasing adhesion and, hence, catechol would take a major role in the curing process of the systems.

In the case of adding cross-linker, **p(1-6)-1k** had and adhesive strength of 8.2 ± 1.7 kPa (n=6) with $NaIO_4$ and 7.8 ± 1.4 kPa (n=6) with $FeCl_3$ after 5 min. When the cross-linker was added after 6 h, the adhesion of **p(1-6)-1k** was 12.3 ± 1.7 kPa (n=6) with $NaIO_4$ and 12.6 ± 0.4 kPa (n=6) with $FeCl_3$ (Figure 4.13c). Nevertheless, when the cross-linker was added to **p2-2k**, the adhesive strength remained low, being 2.9 ± 1.0 kPa (n=6) for $NaIO_4$ and 2.4 ± 1.0 kPa (n=6) for $FeCl_3$ after 5 min and 2.3 ± 0.6 kPa (n=6) for $NaIO_4$ and 2.1 ± 0.7 kPa (n=6) for $FeCl_3$ after 6 h (Figure 4.13d). The fact that the adhesive strength of **p2-2k** did not change with the addition of $NaIO_4$ and $FeCl_3$ would reinforce the fact that these cross-linking agents are favoring cohesion through catechols mainly.

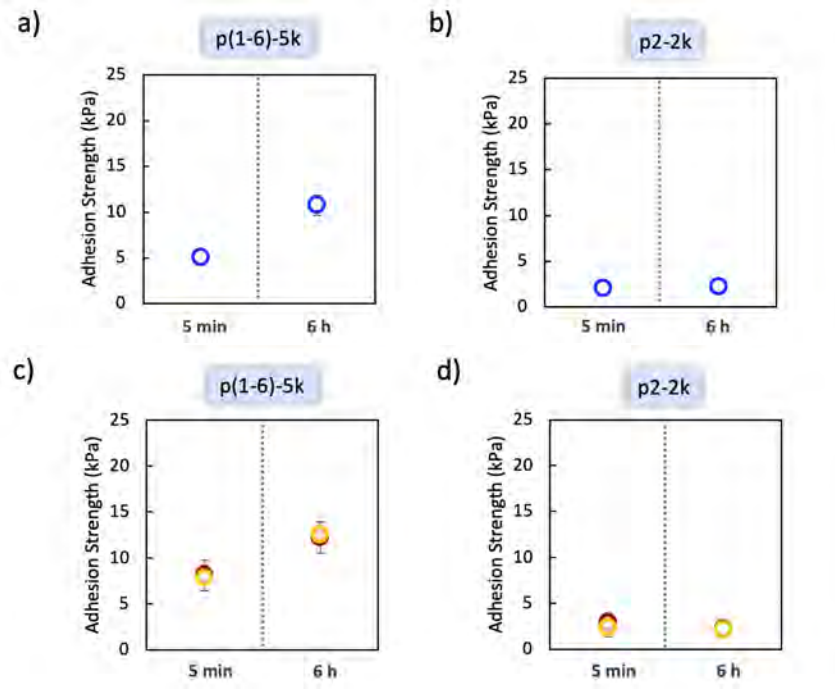


**Figure 4.13.** a) Adhesion results of **p(1-6)-1k** on porcine skin after 5 min and 6 h of curing time, b) adhesion results of **p2-2k** on porcine skin after 5 min and 6 h of curing time, c) adhesion results of **p(1-6)-1k** on porcine skin after 5 min and 6 h of curing time and cross-linking via $NaIO_4$ (red) or $FeCl_3$ (yellow), and d) adhesion results of **p2-2k** on porcine skin after 5 min and 6 h of curing time and cross-linking via $NaIO_4$ (red) or $FeCl_3$ (yellow).

The highest adhesion values obtained with these novel catechol poly(disulfide)s

formulations (18.9 ± 1.5 kPa for **p1-0.9k** and 12.6 ± 0.4 kPa for **p(1-6)-1k**) are within the range of adhesion of commercial products and other non-commercial formulations based on catechol chemistry (see Figure 4.14). These preliminary results with **p1-0.9k** and **p(1-6)-1k** demonstrate the potential of these compounds to reach end in a commercial product in terms of performance.

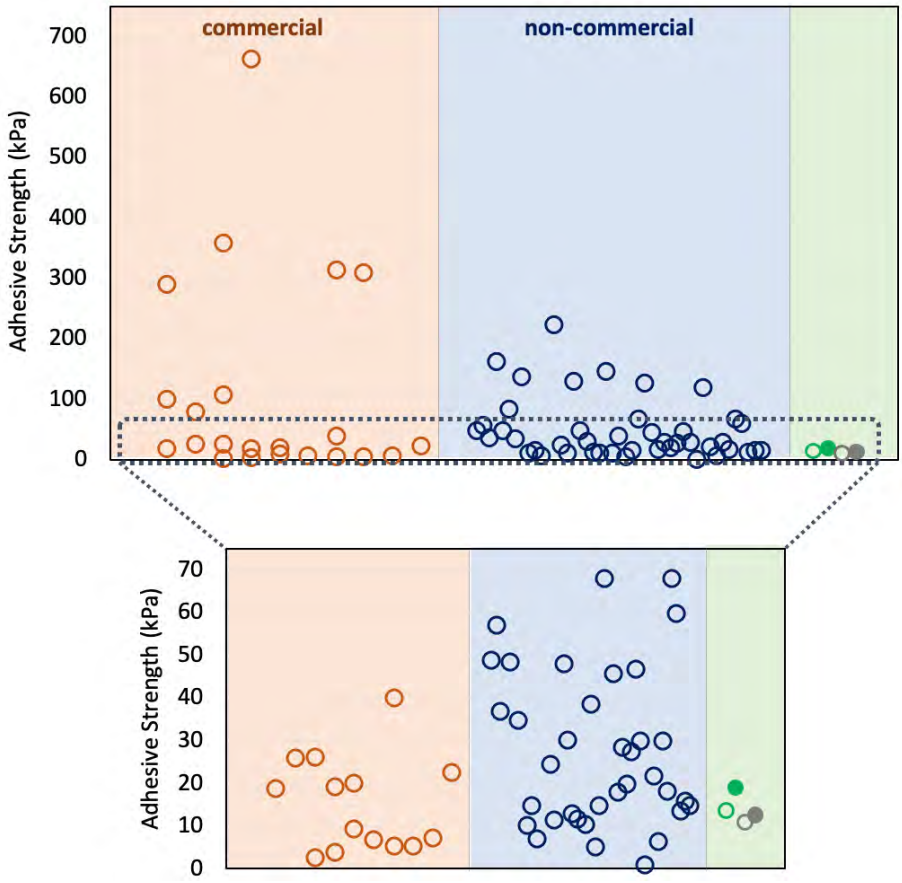


**Figure 4.14.** Benchmarking study of the adhesive performance of **p1-0.9k** and **p(1-6)-1k** with respect commercial products and other non-commercial reported tissue adhesives based on catechol containing formulations. In the green region they are represented the results from the present work, in green the results of **p1-0.9k** and in violet the results of **p(1-6)-1k** (open markers without cross-linker and filled markers with cross-linkers).

### 4.4.2 Sealing properties of adhesive formulations

The sealing ability of catechol poly(disulfide)s formulations has been evaluated *ex vivo* on porcine intestine following the protocol stablished in ASTM F2392-04 to test the burst strength of surgical adhesives. The formulation of interest was placed on the porcine intestine covering completely a 3 mm hole preformed with a biopsy punch. Once the hole was sealed, the material was left curing for five minutes. The sealing performance was recorded with a sensor by obtaining the burst pressure after injecting PBS solution with a syringe pump. For further details of the protocol followed check Experimental Section 4.7 on page 154

The burst pressure of **p1-0.9k** obtained after 5 min curing was 2.5 ± 0.9 mmHg. The addition of iron (II) acetate over **p1-0.9k** ended in a burst strength of 4.1 ± 1.6 mmHg, which is not a significant increase. Qualitatively it could be observed that, despite some change in the color confirming catechol/iron coordination, no clear change in the consistency was achieved. The use of $NaIO_4$ as cross-linker, though, increased the burst pressure up to 9.8 mmHg, but no drastic change in the consistency was seen qualitatively. The difference in performance could be related to the cross-linking mechanism and its dependency on the pH in the case of the catechol/iron complex. Ferrous solutions are only stable at pHs below 5. However at those pHs, catechol/iron mono-complex is formed and, hence, the cross-linking is not efficient. In the case of the cross-linking via catechol oxidation by $NaIO_4$, there is no dependency on the pH and the cross-linking can occur properly.

The poor solubility of **p1-0.9k** in aqueous solution is another parameter which could hinder the proper cross-linking of the system, by reducing the cross-linking points due to the bad mixture between the polymer and the aqueous solution of cross-linker. To overcome this issue, **p(1-6)-1k** has been studied since its ethylene glycol core is expected to enhance the absorption of water and improve the mixing between polymer and cross-linker solution.

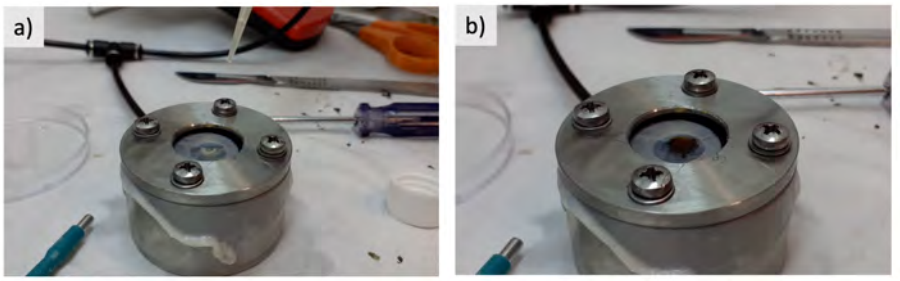


**Figure 4.15.** Pictures of the burst pressure testing system with **p(1-6)-1k** a) before addition of cross-linker and b) after addition of $NaIO_4$.

In the case of **p(1-6)-1k**, a burst pressure of 2.6 ± 1.7 mmHg is obtained after 5 min curing when adding the iron (II) acetate and no change in the consistency is observed. Nonetheless, when adding the $NaIO_4$ solution, the burst pressure increases up to 40.5 ± 9.2 and fast gelation on the surface is seen. These results show a significant increase in the sealing performance of **p(1-6)-1k** with respect to **p1-0.9k** (see Figure 4.16). However, further optimization of the formulation is required to reach values close to the performances shown by commercial products (around 130 mmHg for PREVELEAK® and 300 mmHg for BioGlue®)

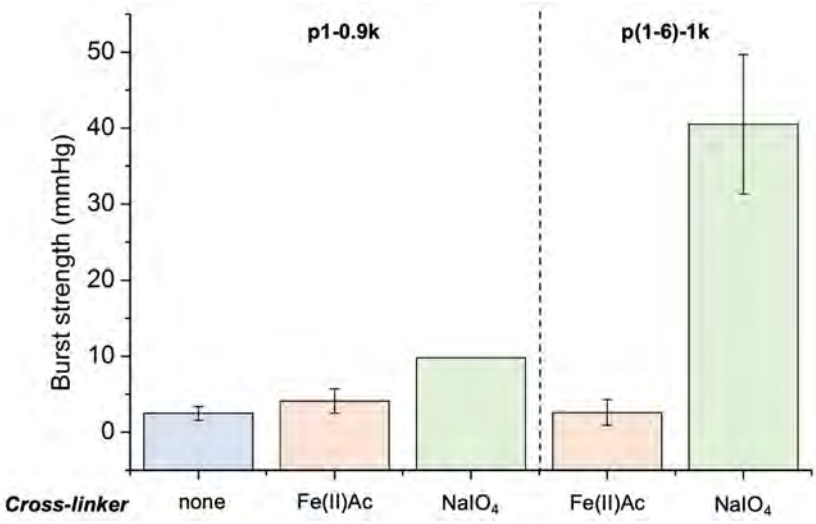


**Figure 4.16.** Burst pressure results of **p1-0.9k** and **p(1-6)-1k** and adhesive formulations with iron (II) acetate and $NaIO_4$ as cross-linking agents. Standard deviation are presented for those samples with replicates (n = 5).

## 4.5 Biocompatibility of tissue adhesive formulations

Aiming to assess the full potential of the adhesive and sealant formulations of the synthesized catechol poly(disulfide)s **p1-0.9k** and **p(1-6)-1k** for biomedical applications, the *in vitro* toxicity studies and posterior *in vivo* intradermal reactivity assay of the extracts were performed following ISO10993-5, ISO10993-10 and ISO10993-12.

### 4.5.1 *In vitro* cell viability

The cytotoxicity evaluation of **p1-0.9k** showed cell viabilities of 101.63 ± 4.05 % and 96.64 ± 0.63 % for the extracts obtained at 24 and 72 h (see Figure 4.17a), indicating good biocompatibility of this material. In the case of **p(1-6)-1k**, the cell viabilities were 19.79 ± 1.24 % and 28.62 ± 0.68 % for the extracts obtained at 24 and 72 h, which implies toxicity of the extracts of **p(1-6)-1k**.[g] However, cytotoxicity evaluation of 1:2 dilutions of original extracts[h] presented cell viabilities of 104.66 ± 3.64 % and 99.85 ± 1.24 % for the 24 and 72 h extracts respectively (Figure 4.17c). These result would prove that **p(1-6)-1k** is toxic at high amounts, but certain concentrations could be tolerated as demonstrate results from 1:2 dilutions.

Due to the toxicity presented by **p(1-6)-1k**, it was decided to evaluate the biocompatibility of **p(1-6)-45k**. In this case, cell viabilities were 93.21 ± 2.33 % and 86.49 ± 0.15 % for the extracts obtained at 24 and 72 h (see Figure 4.17b), indicating good biocompatibility of the material.

### 4.5.2 *In vivo* intradermal reactivity

The biocompatibility studies *in vivo*, were performed on New Zealand White rabbits (n=2). Extracts on physiological saline media from polymers **p1-0.9k**, **p(1-6)-1k** and **p(1-6)-45k** were evaluated after the subcutaneous injection of 200 $\mu$L.[i] The evaluation of the injection sites was done at 24, 48 and 72 h post injection as seen in Figure 4.18.

The scoring of erythema and edema on the different injection sites injection sites (Figure 4.19) revealed that **p1-0.9k**, **p(1-6)-1k** and **p(1-6)-45k** did not

[g] As defined by ISO10993-5, 'reduction of cell viability by more than 30 % is considered a cytotoxic effect.'

[h] Original extracts were obtained from incubations of 200 mg/mL of media.

[i] Generally, three injection sites were tested on each rabbit. In the cases of **p1-0.9k**, **p(1-6)-1k** only two sites could be tested due to the reduction of volume of the extract obtained which occurred from water absorption of the polymers

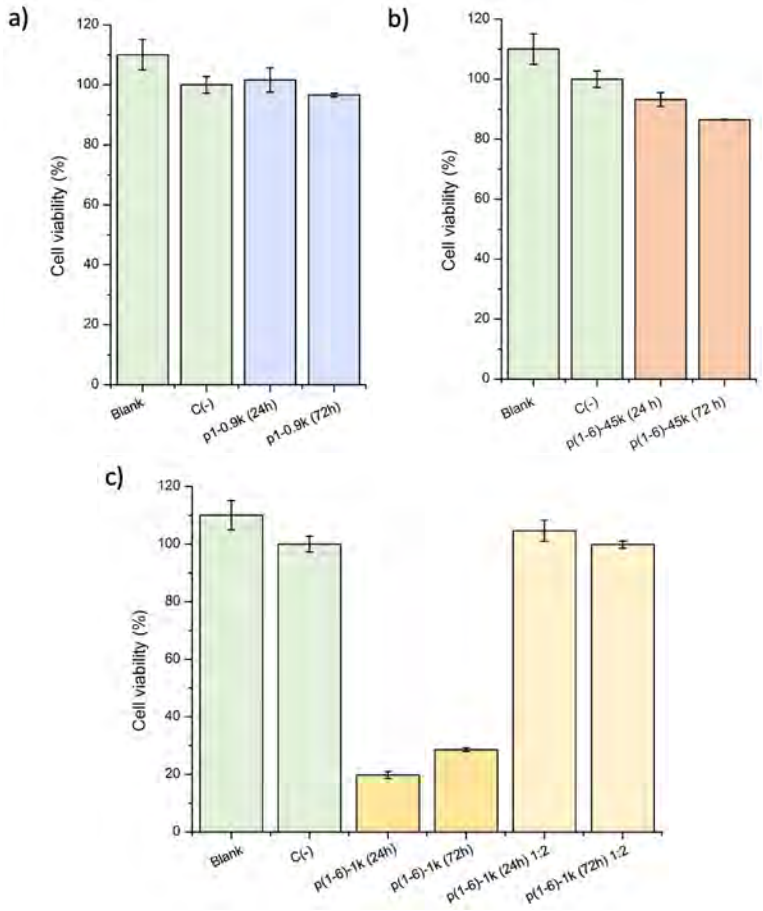


**Figure 4.17.** *In vitro* cell viabilities of a) **p1-0.9k**, b) **p(1-6)-45k**, and c) **p(1-6)-1k**. Blank results correspond to extraction media, DMEM, and C(-) to the negative control of PP standard.

show intradermal reactivity and, thus, passed the assay. Control samples coincides with the one presented in the study of **p1-50k** on Figure 3.29 of page 89.

The current results show that this new family of catechol poly(disulfide)s do not present immunologic response *in vivo* after extraction in saline media and so they are promising candidates for the development of novel compounds for biomedical application.

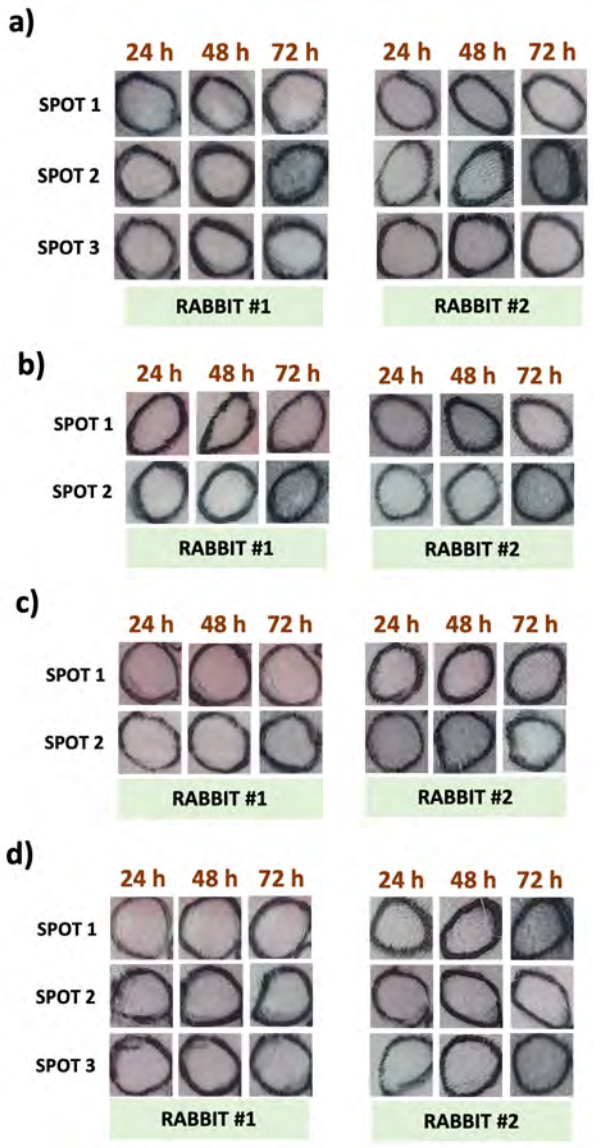


**Figure 4.18.** Images of the injection sites of a) control of physiological saline media, b) extract of **p1-0.9k** c) extracts of **p(1-6)-1k** and d) extracts of **p(1-6)-45k**. All infection sites were monitored at 24, 48 and 72 h.

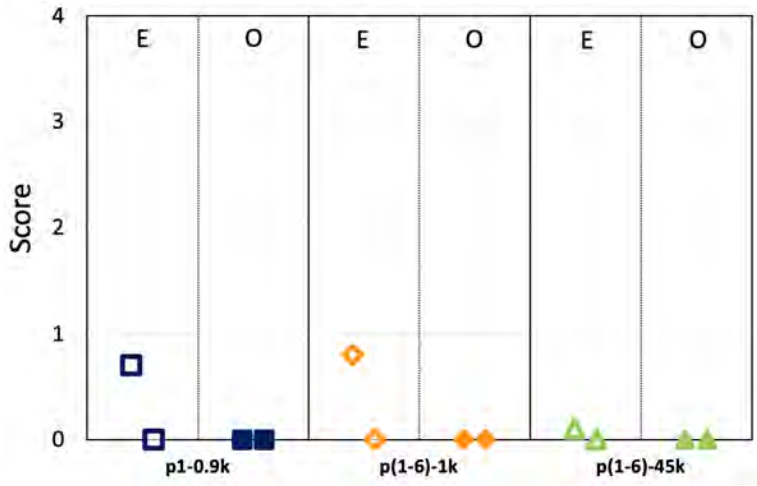


**Figure 4.19.** Results of the scoring of erythema (E) and edema (O) of **p1-0.9k**, **p(1-6)-1k** and **p(1-6)-45k** extracts in physiological saline media.

## 4.6 Polymer stability in biological environments

Another important aspect of materials aimed for biomedical application is their stability and lifetime. Especially in the case of tissue adhesives and sealants, their lifetime has to be directly related to the final application of the material.

To study these features of catechol poly(disulfide)s, polymer **p1-0.9k** was incubated under different media and times, trying to mimic physiological conditions and considering environments that could affect disulfide and ester bonds present in the polymers.

### 4.6.1 Stability in saline media: the pH and redox factor

Initially, polymer reduction was studied indirectly by following up the oxidation of DTT in a 20 mM and pH 7.4 PBS solution in $D_2O$ with presence or absence of **p1-0.9k**. This study revealed faster oxidation of DTT most likely by **p1-0.9k**, though, this result cannot be directly correlated to the disulfide reduction of polymer chain (Figure 4.20).

To clarify if disulfide reduction takes place and, hence, degradation of the polymer, the final water insoluble polymeric material was studied. The degradation of homopolymer **p1-0.9k** was followed by $^1$H NMR and GPC during two weeks and analyzed with MALDI-TOF to check potential cleavage of disulfide and ester bond.

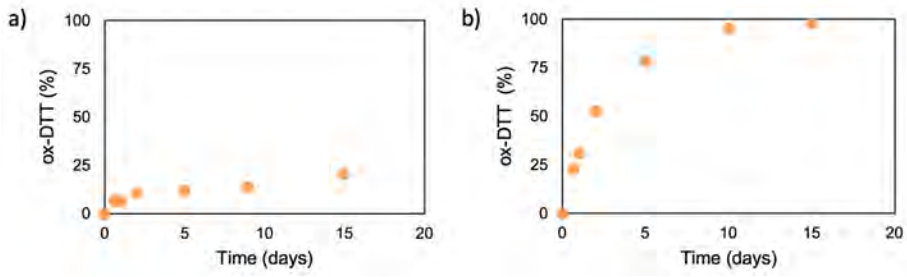


**Figure 4.20.** On the top, kinetics of the oxidation of DTT on atmospheric conditions. On the bottom, kinetics of the oxidation of DTT on atmospheric conditions and presence of **p1-0.9k**.

Three different incubation media were tested: a) PBS 10 mM pH 7.4, b) PBS 10 mM pH 7.4 + DTT 20 mM and c) acetate buffer 10 mM pH 4.9. The ratio between the integrals of the signals at 2.70 and 2.95 ppm allow us to estimate the degree of polymerization of the reaction since signal at 2.95 ppm comes from the methylene next to disulfide bond. The variation between the integrals of this region could indicate thiol oxidation and disulfide reduction. Besides, the possible appearance of a peak at 3.50 ppm would indicate the cleavage of ester bond from the core of the monomeric subunit.

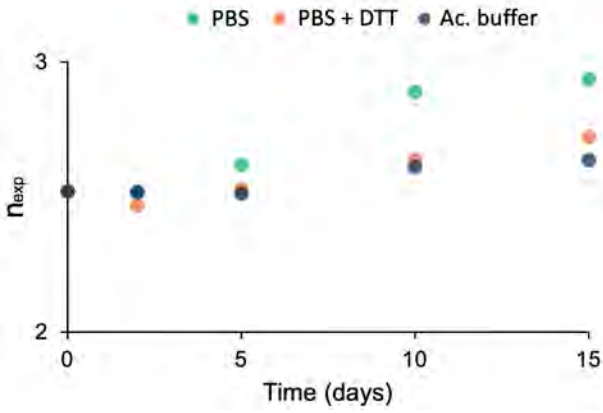


**Figure 4.21.** Change of average number of subunits ($n$) of **p1-0.9k** with time in different media obtained from $^1$H NMR analysis. In green, results from the incubation on PBS 10 mM pH 7.4; in orange from the incubation in PBS 10 mM pH 7.4 + DTT 20 mM; and in blue from the incubation in acetate buffer 10 mM pH 4.9.

The analysis of $^1$H NMR spectra pointed out that hydrolysis of ester bond did not take place under the conditions of study, since there was no appearance of

any peak at 3.50 ppm which would be directly related to the presence of free -OH generated from the ester hydrolysis. The study of the degree of polymerization in each case showed that, in general, there was no big difference in the degree of polymerization between the beginning and the end of the study if considered thiol/disulfide ratio from the signals at 2.70 and 2.95 ppm (Figure 4.21). In the system with DTT it was observed a small disulfide reduction after 2 hours ($\approx$ 2 %), but no complete reduction was achieved. Another general behavior observed was that in all cases there was a slight increase in the degree of polymerization with time. This would make sense from the point of view that this system can be oxidized due to oxygen presence through two different points. Either free thiols can be oxidized to disulfides or catechols can be oxidized to quinone, increasing the degree of polymerization. Besides, this effect is expected to be less prominent at lower pHs and in presence of reducing agents such as DTT as it was observed in the results.

Although this study gave some new insights of the system, no clear degradation through disulfide cleavage has been observed. Since **p1-0.9k** is insoluble in water, although it can absorb some, it could be possible that degradation through disulfide cleavage would be hindered. If the reduction process is not fast enough and does occur mainly in the surface of the polymer, the potential reduction could be countered by the intrinsic oxidation of the system.

In the case of degradation through ester hydrolysis, the insolubility would take a role, but at the same time, although the conditions tried were thought to simulate physiological ones, the conditions tested are not the most convenient to induce the hydrolysis. Basic media or the presence of enzymes could help the hydrolysis process of this polymer.

### 4.6.2 Stability in presence of enzymes

To evaluate the potential enzymatic degradation, **p1-0.9k** was incubated in PBS at 37 °C in presence of esterase, thioredoxin and a combination of both.

In this case the final polymer was analyzed after 15 and 30 days of incubation with enzyme. Qualitatively, no degradation was observed in any of the combinations considering visible polymer dissolution. In fact, in the incubations where esterase was present, it was seen the formation of a polymeric film on the bottom of the vial. That polymeric film was insoluble in DCM and THF, while initial **p1-0.9k** was, suggesting a potential cross-linking in the system, most probably from the reaction catechol/protein or thiol/protein. Despite this insolubility, $^{1}$H NMR, GPC and MALDI-TOF were performed, analyzing the soluble fraction in all cases.

The analysis of GPC elugrams (Figure 4.22) must be correlated with the qualitative observations. In the incubations in presence of esterase, it is seen an

increase in the molecular weight during the first 15 days. After 30 days, although it seems to be degraded by the disappearance of high molecular weight species, this result can be misunderstood, because the signal observed is coming from the soluble fraction which is the minor part of the whole polymer. In the case of presence of thioredoxin, the molecular weight seems to increase with time instead of being reduced, meaning that, if any reduction of disulfide is achieved by thioredoxin, the cleavage of disulfide bond is lower than the molecular weight increase by the intrinsic oxidation of the system previously described.

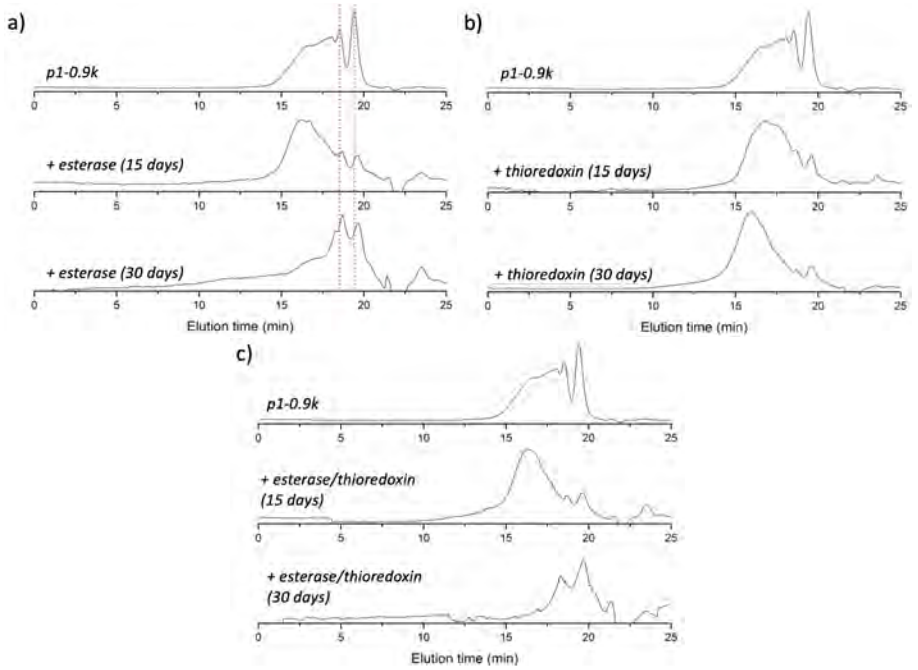


**Figure 4.22.** GPC elugrams of the soluble fraction in THF of **p1-0.9k** after incubation 15 and 30 days in presence of a) esterase, b) thioredoxin and c) esterase + thioredoxin showing the evolution of the polymer with time.

$^{1}$H NMR analysis did not give conclusive data (see Annex). In the case of esterase presence, the lack of peak around 3.5 ppm would indicate that the ester bond was not cleaved. However, it must be considered that only the soluble fraction was possible to be analyzed meaning that we cannot confirm cleavage but cannot be completely discarded that occurred in the insoluble fraction. For the thioredoxin system, free thiols signals could not be considered for the analysis, as some water was entrapped in the polymer despite the long drying process, and

signals of free thiols and water practically overlap in $CDCl_3$. If the signals at 2.70 and 2.95 ppm corresponding to free thiol and disulfide are considered, it would be concluded that in all cases there is oxidation towards disulfide formation. Although this could be expected in esterase system because it should not affect disulfide bond, in those cases were thioredoxin is present, it would be expected some disulfide cleavage.

To gain deeper information of the system MALDI-TOF was carried out. MALDI-TOF spectrum revealed that there is disulfide cleavage in systems containing thioredoxin. If low molecular weight species are checked, it can be observed that the ratio of linear species increased with respect cyclic ones taking into account intensities when thioredoxin was present alone (Figure 4.23). Oppositely, in the systems where esterase was present, the ratio of linear species decreased or is negligible, which is in accordance with the oxidation of the system observed by $^1$H NMR. Although $^1$H NMR shows oxidation in all the cases, these MALDI-TOF analysis would indicate that in the systems where thioredoxin is present, disulfide bond can be cleaved indeed. The mismatch between the observations in $^1$H NMR and MALDI-TOF in thioredoxin containing systems could be caused by the effect of longer polymeric/oligomeric species. In fact, GPC elugrams shows that the number of smallest oligomers (higher elution times) is reduced with the time. Although MALDI-TOF would demonstrate the expected cleavage of disulfides in low molecular weight oligomers, the predominant effect taking place seems to be the intrinsic oxidation of the system and other side reactions occurring between catechol poly(disulfide)s and the proteins.

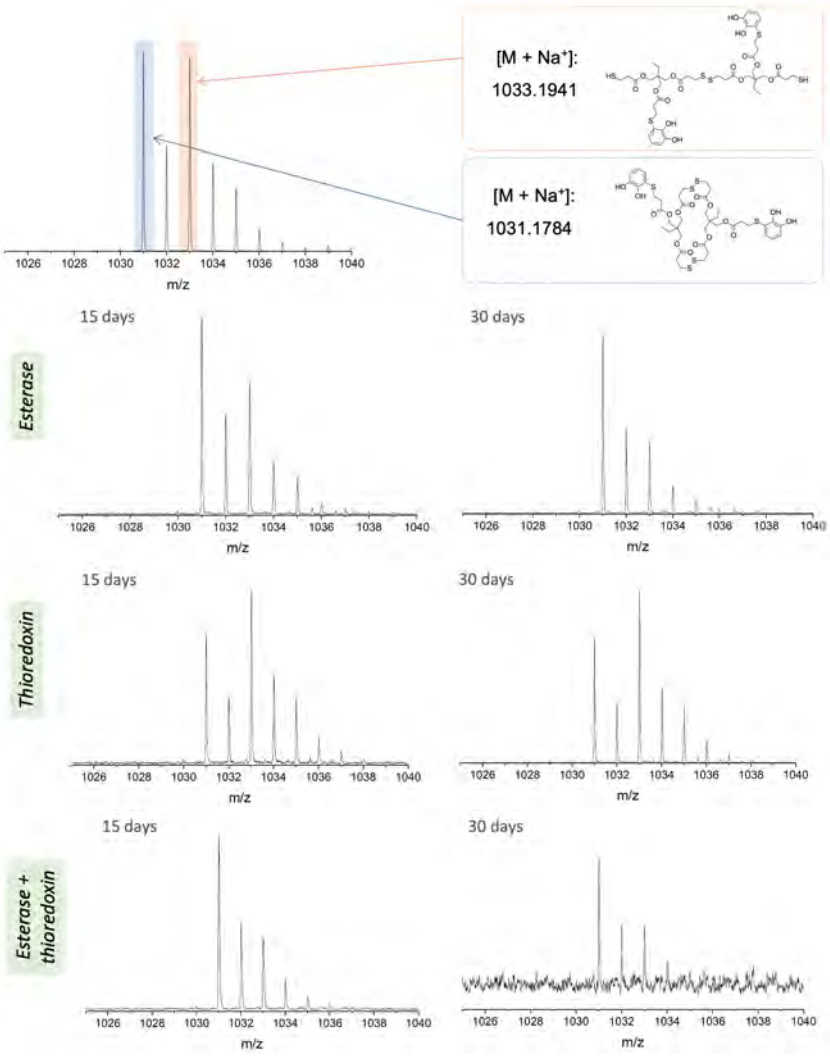


**Figure 4.23.** MALDI-TOF spectrum showing the evolution of the peak corresponding to the dimer after 15 and 30 days of incubation in presence of esterase, thioredoxin and their combination.

## 4.7 Experimental section

### 4.7.1 Synthesis of p1

For the optimization process, monomer **1** (100 mg, 0.2 mmol) and sodium bicarbonate (25, 27 or 33 mg, for the reactions of 0.75, 0.80 and 0.90 equivalents respectively) were mixed in EtOH 96 % (75 $\mu$L) in a small round bottom flask. Then, a solution of iodine (37.6, 40.2 or 45.2 for the reactions of 0.75, 0.80 and 0.90 equivalents respectively) dissolved in EtOH 96 % (375 $\mu$L) was added over the previous one dropwise. Once added, the reaction was left under magnetic stirring at 800 rpm for 15 min at room temperature. The final mixture was dried under reduced pressure. The oligomeric fraction was isolated by extracting the mixture in DCM:$H_2O$ to remove the excess of salts. The organic phase was collected, dried with anhydrous $Na_2SO_4$ and filtered. The final product **p1-0.9k** was obtained after drying the solvent under reduced pressure for 48 h.

In the scaled up synthesis of **p1-0.9k**, monomer **1** (506 mg, 1.0 mmol) and $NaHCO_3$ (134.4 mg, 1.6 mmol) were mixed in EtOH 96 % (0.5 mL). Then, a solution of iodine (190.5 mg, 0.75 mmol) dissolved in EtOH 96 % (1.5 mL) was added over the previous one at 300 $\mu$L/min with a syringe pump. Once added, the reaction was left under magnetic stirring at 800 rpm for 20 min at room temperature. The final mixture was dried under reduced pressure. The oligomeric fraction was isolated by extracting the mixture in DCM:$H_2O$ to remove the excess of salts. The organic phase was collected, dried with anhydrous $Na_2SO_4$ and filtered. The final product **p1-0.9k** was obtained after drying the solvent under reduced pressure for 48 h affording a colorless viscous polymer (412 mg).

**IR(neat)**: ($cm^{-1}$) 3407, 2968, 2938, 1726, 1635, 1587, 1559, 1541, 1458, 1411, 1387, 1350, 1277, 1223, 1159, 1131, 1056, 1015, 991, 928, 898, 852, 824, 777, 728, 701, 667, 638, 567.

### 4.7.2 Synthesis of p(1-6)

For the synthesis of **p(1-6)-1k**, monomer **1** (253 mg, 0.5 mmol), dithiol **6** (81.4 $\mu$L, 0.5 mmol) and sodium bicarbonate (147.0 mg, 1.75 mmol) were mixed in EtOH 96 % (500 $\mu$L). Then, a solution of iodine (211.0 mg, 0.83 mmol) dissolved in EtOH 96 % (1.5 mL) was added at 300 $\mu$L/min with a syringe pump. Once added, the reaction was left under magnetic stirring at 800 rpm for 20 min at room temperature. The final mixture was dried under reduced pressure. The oligomeric fraction was isolated by extracting the mixture in DCM:$H_2O$ to remove the excess of salts. The organic phase was collected, dried with anhydrous $Na_2SO_4$ and filtered. The final product was obtained after drying the solvent under reduced pressure for 48 h affording a colorless viscous polymer (321 mg).

For copolymerization study of **p(1-6)-nk**, monomer **1** and **6** (0.20 mmol in total; 0.15 mmol monomer **1** and 0.05 mmol **6** for 75:25, 0.10 mmol monomer **1** and 0.10 mmol **6** for 50:50 or 0.05 mmol monomer **1** and 0.15 mmol **6** for 25:75) were dissolved in EtOH 96 % (5 mL) in a round bottom flask. Then, a solution of iodine (75.5 mg, 0.30 mmol) dissolved in EtOH 96 % (1.5 mL) was added over the previous one at 300 $\mu$L/min with a syringe pump. Once added, the reaction was left under magnetic stirring at 500 rpm for 20 min at room temperature. The white precipitated polymer obtained was washed a minimum of 5 time with EtOH 96 % until excess of iodine was fully removed. The final product was dried under reduced pressure for 24 h. The reaction was performed at the molar ratios 75:25, 50:50 and 25:75 of **1**:**6**.

### 4.7.3 Synthesis of p2-2k

Trimethylolpropane tris(3-mercaptopropionate) **2** (500 mg, 1.25 mmol) and sodium bicarbonate (174 mg, 2.05 mmol) were mixed in EtOH 96 % (625 $\mu$L). Then, a solution of iodine (238, 0.94 mmol, 0.75 eq.) dissolved in 1.9 mL of EtOH 96 % was added over the previous one at 300 $\mu$L/min with a syringe pump. Once added, the reaction was left under magnetic stirring at 800 rpm for 20 min at room temperature. The final mixture was dried under reduced pressure. The oligomeric fraction was isolated by extracting the mixture in DCM:$H_2O$ to remove the excess of salts. The organic phase was collected, dried with anhydrous $Na_2SO_4$ and filtered. The final product was obtained after drying the solvent under reduced pressure for 48 h affording a colorless viscous polymer (320 mg).

### 4.7.4 Adhesion test on porcine skin

#### 4.7.4.1 Porcine skin and sample preparation

Porcine skin from the flank of the pig was bought on local butcher and stored at -4 °C until used. After defrosted, porcine skin was cut using a biopsy punch (Miltex) of 6 mm and the fat layer was removed. The substrates were immersed in PBS 1x (GIBCO) overnight at 4 °C.

10 $\mu$L of **p1-0.9k**, **p(1-6)-1k** or **p2-2k** were applied on a porcine skin substrate after removing excess of water and two substrates were joined together. Adhered substrates were left curing during 5 min or 6 h before testing keeping them in a petri dish with PBS 1x and gauze to preserve the samples from dryness.

#### 4.7.4.2 Pull off test procedure

Adhesion testing on porcine skin was performed with a universal testing machine (UTM, INSTRON 5583) equipped with 250 N loading sensor.

The external part of porcine skin of the sample was attached to a flat surface using an instant adhesive (Loctite®, Henkel) and a preloading of 1 N during 1 min was applied before measuring the adhesion force.

For cross-linker studies, after a first measurement, 10 $\mu$L of 270 mM ($NaIO_4$ or $FeCl_3$) for **p1-0.9k** and polytris or 175 mM ($NaIO_4$ or $FeCl_3$) for **p(1-6)-1k** were added. A preloading force of 1 N was applied and the pull-off test performed after curing for 5 min in presence of the cross-linking agent.

## 4.7.5 Sealing measurements

### 4.7.5.1 Sample preparation

Sausage casing from porcine intestine was bought on local butcher, sliced in cylindrical fragments of 5 cm in length and stored at -4 °C until used. Before its use, sausage casing was kept soaked in PBS pH 7.4 for 2 hours. Each slice was cut to get a flat surface and a 3 mm hole was done in the center with a 3 mm biopsy punch.

### 4.7.5.2 Burst pressure test

The burst pressure of **p1-0.9k** and **p(1-6)-1k** was tested following the standard test method on ASTM F2392-04. 80 $\mu$L of the adhesive formulation was placed on the hole of the substrate and was left during 10 min of curing. In the case of cross-linker study, 12 $\mu$L of an iron (II) acetate or $NaIO_4$ solution 0.25 M was added over the sealant. Afterwards, the test was proceeded by increasing the pressure of the system with a syringe pump with PBS at 2 mL/min rate until pressure showed by the pressure recording unit went down. A minimum of 5 replicates were performed for each formulation.

## 4.7.6 *In vitro* cell viability and *in vivo* intradermal reactivity

**Extract preparation**. The extracts of polymers **p1-0.9k** and **p(1-6)-1k** was obtained by immersing the polymeric materials in a ratio of 0.2 g/mL of extract media, using DMEM (Invitrogen) or saline media CLEANCLE® (JW Pharmaceutical) for the *In vitro* cell viability and *in vivo* intradermal reactivity respectively. Polymer **p(1-6)-45k** was adsorbed on PP textile (DH Material Medico, Barcelona, Spain) which was cut in substrates of 5 x 1 cm in size with a laser cutter. The adsorption was achieved by immersing the PP textile substrate into 50 mg/mL solution of **p(1-6)-45k** in DCM and drying it under reduced pressure to get a fully coated substrate. PP textile substrates were properly coated with 2.3 $\pm$ 0.6 mg/cm$^2$ of **p(1-6)-45k** on average (n=5). An extraction ratio of 6

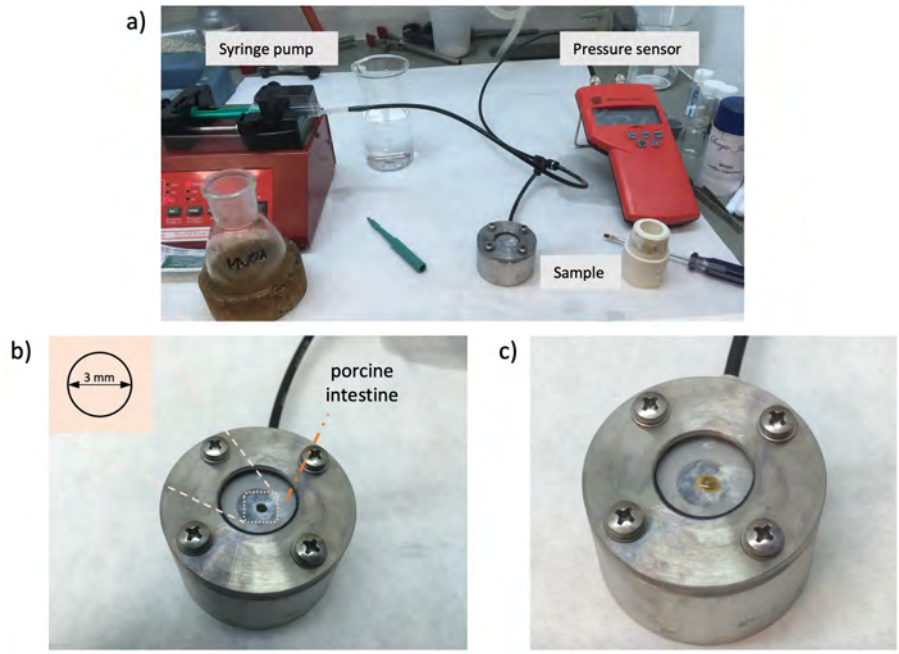


**Figure 4.24.** a) Whole system with the syringe pump and the pressure sensor for burst pressure measurement, b) porcine intestine on the testing device with the 3 mm diameter hole, and c) sample of **p1-0.9k** already prepared for being tested.

$cm^2$/mL was applied to obtain the corresponding extracts on DMEM (Invitrogen) or saline media CLEANCLE® (JW Pharmaceutical). All extraction ratios have been set following the considerations described in ISO10993-12.

**Procedure**. Experimental protocol for *in vitro* cell viability and *in vivo* intradermal reactivity evaluation of **p1-0.9k**, **p(1-6)-1k** and **p(1-6)-45k** were the same of those described on Section 3.8.6 and 3.8.7.

### 4.7.7 Stability studies in saline media

For the stability studies, three different buffer solutions were checked: PBS 10 mM pH 7.4, PBS 10 mM pH 7.4 + DTT 20 mM and acetate buffer 10 mM pH 4.9. Polymer **p1-0.9k** was immersed to get a concentration of 5 mg/mL. The system was kept under constant agitation during 15 days at room temperature. At the time of evaluation, the aqueous solution was removed, the insoluble polymer washed with water and dried under reduced pressure for 48 h and analyzed by

$^{1}$H NMR.

### 4.7.8 Stability studies with enzymes

Polymer **p1-0.9k** was immersed in PBS 10 mM pH 7.4 at a concentration of 5 mg/mL. Then 167 $\mu$L of a stock solution of enzyme (esterase and/or thioredoxin) was added. The stock solution of esterase was prepared by dissolving 30 mg of esterase from porcine liver in 10 mL of PBS 10 mM pH 7.4 ($\approx$ 60 U/mL). For thioredoxin, 1 mg of thioredoxin from *E. Coli* was dissolved in 10 mL of PBS 10 mM pH 7.4 ($\approx$ 0.3 U/mL). The enzymatic degradation was studied during 30 days in presence of esterase, thioredoxin and the combination of both. During the study, all samples were kept in an incubator to simulate enzymatic activity at physiological conditions. Each 3-4 days, the supernatant of the samples was replaced, and fresh enzyme solution was added (167 $\mu$L) to ensure full enzymatic activity along the study.

# CHAPTER 5

# General conclusions

In the present thesis, the polymerization and application of catechol poly(disulfide)s as adhesives have been studied for their use in the biomedical field. After the rigorous analysis during the different stages of the optimization and characterization process, the conclusions of the thesis are summarized next:

- To obtain high purity in monomer **1** is required to perform three purification steps: i) purification of starting tristhiol **2** to remove impurity **9**; ii) first purification by flash column chromatography to remove the cyclic side product **11** and the double addition product **12**; and iii) reduction process and posterior purification by flash column chromatography to remove traces of disulfide **10**.

- The 'blank' monomer containing 3,4-dimethoxy benzyl group **8** could be synthesized and isolated following thiol-ene approach, while benzyl functionalized monomer **7** could not be completely isolated and used as reference.

- From the model polymerization reaction of dithiol with iodine, it could be concluded that chain growth of 1,6-hexandithiol **5** polymerization can be maximized by pushing reaction equilibria adding higher stochiometries of iodine and with the presence of bases such as $NaHCO_3$ or sodium salicylate.

- From the optimization of polymerization of monomer **1**,it could be concluded that is possible to obtain catechol poly(disulfide)s **p1** with $n \approx 100$ (50.000 g/mol) working at 0.04 M and 1.5 equivalents of iodine.

- Monomer **8** can be polymerized to obtain reference poly(disulfide)s **p8** with $n \approx 66$ (37.000 g/mol) working at 0.04 M and 1.5 equivalents of iodine in presence of salicylate.

- Catechol poly(disulfide)s **p1** presents adhesion values from 1 to 4 MPa and has substrate dependent behavior, with cohesive failure in most cases. Reference poly(disulfide)s **p8** presented poor adhesion values demonstrating the importance of catechol functionality in the final adhesion of the material.

- The adhesion of catechol poly(disulfide)s **p1** is reversible after several bonding/debonding processes induced by heat, showing remarkable increase of the adhesive strength on titanium substrates.

- The UV-Vis analysis on surface of the substrates containing the adhesive layer of **p1-50k** demonstrated the coordination of catechol on stainless steel specimens with the appearance of a broad band with $\lambda_{max}$ around 576 nm.

- Cyclic catechol disulfides **p1-cyc** could be isolated from the soluble fraction during polymerization of monomer **1**. The characterization of **p1-cyc** by DOSY and MALDI-TOF showed the presence of macrocycles up to the hexamer, being able to isolate cyclic monomer **c1** by flash column chromatography.

- Through heat-induced ROP, it was possible to polymerize cyclic catechol disulfides **p1-cyc** to obtain reversible adhesives with adhesion performances ranging from 1.5 to 3 MPa depending on the substrate.

- Oligomeric formulations from homopolymer **p1-0.9k** and copolymer **p(1-6)-1k** could be used as tissue adhesives, showing adhesive strengths of 14.8 and 10.8 kPa on wet porcine skin. The adhesive performances of these formulations could be improved up to 18.9 and 12.6 kPa respectively by adding cross-linker such as $NaIO_4$ or $FeCl_3$.

- For sealing purposes, copolymer **p(1-6)-1k** showed the highest performance on porcine intestine, reaching values up to 40.5 mmHg.

- Homopolymer **p1-0.9k** exhibited high stability on simulated physiological media and in presence of enzymes like esterase and thioredoxin.

- The promising results of the *in vitro* and *in vivo* studies of all the homopolymers **p1** and copolymers **p(1-6)** tested during this work revealed the good biocompatibility of the materials as defined by ISO 10993, which demonstrates the high potential of these materials in the biomedical field.

Throughout the present work a series of novel materials have been synthesized and characterized in depth, showing the feasibility and applicability of catechol poly(disulfide)s. The efforts on different aspects of the synthesis and polymerization process have revealed the peculiarities of the interplay between catechol, thiols and disulfides present in these new compounds and polymers, and the crucial role of catechol on their adhesion. The promising results from this thesis set the precedents for further development in the near future of catechol poly(disulfide)s with potential application on the biomedical field.

# Bibliography


(1) Queiroz, C.; Mendes Lopes, M. L.; Fialho, E.; Valente-Mesquita, V. L. *Food Rev. Int.* **2008**, *24*, 361–375.

(2) D'Ischia, M.; Napolitano, A.; Pezzella, A.; Meredith, P.; Sarna, T. *Angew. Chemie - Int. Ed.* **2009**, *48*, 3914–3921.

(3) Vincent, J. F.; Hillerton, J. E. *J. Insect Physiol.* **1979**, *25*, 653–658.

(4) Zhao, M.; Bai, L.; Jang, J. *Appl. Surf. Sci.* **2020**, *511*, 1–8.

(5) Priemel, T.; Palia, R.; Babych, M.; Thibodeaux, C. J.; Bourgault, S.; Harrington, M. J. *Proc. Natl. Acad. Sci. U. S. A.* **2020**, *117*, 7613–7621.

(6) Waite, J. H.; Tanzer, M. L. *Science* **1981**, *212*, 1038–1040.

(7) Gebbie, M. A.; Wei, W.; Schrader, A. M.; Cristiani, T. R.; Dobbs, H. A.; Idso, M.; Chmelka, B. F.; Herbert Waite, J.; Israelachvili, J. N. *Nat. Chem.* **2017**, *9*, 473–479.

(8) Yu, J.; Wei, W.; Danner, E.; Ashley, R. K.; Israelachvili, J. N.; Waite, J. H. *Nat. Chem. Biol.* **2011**, *7*, 588–590.

(9) Yang, J.; Cohen Stuart, M. A.; Kamperman, M. *Chem. Soc. Rev.* **2014**, *43*, 8271–8298.

(10) Uchimiya, M.; Stone, A. T. *Chemosphere* **2009**, *77*, 451–458.

(11) Patil, N.; Jérôme, C.; Detrembleur, C. *Prog. Polym. Sci.* **2018**, *82*, 34–91.

(12) Litwinienko, G.; Mulder, P. *J. Phys. Chem. A* **2009**, *113*, 14014–14016.

(13) Shin, H. S.; Satsu, H.; Bae, M. J.; Totsuka, M.; Shimizu, M. *Nutrients* **2017**, *9*, 1–12.

(14) Pinnataip, R.; Lee, B. P. *ACS Omega* **2021**, *6*, 5113–5118.

(15) Della Vecchia, N. F.; Avolio, R.; Alfè, M.; Errico, M. E.; Napolitano, A.; D'Ischia, M. *Adv. Funct. Mater.* **2013**, *23*, 1331–1340.

(16) Greco, G.; Panzella, L.; Verotta, L.; D'Ischia, M.; Napolitano, A. *J. Nat. Prod.* **2011**, *74*, 675–682.

(17) Kim, E.; Panzella, L.; Micillo, R.; Bentley, W. E.; Napolitano, A.; Payne, G. F. *Sci. Rep.* **2015**, *5*, 1–14.

(18) Ito, S.; Wakamatsu, K.; Ozeki, H. *Pigment Cell Res.* **2000**, *13*, 103–109.

(19) Iacomino, M.; Mancebo-Aracil, J.; Guardingo, M.; Martín, R.; D'Errico, G.; Perfetti, M.; Manini, P.; Crescenzi, O.; Busqué, F.; Napolitano, A.; D'Ischia, M.; Sedó, J.; Ruiz-Molina, D. *Int. J. Mol. Sci.* **2017**, *18*, DOI: 10.3390/ijms18102169.

(20) Ito, S.; Prota, G. *Experientia* **1977**, *33*, 1118–1119.

(21) Zhao, H.; Waite, J. H. *J. Biol. Chem.* **2006**, *281*, 26150–26158.

(22) Valois, E.; Hoffman, C.; Demartini, D. G.; Waite, J. H. *Langmuir* **2019**, *35*, 15985–15991.

(23) Lee, Y.; Chung, H. J.; Yeo, S.; Ahn, C. H.; Lee, H.; Messersmith, P. B.; Park, T. G. *Soft Matter* **2010**, *6*, 977–983.

(24) Krüger, J. M.; Börner, H. G. *Angew. Chemie - Int. Ed.* **2021**, *60*, 6408–6413.

(25) Mancebo-Aracil, J.; Casagualda, C.; Moreno-Villaécija, M. Á.; Nador, F.; García-Pardo, J.; Franconetti-García, A.; Busqué, F.; Alibés, R.; Esplandiu, M. J.; Ruiz-Molina, D.; Sedó-Vegara, J. *Chem. - A Eur. J.* **2019**, *25*, 12367–12379.

(26) Saiz-Poseu, J.; Mancebo-Aracil, J.; Nador, F.; Busqué, F.; Ruiz-Molina, D. *Angew. Chemie - Int. Ed.* **2019**, *58*, 696–714.

(27) Lin, Q.; Gourdon, D.; Sun, C.; Holten-Andersen, N.; Anderson, T. H.; Waite, J. H.; Israelachvili, J. N. *Proc. Natl. Acad. Sci. U. S. A.* **2007**, *104*, 3782–3786.

(28) Hwang, D. S.; Harrington, M. J.; Lu, Q.; Masic, A.; Zeng, H.; Waite, J. H. *J. Mater. Chem.* **2012**, *22*, 15530–15533.

(29) Chirdon, W. M.; O'Brien, W. J.; Robertson, R. E. *J. Biomed. Mater. Res. - Part B Appl. Biomater.* **2003**, *66*, 532–538.

(30) Saiz-Poseu, J.; Alcón, I.; Alibés, R.; Busqué, F.; Faraudo, J.; Ruiz-Molina, D. *CrystEngComm* **2012**, *14*, 264–271.

(31) Saiz-Poseu, J.; Sedõ, J.; García, B.; Benaiges, C.; Parella, T.; Alibés, R.; Hernando, J.; Busqué, F.; Ruiz-Molina, D. *Adv. Mater.* **2013**, *25*, 2066–2070.

(32) Li, S.-C.; Chu, L.-N.; Gong, X.-Q.; Diebold, U. *Science* **2010**, *328*, 882–885.

(33) Akram Bhuiyan, M. S.; Roland, J. D.; Liu, B.; Reaume, M.; Zhang, Z.; Kelley, J. D.; Lee, B. P. *J. Am. Chem. Soc.* **2020**, *142*, 4631–4638.

(34) Zhang, W.; Wang, R.; Sun, Z. M.; Zhu, X.; Zhao, Q.; Zhang, T.; Cholewinski, A.; Yang, F.; Zhao, B.; Pinnaratip, R.; Forooshani, P. K.; Lee, B. P. *Chem. Soc. Rev.* **2020**, *49*, 433–464.

(35) Zhang, L.; Liu, M.; Zhang, Y.; Pei, R. *Biomacromolecules* **2020**, *21*, 3966–3983.

(36) Hong, S.; Wang, Y.; Park, S. Y.; Lee, H. *Sci. Adv.* **2018**, *4*, 1–11.

(37) Sever, M. J.; Weisser, J. T.; Monahan, J.; Srinivasan, S.; Wilker, J. J. *Angew. Chemie - Int. Ed.* **2004**, *43*, 448–450.

(38) Sever, M. J.; Wilker, J. J. *J. Chem. Soc. Dalt. Trans.* **2004**, *4*, 1061–1072.

(39) Holten-Andersen, N.; Harrington, M. J.; Birkedal, H.; Lee, B. P.; Messersmith, P. B.; Lee, K. Y. C.; Waite, J. H. *Proc. Natl. Acad. Sci. U. S. A.* **2011**, *108*, 2651–2655.

(40) Menyo, M. S.; Hawker, C. J.; Waite, J. H. *Soft Matter* **2013**, *9*, 10314–10323.

(41) Krogsgaard, M.; Hansen, M. R.; Birkedal, H. *J. Mater. Chem. B* **2014**, *2*, 8292–8297.

(42) Włodarczyk-Biegun, M. K.; Paez, J. I.; Villiou, M.; Feng, J.; Del Campo, A. *Biofabrication* **2020**, *12*, 1–16.

(43) Holm Agergaard, A.; Sommerfeldt, A.; Uttrup Pedersen, S.; Birkedal, H.; Daasbjerg, K. *Angew. Chemie Int. Ed.* **2021**, 1–8.

(44) Bijlsma, J.; de Bruijn, W. J.; Hageman, J. A.; Goos, P.; Velikov, K. P.; Vincken, J. P. *Sci. Rep.* **2020**, *10*, 1–11.

(45) Xu, C.; Chen, Y.; Si, Y.; Yan, Y.; Kayitmazer, A. B.; Ding, Y.; Qian, W.; Zheng, Z.; Cao, S.; Xu, Y. *Adv. Mater. Interfaces* **2021**, *8*, 2001955–2001965.

(46) Zhang, Y.; Zhao, Y.; Xia, S.; Tao, L.; Wei, Y. *Macromol. Rapid Commun.* **2020**, *41*, 1900533–1900539.

(47) Moon, J.; Huh, Y.; Park, J.; Kim, H. W.; Choe, Y.; Huh, J.; Bang, J. *ACS Appl. Polym. Mater.* **2020**, *2*, 2444–2451.

(48) Putnam, A. A.; Wilker, J. J. *Soft Matter* **2021**, *17*, 1999–2009.

(49) Baby, M.; Periya, V. K.; Sankaranarayanan, S. K.; Maniyeri, S. C. *Appl. Surf. Sci.* **2020**, *505*, 144414–144424.

(50) Jenkins, C. L.; Siebert, H. M.; Wilker, J. J. *Macromolecules* **2017**, *50*, 561–568.

(51) Lee, H.; Dellatore, S. M.; Miller, W. M.; Messersmith, P. B. *Science* **2007**, *318*, 426–430.

(52) Sung, M. K.; Rho, J.; Choi, I. S.; Messersmith, P. B.; Lee, H. *J. Am. Chem. Soc.* **2009**, *131*, 13224–13225.

(53) Hong, S.; Kim, J.; Na, Y. S.; Park, J.; Kim, S.; Singha, K.; Im, G. I.; Han, D. K.; Kim, W. J.; Lee, H. *Angew. Chemie - Int. Ed.* **2013**, *52*, 9187–9191.

(54) Lim, C.; Huang, J.; Kim, S.; Lee, H.; Zeng, H.; Hwang, D. S. *Angew. Chemie - Int. Ed.* **2016**, *55*, 3342–3346.

(55) Yu, L.; Liu, X.; Yuan, W.; Brown, L. J.; Wang, D. *Langmuir* **2015**, *31*, 6351–6366.

(56) Zhang, H.; Yu, L.; Ma, X.; Peng, Y.; Hu, J.; Ruan, S. *Appl. Surf. Sci.* **2020**, *510*, 1–10.

(57) Liebscher, J.; Mrówczyński, R.; Scheidt, H. A.; Filip, C.; Haìdade, N. D.; Turcu, R.; Bende, A.; Beck, S. *Langmuir* **2013**, *29*, 10539–10548.

(58) Barclay, T. G.; Hegab, H. M.; Clarke, S. R.; Ginic-Markovic, M. *Adv. Mater. Interfaces* **2017**, *4*, 1–20.

(59) Barrett, D. G.; Sileika, T. S.; Messersmith, P. B. *Chem. Commun.* **2014**, *50*, 7265–7268.

(60) Wang, H.; Wu, J.; Cai, C.; Guo, J.; Fan, H.; Zhu, C.; Dong, H.; Zhao, N.; Xu, J. *ACS Appl. Mater. Interfaces* **2014**, *6*, 5602–5608.

(61) Qiu, W. Z.; Yang, H. C.; Wan, L. S.; Xu, Z. K. *J. Mater. Chem. A* **2015**, *3*, 14438–14444.

(62) Iacomino, M.; Paez, J. I.; Avolio, R.; Carpentieri, A.; Panzella, L.; Falco, G.; Pizzo, E.; Errico, M. E.; Napolitano, A.; Del Campo, A.; D'Ischia, M. *Langmuir* **2017**, *33*, 2096–2102.

(63) Suárez-García, S.; Sedó, J.; Saiz-Poseu, J.; Ruiz-Molina, D. *Biomimetics* **2017**, *2*, 1–17.

(64) Kim, M. H.; Lee, J. N.; Lee, J.; Lee, H.; Park, W. H. *ACS Biomater. Sci. Eng.* **2020**, *6*, 3103–3113.

(65) Liu, Y.; Ai, K.; Lu, L. *Chem. Rev.* **2014**, *114*, 5057–5115.

(66) Tran, H. Q.; Batul, R.; Bhave, M.; Yu, A. *Biotechnol. J.* **2019**, *14*, 1–12.

(67) Nador, F.; Guisasola, E.; Baeza, A.; Villaecija, M. A. M.; Vallet-Regí, M.; Ruiz-Molina, D. *Chem. - A Eur. J.* **2017**, *23*, 2753–2758.

(68) Moreno-Villaécija, M. Á.; Sedó-Vegara, J.; Guisasola, E.; Baeza, A.; Regí, M. V.; Nador, F.; Ruiz-Molina, D. *ACS Appl. Mater. Interfaces* **2018**, *10*, 7661–7669.

(69) Guyot, C.; Cerruti, M.; Lerouge, S. *Mater. Sci. Eng. C* **2021**, *118*, 1–9.

(70) Park, M. K.; Li, M. X.; Yeo, I.; Jung, J.; Yoon, B. I.; Joung, Y. K. *Carbohydr. Polym.* **2020**, *248*, 1–11.

(71) Zheng, Z.; Bian, S.; Li, Z.; Zhang, Z.; Liu, Y.; Zhai, X.; Pan, H.; Zhao, X. *Carbohydr. Polym.* **2020**, *249*, 1–12.

(72) Zhou, D.; Li, S.; Pei, M.; Yang, H.; Gu, S.; Tao, Y.; Ye, D.; Zhou, Y.; Xu, W.; Xiao, P. *ACS Appl. Mater. Interfaces* **2020**, *12*, 18225–18234.

(73) Yang, B.; Song, J.; Jiang, Y.; Li, M.; Wei, J.; Qin, J.; Peng, W.; Lasaosa, F. L.; He, Y.; Mao, H.; Yang, J.; Gu, Z. *ACS Appl. Mater. Interfaces* **2020**, *12*, 57782–57797.

(74) Yang, Z.; Huang, R.; Zheng, B.; Guo, W.; Li, C.; He, W.; Wei, Y.; Du, Y.; Wang, H.; Wu, D.; Wang, H. *Adv. Sci.* **2021**, *2003627*, 1–12.

(75) Shao, Z.; Hu, X.; Cheng, W.; Zhao, Y.; Hou, J.; Wu, M.; Xue, D.; Wang, Y. *Nanoscale* **2020**, *12*, 18771–18781.

(76) Tang, Z.; Zhao, M.; Wang, Y.; Zhang, W.; Zhang, M.; Xiao, H.; Huang, L.; Chen, L.; Ouyang, X.; Zeng, H.; Wu, H. *Int. J. Biol. Macromol.* **2020**, *144*, 127–134.

(77) Wei, K.; Senturk, B.; Matter, M. T.; Wu, X.; Herrmann, I. K.; Rottmar, M.; Toncelli, C. *ACS Appl. Mater. Interfaces* **2019**, *11*, 47707–47719.

(78) Hu, C.; Long, L.; Cao, J.; Zhang, S.; Wang, Y. *Chem. Eng. J.* **2021**, *411*, 1–16.

(79) Huang, J.; Jiang, Y.; Liu, Y.; Ren, Y.; Xu, Z.; Li, Z.; Zhao, Y.; Wu, X.; Ren, J. *Bioact. Mater.* **2021**, *6*, 770–782.

(80) Desai, M. S.; Chen, M.; Hong, F. H. J.; Lee, J. H.; Wu, Y.; Lee, S. W. *Biomacromolecules* **2020**, *21*, 2938–2948.

(81) Scalzone, A.; Bonifacio, M. A.; Cometa, S.; Cucinotta, F.; De Giglio, E.; Ferreira, A. M.; Gentile, P. *Front. Bioeng. Biotechnol.* **2020**, *8*, 1–14.

(82) Pang, H.; Zhao, S.; Mo, L.; Wang, Z.; Zhang, W.; Huang, A.; Zhang, S.; Li, J. *J. Appl. Polym. Sci.* **2020**, *137*, 1–10.

(83) Li, S.; Chen, N.; Li, X.; Li, Y.; Xie, Z.; Ma, Z.; Zhao, J.; Hou, X.; Yuan, X. *Adv. Funct. Mater.* **2020**, *30*, 1–13.

(84) Yi, J.; Nguyen, K. C. T.; Wang, W.; Yang, W.; Pan, M.; Lou, E.; Major, P. W.; Le, L. H.; Zeng, H. *ACS Appl. Bio Mater.* **2020**, *3*, 8943–8952.

(85) Lee, B. P.; Dalsin, J. L.; Messersmith, P. B. *Biomacromolecules* **2002**, *3*, 1038–1047.

(86) Brubaker, C. E.; Kissler, H.; Wang, L. J.; Kaufman, D. B.; Messersmith, P. B. *Biomaterials* **2010**, *31*, 420–427.

(87) Liu, Y.; Meng, H.; Konst, S.; Sarmiento, R.; Rajachar, R.; Lee, B. P. *ACS Appl. Mater. Interfaces* **2014**, *6*, 16982–16992.

(88) Matos-Pérez, C. R.; White, J. D.; Wilker, J. J. *J. Am. Chem. Soc.* **2012**, *134*, 9498–9505.

(89) Anderson, T. H.; Yu, J.; Estrada, A.; Hammer, M. U.; Waite, J. H.; Israelachvili, J. N. *Adv. Funct. Mater.* **2010**, *20*, 4196–4205.

(90) Degen, G. D.; Stow, P. R.; Lewis, R. B.; Andresen Eguiluz, R. C.; Valois, E.; Kristiansen, K.; Butler, A.; Israelachvili, J. N. *J. Am. Chem. Soc.* **2019**, *141*, 18673–18681.

(91) Wonderly, W. R.; Cristiani, T. R.; Cunha, K. C.; Degen, G. D.; Shea, J. E.; Waite, J. H. *Macromolecules* **2020**, *53*, 6767–6779.

(92) Grewal, M. S.; Yabu, H. *RSC Adv.* **2020**, *10*, 4058–4063.

(93) Jones, T. A.; Wilker, J. J. *ACS Appl. Polym. Mater.* **2020**, *2*, 4632–4639.

(94) Nishimori, K.; Tenjimbayashi, M.; Naito, M.; Ouchi, M. *ACS Appl. Polym. Mater.* **2020**, *2*, 4604–4612.

(95) Jiang, J.; Wan, W.; Ge, L.; Bu, S.; Zhong, W.; Xing, M. *Chem. Commun.* **2015**, *51*, 8695–8698.

(96) Wang, J.; Zhu, H.; Chen, G.; Hu, Z.; Weng, Y.; Wang, X.; Zhang, W. *Macromol. Rapid Commun.* **2014**, *35*, 1061–1067.

(97) Panchireddy, S.; Grignard, B.; Thomassin, J. M.; Jerome, C.; Detrembleur, C. *ACS Sustain. Chem. Eng.* **2018**, *6*, 14936–14944.

(98) Jenkins, C. L.; Meredith, H. J.; Wilker, J. J. *ACS Appl. Mater. Interfaces* **2013**, *5*, 5091–5096.

(99) Bang, E. K.; Lista, M.; Sforazzini, G.; Sakai, N.; Matile, S. *Chem. Sci.* **2012**, *3*, 1752–1763.

(100) Rosenthal-Kim, E. Q.; Puskas, J. E. *Molecules* **2015**, *20*, 6504–6519.

(101) Marvel, C. S.; Olson, L. E. *J. Am. Chem. Soc.* **1957**, *79*, 3089–3091.

(102) Choi, W.; Sanda, F.; Kihara, N.; Endo, T. *J. Polym. Sci. Part A Polym. Chem.* **1998**, *36*, 79–84.

(103) Ding, Y.; Hay, A. S. *Polymer* **1997**, *38*, 2239–2244.

(104) Meng, Y. Z.; Tjong, S. C.; Hay, A. S. *Polymer* **2001**, *42*, 5215–5224.

(105) Goethals, E.; Sillis, C. *Die Makromol. Chemie* **1968**, *119*, 249–251.

(106) Lee, Y.; Koo, H.; Jin, G. W.; Mo, H.; Cho, M. Y.; Park, J. Y.; Choi, J. S.; Park, J. S. *Biomacromolecules* **2005**, *6*, 24–26.

(107) Yamanaka, T.; Endo, K. *Polym. J.* **2007**, *39*, 1360–1364.

(108) Rosenthal, E. Q.; Puskas, J. E.; Wesdemiotis, C. *Biomacromolecules* **2012**, *13*, 154–164.

(109) Rosenthal-Kim, E. Q.; Puskas, J. E. *Pure Appl. Chem.* **2012**, *84*, 2121–2133.

(110) Virtue, R. W.; Lewis, H. B. *J. Biol. Chem.* **1934**, *104*, 415–421.

(111) Oester, M. Y.; Danehy, J. P. *J. Org. Chem.* **1967**, *35*, 1491–1495.

(112) Danehy, J. P.; Doherty, B. T.; Egan, C. P. *J. Org. Chem.* **1971**, *36*, 2525–2530.

(113) Danehy, J. P.; Egan, C. P.; Switalski, J. *J. Org. Chem.* **1971**, *36*, 2530–2534.

(114) Houk, J.; Whitesides, G. M. *Tetrahedron Lett.* **1989**, *45*, 91–102.

(115) Tam-Chang, S. W.; Stehouwer, J. S.; Hao, J. *J. Org. Chem.* **1999**, *64*, 334–335.

(116) Amaratunga, W.; Milne, J.; Santagati, A. *J. Polym. Sci. Part A Polym. Chem.* **1998**, *1*, 379–390.

(117) Endo, K.; Shiroi, T.; Murata, N.; Kojima, G.; Yamanaka, T. *Macromolecules* **2004**, *37*, 3143–3150.

(118) Ishida, H.; Kisanuki, A.; Endo, K. *Polym. J.* **2009**, *41*, 110–117.

(119) Dang, C.; Wang, M.; Yu, J.; Chen, Y.; Zhou, S.; Feng, X.; Liu, D.; Qi, H. *Adv. Funct. Mater.* **2019**, *29*, 1–9.

(120) Rosenthal-Kim, E. Q.; Agapov, R. L.; Puskas, J. E. *Eur. Polym. J.* **2015**, *65*, 232–237.

(121) Zhang, Q.; Shi, C. Y.; Qu, D. H.; Long, Y. T.; Feringa, B. L.; Tian, H. *Sci. Adv.* **2018**, *4*, 1–9.

(122) Matsumura, S.; Hlil, A. R.; Lepiller, C.; Gaudet, J.; Guay, D.; Shi, Z.; Holdcroft, S.; Hay, A. S. *J. Polym. Sci. Part A Polym. Chem.* **2008**, *46*, 7207–7224.

(123) Ding, Y.; Hay, A. S. *Macromolecules* **1996**, *29*, 4811–4812.

(124) Ding, Y.; Hay, A. S. *Macromolecules* **1996**, *29*, 6386–6392.

(125) Basak, D.; Kumar, R.; Ghosh, S. *Macromol. Rapid Commun.* **2014**, *35*, 1340–1344.

(126) Ruiz Molina, D.; Sedó Vegara, J.; Mancebo Aracil, J., CATECHOL–DERIVATIVE COMPOUNDS AND THEIR USE, EP3438093B1, 2017.

(127) *European Medicines Agency website.* https://www.ema.europa.eu/en/human-regulatory/overview/medical-devices (accessed 2021-10–06).

(128) *Henkel website.* https://www.henkel-adhesives.com/es/es/industrias/medical/medical-devices.html (accessed 2021-10–02).

(129) *'5 types of medical grade adhesives for fast production speeds' – G A Lindberg ChemTech Blogg*, https://www.galindberg.se/blogg/5-fast-medical-adhesives/l (accessed 2021-10–02).

(130) Hohl, D. K.; Weder, C. *Adv. Opt. Mater.* **2019**, *7*, 1–25.

(131) Ito, S.; Akiyama, H.; Sekizawa, R.; Mori, M.; Yoshida, M.; Kihara, H. *ACS Appl. Mater. Interfaces* **2018**, *10*, 32649–32658.

(132) Balkenende, D. W.; Olson, R. A.; Balog, S.; Weder, C.; Montero De Espinosa, L. *Macromolecules* **2016**, *49*, 7877–7885.

(133) Heinzmann, C.; Coulibaly, S.; Roulin, A.; Fiore, G. L.; Weder, C. *ACS Appl. Mater. Interfaces* **2014**, *6*, 4713–4719.

(134) Liu, J.; Tan, C. S. Y.; Scherman, O. A. *Angew. Chemie - Int. Ed.* **2018**, *57*, 8854–8858.

(135) Michal, B. T.; Spencer, E. J.; Rowan, S. J. *ACS Appl. Mater. Interfaces* **2016**, *8*, 11041–11049.

(136) Fortman, D. J.; Snyder, R. L.; Sheppard, D. T.; Dichtel, W. R. *ACS Macro Lett.* **2018**, *7*, 1226–1231.

(137) Lee, D.; Bae, H.; Ahn, J.; Kang, T.; Seo, D. G.; Hwang, D. S. *Acta Biomater.* **2020**, *103*, 92–101.

(138) Wuts, P. G. M., *Protection for the Hydroxyl Group, Including 1,2- and 1,3-Diols*, 5th; Wuts, P. G. M., Ed.; Wiley: 2014, pp 17–471.

(139) Hoyle, C. E.; Lowe, A. B.; Bowman, C. N. *Chem. Soc. Rev.* **2010**, *39*, 1–34.

(140) Berteotti, A.; Vacondio, F.; Lodola, A.; Bassi, M.; Silva, C.; Mor, M.; Cavalli, A. *ACS Med. Chem. Lett.* **2014**, *5*, 501–505.

(141) Zeynizadeh, B. *J. Chem. Res. - Part S* **2002**, 564–566.

(142) Pruckmayr, G.; Dreyfuss, P.; Dreyfuss, M. P. *Kirk-Othmer Encycl. Chem. Technol.* **2000**, *1*, 1–30.

(143) Cataldo, F. *Eur. Polym. J.* **1996**, *32*, 1297–1302.

(144) Capello, C.; Fischer, U.; Hungerbühler, K. *Green Chem.* **2007**, *9*, 927–934.

(145) Danner, E. W.; Kan, Y.; Hammer, M. U.; Israelachvili, J. N.; Waite, J. H. *Biochemistry* **2012**, *51*, 6511–6518.

(146) Have, G.; Wettabilities, S.; Laibinis, P. E.; Whitesides, G. M. *J. Am. Chem. Soc.* **1995**, 1990–1995.

(147) Laibinis, P. E.; Whitesides, G. M. *J. Am. Chem. Soc.* **1992**, 9022–9028.

(148) Robert Campbell, J. *J. Org. Chem.* **1962**, *27*, 2207–2209.

(149) Fan, X.; Lin, L.; Dalsin, J. L.; Messersmith, P. B. *J. Am. Chem. Soc.* **2005**, *127*, 15843–15847.

(150) Sánchez-De-Armas, R.; San-Miguel, M. A.; Oviedo, J.; Márquez, A.; Sanz, J. F. *Phys. Chem. Chem. Phys.* **2011**, *13*, 1506–1514.

(151) Wang, Z.; Tian, H.; He, Q.; Cai, S. *ACS Appl. Mater. Interfaces* **2017**, *9*, 33119–33128.

(152) Imbernon, L.; Oikonomou, E. K.; Norvez, S.; Leibler, L. *Polym. Chem.* **2015**, *6*, 4271–4278.

(153) Abul-Futouh, H.; Almazahreh, L. R.; Harb, M. K.; Görls, H.; El-khateeb, M.; Weigand, W. *Inorg. Chem.* **2017**, *56*, 10437–10451.

(154) Wang, S.; Witek, J.; Landrum, G. A.; Riniker, S. *J. Chem. Inf. Model.* **2020**, *60*, 2044–2058.

(155) Freeman, F.; Angeletakis, C. N.; Maricich, T. J. *Org. Magn. Reson.* **1981**, *17*, 53–58.

(156) Kortüm, G.; Braun, W.; Herzog, G. *Angew. Chemie - Int. Ed.* **1963**, *2*, 333–404.

(157) Bao, Z.; Gao, M.; Sun, Y.; Nian, R.; Xian, M. *Mater. Sci. Eng. C* **2020**, *111*, 1–15.

(158) Donkerwolcke, M.; Burny, F.; Muster, D. *Biomaterials* **1998**, *19*, 1461–1466.

(159) Ma, Z.; Bao, G.; Li, J. *Adv. Mater.* **2021**, *33*, 1–29.

(160) Taboada, G. M.; Yang, K.; Pereira, M. J.; Liu, S. S.; Hu, Y.; Karp, J. M.; Artzi, N.; Lee, Y. *Nat. Rev. Mater.* **2020**, *5*, 310–329.

(161) Bal-Ozturk, A.; Cecen, B.; Avci-Adali, M.; Topkaya, S. N.; Alarcin, E.; Yasayan, G.; Li, Y. C. E.; Bulkurcuoglu, B.; Akpek, A.; Avci, H.; Shi, K.; Shin, S. R.; Hassan, S. *Nano Today* **2021**, *36*, 1–25.

(162) *'A Sticky Situation: SuperGlue in Warfare' – War History Online*, https://www.warhistoryonline.com/history/history-of-the-super-glue.html (accessed 2021-09–15).

(163) Bhagat, V.; Becker, M. L. *Biomacromolecules* **2017**, *18*, 3009–3039.

(164) *Progel product website*, https://www.bd.com/en-us/offerings/capabilities/-biosurgery/sealants/progel-pleural-air-leak-sealant (accessed 2021-09–25).

(165) *Auction of patent assets announcement*, https://www.prweb.com/releases/-patent_and_trademark_assets_related_to_absorbable_surgical_adhesives_and_-sealants_owned_by_cohera_medical_inc_to_sell_on_february_25_2019_in_private_-auction/prweb16084779.html (accessed 2021-05–10).

(166) Ryu, J. H.; Lee, Y.; Kong, W. H.; Kim, T. G.; Park, T. G.; Lee, H. *Biomacromolecules* **2011**, *12*, 2653–2659.

(167) Hong, S. H.; Ryu, J. H.; Lee, H. *J. Ind. Eng. Chem.* **2019**, *79*, 425–430.

(168) Wang, L.; Zhang, X.; Yang, K.; Fu, Y. V.; Xu, T.; Li, S.; Zhang, D.; Wang, L. N.; Lee, C. S. *Adv. Funct. Mater.* **2020**, *30*, 1–14.

(169) Liu, Y.; Cheong NG, S.; Yu, J.; Tsai, W. B. *Colloids Surfaces B Biointerfaces* **2019**, *174*, 316–323.

(170) Burke, S. A.; Ritter-Jones, M.; Lee, B. P.; Messersmith, P. B. *Biomed. Mater.* **2007**, *2*, 203–210.

(171) Murphy, J. L.; Vollenweider, L.; Xu, F.; Lee, B. P. *Biomacromolecules* **2010**, *11*, 2976–2984.

(172) Brubaker, C. E.; Messersmith, P. B. *Biomacromolecules* **2011**, *12*, 4326–4334.

(173) Chung, H.; Grubbs, R. H. *Macromolecules* **2012**, *45*, 9666–9673.

(174) Sun, F.; Bu, Y.; Chen, Y.; Yang, F.; Yu, J.; Wu, D. *ACS Appl. Mater. Interfaces* **2020**, *12*, 9132–9140.

(175) Guo, J.; Kim, G. B.; Shan, D.; Kim, J. P.; Hu, J.; Wang, W.; Hamad, F. G.; Qian, G.; Rizk, E. B.; Yang, J. *Biomaterials* **2017**, *112*, 275–286.

(176) Mehdizadeh, M.; Weng, H.; Gyawali, D.; Tang, L.; Yang, J. *Biomaterials* **2012**, *33*, 7972–7983.

(177) Zhu, W.; Peck, Y.; Iqbal, J.; Wang, D. A. *Biomaterials* **2017**, *147*, 99–115.

(178) Sedó, J.; Saiz-Poseu, J.; Busqué, F.; Ruiz-Molina, D. *Adv. Mater.* **2013**, *25*, 653–701.

(179) Kord Forooshani, P.; Lee, B. P. *J. Polym. Sci. Part A Polym. Chem.* **2017**, *55*, 9–33.

(180) Barros, N. R. et al. *Biomater. Sci.* **2021**, 1–38.

(181) *'Kensey Nash Corporation Pays $20M For VC-Backed Nerites Corporation' – Biospace News*, https://www.biospace.com/article/releases/kensey-nash-corporation-pays-20m-for-vc-backed-nerites-corporation-/ (accessed 2020-09–20).

(182) Messersmith, P. B.; Jeffrey, D.; Lee, B. P.; Burke, S. A., DOPA-FUNCTIONAL
bibrangedash IZED, BRANCHED, POLY(AKLYLENE OXIDE) ADHESIVES, US2008247984A1, 2008.

(183) Jeffrey, D.; Lee, B. P.; Vollenweider, L.; Silvary, S.; Murphy, J. L.; Xu, F.; Spitz, A.; Lyman, A., MULTI–ARMED CATECHOL COMPOUND BLENDS, US2010113828A1, 2010.

(184) Lee, B. P.; Vollenweider, L.; Murphy, J. L.; Xu, F.; Dalsin, J.; Virosco, J.; Lew, W.; White, J., BIOADHESIVE CONSTRUCTS, US2010137902A1, 2010.

(185) *Innotherapy, Inc. website.* https://innotherapy.com/pipeline/ (accessed 2021-09–10).

(186) Yan, S.; Wang, W.; Li, X.; Ren, J.; Yun, W.; Zhang, K.; Li, G.; Yin, J. *J. Mater. Chem. B* **2018**, *6*, 6377–6390.

(187) Chen, T.; Chen, Y.; Rehman, H. U.; Chen, Z.; Yang, Z.; Wang, M.; Li, H.; Liu, H. *ACS Appl. Mater. Interfaces* **2018**, *10*, 33523–33531.

(188) Han, L.; Wang, M.; Li, P.; Gan, D.; Yan, L.; Xu, J.; Wang, K.; Fang, L.; Chan, C. W.; Zhang, H.; Yuan, H.; Lu, X. *ACS Appl. Mater. Interfaces* **2018**, *10*, 28015–28026.

(189) Bai, Z.; Dan, W.; Yu, G.; Wang, Y.; Chen, Y.; Huang, Y.; Yang, C.; Dan, N. *RSC Adv.* **2018**, *8*, 42123–42132.

(190) Fan, C.; Fu, J.; Zhu, W.; Wang, D. A. *Acta Biomater.* **2016**, *33*, 51–63.

(191) Kim, J. Y.; Ryu, S. B.; Park, K. D. *J. Ind. Eng. Chem.* **2018**, *58*, 105–112.

(192) Kim, B. J.; Oh, D. X.; Kim, S.; Seo, J. H.; Hwang, D. S.; Masic, A.; Han, D. K.; Cha, H. J. *Biomacromolecules* **2014**, *15*, 1579–1585.

(193) Jeon, E. Y.; Hwang, B. H.; Yang, Y. J.; Kim, B. J.; Choi, B. H.; Jung, G. Y.; Cha, H. J. *Biomaterials* **2015**, *67*, 11–19.

(194) Lu, D.; Li, Y.; Wang, X.; Li, T.; Zhang, Y.; Guo, H.; Sun, S.; Wang, X.; Zhang, Y.; Lei, Z. *J. Mater. Chem. B* **2018**, *6*, 7511–7520.

(195) Zhang, H.; Bré, L. P.; Zhao, T.; Zheng, Y.; Newland, B.; Wang, W. *Biomaterials* **2014**, *35*, 711–719.

(196) Kim, M.; Ondrusek, B. A.; Lee, C.; Douglas, W. G.; Chung, H. *J. Polym. Sci. Part A Polym. Chem.* **2018**, *56*, 1564–1573.

(197) Mehdizadeh, M.; Weng, H.; Gyawali, D.; Tang, L.; Yang, J. *Biomaterials* **2012**, *33*, 7972–7983.

(198) Lu, X.; Shi, S.; Li, H.; Gerhard, E.; Lu, Z.; Tan, X.; Li, W.; Rahn, K. M.; Xie, D.; Xu, G.; Zou, F.; Bai, X.; Guo, J.; Yang, J. *Biomaterials* **2020**, *232*, 119719.

(199) Han, X.; Meng, G.; Wang, Q.; Cui, L.; Wang, H.; Wu, J.; Liu, Z.; Guo, X. *J. Biomater. Appl.* **2019**, *33*, 915–923.

(200) Wang, R.; Li, J.; Chen, W.; Xu, T.; Yun, S.; Xu, Z.; Xu, Z.; Sato, T.; Chi, B.; Xu, H. *Adv. Funct. Mater.* **2017**, *27*, DOI: 10.1002/adfm.201604894.

(201) Li, S.; Chen, N.; Li, X.; Li, Y.; Xie, Z.; Ma, Z.; Zhao, J.; Hou, X.; Yuan, X. *Adv. Funct. Mater.* **2020**, *30*, 1–13.

(202) Lu, D.; Wang, H.; Li, T.; Li, Y.; Dou, F.; Sun, S.; Guo, H.; Liao, S.; Yang, Z.; Wei, Q.; Lei, Z. *ACS Appl. Mater. Interfaces* **2017**, *9*, 16756–16766.

(203) Hu, S.; Pei, X.; Duan, L.; Zhu, Z.; Liu, Y.; Chen, J.; Chen, T.; Ji, P.; Wan, Q.; Wang, J. *Nat. Commun.* **2021**, *12*, DOI: 10.1038/s41467-021-21989-5.

(204) Zhou, J.; Bhagat, V.; Becker, M. L. *ACS Appl. Mater. Interfaces* **2016**, *8*, 33423–33429.

(205) Narayanan, A.; Kaur, S.; Peng, C.; Debnath, D.; Mishra, K.; Liu, Q.; Dhinojwala, A.; Joy, A. *Biomacromolecules* **2019**, *20*, 2577–2586.

# CHAPTER 6

# Annex

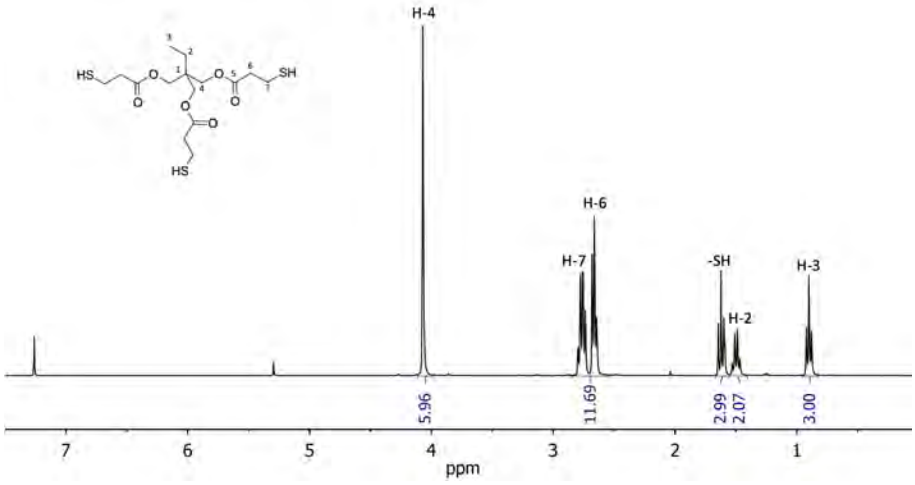


**Figure 6.1.** $^{1}$H NMR spectrum and assignments of compound **2**.

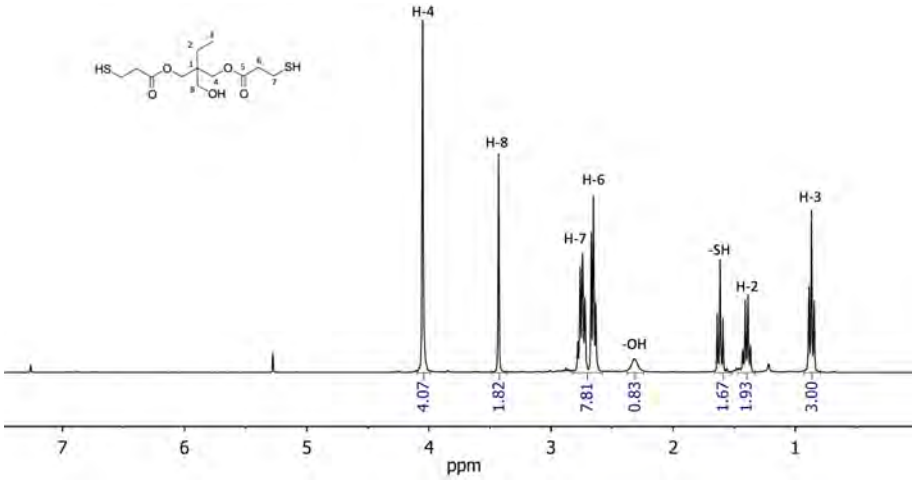


**Figure 6.2.** $^{1}$H NMR spectrum and assignments of compound **9**.

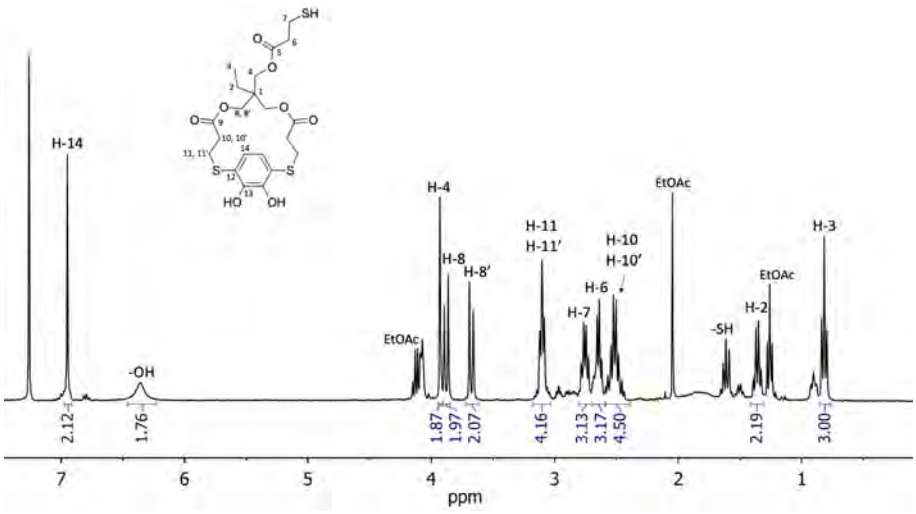


**Figure 6.3.** $^{1}$H NMR spectrum and assignments of compound **11**.

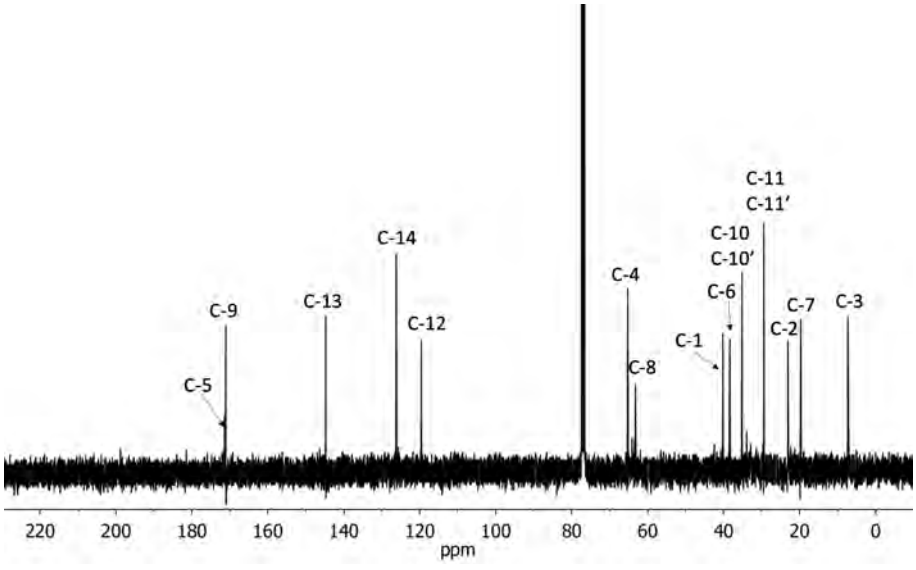


**Figure 6.4.** $^{13}$C NMR spectrum and assignments of compound **11**.

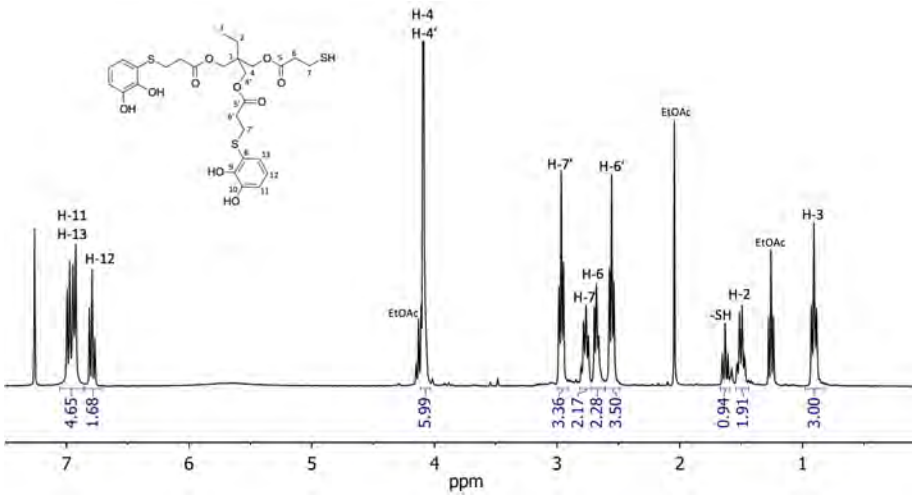


**Figure 6.5.** $^{1}$H NMR spectrum and assignments of compound **12**.

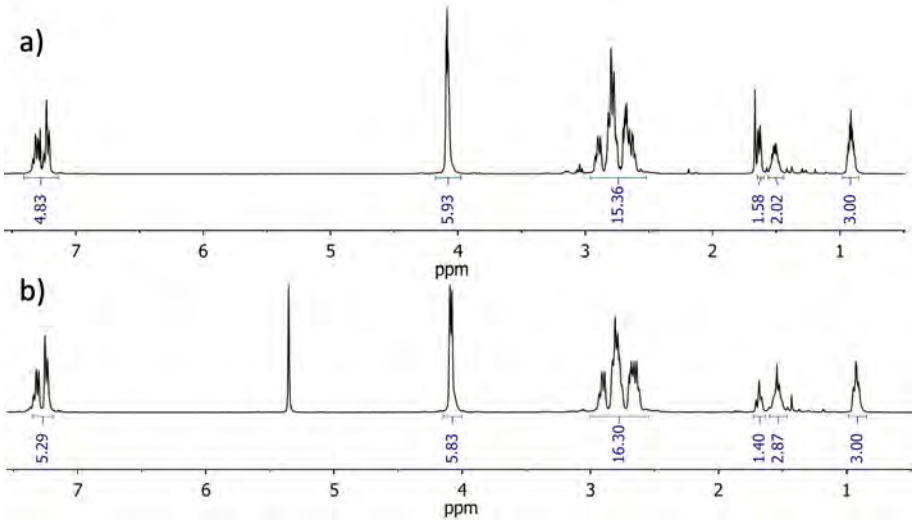


**Figure 6.6.** a) $^{1}$H NMR of the crude of reaction from the synthesis of **7** and b) $^{1}$H NMR of the third fraction from purification considered the most pure containing **7**

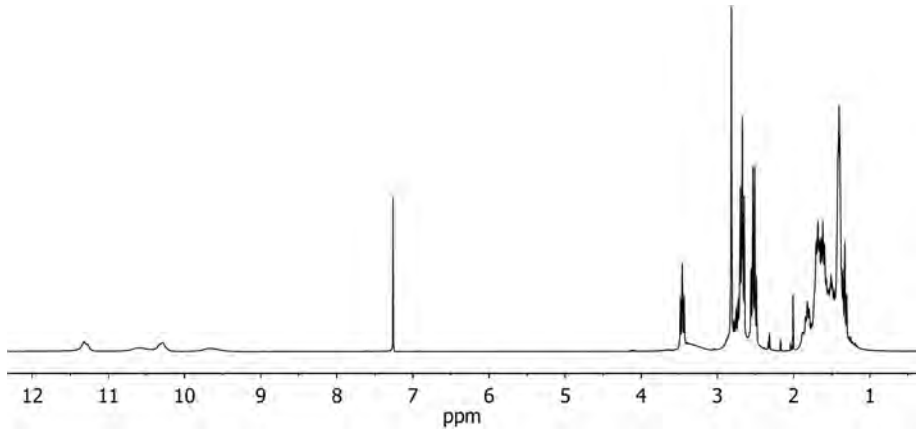


**Figure 6.7.** $^{1}$H NMR spectrum of product of polymerization of **5** in ACN after 12 hours of reaction.

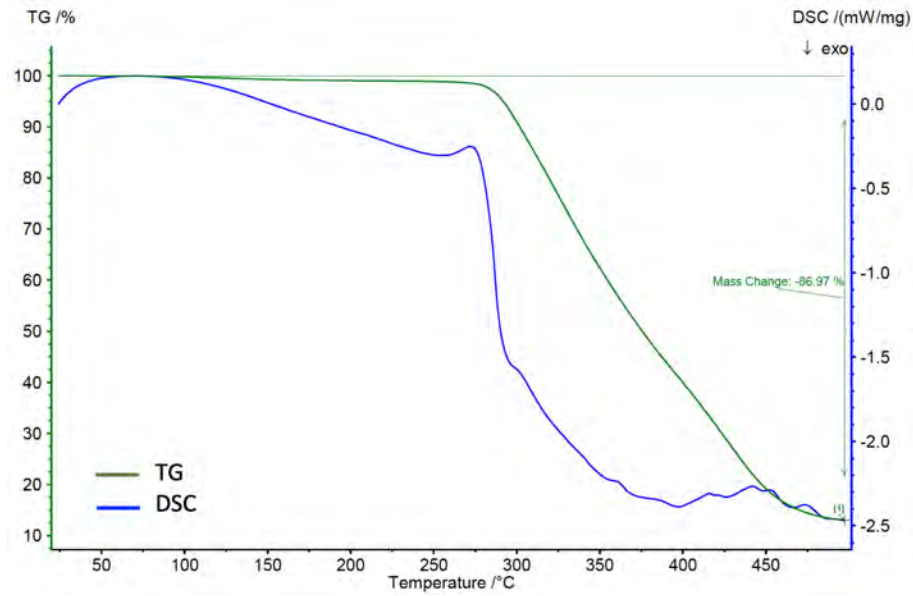


**Figure 6.8.** TGA and DSC analysis of **p1-50k**.

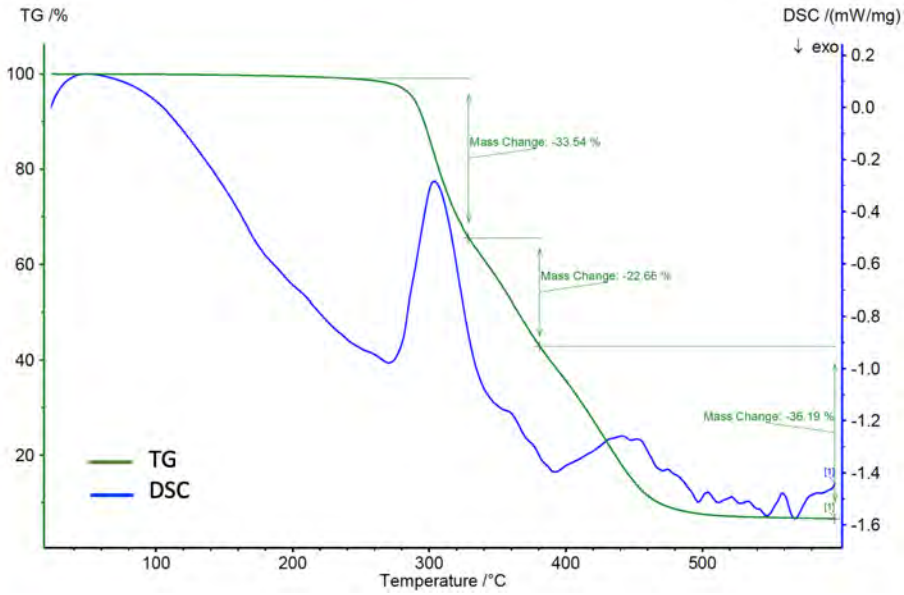


**Figure 6.9.** TGA and DSC analysis of **p8-37k**.

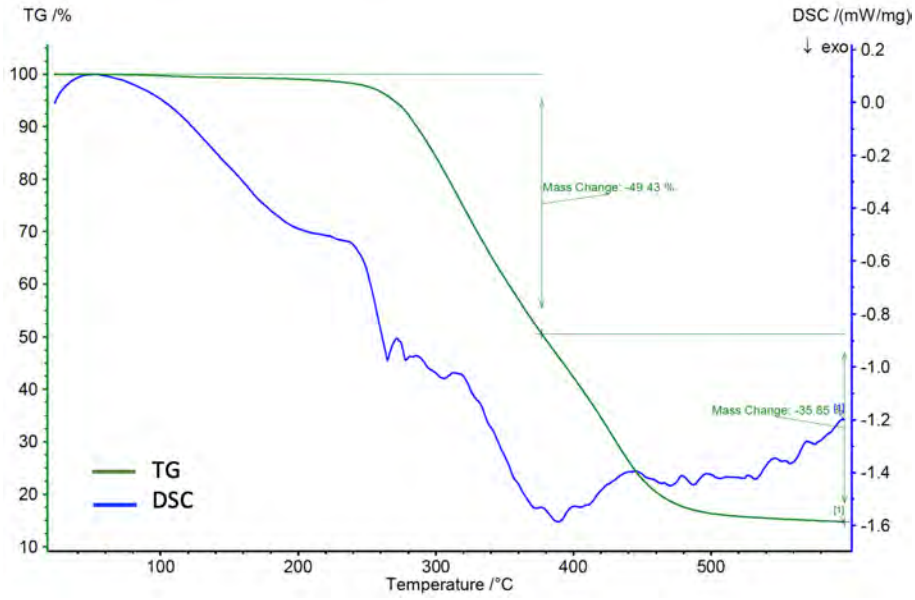


**Figure 6.10.** TGA and DSC analysis of ROP product of **p1-cyc**.

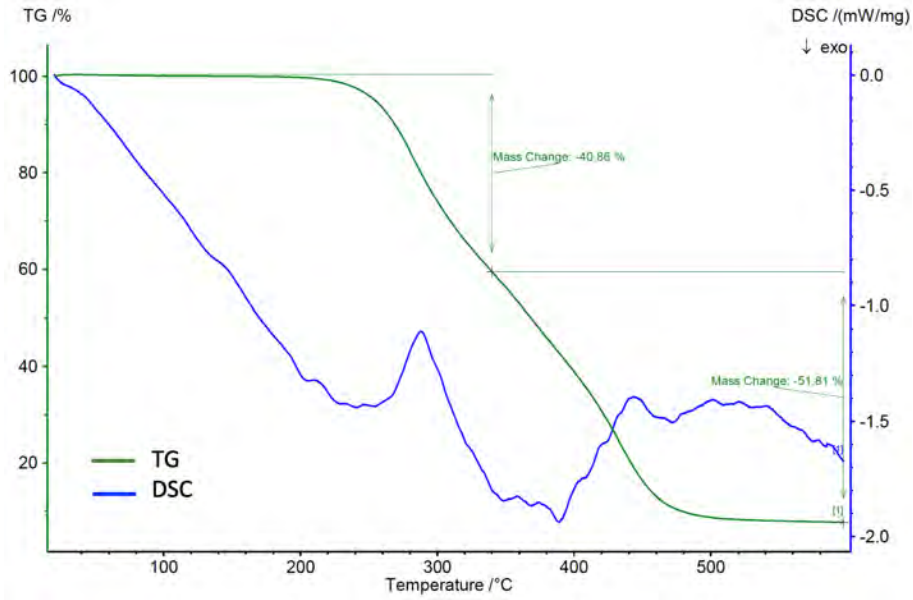


**Figure 6.11.** TGA and DSC analysis of ROP product of **p8-cyc**.

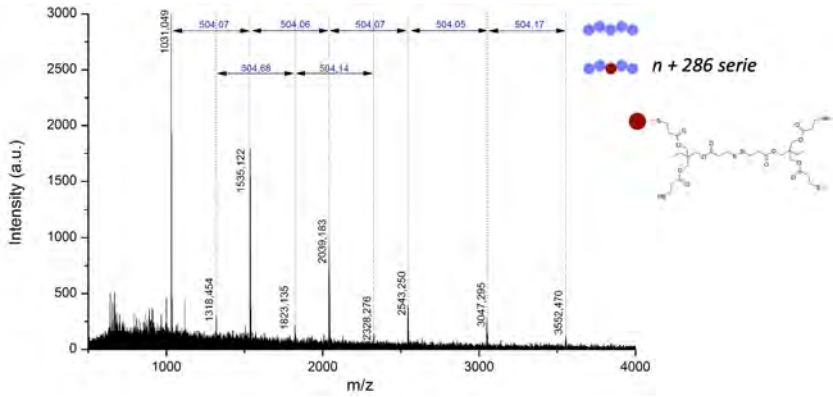


**Figure 6.12.** MALDI-TOF and peak assignments of **p1-nk** from the polymerization reaction at 0.04 M, 0.8 equivalents of iodine and 10 min of reaction time.

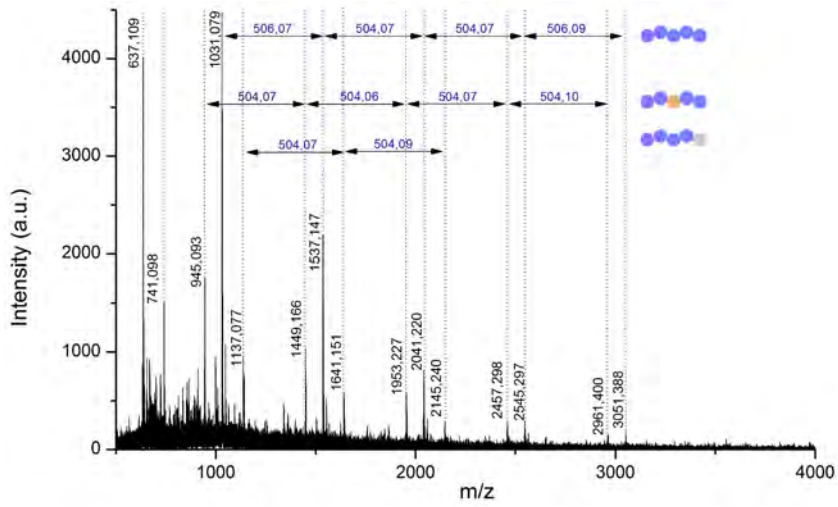


**Figure 6.13.** MALDI-TOF and peak assignments of **p1-nk** from the polymerization reaction at 0.4 M, 0.8 equivalents of iodine and 10 min of reaction time.

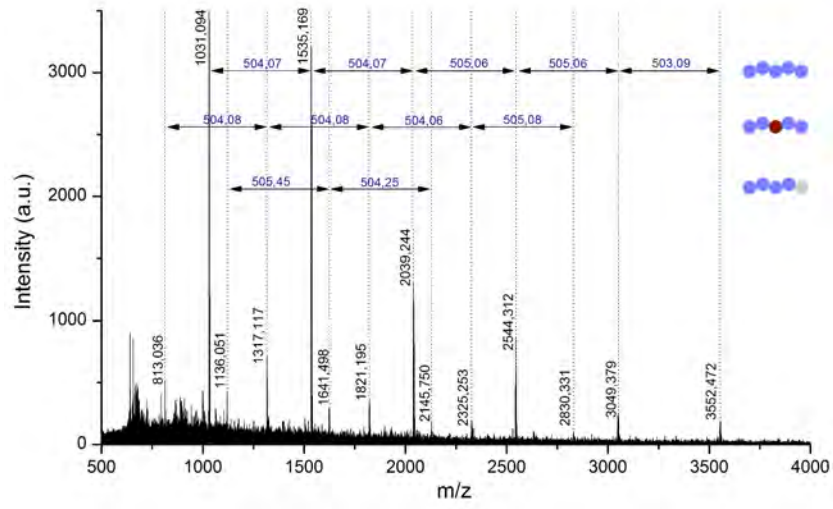


**Figure 6.14.** MALDI-TOF and peak assignments of **p1-nk** from the polymerization reaction at 0.04 M, 1.05 equivalents of iodine and 10 min of reaction time.

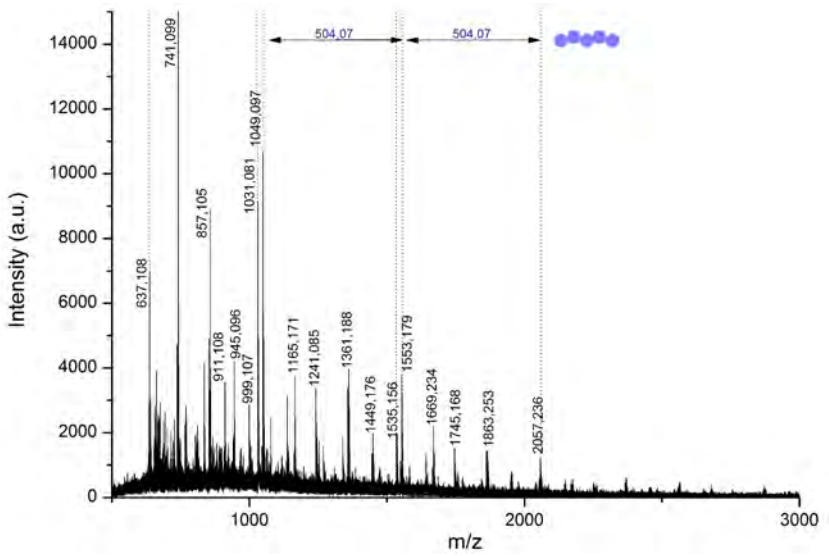


**Figure 6.15.** MALDI-TOF and peak assignments of **p1-nk** from the polymerization reaction at 0.4 M, 1.05 equivalents of iodine and 4 h of reaction time.

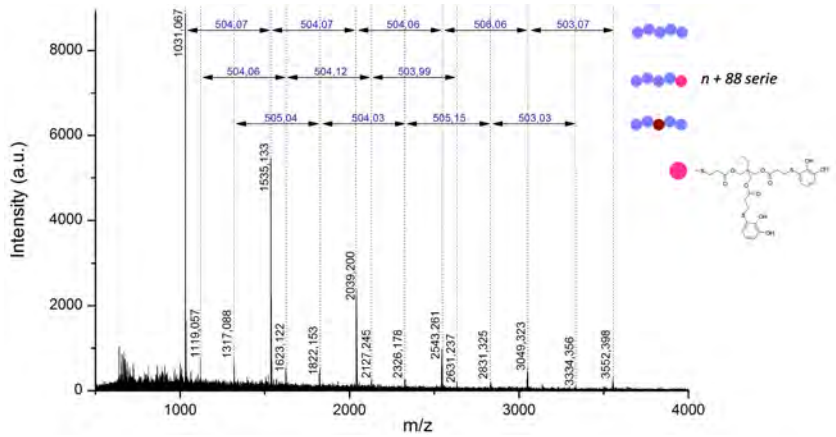


**Figure 6.16.** MALDI-TOF and peak assignments of **p1-nk** from the polymerization reaction at 0.04 M, 1.05 equivalents of iodine and 4 h of reaction time.

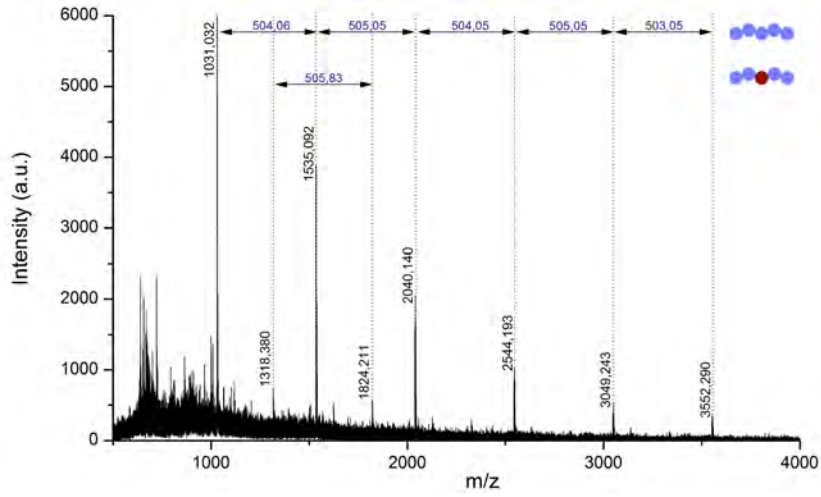


**Figure 6.17.** MALDI-TOF and peak assignments of **p1-nk** from the polymerization reaction at 0.04 M, 0.8 equivalents of iodine and 4 h of reaction time.

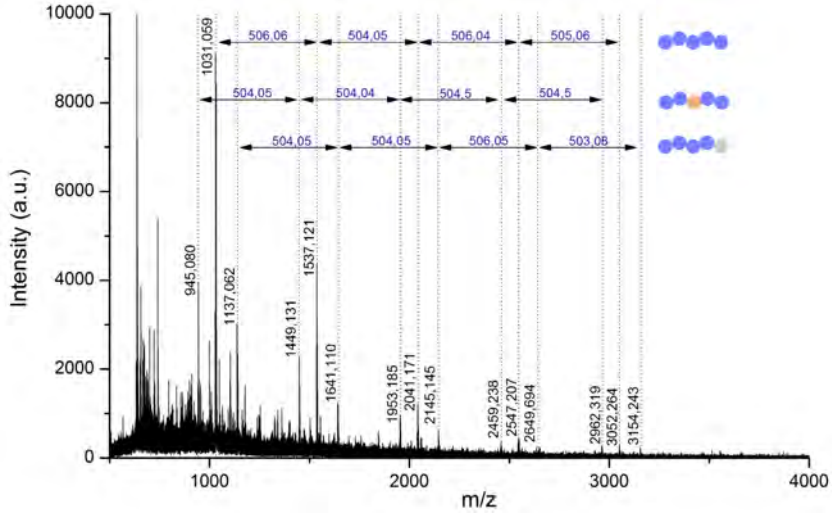


**Figure 6.18.** MALDI-TOF and peak assignments of **p1-nk** from the polymerization reaction at 0.4 M, 1.05 equivalents of iodine and 10 min of reaction time.

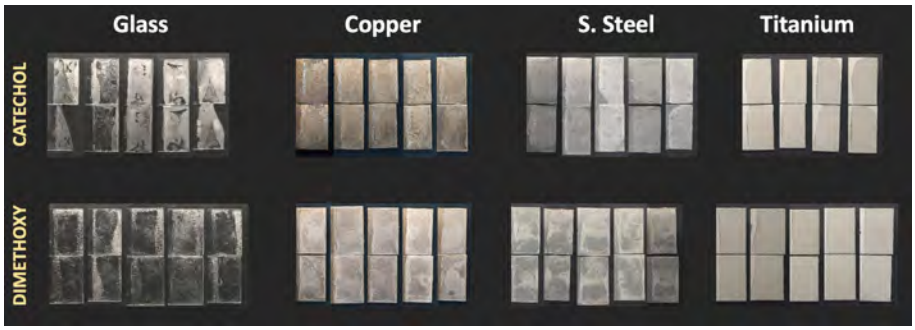


**Figure 6.19.** Pictures of the substrates after last measurement showing the cohesive failure in the samples and the substrate failure in some glass specimens. Falta Aluminio!!!

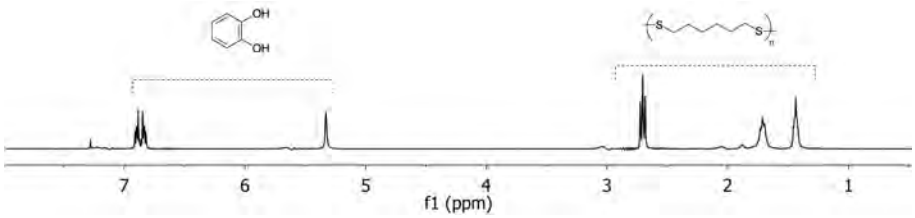


**Figure 6.20.** $^{1}$H NMR spectrum of product from reaction of **p5-16k** and pyrocatechol **3** at 120 °C for 1 hour.

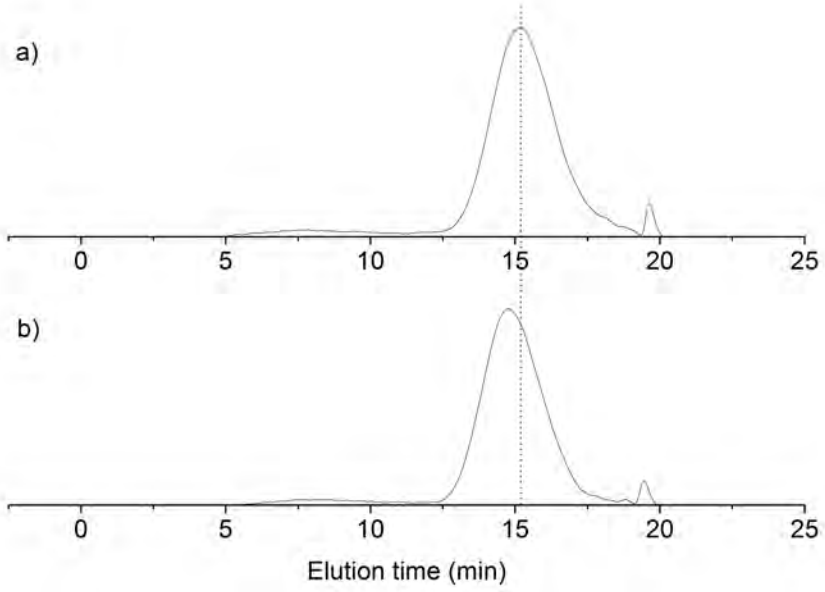


**Figure 6.21.** GPC of a) **p5-16k** before reaction and b) after reaction with pyrocatechol **3** heating up at 120 °C for 1 hour.

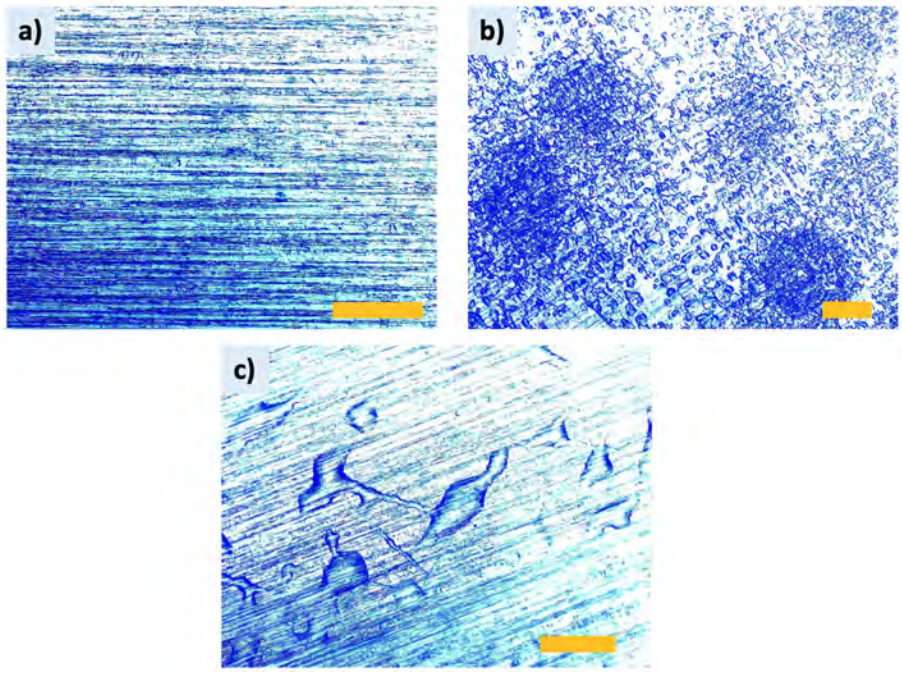


**Figure 6.22.** Optical microscopy images of a) pristine stainless steel, b) stainless steel with **p1-50k** and c) stainless steel with **p8-37k**. Scale bars: 200 $\mu$m.

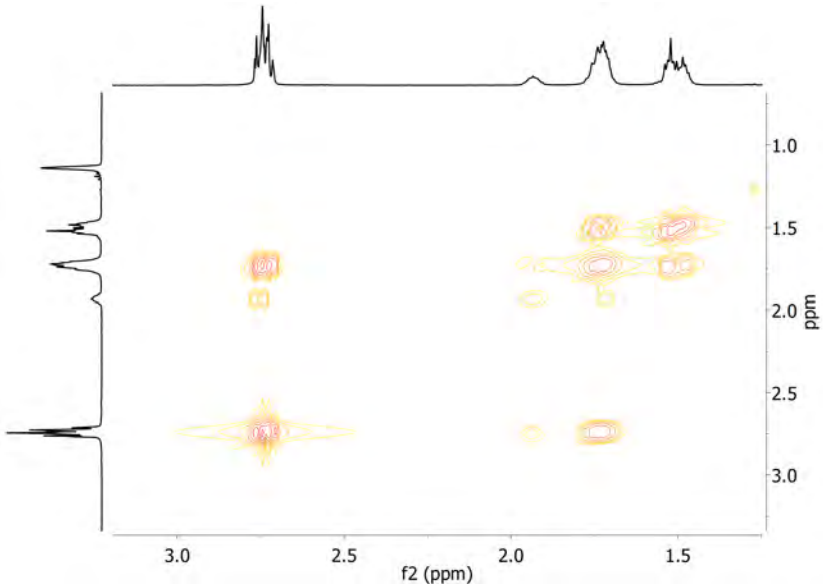


**Figure 6.23.** $^{1}$H-$^{1}$H COSY analysis of supernatant of polymerization of **5**.

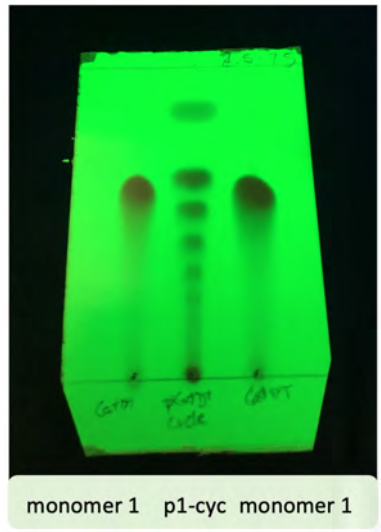


**Figure 6.24.** TLC under UV light of **p1-cyc** showing the separated spots of the different cyclic species.

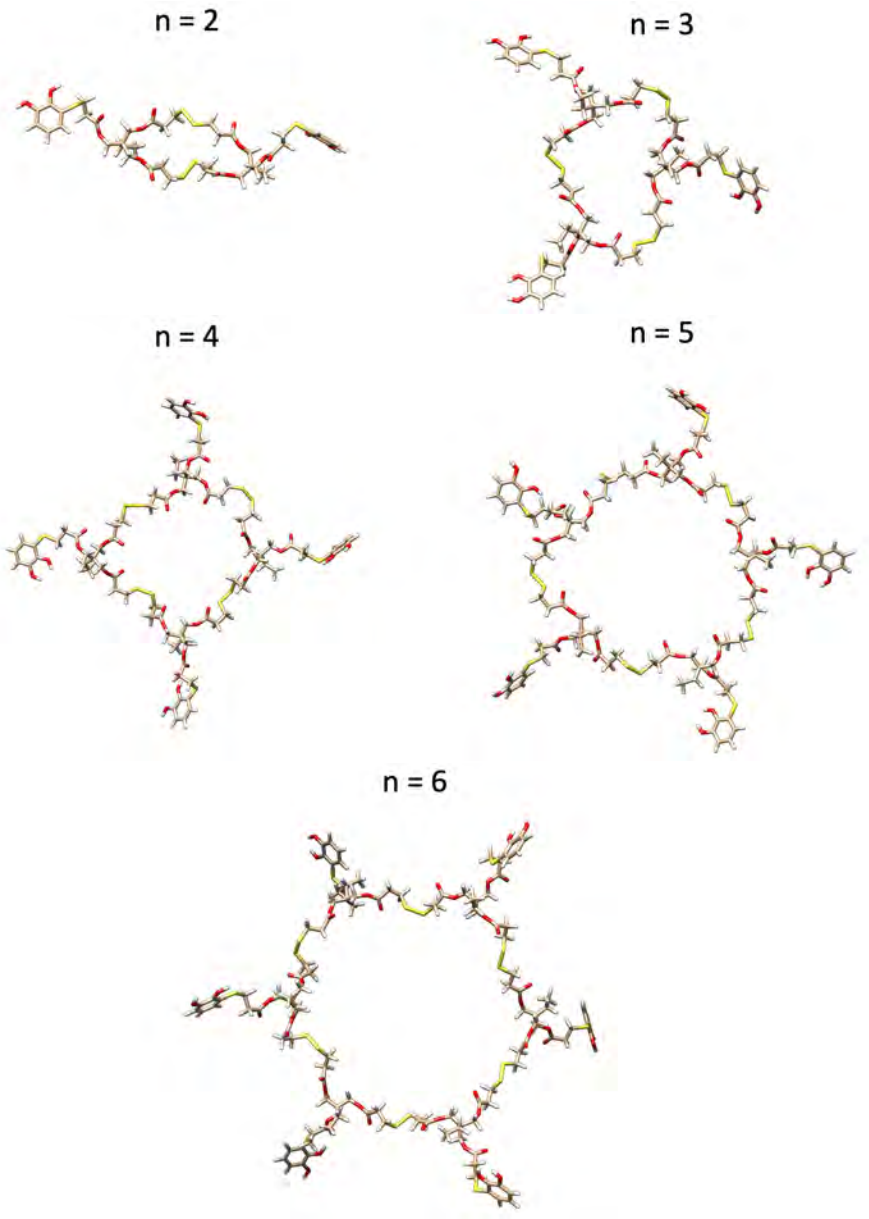


**Figure 6.25.** Conformers obtained with the improved ETKDG conformer generator of the catechol disulfide macrocycles observed in DOSY.

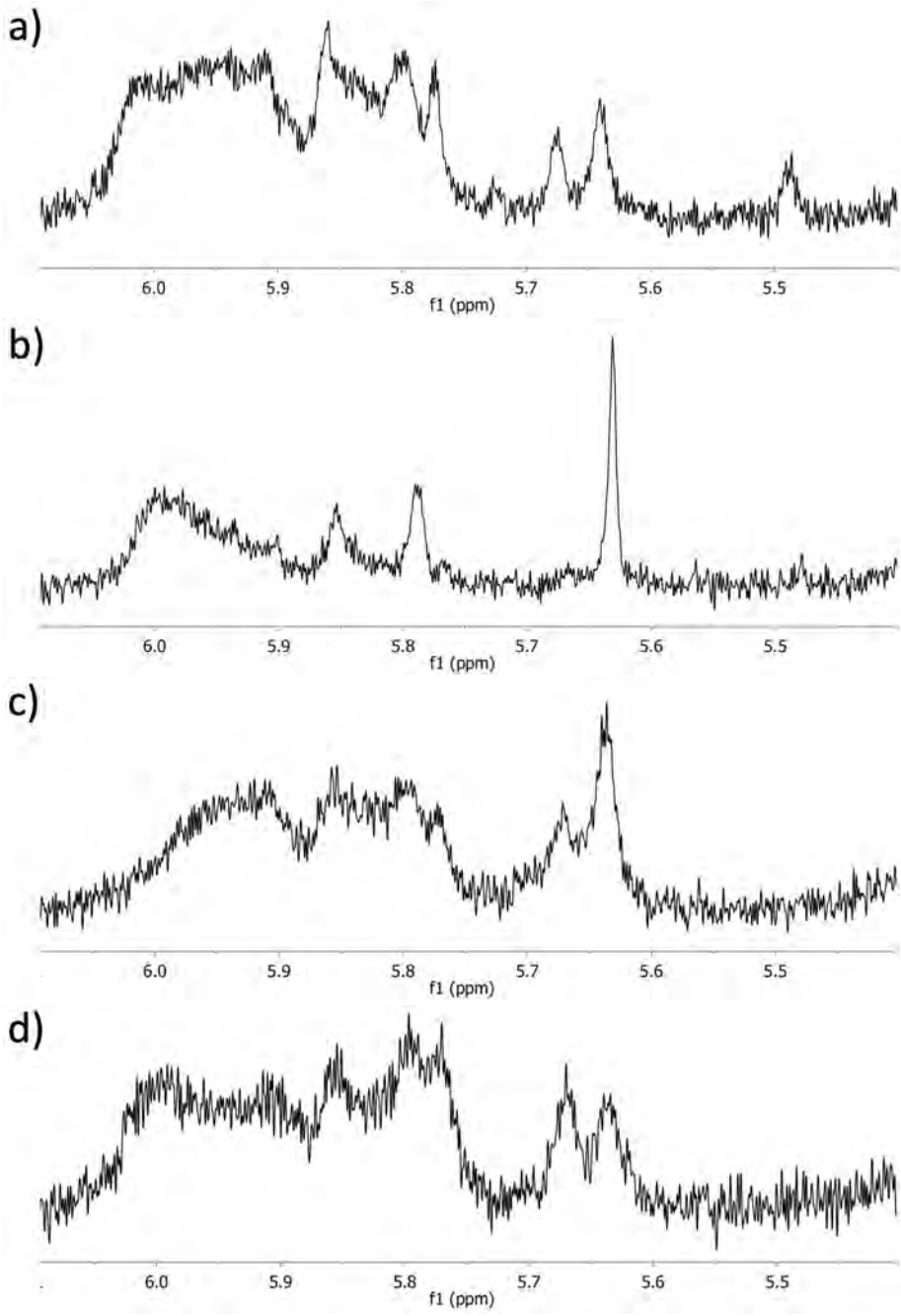


**Figure 6.26.** $^{1}$H NMR of −OH region from the soluble fraction of the synthesis of **p1-nk** with 0.75 eq. of iodine at different concentrations, a) 20 mM, b) 10 mM, c) 5 mM and d) 1 mM. Data courtesy of Pau Delgado Melgares.

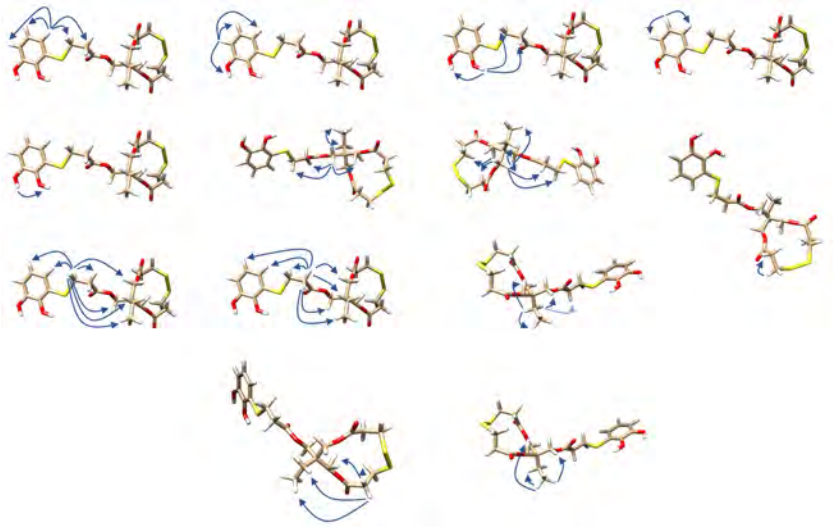

**Figure 6.27.** NOE assignments of cyclisized monomer **c1**

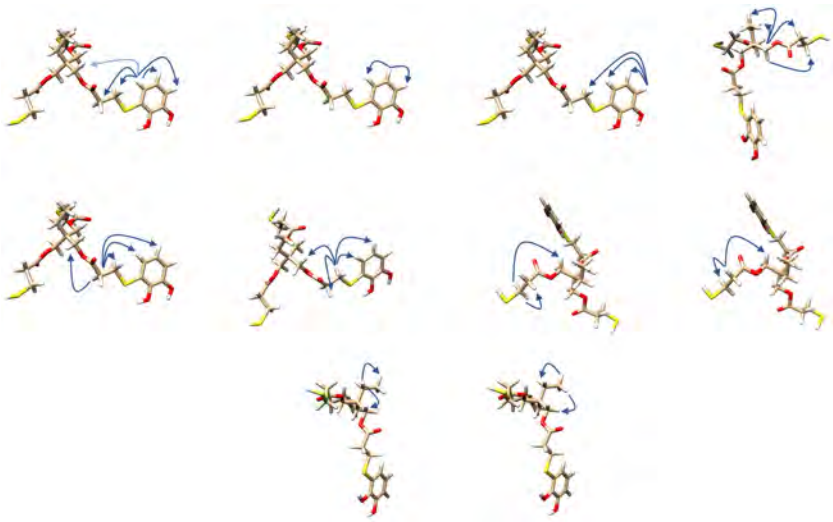

**Figure 6.28.** NOE assignments of monomer **1**

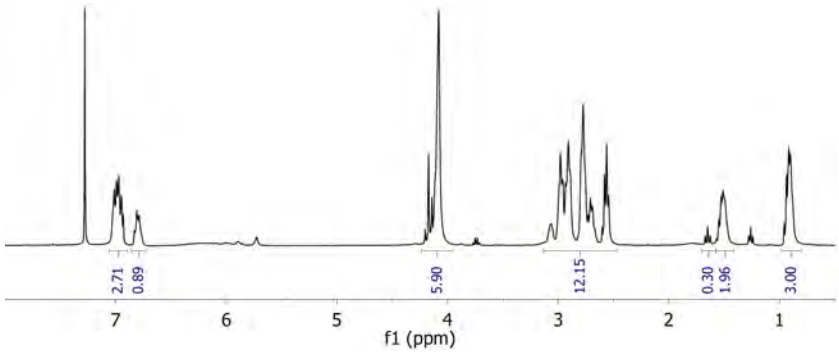


**Figure 6.29.** $^{1}$H NMR of synthesis of **p1-0.9k** from the polymerization of monomer **1** with 0.75 equivalents of iodine.

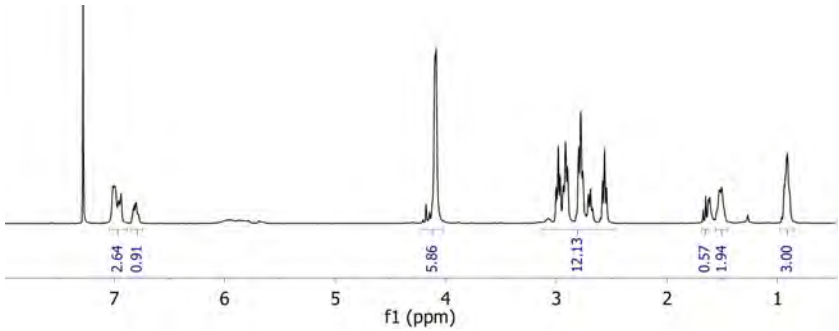


**Figure 6.30.** $^{1}$H NMR of synthesis of **p1-1.5k** from the polymerization of monomer **1** with 0.8 equivalents of iodine.

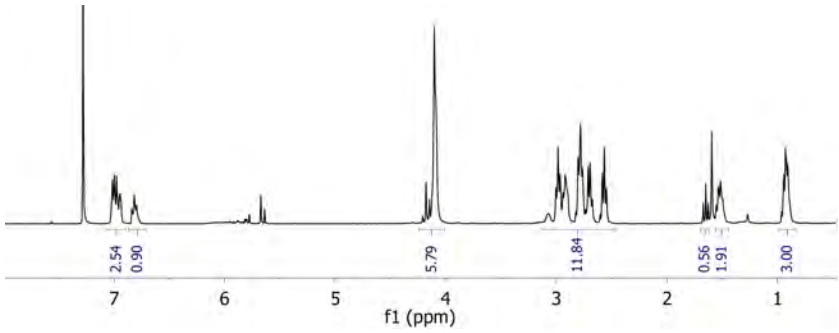


**Figure 6.31.** $^{1}$H NMR of synthesis of **p1-1.2k** from the polymerization of monomer **1** with 0.9 equivalents of iodine.

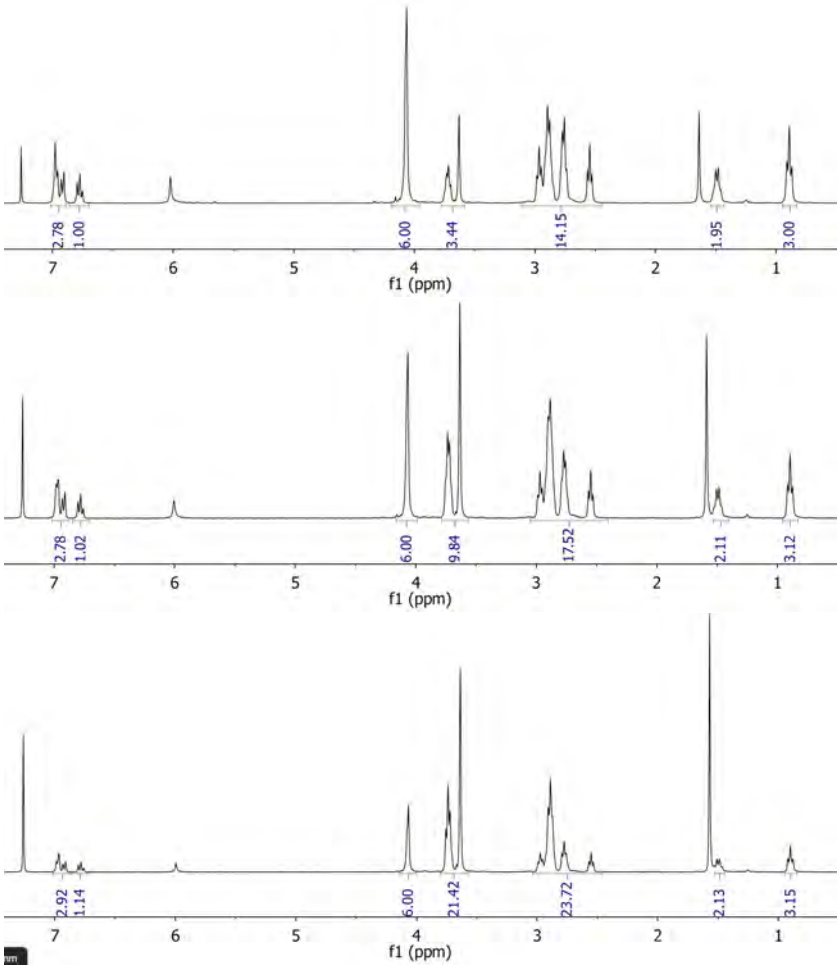


**Figure 6.32.** From top to bottom, $^{1}$H NMR of **p(1-6)-61k**, **p(1-6)-45k** and **p(1-6)-39k** obtained from the copolymerization of monomer **1** with dithiol **6** at the ratios 75:25, 50:50 and 25:75, respectively.

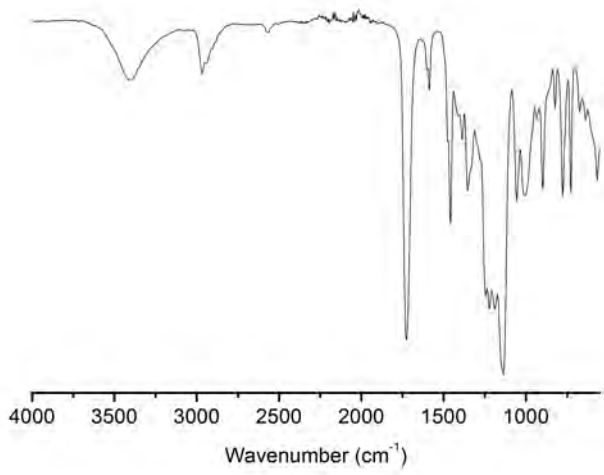


**Figure 6.33.** FT-IR of monomer **1**

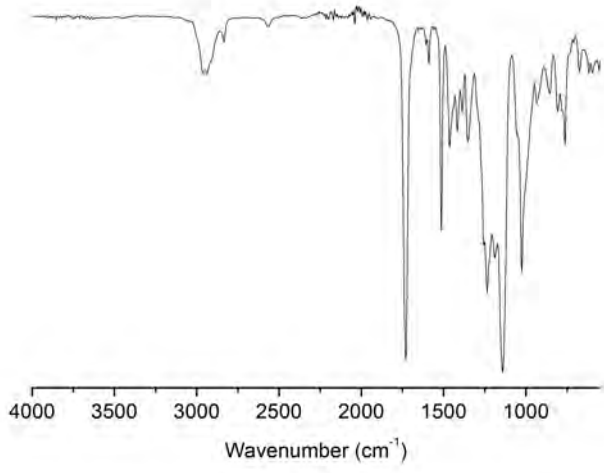


**Figure 6.34.** FT-IR of monomer **8**

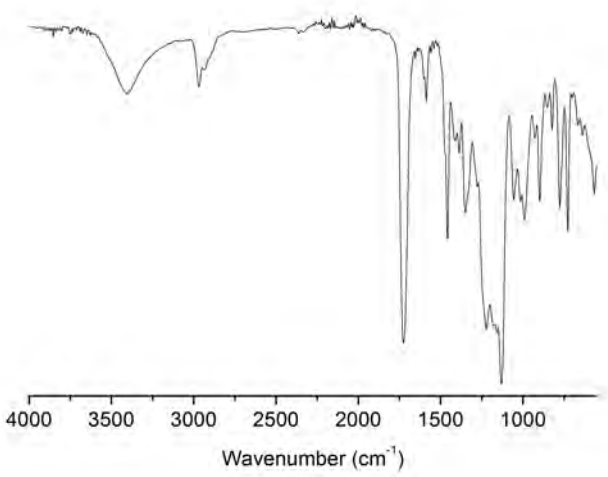


**Figure 6.35.** FT-IR of monomer **p1-50k**